THESIS AND ABSTRACT

Investigation of the biological role of iASPP *in vivo*.

Mario Notari

Green Templeton College

Ludwig Institute for Cancer Research, ORCB
Nuffield Department of Clinical Medicine
University of Oxford

Word count: 49’018

Trinity Term 2011

Table of contents

ABSTRACT **1**

Publications **2**

Acknowledgments **3**

Abbreviation **4**

Chapter 1 ..... **8**

General Introduction **8**

1.1 p53 and its family members: overview. 8

1.1.1 TP53 gene and p53 protein structure. 10

1.1.2 *TP63* and *TP73* genes and protein structures. 11

1.1.3 p53 is a master regulator of various cellular responses. 14

1.1.3.1 Apoptosis: overview. 16

1.1.3.2 p53 and its role in apoptosis. 20

1.1.3.3 p63, p73 and their role in apoptosis. 22

1.1.4 The p53 family of proteins in normal development. 23

1.1.4.1 p53. 23

1.1.4.2 p53 inhibitors: mdm2 and mdm4 are essential for embryonic development and heart function. 25

1.1.4.3 p63 and p73. 27

1.2 The ASPP family of proteins: new co-activators of p53 and its family members.....29
1.2.1 Identification of the ASPP family, protein structure and expression. 29
1.2.2 Functions of the ASPP proteins. 33
1.2.2.1 ASPP1 and ASPP2.....33
1.2.2.2 iASPP.....34
1.2.3 Regulation of ASPP proteins expression. 36
1.2.3.1 ASPP1 and ASPP2.....36
1.2.3.2 iASPP.....37
1.2.4 ASPP proteins and cancer. 37
1.2.4.1 ASPP1 and ASPP2 as tumour suppressor genes. 37
1.2.4.2 iASPP as an oncogene. 38
1.2.5 The ASPP family in development. 39
1.2.5.1 ASPP1 and ASPP2 in development. 39
1.2.5.2 iASPP and wa3 mice: spontaneous mutation of PPP1R13L protein in mice. 41
1.3 Mammalian cardiovascular system: an overview. 43
1.3.1 Heart: function, structure and development. 43
1.3.2 Cardiomyocytes. 45
1.3.3 Diseases of the myocardium: cardiomyopathies. 51
1.3.3.1 Hypertrophic cardiomyopathy. 54
1.3.3.2 Dilated cardiomyopathy. 55
1.3.3.3 Arrhythmogenic right ventricular cardiomyopathy/dysplasia. 57
▪Naxos and Carvajal diseases. 58
1.3.3.4 Restricted cardiomyopathy. 60
1.3.2.5 Desmosomes and diseases 61

1.3.4 Signaling pathways involved in the adaptive and maladaptive response in cardiomyopathy. 63

1.3.4.1 Myocyte hypertrophy and the apoptotic pathway....64

1.3.4.2 Cytoskeletal pathway and dilated cardiomyopathy. 65

1.3.4.3 PI3K-Akt axis and TNF-α-NFk-B pathways. 66

1.3.4.4.Wnt/β-catenin signaling pathway in heart. 68

1.3.5 Cardiotoxicity of anticancer drugs....69

1.4 Mammalian skin: overview. 73

1.4.1 Hair follicles: structure and development. 73

1.4.2 Epidermis and the stratification process. 76

1.4.2.1 p63 expression is essential for epithelial development....79

1.5 Aim of the study. 83

Chapter 2 84

Materials and Methods 84

2.1 Animals. 84

2.2 Breeding. 84

2.3 Genotyping. 85

2.3.1 DNA extraction from ear biopsies. 85

2.3.2 iASPP$^{flox/flox}$ genotyping. 85

2.3.3 iASPP$^{\Delta 8/\Delta 8}$;Cre^{+} genotyping. 86

2.4 Materials. 87

2.4.1 Reagents. 87

2.4.1 SDS-polyacrylamide Gels. 96

2.4.3 Cell lines. 100
2.5 Methods. 100
2.5.1 Tissue Culture. 100
2.5.2 DNA techniques. 102
2.5.3 Protein manipulation. 103
2.5.4 Cell-based assay. 106
2.5.5 Mouse work. 107
2.5.6 Computer images. 113
2.5.7 Statistics. 113

Chapter 3 114

***RESULTS*....114**

Generation of iASPP$^{flox/flox}$ mice: a conditional knockout system for the depletion of iASPP protein *in vivo*. 114

3.1 Introduction. 114
3.1.1 Traditional knockout technology vs. conditional knockout technology. 114
3.2 Results 118
3.2.1 Generation of iASPP$^{flox/flox}$ mice. 118
3.2.1.1 Validation of Cre-loxP for the deletion of iASPP exon 8 *in vitro*. 122
3.2.2 Generation of iASPP$^{\Delta 8/\Delta 8}$ mice. 123
3.2.2.1 Confirmation of genomic excision of loxP-flanked sites in Cre-expressing mice. 123
3.2.2.2 Confirmation of iASPP deficiency in iASPP$^{\Delta 8/\Delta 8}$ tissue and primary cells. 125
3.2.3 iASPP deficiency leads to high mortality rates in mice. 127
3.2.4 Investigation of expression and cellular localisation of iASPP *in vivo*. 129
3.3 Discussion and conclusion. 132

Chapter 4 135

RESULTS 135

iASPP is required for normal functioning of the heart and its development *in vivo*.. 135

4.1 Introduction. 135

4.2 Results 136

4.2.1 Loss of iASPP leads to a shorter life span *in vivo*. 136

4.2.2 iASPP-deficient mice display Arrhythmogenic Right Ventricular Cardiomyopathy (ARVC). 137

4.2.2.1 iASPP-depleted mice exhibit morphological and molecular evidence of cardiac dysfunction. 137

4.2.2.2 *In vivo* MR imaging reveal impaired function and performance of the cardiac muscle of iASPP$^{\Delta 8/\Delta 8}$ mice. 143

4.2.2.3 iASPP-null hearts display typical features of ARVC. 147

4.2.2.4 Spontaneous ventricular arrhythmias in iASPP-deficient mice. 151

4.2.3 Alteration of the intercalated disc complexes is associated with loss of iASPP *in vivo*. 153

4.2.4 Loss of iASPP expression is the direct cause of the ARVC phenotype in iASPP$^{\Delta 8/\Delta 8}$ mice. 159

4.2.4.1 Young iASPP$^{\Delta 8/\Delta 8}$ mice showed morphological and molecular evidence of a remodelling process in the heart. 159

4.2.4.2 Embryonic iASPP$^{\Delta 8/\Delta 8}$ hearts demonstrate defects in the morphology and structure of the myocardium. 162

4.2.4.3 Validation of episcopic analyses by cellular and molecular investigation of iASPP-null embryonic hearts. 168

4.2.5 Investigation of the molecular mechanism(s) underlying the ARVC pathology in iASPP$^{\Delta 8/\Delta 8}$ mice. 173

4.2.5.1 Loss of iASPP induces apoptosis in young and embryonic mouse hearts. 173

4.2.5.2 iASPP$^{\Delta 8/\Delta 8}$ ARVC is not dependent on p53 or its family members....177

4.2.5.2.1 iASPP$^{\Delta 8/\Delta 8}$;p53$^{-/-}$ mice: loss of p53 alleles only rescues the local fibrotic deposits, and not the dilated cardiomyopathy in iASPP$^{\Delta 8/\Delta 8}$ mice.....177

4.2.4.2.2 p63$^{+/-}$;iASPP$^{\Delta 8/\Delta 8}$ does not alleviate iASPP$^{\Delta 8/\Delta 8}$-dependent ARVC.182

4.3 Summary and discussion 184

Chapter 5 195

***RESULTS*.....195**

iASPP loss results in impaired epidermal formation. 195

5.2 Results.....195

5.2.1 iASPP$^{\Delta 8/\Delta 8}$ mice showed abnormal hair follicle organisation.....195

5.2.2 iASPP is an important regulator of epithelial stratification *in vivo*. 198

5.2.3 iASPP is predominantly expressed in the basal layer of stratified epithelia *in vivo*.....201

5.2.4 iASPP is a negative regulator of keratinocyte differentiation. 203

5.2.5 iASPP deficiency does not affect epithelial cell-to-cell junctions.....208

5.2.6 iASPP binds p63 and antagonises the transcriptional activity of TAp63. .210

5.2.7 Genetic interaction between the iASPP and p63 proteins in mouse epidermis: generation of iASPP$^{\Delta 8/\Delta 8}$;p63$^{+/.}$.....213

5.3 Summary and discussion. 216

Chapter 6.....222

***Conclusions and future work* 221**

6.1 iASPP$^{flox/flox}$ mice: a new conditional mouse model to investigate the biological importance of iASPP *in vivo*.....221

6.2 iASPP and ARVC: are iASPP$^{\Delta 8/\Delta 8}$ mice a new *in vivo* model with which to study ARVC?.....222

6.3 iASPP and ARVC: iASPP as a new component of the intercalated disc junctions in the myocardium. 224

6.4 iASPP and Naxos-Carvajal syndrome. 226

6.5 iASPP and cardiotoxicity of anticancer drugs. 228

6.6 iASPP as a new modulator of TAp63 transcriptional activity. 229

Bibliography 231

ABSTRACT

Investigation of the biological role of iASPP *in vivo.*

LICR, ORCB, NDM, University of Oxford – Green Templeton College
Degree of Doctor of Philosophy
Mario Notari

The p53 family of transcription factors, which comprises the products of the *TP53, TP63* and *TP73* genes, is at the hub of different signalling pathways that determine the fate of a cell. *In vitro*, the p53 family posses a tumour suppressive function. However, *in vivo*, although p53-deficient mice develop spontaneous tumours, p73 and p63 KO animals show defects in neuronal and epidermal development, respectively. The ASPP family of proteins also consists of three members: ASPP1, ASPP2 and iASPP. They are evolutionarily conserved binding partners and specific regulators of p53-, p63- and p73- mediated apoptosis *in vitro*. In contrast to ASPP1 and ASPP2, the biological significance of iASPP *in vivo* and the possible interaction with p53 family members remains unclear, and it is the subject of this study.

To investigate the role of iASPP *in vivo*, a transgenic mouse model was generated in which iASPP expression is controlled by the Cre/loxP recombination system. Deletion of iASPP resulted in the development of a cardiocutaneous disorder which displayed features of Arrhythmogenic Right Ventricular Cardiomyopathy (ARVC), defects in hair follicle position and impaired epithelial stratification. iASPP loss resulted in a sudden, premature and arrhythmic mode of death of all iASPP mutant mice. iASPP deficiency induced p53-dependent apoptosis in embryonic hearts and dilation of the right ventricle, however, the inactivation of p53 alleles only rescued the fibro-fatty deposits present in iASPP KO hearts. Mechanistically, iASPP locates at the polar ends of cardiomyocytes where it matches the location of other proteins known to be involved in the etiology of ARVC and in maintaining the integrity of intercalated discs. Loss of iASPP also resulted in increased differentiation of primary keratinocytes both *in vitro* and *in vivo*. Consistent with this, iASPP bound p63 and inhibited the transcriptional activity of both TAp63α and ΔNp63 *in vitro*, and regulated the expression level of p63-regulated genes such as envoplakin.

These results demonstrate that iASPP prevents cardiocutaneous disorder through its ability to inhibit p53-induced apoptosis and to influence the integrity of intercalated disc. Moreover, iASPP is also an important regulator of p63 and is involved in controlling epithelial stratification in vivo.

Publications

Notari Mario[#], Hu Ying[#], Koch Sofia, Lu Min, Ratnayaka Indrika, Zhong Shan, Baer Caroline, Pagotto Anna, Goldin R, Salter Victoria, Candi Eleonora, Melino Gery, Lu Xin. **Inhibitor of apoptosis-stimulating protein of p53 (iASPP) prevents senescence and is required for epithelial stratification.** *Proc Natl Acad Sci USA 2011 Oct 4;108(40):16645-50. Epub 2011 Sep 19.*

Notari Mario[#], Hu Ying[#], Dupays Laurent, Yavari Arash, Carr Carolyn, Zhong Shan, Indrika Ratnayaka, Opel Aaisha, Tinker Andrew, Clarke Kieran, Watkins Hugh, Mohun Tim and Lu Xin. iASPP prevents cardiocutaneous disorder by inhibiting p53-induced apoptosis and maintaining desmosomal integrity. Nature Medicine (under consideration 2011).

[#] *These authors contributed equally*

Acknowledgments

I would like to express my gratitude, first of all, to my supervisor Prof. Xin Lu for giving me the opportunity to have this wonderful experience. Thank you for all the support, suggestions, guidance and expertise you have given me during my four years at the Ludwig Institute for Cancer Research (LICR), not forgetting the well-needed enthusiasm and encouragement when presenting negative results.

A big thank you goes out to all my colleagues, past and present, who have made my life inside the lab so pleasant and the Institute such a friendly place to work. I have truly made some wonderful friends at the LICR, both in London and Oxford. Liz and Chris who helped me with all the little technical difficulties or questions I had throughout my project. Shan who taught me how to work with mice and helped me with the iASPP$^{\Delta 8/\Delta 8}$ mouse colony. Alex who dealt with all the paper work during my DPhil course of study, and always had something "not science" related to say at lunch. Indi for cutting all my paraffin blocks, Mark for a great amount of work on the confocal microscope, Neil for making the lab a good place to work. Ying, whose research has contributed greatly to my project, Claire Beveridge, whose help and advice has been invaluable. To all my fellow DPhil students in the Institute: there is hope. Special thanks go out to Luca and Anna: thanks for bringing a bit of "italianity" into the lab….without you I would have gone insane. A big thank you goes to the espresso coffee machine…without it, I am not sure I would have survived the countless late nights in the lab.

Next, I would like to thank all our collaborators. T.J. Mohun who performed all the episcopic reconstruction analysis, and Laurent Dupay who showed me how to dissect an embryonic mouse heart. Arash Yavari and Mo who helped and advised me on the ECG part of the project. Carolyn Carr and Kieran Clarke who helped me with the live MRI imaging study.

Then, I should not forget to mention my "Italian friends" here in Oxford (Cristiano- beyond doubt a wonderful engineering mind, Luca and Anna- thanks for putting up with me as colleagues and friends, Eleonora and Hilde- thanks for making our place in Oxford feel like home and Massimo- my usual football buddy and sometimes life coach), my "English friends": Tim…thanks buddy, Wiggie and Carlio. To Libby, whose late chats on the couch make my life a lot easier. My London and ex-London friends: Becks, Bel, James, Gerardo and Fizzy: you guys are wonderful. Thanks for reminding me that there is a life outside the lab. To my "Italian Italian friends": Denny, Gina, Force, Ercolino, Sala, Azza, Kitoz, Nico, Lillo and i ragazzi del Tintoretto…Thanks guys for everything, you made me what I am now. Special thanks also go out to Ricca, Gonfio, Babu e "la Vaca", who have truly always been there when I needed the most.

And last but not least, a tremendous special thank you to my family: Truly, this thesis is for you. You always believed in me and supported all my decisions, even when they meant leaving you, my country and my friends…THANKS, without your love I could not have finished my studies abroad. To my wonderful Mum and my amazing Dad whose sacrifices and guidance make me a Doctor in Philosophy. To my two fantastic Sisters and my extraordinary nephew Cristiano, who I care for very much...Thanks for always being there for me.

Abbreviation

- **3D** : Three-dimensional
- **4-OHT** : 4 hydroxyltamoxifen
- **ΔN** : Delta-N

- **a.a**. : Amino acids
- **AEC** : Ankyloblepharon-ectodermal dysplasia
- **AL** : Acute leukemia
- **ANP** : Atrial nautrietic peptide
- **ARVC** : Arrhythmogenic right ventricular cardiomyopathy
- **ASPP** : Apoptotic stimulating protein of p53
- **ATM** : Ataxia Telangiectasia
- **ATP** : Adenosine triphospate

- **bp**: Base-pair
- **Bbp** : Bcl-2 binding protein
- **BH** : Bcl-2 homology domain
- **BMP** : Bone morphogenic protein
- **BrdU** : Bromodeoxyuridine

- **Ca^{2+}** : Calcium
- **Chk2** : Check point kinase 2
- **Chip** : Cromatine immunoprecipitation
- **CDK** : Cyclin-dependant kinase
- **CHF**: Congestive heart failure
- **CML** : Chronic myelogenus leukemia
- **CMV** : Cytomegalovirus
- **CNS** : Central nervous system

- **Dsh-1** : Dishevelled-1
- **DBD** : DNA binding domain
- **DCM** : Dilated cardiomyopathy
- **DD** : Death domain
- **DNA** : Deoxyribonuclei acid
- **DSC2** : Desmocollin 2
- **DSG2** : Desmoglein 2
- **DSP** : Desmoplakin

- **E1** : Ubiquitin activating enzyme
- **E13.5** : Embryonic day 13.5
- **E14.5** : Embryonic day 15.5
- **E16.5** : Embryonic day 16.5
- **E18.5** : Embryonic day 18.5

- **E2** : Ubiquitin coniugated enzyme
- **E3** : Ubiquitin ligase enzyme
- **Ex2** : Exon 2
- **Ex2/3** : Exon2 and exon3
- **ECC** : Ectrodactyly-ectodermal dysplasia
- **ECG** : Electrocardiogram
- **ECM** : Extracellular matrix
- **ED** : Ectodermal dysplasia
- **ES** : Embryonic stem cell
- **ESTs** : Expressed sequence tags
- **EtBr** : Ethidium bromide
- **EVPL** : Envoplakin

- **FADD** : Fas-associated death domain
- **Flox** : LoxP-flanked
- **Fz-2** : Frizzled-2

- **Gr**: Granular layer

- **H&E** : Haematoxylin and eosin
- **HAT** : Histone Acetylate transferase
- **HCM** : Hypertrophic cardiomyopathy
- **HF** : Heart failure
- **HREM** : High-resolution episcopic microscopy

- **iASPP** : Inhibitor of apoptotic stimulating protein of p53
- **iASPP$^{\Delta 8/\Delta 8}$** : Homozygous iASPP gene knockout
- **iASPP$^{\Delta 8/+}$** : Heterozygous iASPP gene expression
- **iASPP$^{+/+}$** : Homozygous iASPP gene wild type
- **IAP** : Inhibitor of apoptosis protein
- **IGF-1** : Insulin like growth factor-1
- **ID** : Intercalated disc

- **Kb** : Kilo base pair
- **KD** : Kilo daltons
- **K1** : Keratin 1
- **K5** : Keratin 5
- **K6 :** Keratin6
- **K10** : Keratin 10
- **K14** : Keratin 14
- **K18 :** Keratin 18
- **KO** : Knockout
- **KC** : Mouse keratinocyte

- **LA** : Left atrium
- **LIF** : Leukemis inhibitory factor
- **LV** : Left ventricle
- **LVD** : Left ventricular dysfunction

- **LVEF** : Left ventricular ejection fraction

- **Mdm2** : Murine double minute 2
- **Mdm4** : Murine double minute 4
- **MEF**: Mouse embryonic fibroblast
- **MRI** : Magnetic resonance imaging

- **n=** : Number equal
- **NFκB** : Nuclear factor κ B
- **NCBI** : National center for biotechnology information
- **NKIP1** : NFκB interacting protein 1

- **OD** : Oligomerization domain
- **ORF** : Open reading frame

- **p5** : Postanatal day 5
- **p7** : Postanatal day 7
- **p10** :Postanatal day 10
- **P1** : Promoter 1
- **P2** : Promoter 2
- **PCR** : Polymerase chain reaction
- **PF :** Pemphigus foliaceus
- **PIG** : P53-induce gene
- **PI3K** : Phosphoinositde-3-phosphate kinase
- **PLK** : Plakoglobin
- **PPP1R13L** : protein phosphatase 1, regulatory (inhibitor) subunit 13 like(iASPP gene)
- **PR** : Prolin rich
- **PKP** : Plakophillin
- **PV :** Pemphigus vulgaris

- **Rb** : Retinoblastome gene
- **RA** : Right atrium
- **RAI** : RelA-associate inhibitor
- **RCM** : Restricted cardiomyopathy
- **ROS** : Reactive oxygen species
- **RV** : Right ventricle

- **Shh**: Sonic hedgehog
- **snRNAi** : Small nucleotide RNA inhibitor
- **Sp** : Spinous layer
- **SAM** : Sterile alfa motifs
- **SC** : Stratum corneum
- **SD** : Standard deviation
- **SH3** : SRC homology 3
- **SPPK :** Striate palmoplantar keratosis
- **SR** : Sarcoplasmatic reticulum
- **STAT** : Signal trasducers and activators of transcription

- **TA** : Transactivation
- **TBP** : TATA-binding protein
- **TFIID** : Transcription factor II D
- **TNF-α** : Tumor necrosis factor-α
- **TNFR** : Tumor necrosis factor receptor
- **TP53** : Tumor protein 53
- **TP63** : Tumor protein 63
- **TP73** : Tumor protein 73
- **TUNEL** : terminal deoxynucleotidyl transferase biotin-UTP nick end labelling

- **UV** : Ultraviolet

- **Wa3** : Wave 3 mice, iASPP knockout mice
- **WHO** : World health organization
- **WT** : Wild type

Chapter 1
General Introduction

The work described in this thesis was set out to investigate the biological and functional importance of iASPP protein *in vivo*. The well-established function of the ASPP family of proteins described in the literature is related to their ability to influence the apoptotic activity of the tumour suppressor p53. Hence, p53 and its family members will first be briefly introduced, as well as their function in tissue homeostasis and development. The known information about the ASPP family members will then be described, followed by a general introduction to the biology and major pathologies of the heart and skin, where the major biological effects *in vivo* of loss of iASPP expression were observed.

1.1 p53 and its family members: overview.

The *TP53* gene, which encodes all of the isoforms of the p53 tumour suppressor protein, is one of the most studied genes in cancer research. Over the past 10 years, more than 4,000 publications have appeared in various scientific journals, all focussing on p53 and its regulation in cancer (Pub Med Medline search source). p53 was the first tumour suppressor protein to be identified, although its function as such was only identified 10 years later through the pioneering work of Baker and Finley in 1989 (Baker, Fearon et al. 1989; Finlay, Hinds et al. 1989). It was first believed to be an oncogene: a gene that stimulates cell growth and proliferation under normal conditions. However, subsequent publications appeared in scientific journals that disputed this idea, until Baker and Finlay independently demonstrated that p53's oncogenic activity was due to a mutated form of the

protein and instead proposed that functions as a tumour suppressor: a gene that inhibits cell growth and proliferation under normal conditions (Vogelstein, Lane et al. 2000).

Following more than 30 years of intensive investigation of p53, we now know that damage to *TP53* is one of the most frequent genetic alterations that occur during tumourigenesis, as p53 is mutated more than 50% of human cancers (see the IARC *TP53* mutations website). In those that do not have mutated p53, its function is frequently altered through binding with viral proteins or its pathways are affected by inactivated proteins (Vogelstein, Lane et al. 2000).

Molecular and biochemical analysis has revealed that p53 is a nuclear phosphoprotein; it is a sequence-specific DNA binding factor that plays a central role in controlling tissue homeostasis in response to different stimuli, by enhancing or repressing the transcription of genes that regulate a variety of cellular processes including: cellular senescence, differentiation, cell-cycle arrest and apoptosis (Vogelstein, Lane et al. 2000; Slee, O'Connor et al. 2004). This ability makes p53 an important tumor suppressor, and has subsequently initiated a large amount of research in this area (Lowe, Cepero et al. 2004).

Over a decade after the initial discovery of p53, two further proteins with structural similarly to p53 were discovered. The first p53 related gene was identified by Caput and colleagues in 1997, and they called it p73 due to its molecular weight (Kaghad, Bonnet et al. 1997). Soon after, several groups independently identified the third member of the family, p63 (Osada, Ohba et al. 1998; Yang, Kaghad et al. 1998; Tan, Bian et al. 2001). Although p63 and p73 are genetic paralogues of p53, their molecular structure is more similar to each other than that of p53. However, they can perform certain “p53-like activities” such as binding specific DNA sequences, forming homodimers and, most importantly, inducing apoptosis and cell cycle arrest *in vitro* (Osada, Ohba et al. 1998; Yang, Kaghad et al. 1998). Nevertheless, in contrast with p53’s function as a tumour suppressor, p63 and p73 are only rarely mutated in cancer. Severe developmental abnormalities were observed in p63 or p73 knock-out (KO) mice, indicating a non-redundant function with p53 and suggesting a peculiar role of each of these proteins *in vivo*.

1.1.1 *TP53* gene and p53 protein structure.

In mammals, the "tumor protein" 53 gene (*TP53*) is composed of 11 exons and several splice variants exist *(figure 1.1)*. FLp53 is 393 amino acids long and contains four main functional domains: a transcription activation domain (TA) (residues 1-42), proline rich region (PR) consisting of five PXXP repeats (residues 61-94), a DNA-binding domain (DBD) (residues 102-292) required for sequence specific DNA binding, and finally an oligomerisation domain (OD) (residues 324-355) *(figure 1.1)*. Moreover, the C-terminus contains a nuclear localisation signal and functions as a negative regulatory domain (Vousden and Lu 2002). Within the N-terminus, p53 contains an acidic domain found and described in other well characterized transcription factor that functions both in recruiting the transcriptional machinery or can interact with activators such as p300 or the ubiquitin ligase mdm2. Through the DBD, p53 has the ability to interact with double strand DNA sequences consisting of at least two repeats of the consensus sequence 5'-PuPuPuC(A/T)-(T/A)GPyPyPy-3', and it is known to bind as a tetramer to these specific consensus DNA sequences (el-Deiry, Kern et al. 1992). The *TP53* gene encodes two primary transcripts that are controlled from two different promoters: P1 and P2 (Murray-Zmijewski, Lane et al. 2006) *(figure 1.1)*. Transcripts produced from the P1 promoter generate full-length p53 proteins (FLp53). Recently, however, a P1' promoter has been discovered within exon one that generates a p53 protein lacking the first 40 amino acids (a.a.), although it still contains part of the TA and can transactivate transcription through a second TA domain (Zhu, Zhou et al. 1998). In contrast, transcripts generated from the P2 promoter do not have the TA domain (Δ133p53) and result in the expression of a terminally truncated protein that acts as a dominant negative isoform of the protein. Moreover, exon 9 can be alternatively spliced to produce 3 different p53 isoforms: FLp53α, -β and -γ, where β and γ lack of part of the OD domain (Murray-Zmijewski, Lane et al. 2006) *(figure1.1)*

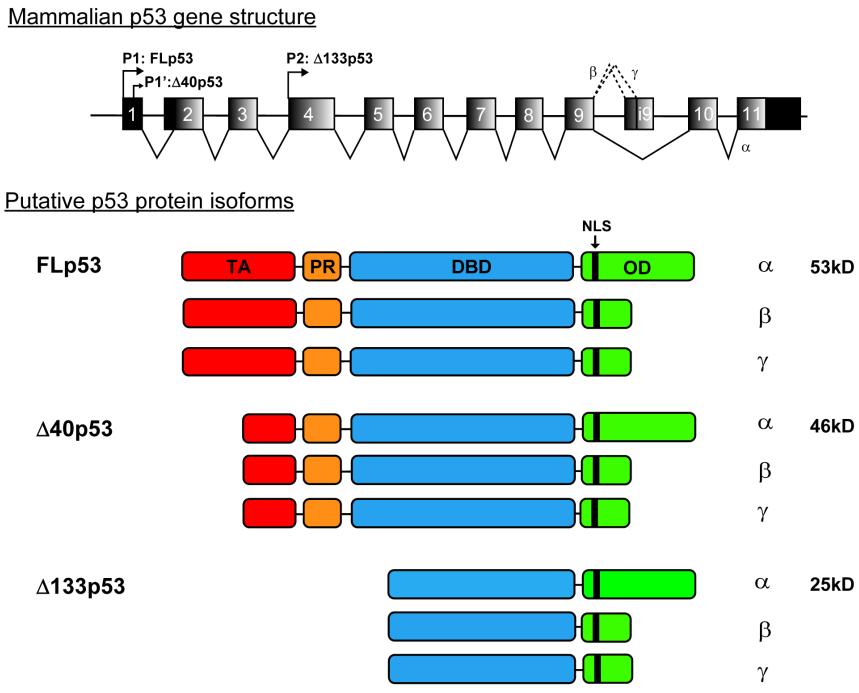


Figure 1.1: *TP53* gene and structure of p53 protein and its isoforms. Schematic overview of p53 gene structure: alternative splicing (α,β,γ) and alternative promoters (P1, P1' and P2) are indicated. The promoter P1 leads to the expression of FLp53, which is a 393 amino acid long protein, containing a transactivation (TA), proline rich (PR), DNA binding (DBD) and oligomerisation domain. The P1' promoter encodes Δ40p53 isoforms that lacks the first 40 a.a. and acts as a dominant negative inhibitor of the full-length protein. The P2 promoter, located in intron 4, leads to the expression of the Δ133p53 isoform which lacks the N-terminus. Different domains are represented by different colours. The black bar represents the nuclear localisation signal (NLS), which is indispensable for relocating the different protein isoforms into the nucleus.

1.1.2 *TP63* and *TP73* genes and protein structures.

The *TP63* and *TP73* genes of the mouse are located on chromosomes 3 (3q27-29) and 1 (1q36) respectively. Mammalian p63 is 680 a.a. long, and figure 1.2 shows its main structural domains. Like p53, it contains a TA domain at its N-terminus, a DBD which has 60% a.a. identity to the DBD of p53 and an OD. In addition, the α isoforms contain a sterile alpha motif (SAM), which in other molecules has been implicated in protein-protein interactions, and two PR domains *(figure 1.2)*. The *TP63* gene was the first gene discovered that possesses an internal promoter and, like *TP53*, contains two different promoters named P1 and P2 (Yang, Kaghad et al. 1998).

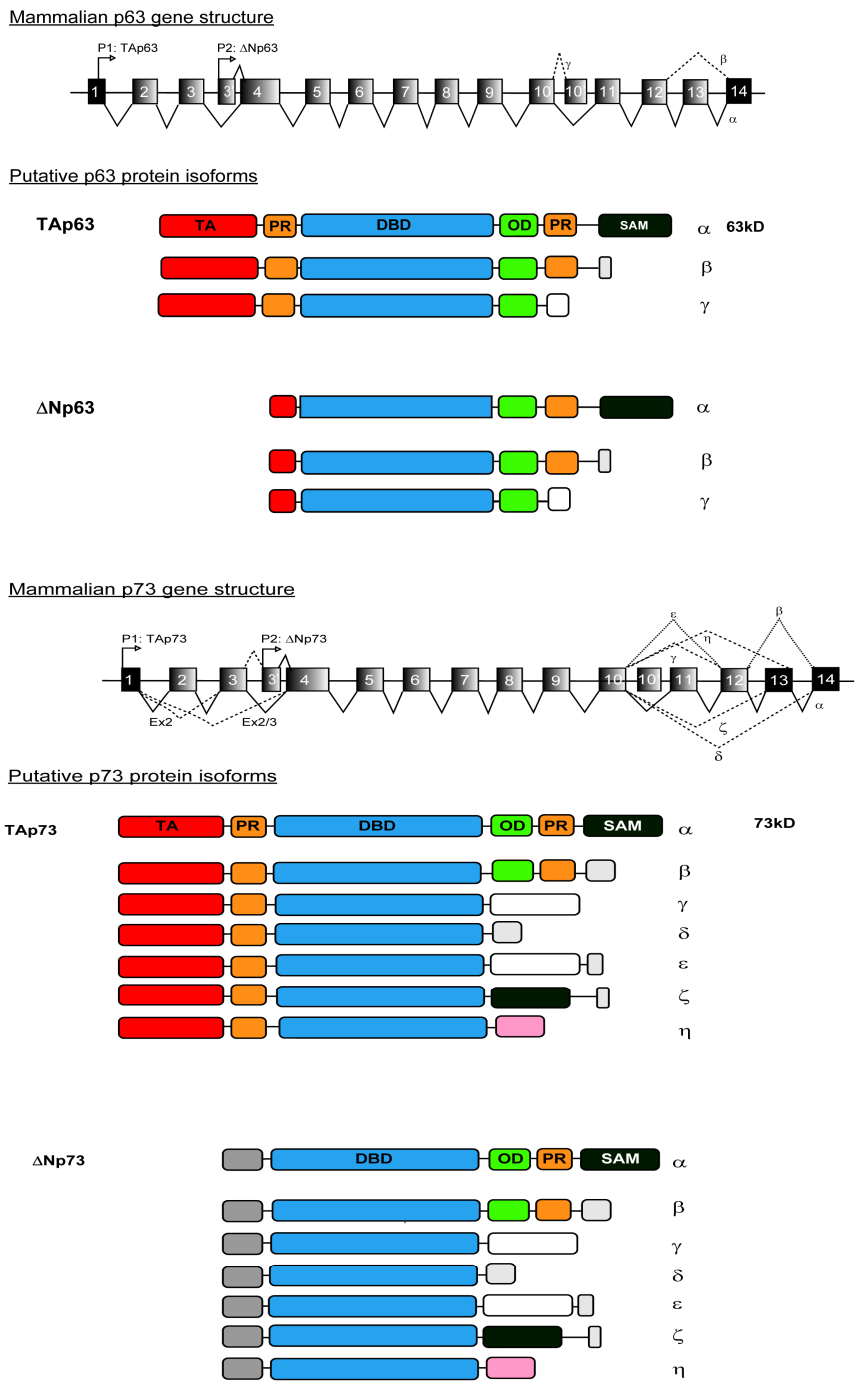


Figure 1.2: *TP63* and *TP73* gene structures and their putative proteins isoforms. Schematic overview of p63 *(previous page)* and p73 gene *(above)* structure: alternative splicing (α,β,γ for *TP63*; α,β,γ,ζ,δ,ε and η for *TP73*) and alternative promoters (P1 and P2) are indicated. Both the p63 and p73 genes can be transcribed from an alternative promoter (P2), leading to the expression of N-terminally truncated forms (ΔN), while full-length isoforms (TA) are encoded by the P1 promoter. Alternative splicing of exon 2 (Ex2) or exons 2 and 3 (Ex2/3) occurs only in the *TP73* gene, making it possible that there are 28 p73 protein isoforms, but so far only 14 have been identified. Both proteins contain a transactivation (TA), proline rich (PR), DNA binding (DBD) and oligomerisation (OD) domain, on top of an additional PR domain and a sterile alpha motif (SAM) domain, which serves as a putative protein interaction domain. Different domains are represented by different colors.

The P2 promoter, which is located at the 3' end of exon 3, generates all the amino terminally truncated isoforms (ΔNp63), which lack the TA domain *(figure 1.2)*. In contrast, the P1 promoter generates all of the full length isoforms, and are called transactivating proteins (TAp63). The *TP63* gene expresses at least three different spliced variants that generate three different C-terminal proteins (isoforms α, β, γ). Altogether, the gene can be transcribed and translated to give six different protein isoforms. The TAp63 proteins can bind to DNA through p53-responsive elements on the promoters of different target genes and activate their transcription. Such activation can induce either apoptosis or cell cycle arrest *in vitro* (Yang, Kaghad et al. 2002), however, recent studies have revealed that p63-responsive elements are slightly different from ones that are responsive to p53, and confer a different responsiveness to p63 when compare to p53 (Osada, Park et al. 2005).

The mammalian p73 gene is composed of 15 exons and, like p53 and p63, can be transcribed from various alternative promoters (Stiewe, Zimmermann et al. 2002). p73's protein structure is highly similar to that of p63 *(figure 1.2).* p73 has an N-terminal TA domain, a DBD which shares 86% of homology which p63, an OD and a SAM domain, which share 53% identity with p63 (Melino, Lu et al. 2003) *(figure 1.2).* The TAp73 are generated from a promoter located upstream of exon 1 (P1), while the amino terminal truncated isoforms are generated from the activity of the P2 promoter on exon 3. In addition, seven different C-terminal spliced variants (α, β, γ, δ, ζ and η) can be generated by different rearrangement of the mRNA. Moreover, exons 2 and 3 can be alternatively spliced (not shown), bringing the total number of different mRNAs that can be translated into different p73 protein isoforms to 28 (Melino, Lu et al. 2003) *(figure 1.1)*. Data generated from Marin and colleagues suggested that, like p53 and p63, p73 isoforms can regulate both apoptosis and cell-cycle arrest, although its role is less-well understood than that of p53 (Irwin, Marin et al. 2000). Both the p63 and p73 -ΔN isoforms were thought to act as dominant negative isoforms of the two proteins (Melino, Lu et al. 2003). However, recent studies have revealed the presence of a second TA domain, and ΔNp63 is now known to be a key transcription factor for the renewal of the epidermis in mammals (Candi, Cipollone et al. 2008).Recent studies also indicate

that p73 can bind slightly different DNA recognition sequences from p53-responsive elements, conferring specificity to the activation of genes by p73 proteins but not p53 (Sasaki, Naishiro et al. 2005).Although recent investigations have provided new insights into the different roles of p53, its ability to induce apoptosis represents the major pathway by which it can act as a tumour suppressor. Evidence suggests that p63 and p73 exert part of their function as tumour suppressors by mediating the apoptotic response in various cellular contexts, however, their role is more dramatic in the development of specific organs than as apoptotic stimulators *in vivo*.

1.1.3 p53 is a master regulator of various cellular responses.

The balance between pro- and anti-apoptotic molecules must be tightly regulated in order to enable the fine equilibrium between the life and death of cells within a multicellular organism. The growth inhibitory response plays an important role in tissue homeostasis because it acts as a protective mechanism to prevent DNA-damaged cells, which have acquired abnormal oncogenic signals, to proliferate rapidly and form malignancies. As already mentioned, p53 can influence many aspects of cell life via the pathways of growth inhibitory responses such as the apoptotic pathway, cell cycle arrest and DNA repair, cellular senescence and differentiation. For this reason, p53 has been classed as a “tumor suppressor”, and its tumor suppressive function is mainly achieved through its ability to regulate the transcription of target genes important for the inhibition of cell proliferation *(figure 1.3)*. This is reinforced by the fact that most of the mutations in *TP53* found in cancers are within the DNA binding domain (www-p53.iarc.fr), and these mutations mostly prevent p53 from bind to DNA thus preventing it from activating transcription (Yee and Vousden 2005). To activate gene transcription, p53 is able to interact and influence with the basal transcription machinery via its N-terminal TA domain. In fact, it can recruit HAT (Histone Acetylate Transferase) proteins in order to acetylate histone proteins and remodel the chromatin into a more accessible conformation. Alternatively, in a cooperative manner, it can also induce histone methylation by binding and activating two methyl-transferase enzymes: CARM1 and PRTM1 (An, Kim et al. 2004). It has also

been demonstrated that p53 can repress transcription by joining with and sequestering the TATA-binding protein (TBP), which is a fundamental component of the transcription factor II D (TFIID) complex, required for RNA polymerase to activate transcription (Seto, Usheva et al. 1992). Moreover, recent analyses based on the human genome have calculated that p53 could bind up to 542 consensus sequences (Wei, Wu et al. 2006). It is, therefore, clear that p53 is involved in the regulation of numerous pathways and cellular responses, among which the regulation of cell cycle arrest and apoptosis are the most studied and best characterised functions of p53.

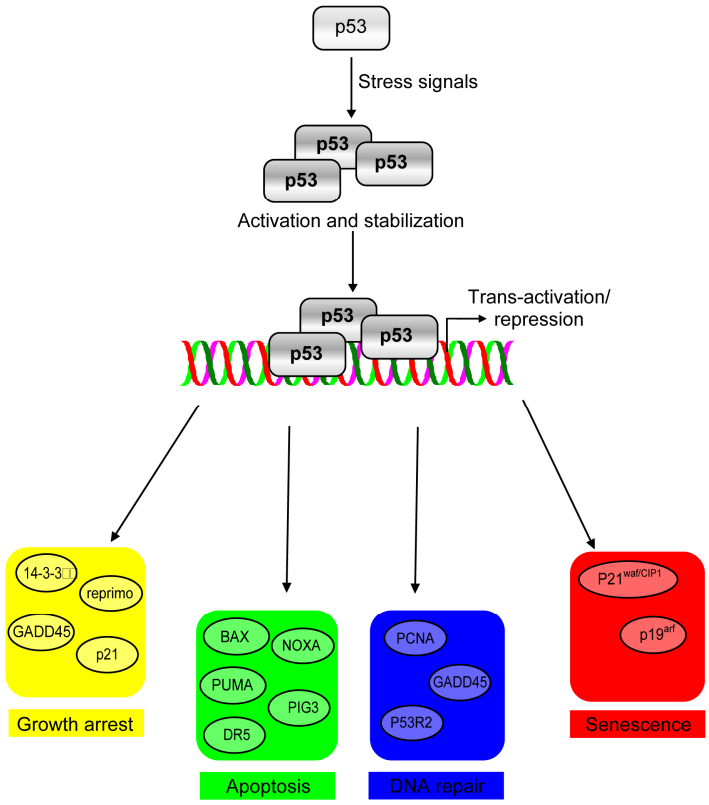


Figure 1.3: Schematic view of p53's mechanisms of action. The transcription factor p53 can activate or repress many genes upon stabilisation and activation by multiple stress signals. p53 has been shown to induce growth arrest, apoptosis, DNA repair and senescence by altering the expression of various genes, some of which are indicated in this simplified diagram.

1.1.3.1 Apoptosis: overview.

Programmed cell death or apoptosis is a normal process in tissue homeostasis, and describes the controlled death of a cell by genetic stimuli. Apoptosis plays a fundamental role in the maintenance of tissue homeostasis and in controlling cell number during development (Prindull 1995). Although first described more than 30 years ago, in reality the process was observed much earlier (Kerr, Wyllie et al. 1972). Apoptosis is distinct from another form of cell death called necrosis, in which uncontrolled cell death leads to lysis of cells and the release of their contents into the extracellular space, inducing an inflammatory response (Wyllie 1997). In programmed cell death, in contrast, a synchronised succession of events occurs such as membrane blebbing, cell shrinking, chromatin condensation and DNA fragmentation (Wyllie 1997). Eventually, cells disintegrate into small, membrane-based apoptotic bodies, followed by the intervention of (usually) macrophages that clear the apoptotic bodies to avoid the stimulation of an inflammatory response.

To date, two main apoptotic pathways have been described in mammals: the extrinsic (or death receptor) pathway and the intrinsic (or mitochondrial) pathway. These two pathways, although distinct from each other, converge on the activation of enzymes called caspases that drive the terminal events of programmed cell death (Thornberry and Lazebnik 1998). In fact, the caspases (Cysteine ASPartyl proteASEs) are a family of enzymes that function as the executioners of the apoptotic program. They are cysteine proteases that specifically cleave substrates at an Asp-xxx bond, although each caspase has it own substrate specificity (Thornberry and Lazebnik 1998). Caspase are synthesised as inactive precursors containing an N-terminal prodomain, a large subunit (p20) and a small subunit (p10). Upon apoptosis signals are activated, the inactive precursor is cleaved and loses its protodomain, and two large subunits and two small subunits assemble to form an active heterotetramer (Walker, Talanian et al. 1994). There are currently 14 caspases which are divided into 3 different categories: inflammatory caspases, which contain enzymes involved in the inflammatory response rather than apoptosis; apoptotic initiator caspases that lie upstream in the activation cascade, characterised by a longer pro-domain containing either a death receptor domain (caspase-8 and -10) or a caspase recruitment/activation domain (caspase-2 and -9) that allows them

to interact with modulator molecules; and finally, apoptotic effector caspases (caspase-3, -6 and -7), which are characterised by a short prodomain and are responsible for cleaving many cellular substrates within the cell to actually induce cell death (Degterev, Boyce et al. 2003).

As mentioned above, apoptosis can be activated by two classical pathways: the extrinsic and intrinsic pathways. In the extrinsic apoptotic pathway, programmed cell death can be triggered by external signals (ligands) which activate death receptors *(figure 1.4)*. Death receptors are part of the tumor necrosis factor receptor (TNFR) superfamily of proteins. The main death receptors involved in the activation of the extrinsic pathway are: the TNF receptor-1 (TNRF-1), FAS (CD95) and the trail receptors DR4 and DR5 (Jin and El-Deiry 2005). Here, only the FAS pathway is discussed as an example of the extrinsic apoptosis activation process by death receptors, as they all follow the same cascade of events. It is worth noting that these receptors also activate a variety of other pathways depending on cell type, external conditions and tissue specificity. Upon FAS ligand binding to its receptor on the external part of the membrane, clustering of the intracellular part of the receptors called death domain (DD) is induced, which allows the binding of the adaptor protein FADD (Fas-associated death domain). FADD, as a consequence, can bind pro-caspase 8. This complex was named the DISC pathway (Jin and El-Deiry 2005). The formation of the DISC complex induces the conversion of procaspase-8 to its active form, caspase-8, by autoproteolytic cleavage of the enzyme. Active caspase-8 is then able to interact with and process procaspase-3 into its active form, which drives the following apoptotic events *(figure 1.4)*.

In the intrinsic apoptotic pathway, apoptosis is triggered by intrinsic signals within the cell, and mitochondria are the key regulators of the process *(figure 1.4)*. The fundamental event in the intrinsic apoptotic pathway occurs when the outer membranes of the mitochondria (membrane-enclosed organelles that support the oxidative “respiratory” process by producing energy in the form of ATP molecules) are permeabilised as a result of the activation of members of the Bcl-2 family.

There are about 20 Bcl-2 family members, all of which have either pro- or anti-apoptotic functions, and are generally classified into three different categories according to the presence of up to four

BH domains into their structure. The first group comprises anti-apoptotic proteins that promote cell survival, and includes Bcl-2, Bcl-XL and Bcl-W. Structurally, they contain four bcl-2 homology domains (BH). The pro-apoptotic members, in contrast, are spread across two groups: the multi-BH domain group including BAX, BOK and BAK, which share only three BH domains; and the BH3 only proteins such as BID, BAD, NOXA and PUMA. Both pro-apoptotic groups seems to be required for the activation of the intrinsic apoptotic pathway, although studies have suggested that the damage-sensing BH3-only proteins may work upstream of BAX and BAK, as cells deficient in those proteins cannot induce apoptosis (Zong, Lindsten et al. 2001). The actual mechanism by which the outer membrane of the mitochondrion is permeabilised is still controversial, but once it is achieved the apoptotic pathway is perpetuated through either the release of pro-apoptotic molecules, such as cytochrome C, or by loss of function of the mitochondrion such as a deficiency in the electrochemical gradient that in turn impairs energy production *(figure 1.4)*. When cytochrome C is released from the inner space of the mitochondrion, it activates the apoptosis protease activating factor 1 (apaf-1) adaptor protein and forms a complex called the apoptosome, which is the fundamental complex needed to trigger the apoptotic pathway and activate the caspase enzymes (Li, Nijhawan et al. 1997). In fact, using ATP, the complex can cleave and convert procaspases into their active forms which, in turn, are able to activate effector caspases such as caspase-3. The second group of proteins that is induced by mitochondrial permeabilisation by the Bcl-2 family of proteins are the inhibitor of apoptosis antagonists, including smac/DIABLO, HtrA2/Omi and GSPT1/eRF3. Inhibitor of apoptosis proteins (IAPs) can slow down the apoptotic process by binding and inhibiting the activation of caspase enzymes (Li, Nijhawan et al. 1997).

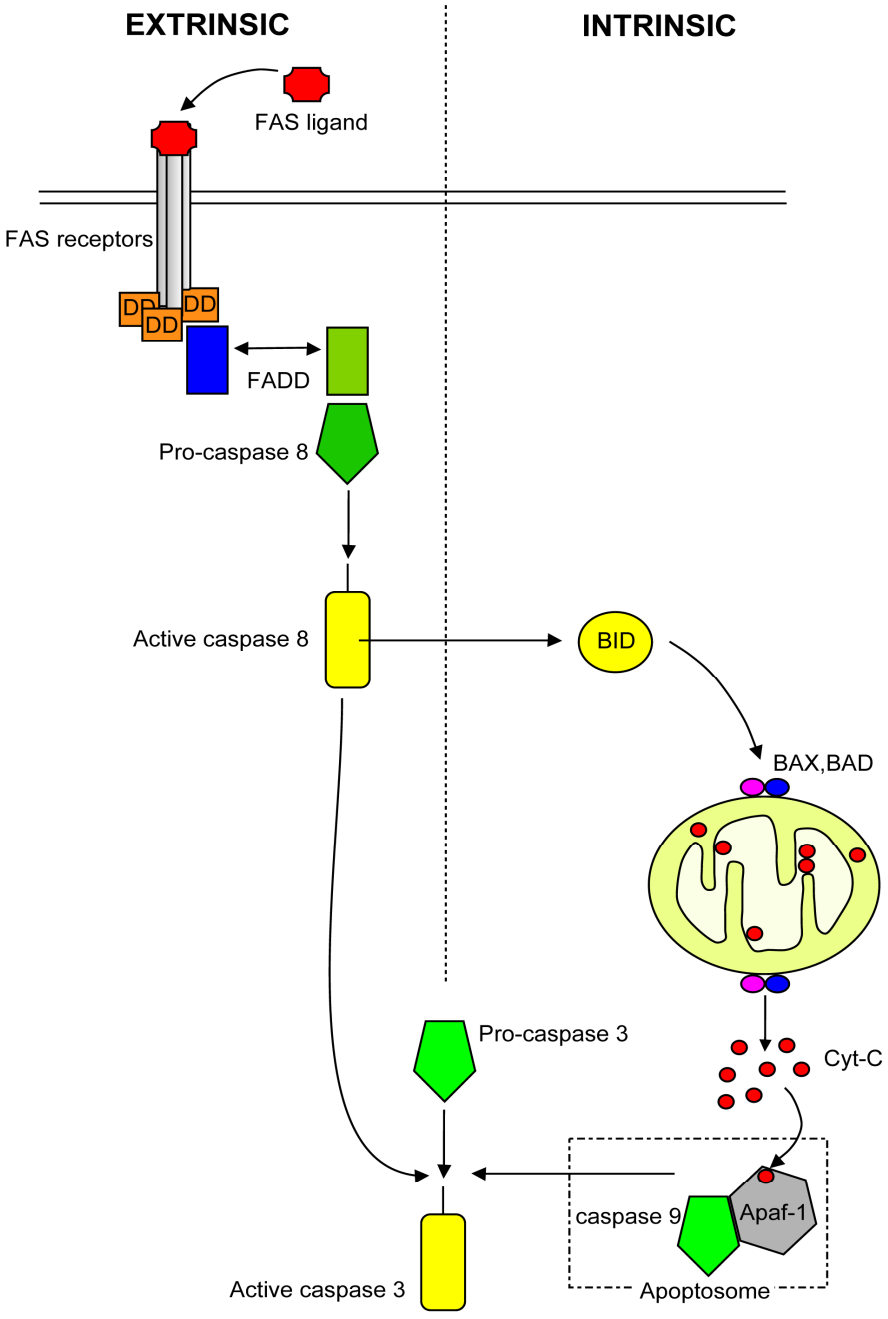


Figure 1.4: Simplified view of the extrinsic and intrinsic apoptotic pathways. Apoptosis can be activated by the death receptor (extrinsic) or mitochondrial (intrinsic) pathways, both of which converge in the activation of an effector caspase (active caspase 3). Extrinsic pathway: FAS ligand (red) induces the trimerisation of its receptor (FAS receptor), which leads to the recruitment of the other components of the death-inducing complex. The adaptor protein FADD interacts with FAS receptor through its DD domain and allows the recruitment and activation of caspase-8. Intrinsic pathway: as a result of the activation of Bcl-2 family members (BAX, BID and others), the permeabilisation of the outer membrane of the mitochondria allows the release of cytochrome C (Cyt-3). Cyt-3 can then activate caspase 9 through the formation of the apoptosome complex. Caspases 8 and 9 can both activate caspase 3 which sets the apoptotic process in motion.

1.1.3.2 p53 and its role in apoptosis.

The apoptotic function of p53 is thought to be its most evolutionarily conserved function. In fact, simple organisms such as *C. elegans* and *D. melanogaster* possess homologues of human p53 which are only able to induce programmed cell death, and not cell cycle arrest or other p53-related functions (Ollmann, Young et al. 2000; Schumacher, Hofmann et al. 2001). p53 triggers apoptosis by trans-activating and trans-repressing the expression of genes implicated in both the intrinsic and extrinsic apoptotic pathways *(figure 1.3)*. In fact, pro-apoptotic genes, of both the intrinsic and extrinsic pathways have been reported to be induced by p53, including the death receptor FAS (Muller, Wilder et al. 1998), the trail receptor DR5 (Wu, Burns et al. 1997) and several members of the Bcl-2 family of proteins like NOXA and PUMA (Oda, Ohki et al. 2000; Yu, Zhang et al. 2001) *(figure 1.5)*. Interestingly, KO mice models have shown that the latter, a pro-apoptotic protein, is essential for p53-mediated apoptosis as PUMA deficient mice have almost all of the apoptotic function deficiencies observed in p53-null mice (Yu and Zhang 2003). p53 can also modulate the intrinsic apoptotic pathway at the level of the apoptosome, by increasing the transcription and therefore the expression of APAF-1 (Robles, Bemmels et al. 2001). Finally, genes encoding redox-regulating enzymes, cytoplasmic proteins that generate reactive oxygen species (ROS), called PIG (p53-induced) genes cause damage to the mitochondrial membrane and initiate apoptotic events. Among PIG genes, the best characterized is a quirine oxidoreductase homologue PIG3 (Contente, Dittmer et al. 2002). It is worth noting that several studies have shown that p53 can also induce apoptosis via transcription- independent mechanisms (Caelles, Helmberg et al. 1994; Gao and Tsuchida 1999). Indeed, p53 can translocate to the mitochondria following DNA damage or hypoxia, where it can directly interact with anti-apoptotic components such as Bcl-2 and Bcl-XL, and contribute directly to apoptotic signalling in the mitochondria.

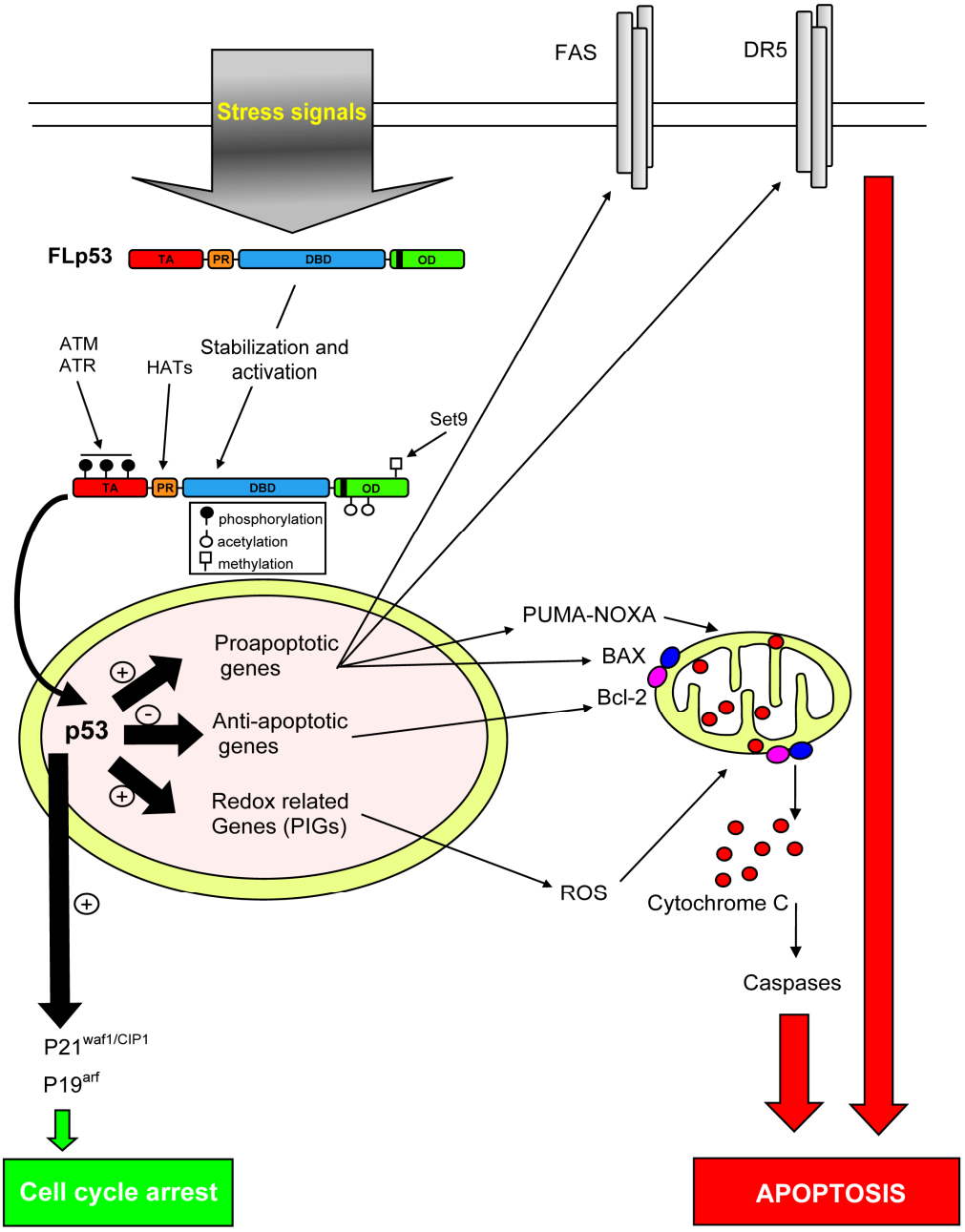


Figure 1.5: Upon stabilisation and activation, p53 can induce cell cycle arrest or apoptosis. This diagram represents how p53 can drive apoptosis and cell cycle arrest at various levels, by regulating the expression of different groups of genes involved in the intrinsic and extrinsic pathways, or the cell cycle arrest processes. Upon stress signals, FLp53 is post-translationally modified. ATM, ATR *(top left)* and Ser9 *(center)* enzymes are shown.. It is believed that post-translational modifications play a fundamental role in the stabilisation of the protein, and specify the selectivity of p53 target genes. p53 is known to translocate into the nucleus where it can transactivate (+) or transrepress (-) various genes important for activate apoptosis (red) or cell-cycle arrest (green). In particular, p53 can drive apoptosis at various levels by regulating the expression of genes involved in the intrinsic (PUMA, NOXA, bax and Bcl-2) or extrinsic pathways (FAS, DR5). On the other hand, p53 can also drive cell cycle arrest by transactivating $p21^{waf1/CIP1}$ and $p19^{arf}$.

1.1.3.3 p63, p73 and their role in apoptosis.

p63 and p73 are functionally and structurally related to p53. However, their roles in tumor suppression remain unclear. To date, only a small percentage of human tumours have been demonstrated to harbor mutations in the *TP63* or *TP73* genes (Irwin and Kaelin 2001). Nevertheless, overexpression of p63 or p73 isoforms has been found in human tumours. In particular ΔNp63 has been reported to be up-regulated in head and neck squamous cell carcinoma (Weber, Bellmann et al. 2002; Dominguez, Garcia et al. 2006; Wager, Guilhot et al. 2006), while ΔNp73 was found to be overexpressed in gliomas as well as colon carcinoma (Dominguez et al., 2006; Wager et al., 2006). More recent investigations using RT-PCR experiments combined with immunohistochemistry using p63- and p73-specific antibodies have demonstrated increased or reduced expression of TA or ΔN isoforms in human cancer. For instance, Park et al. showed that a substantial set of bladder tumours lose the expression of TA isoforms and instead have increased expression of ΔNp63. This suggests that abnormal expression of p63 is a frequent event in bladder carcinogenesis, which contributes to the progression of disease (Park, Lee et al. 2000). Moreover, it has been reported that some types of leukemias, particularly chronic myelogenous leukemia (CML), have mutations in the *TP63* gene (Yamaguchi, Inokuchi et al. 2001), reinforcing the hypothesis that p63 may act as tumour suppressor. Finally, the analysis of age-dependent tumour formation in mice carrying mutations in their DBD has shown that such animals are more prone to tumour formation, demonstrating a central role for p63 and p73 in tumour suppression (Flores, Sengupta et al. 2005). However, two other independent studies have shown that p73 knock-out mice and p63 heterozygous mice do not develop spontaneous tumours (Yang, Walker et al. 2000; Keyes, Vogel et al. 2006), making the literature on the possible role of p63 and p73 being tumour suppressors even more complex and controversial.

1.1.4 The p53 family of proteins in normal development.

1.1.4.1 p53.

The role of p53 as a potent tumour suppressor both *in vivo* and *in vitro* is clear, as demonstrated by the fact that inactivation of the p53 pathway is a fundamental step in the development of the majority of human and rodent tumours. However, recent studies have demonstrated that under physiological conditions, p53 family members are also necessary for the expression of genes involved in differentiation, cell adhesion, motility, angiogenesis and translation (Riley, Sontag et al. 2008). KO studies using transgenic mice indicate that many tumour suppressor genes are essential for normal development, such as the Retinoblastoma (Rb) gene (Classon and Harlow 2002). Organ formation involves proliferation, differentiation and apoptotic processes, which need to be tightly regulated in different cell populations. This fundamental regulation is usually controlled by a particular tumour suppressor gene. The discovery that p53 mRNA expression is present in developing mouse embryos (Rogel, Popliker et al. 1985; Schmid, Lorenz et al. 1991), and that both p53 mRNA and protein are expressed up to embryonic day 11.5 and dramatically decrease after that time point (Louis, McFarland et al. 1988), initially suggested a role for p53 in development. Moreover, Schmid and colleagues showed by *in situ* hybrydisation that, during organogenesis in mouse embryos, p53's expression pattern becomes tissue specific and that terminally differentiated tissues exhibit reduced expression of p53 (Schmid, Lorenz et al. 1991). Hence, the demonstration by Donehower and colleagues in 1992 that p53 deficient mice are viable and do not show any developmental defects came as a surprise (Donehower, Harvey et al. 1992). More recent investigations of p53-null offspring, however, have revealed that a substantial fraction of p53-null pups have developmental abnormalities indicating an important role for p53 in embryonic development (Armstrong, Kaufman et al. 1995). In particular, 8-16% of p53-null newborns presented defects in neural tube development associated with an overgrowth of neural tissue, suggesting a possible role of p53 in neuronal development (Sah, Attardi et al. 1995). Interestingly, these defects were predominately observed in female progeny (Armstrong, Kaufman et al. 1995).

This phenotype is common to other proteins involved in the intrinsic apoptotic pathway, such as Apaf-1 or caspase-3, suggesting that exencephaly results from an absence of cell death in the developing neural tube (Kuida, Zheng et al. 1996; Cecconi, Alvarez-Bolado et al. 1998). Interestingly, no significant difference in the rate of apoptosis was observed when p53-null embryos were compared to wild-type littermates.

The involvement of p53 in embryogenesis comes from another set of experiments, in which over-expression of wild type p53 has been forced during mouse development (Godley, Kopp et al. 1996). This forced overexpression led to impaired in kidney formation and abnormal differentiation of the uretic bud (Godley, Kopp et al. 1996). Early studies of p53 overexpression in lens cells revealed defects in fiber formation and a failure of cells to undergo proper differentiation (Nakamura, Pichel et al. 1995). Finally, the importance of p53 in development is demonstrated by the rescue of the embryonic lethality phenotype in mdm2- and mdm4-null mice by the absence of p53. Mdm2- and mdm4-null mice are embryonically lethal due to over activation of p53 pathway (Jones, Roe et al. 1995; Montes de Oca Luna, Wagner et al. 1995). Taken together, these data imply that the expression level of p53 must be carefully regulated during embryonic development. In the absence of p53, normal development can occur regularly but there is a high risk of embryonic loss. On the other hand, too much p53 can be as harmful as not having the protein at all.

So what is the role of p53 in development then? The answer might lie in two important papers which suggest that p53 acts as a teratological suppressor in development (Nicol, Harrison et al. 1995; Norimura, Nomoto et al. 1996). Both studies demonstrated that the p53 pathway is important for reducing the amount of defective embryos after exposure to genotoxic stimuli such as drugs or radiation. These data suggest that p53 plays a fundamental role in mammalian development, and that its primary role is to coordinate the multicellular adaptive responses to diverse environmental stresses. During development, the response to such environmental stress is of fundamental importance in determining, sensing and eliminating damage embryos, probably by increasing apoptosis.

1.1.4.2 p53 inhibitors: mdm2 and mdm4 are essential for embryonic development and heart function.

Allan Bradley et al. and Guillermina Lozano et al., at the same time, showed that deletion of the mdm2 ($mdm2^{\Delta 2/\Delta 2}$) gene is embryonic lethal in mice (Jones, Roe et al. 1995; Montes de Oca Luna, Wagner et al. 1995). In their independent studies, they showed that no viable $mdm2^{\Delta 2/\Delta 2}$ mice were recovered after birth, suggesting an important role of the protein in mouse development. The increased amount of apoptosis detected in mdm2-null embryos when compared to wild type controls was indicated as the cause for the embryonic lethality. Indeed, inactivation of both p53 alleles completely rescues the lethal phenotype of $mdm2^{\Delta 2/\Delta 2}$ mice (Jones, Roe et al. 1995; Montes de Oca Luna, Wagner et al. 1995; Finch, Donoviel et al. 2002). Rescuing the embryonic lethality with a p53-null background strengthens the importance of mdm2 as an inhibitor of p53 *in vivo*. However, due to the early embryonic lethality, this study can not exclude the possibility of a tissue specific role for mdm2 in different organs. On the other hand, Parant and colleagues were the first to study the role of mdm4 in embryonic development and adult mice (Parant, Chavez-Reyes et al. 2001). They reported a midgestation lethality in embryonic development, when the loss of the mdm4 allele was in a homozygous combination (Parant, Chavez-Reyes et al. 2001). They also proved that the embryonic lethality was dependent on the presence of the *TP53* gene (Parant, Chavez-Reyes et al. 2001), such as in mdm2 null mice (Jones, Roe et al. 1995). Taken together, these results indicate that both mdm4 and mdm2 are critical negative regulators of p53 activity *in vivo*, and that their presence is essential for the correct development of a mouse embryo by balancing the apoptotic activity of p53.

Conditional KO studies of p53 inhibitors in vivo also revealed a fundamental role of mdm2 and mdm4 in heart development and performance (Grier, Xiong et al. 2006; Xiong, Van Pelt et al. 2007). To study the role of mdm2 in the developing heart, Grier and colleagues in 2006 decided to use $mdm2^{flox/flox}$ mice (Grier, Xiong et al. 2006), and crossed them with αMyHC-Cre mice, which

express the recombinase enzyme under the control of the α-myosin heavy-chain promoter (Agah, Frenkel et al. 1997), leading the animals to be deficient for mdm2 expression only in the myocardium (Grier, Xiong et al. 2006). As a result, none of the homozygous mdm2-null pups generated from $mdm2^{+/-}$;αMyHC-Cre^{+} breeding pairs were born, indicating a fundamental role of mdm2 in heart development (Grier, Xiong et al. 2006). Analyses of $mdm2^{-/-}$;αMyHC-Cre^{+} embryos at E9.5 revealed various heart abnormalities. Specifically, thinning of the embryonic ventricular walls and a reduced number of cardiomyocytes were the most prominent abnormalities observed in $mdm2^{\Delta 2/\Delta 2}$;αMyHC-Cre^{+} embryos (Grier, Xiong et al. 2006). It was shown that an increased number of apoptotic cells was evident in hearts derived from homozygous mdm2-null;αMyHC-Cre^{+} embryos, while no difference in proliferation rate was observed between mutant and wild type mice (Grier, Xiong et al. 2006). The *TP53* null allele was introduced into $mdm2^{flox/+}$;αMyHC-Cre^{+} and it was shown that deletion of both p53 and mdm2 rescued the heart abnormalities and the lethal phenotype in $mdm2^{-/-}$;αMyHC-Cre^{+} (Grier, Xiong et al. 2006). Together, these results clearly indicate that mdm2 is a powerful regulator of p53-mediated apoptosis in heart development, and that non-functional mdm2 protein leads the mice to have a shorter life spam.

The role of mdm4 in mouse adult hearts was investigated using $mdm4^{\Delta 2/flox}$ mice (Xiong, Van Pelt et al. 2007) crossed with cardiomyocyte-specific Cre (αMyHC-Cre^{+}) mice (Agah, Frenkel et al. 1997). Surprisingly, loss of mdm4 in mouse heart did not result in embryonic lethality. However, the authors reported that all transgenic mice died within a year but the reason for this shorten life span was not investigated (Xiong, Van Pelt et al. 2007). A year later, Guillermina Lozano's laboratory elegantly explained the reason behind the shorter life expectancy for $mdm4^{\Delta 2/flox}$;αMyHC-Cre^{+} mice (Xiong, Van Pelt et al. 2007). They showed that mice with no mdm4 expression in the heart show severe oedema and heart failure as early as 3 months of age (Xiong, Van Pelt et al. 2007). To explore the cause of the death, homozygous mutant mice were sacrificed and analysed for gross abnormalities, which revealed clear signs of an underlying cardiomyopathic condition (Xiong, Van Pelt et al. 2007). Detailed analysis demonstrated a severe

loss of cardiomyocytes in mdm4$^{-/flox}$;αMyHC-Cre^{+} hearts, and replacement of myocardial tissue with fibrotic deposits (Xiong, Van Pelt et al. 2007). Cell number quantification analyses and terminal deoxynucleotidyl transferase biotin-UTP nick end labelling (TUNEL) assay suggested that the number of cardiomyocytes was decreased, due to increased levels of apoptosis in mutant hearts, suggesting that Mdm4 is important in protecting fully differentiated cardiomyocytes from apoptosis (Xiong, Van Pelt et al. 2007). The p53 conditional allele was introduced into mdm4$^{\Delta 2/flox}$;αMyHC-Cre^{+} mice to understand whether the cardiomyopathy caused by the loss of mdm4 expression was p53 dependent. The deletion of a single p53 allele increased the survival rate and life span of mdm4$^{\Delta 2/flox}$ mice, indicating that loss of mdm4 in the myocardium induces a p53-dependent cardiomyopathy in mice, and that mdm4's inhibition of p53 in adult cardiac tissue is essential for normal heart function (Xiong, Van Pelt et al. 2007).

1.1.4.3 p63 and p73.

Despite the remarkable structural similarity of their DBD and functional similarities observed between p53, p63 and p73, mouse KO technologies have demonstrated that they also have unexpected functional diversity. In fact, deletion of p63 and p73 in mice has shown that they have a more profound effect on normal development and organogenesis than p53 (Mills, Zheng et al. 1999; Yang, Walker et al. 2000). In particular, inactivation of the *TP63* gene has demonstrated the essential role of p63 in limb formation and epithelial morphology (Mills, Zheng et al. 1999). All squamous epithelia and their derivatives are missing in p63-null mice, including teeth, hair, mammary and prostate glands and the sweet and lacrimary glands (Mills, Zheng et al. 1999; Yang, Schweitzer et al. 1999). Most p63-null animals die before or a few days after birth (Yang, Schweitzer et al. 1999). Moreover, studies performed on mature epidermis have demonstrate that ΔNp63 is the main isoform expressed in proliferative keratinocytes, which locate into the basal layer of the epidermis, and its expression is reduced in the suprabasal differentiated layers (Candi,

Rufini et al. 2006). This evidence suggests a pivotal role for p63 in epidermal development as opposed to tumour susceptibility.

Consistent with the role of p63 in epithelial morphogenesis and limb development, heterozygous germ line mutations of p63 are the cause of six rare autosomal dominant disorders that recapitulate, less severely, the phenotype of p63-deficient mice (Celli, Duijf et al. 1999). 29 mutations in the DNA binding domain of p63 have been associated with three forms of ectrodactyly ectodermal dysplasia (EEC) (Celli, Duijf et al. 1999). Interestingly, some of these mutations have mapped and correspond to hotspot of p53 in cancer. On the other hand, ankyloblepharon-ectodermal dysplasia (AEC) mutations are locating in the SAM domain and affect only the α isoforms of the protein (Fomenkov, Huang et al. 2003). Together, these data indicate p63 to be a key regulator of epidermal development, lineage commitment and cell adhesion, however human p63 mutations have a variety of phenotype from skin fragility (AEC dysplasia) tolimb abnormalities (EEC dysplasia). These differences are likely caused by differential activation of p63 target genes by the different mutant p63 proteins. For example, whereas EEC mutants may be able to activate p63 target genes involved in skin development, they might fail to activate target genes required for limb development (Koster 2010).

The *TP73* gene also has distinct developmental roles. It has been showed that ΔNp73 is the predominant isoform in the developing mouse (Pozniak, Radinovic et al. 2000), and *in situ* hybridization shown that its expression is restricted to the brain (Yang, Walker et al. 2000). Consistent with this, p73-null mice exhibit hippocampal abnormalities, malformation of the limbic telencephalon and hydrocephalus, indicating an important role of p73 in neuronal development (Yang, Walker et al. 2000). Of note, p63- and p73-deficient mice lack spontaneous tumour formation, established by the maintenance of a cohort of p63 and p73 mutant mice for more than two years (Yang, Walker et al. 2000). Thus, it is becoming clear that p63 and p73, at least in *in vivo* mammalian systems, are not classical tumour suppressor but have instead evolved their own function as important genes in controlling organogenesis and development.

1.2 The ASPP family of proteins: new co-activators of p53 and its family members.

The "tumor suppressor" ability of p53 to push cells towards programmed cell death or cell cycle arrest has been the subject of intensive study. However, what determines this choice and how p53 decides to choose between life (cell-cycle arrest) and death (apoptosis) are still important questions that remain not completely understood. Better understanding of how p53-dependent apoptosis can be reactivated in tumours retaining wild type p53 has obvious, important implications for the development of new anti-cancer therapies (Murray-Zmijewski, Slee et al. 2008). It has been proposed that various post-translational modifications can influence the ability of p53 to induce cell cycle arrest or apoptosis (Murray-Zmijewski, Slee et al. 2008). Moreover, p63 and p73 have been shown to interact with and enhance p53-apoptotic activity (Flores, Tsai et al. 2002), suggesting that protein-protein interactions could play a fundamental role in the activation of specific genes. The discovery of the ASPP family of proteins offers a new, exciting insight into how p53 discriminates between different cells. Our laboratory, in 2001, identified two novel proteins which regulate the apoptotic function of p53 but not cell cycle arrest, and named them 'ASPP' proteins (Samuels-Lev, O'Connor et al. 2001). Hence, the ASPP family is a newly discovered family of proteins that interacts with and modulates p53-mediated apoptosis, providing another level of regulation for the activity and selectivity of p53 (Sullivan and Lu 2007).

1.2.1 Identification of the ASPP family, protein structure and expression.

The ASPP family is a family of proteins that is evolutionarily conserved from nematodes to vertebrates (Trigiante and Lu 2006) and, in mammals, encompasses three different members: ASPP1, ASPP2 and iASPP. All members of the family share a highly conserved carboxyl-terminal end which contains the signature sequence of three distinct motifs: Ankyrin repeats, SH3-domain and Proline rich region *(figure 1.6)*. The name ASPP also stands for Apoptotic Stimulating Protein

of p53, due to the proteins' biological functions. In particular, the C-terminus of the ASPPs is compost of four ankyrin repeats and one SH3-domain, two common structural domains involved in protein-protein interactions. Indeed this is a characteristic feature of the ASPP proteins as, so far, it is the only family to date that has a structural unit of ankyrin repeats closely juxtaposed to an SH3 domain (Robinson, Lu et al. 2008). In addition, a proline rich domain has been found close to the ankyrin repeats and the SH3 domain, giving the ASPPs the ability to make various complexes with other proteins. The C-terminus is, therefore, the preferred binding site for the ASPPs' binding partners, which include p53 and its family members (Gorina and Pavletich 1996; Robinson, Lu et al. 2008), and also RelA/p65 (Yang, Hori et al. 1999), Bcl-2 (Naumovski and Cleary 1996), adenomatous polyposis coli-like (APCL) (Nakagawa, Koyama et al. 2000), Hepatitis-C core protein (Cao, Hamada et al. 2004), amyloid beta precursor protein-binding protein 1 (APPB1) (Chen, Liu et al. 2003), PP1 (Helps, Barker et al. 1995), YES-associated protein-1 (YAP1) (Espanel and Sudol 2001) and SAM68 (Thornton, Dalgleish et al. 2006).

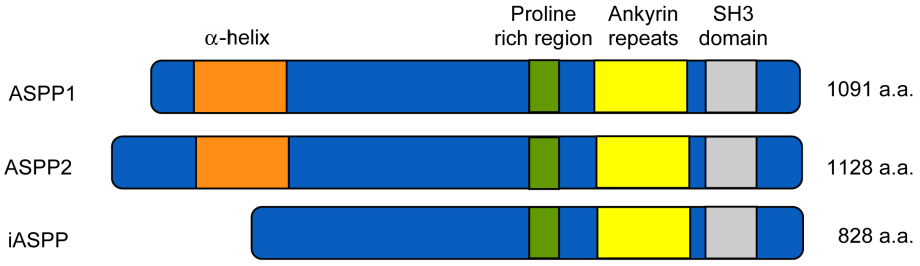


Figure 1.6: The ASPP family of proteins. The ASPP family consists of three members: ASPP1, ASPP2 and iASPP. All three proteins are characterised by three conserved domains in the C-terminus: a proline rich domain, ankyrin repeats and an SH3 domain. In addition, ASPP1 and ASPP2 have an α-helical domain in their N-terminus. The length in amino acids of each protein is indicated.

The first member of the family to be discovered was ASPP2 and it remains the best characterised. It was identified in a yeast-two hybrid screen of a transformed B-cell cDNA library using a fragment of mouse p53 as bait (residues 73-300). The screen identified two novel p53 binding partners, named 53BP1 and 53BP2 (Iwabuchi, Bartel et al. 1994). Interestingly, these two proteins had no sequence similarity, and could both bind the DNA binding domain of wild type p53 but not most of the mutant forms found in human cancers (Joerger, Ang et al. 2005). However, only 53BP2 contain the ASPP signature domains. 53BP2 was initially denominated p53-binding protein 2, until subsequent studies identified it as a smaller fragment of ASPP2 (600-1128) (Iwabuchi, Bartel et al. 1994). Studies on 53BP1, instead, revealed that it is a protein involved in the DNA repair process and completely unrelated to 53BP2 (Joo, Jeffrey et al. 2002). A longer ASPP2 fragment (123-1128) was discovered two years later in another two-hybrid screen, this time using the N-terminal fragment of Bcl-2 (1-188) as a bait, and for this reason it was named it Bbp (Bcl-2 binding protein) (Naumovski and Cleary 1996).

Only in 2001, was the full length ASPP2 finally identified to be a 1228 amino acid long protein and the name ASPP2 given. (Samuels-Lev, O'Connor et al. 2001) *(figure 1.6)*. Takahashi and colleagues, a few years later, demonstrated that the gene encoding full length ASPP2 (named *TP53BP2*) was the same gene that encodes also the shorter form Bbp. In fact, the two proteins are generated by alternative splicing of exon 3 (Takahashi, Kobayashi et al. 2004).

By mRNA expression analysis using northern blot techniques, it was demonstrated that ASPP2/53BP2 is expressed in various human tissues to different degrees (Iwabuchi, Bartel et al. 1994). Iwabuchi et al. showed that the highest expression level of ASPP2 was detectable in skeletal muscle, whereas the lowest was detected in the heart and brain (Iwabuchi, Bartel et al. 1994). In contrast, Yang and colleagues demonstrated that the heart and brain heavily expressed ASPP2 while the liver, instead, did not express ASPP2 at all (Yang, Hori et al. 1999). This inconsistency between the two studies may be due to different conditions in which the organs were harvested, or simply a result of different genders or ages of the mice used, which are not mentioned in the experimental procedures (Yang, Hori et al. 1999). Nevertheless, both groups showed that ASPP2 expression is

conditional to different organs, so to completely appreciate the biological function of ASPP proteins, systematic studies are required to determine their tissue expression levels and study their regulation. In view of above, conditional KO mouse technologies should be helpful in understanding the biological function of ASPP proteins.

In 1998, the first publication in which ASPP1's sequence was reported appeared in a scientific journal (Nagase, Ishikawa et al. 1998). Nagase et al. reported the discovery of a new protein of 928 amino acids long, which they called KIAA0771, with surprisingly high N-terminal homology to 53BP2. Computer examination of different databases using the ASPP2 signature domains, revealed that KIAA0771 is a truncated N-terminal form of a longer protein of 1091 amino acids that was called ASPP1 (Nagase, Ishikawa et al. 1998). Unlike the bond between 53BP2 and ASPP2, 53BP1 is not a splice variant of ASPP1, and to date, no splice variants of this protein have been reported.

The third family member to be identified was iASPP (also named PPP13R1L, RAI and NKIP1) is the most conserved member of the family as it is the only one expressed in *C. elegans* (Bergamaschi, Samuels et al. 2003). iASPP was first discovered as a shorter form of 315 a.a. that functions as a RELA/p65 associated inhibitor (RAI) (Yang, Hori et al. 1999). RAI was initially isolated in human placenta and brain cDNA libraries using NFkB as bait in a yeast-two hybrid assay (Yang, Hori et al. 1999). The latter search, however, reveal two sequences of 2.1 kb and 2.6 kb long, both containing the open reading frame for RAI but differing in the 5' untranslated region (Yang, Hori et al. 1999). In 2004, our laboratory identified a longer form of RAI which was called iASPP. The publication reported that a scrupulous BLAST search (National Centre for Biotechnology Information (NCBI) using the RAI sequence demonstrated the existence of three other sequences with high homology to RAI reported by Yang in 1998. Further comparison of these three new sequences, and those isolated in the original study, demonstrated complete overlap with one of the three new expressed sequence tags (ESTs), which encode for an 828 a.a. long protein. Finally, intron-exon mapping showed that the 2.6 kb sequence initially isolated and the 828 a.a. EST were derived from the same gene, and that the 2.1 kb shorter ORF, which encodes for RAI,

was raised from a single base pair insertion that introduced a new stop codon (Slee, Gillotin et al. 2004).

1.2.2 Functions of the ASPP proteins.

1.2.2.1 ASPP1 and ASPP2.

To date, the most well know function of the ASPP family of proteins is their ability to influence the apoptotic response by enhancing or inhibiting the activity of p53 (Trigiante and Lu 2006). In particular, ASPP1 and ASPP2 interact with p53 and stimulate its apoptotic function, but not cell cycle arrest, by specifically enhancing the p53's transactivation activity on the promoters of pro-apoptotic genes (Samuels-Lev, O'Connor et al. 2001; Bergamaschi, Samuels et al. 2004) *(figure 1.7)*. Indeed, ASPP proteins can interact with p53 and its family member, as demonstrated by the crystal structure of the complex between the C-terminus of the ASPPs and p53's DNA binding domain (Gorina and Pavletich 1996; Robinson, Lu et al. 2008). In particular, the third and fourth ankyrin repeat domains of the ASPPs, in association with their SH3 domain, have been shown to interact with the surface of the DBD of p53 (Gorina and Pavletich 1996; Robinson, Lu et al. 2008). Moreover, ASPP1 and ASPP2 have been shown to stimulate and activate the apoptotic function of p63 and p73 (Bergamaschi, Samuels et al. 2004). This evidence supports the idea that ASPP1 and ASPP2 function as tumor suppressor proteins by cooperating with p53 to eliminate cells, by enhancing its ability to induce cell death. In addition, Bergamaschi and colleagues showed that ASPP1 and ASPP2 inhibit the transforming activity of both RAS and E1A in rat embryonic fibroblasts (Bergamaschi, Samuels et al. 2003), supporting the notion that ASPP1 and ASPP2 act as tumour suppressor proteins. Although not directly involved in p53 binding, the N-terminal domain of ASPP2 is required to enhance p53's apoptotic activity. Bpb is, in fact, less active than the corresponding full length proteins in stimulating p53-dependent genes, indicating that the N-terminus may control the activity of ASPP1 and ASPP2 (Samuels-Lev, O'Connor et al. 2001).

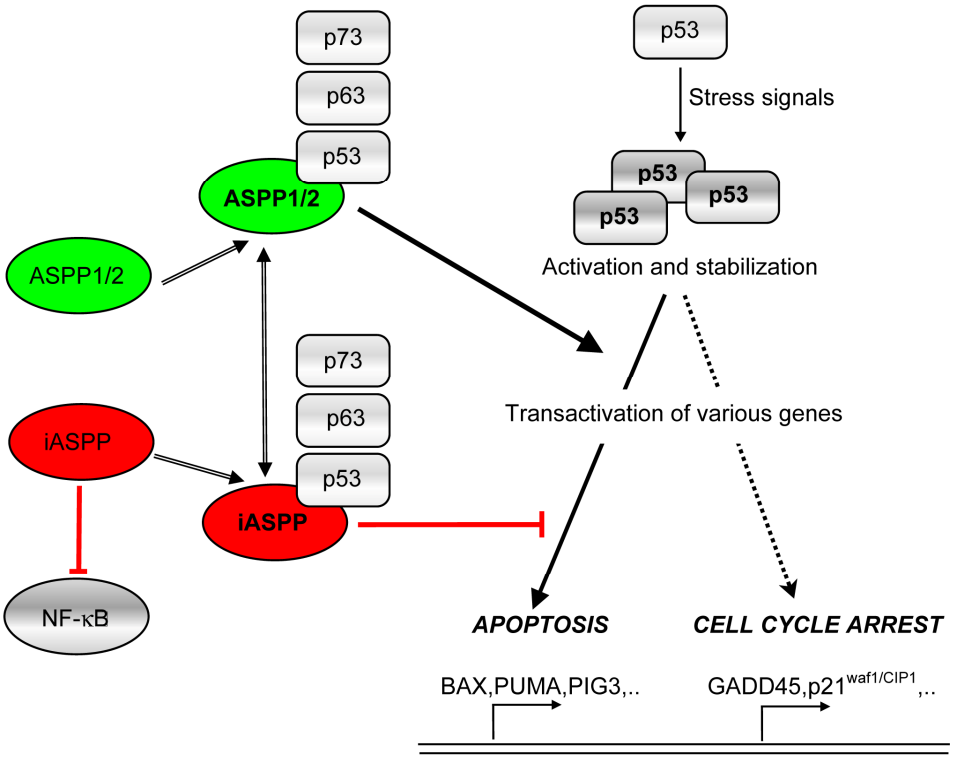


Figure 1.7: Schematic model of ASPP function. Stress signals lead to activation and stabilisation of p53. p53 can then transactivate various genes involved in apoptosis (BAX, PUMA, PIG3) or cell cycle arrest ($p21^{waf1/CIP1}$, GADD45). The ASPP family members ASPP1 and ASPP2 selectively stimulate p53's pro-apoptotic function, while iASPP inhibits it. The ASPPs can also bind p63 and p73 and modulate their apoptotic function as. iASPP has been discovered to be a NFκB (p65RelA) interactor and is known to bind and inhibit its activity. It is thought that mutual exclusion between iASPP and ASPP1 or ASPP2, for binding to the p53 family members, determines the outcome of the cell's fate: i.e. to die or live. However, this represents only a simplified view as many new ASPP binding partners are constantly being discovered.

Moreover, the N-terminus seems to also play a role in specifying the cellular location of the two proteins. Removal of the N-terminus causes them to relocate into the nucleus, while the full length proteins have a classical cytoplasmic location (Samuels-Lev, O'Connor et al. 2001).

1.2.2.2 iASPP.

In contrast with the tumour suppressive function of ASPP1 and ASPP2, iASPP has an inhibitory effect on p53-mediated apoptosis (Bergamaschi, Samuels et al. 2003) *(figure 1.7)*. Over-expression of iASPP specifically reduces the apoptotic activity of p53 by interfering with the transcription of various apoptotic effector genes such as BAX or PIG3 (Bergamaschi, Samuels et al. 2003).

However, consistent with the function of ASPP1 and ASPP2, iASPP does not impair the transcriptional activity of p53 when it is bound to promoters of cell-cycle arrest genes such as *CDKN1A*, which encodes $p21^{WAF1/CIP}$, or GADD45 (Bergamaschi, Samuels et al. 2003). iASPP is the only member of the ASPP family to be found in *C. elegans* (Ce-iASPP) and it appears to be the most conserved member of the family through evolution (Bergamaschi, Samuels et al. 2003). It shares 38% amino acid identity with Ce-iASPP and, interestingly, the ability of iASPP to inhibit p53-mediated apoptosis is conserved from *C. elegans* to humans, as Ce-iASPP can inhibit human p53-mediated apoptosis *in vitro* (Bergamaschi, Samuels et al. 2003). Overexpression of iASPP confers resistance to apoptosis induction by UV radiation, or by exposure to chemotherapeutic agents like cisplatin or doxorubicin, in cultured cells (Bergamaschi, Samuels et al. 2003), supporting the view that iASPP acts as an oncoprotein through its ability to inhibit p53-induced apoptosis. Like ASPP1 and ASPP2, iASPP interacts and binds with p53 through its second and third ankyrin repeats and its SH3 domain, suggesting that iASPP might simply function as a competitive inhibitor of ASPP1 and ASPP2 *(figure 1.7)*. Interestingly, iASPP was shown to bind the DNA binding domain of p53 with higher affinity when it contains a proline residue at codon 72 instead of an arginine. As a consequence, the inhibitory effect of iASPP on the p53Pro72 polymorphism is more pronounced when compared to p53Arg72 (Bergamaschi, Samuels et al. 2006). These data might provide a new mechanism to explain how the p53Arg72 polymorphism is more active in inducing apoptosis. More recently, a newly identified region of p53 outside the core DNA binding domain of p53 has been identified that interacts specifically with iASPP, providing a new mechanism by which iASPP can interfere with the apoptotic function of p53 (Ahn, Byeon et al. 2009).

1.2.3 Regulation of ASPP proteins expression.

1.2.3.1 ASPP1 and ASPP2.

Both ASPP1 and ASPP2 were first identified as smaller proteins, suggesting that their expression might be regulated by alternative splicing at the transcriptional level. Investigation of the *TP53BP2* gene revealed that two different splice variants of ASPP2 can be generated by alternative splicing of exon 3, named respectively 53BP2L (full length ASPP2) and 53BP2S (former Bp2 protein) (Takahashi, Kobayashi et al. 2004). However, little is know about the mechanism that regulates the choice between these two isoforms *in vivo.* At the transcriptional level, two laboratories independently demonstrated that E2F-1 can enhance the transcription of ASPP1 and ASPP2, by binding their promoters and stimulating their expression (Chen, Padiernos et al. 2005; Fogal, Hsieh et al. 2005). E2F-1 can be induced by various DNA damaging agents, which could explain how ASPP1 and ASPP2 are quickly up-regulated upon genotoxic stress. Further studies have suggested that different members of the E2F family have different binding affinities for ASPP1 and ASPP2, adding another level of complexity in understanding how ASPP1 and ASPP2 are regulated (Fogal, Hsieh et al. 2005; Hershko, Chaussepied et al. 2005). Moreover, ASPP1 and ASPP2 can be epigenetically silenced by aberrant methylation of their promoters, like most other tumor suppressor proteins. A recent study showed that these two genes are frequently down-regulated by DNA methylation in hepatitis B virus positive carcinomas (Zhao, Wu et al. 2010), while ASPP1 has been demonstrated to be down-regulated via a similar mechanism in acute lymphoblastic leukemia (Agirre, Roman-Gomez et al. 2006).

At the protein level, UV radiation and various DNA damaging agents have been reported to increased ASPP1 and ASPP2 expression (Lopez, Ao et al. 2000). One study has also shown that proteasomal degradation may be important for the regulation of ASPP2. ASPP2 can be ubiquitinated in its central region and subsequently targeted for proteasomal degradation, while DNA damaging anti-cancer drugs such as antracycline and bortezomib, which inhibits the proteasome pathway, can increase ASPP2 expression (Zhu, Ramos et al. 2005). Finally, the same

group also reported down-regulation of ASPP2 expression in the absence of cellular stress (Zhu, Ramos et al. 2005). However, the mechanisms related to ASPP1 and ASPP2 expression remain poorly understood and it is of fundamental importance to cancer therapy that we understand how to modulate their expression in cancers which retain wild type p53.

1.2.3.2 iASPP.

Like ASPP1 and ASPP2, the history of how full-length iASPP was discovered implies that iASPP expression could be regulated at the transcriptional level by alternative splicing. However, no direct evidence had been shown. Recently, a new open reading frame (ORF) has been identified which encodes for a protein 407 a.a. long, named iASPP-SV. However, iASPP-SV has only been reported in humans. (Zhang, Diao et al. 2007). Unfortunately, very little is known to date about the regulation of iASPP expression both at the transcriptional and translational level. The numerous binding partners of the ASPP family members identified in the past might provide better insight into how iASPP is regulated.

1.2.4 ASPP proteins and cancer.

1.2.4.1 ASPP1 and ASPP2 as tumour suppressor genes.

Given the well-established interaction between the ASPP and p53 family members, it is logical to expect that the ASPPs have an important role in tumourigenesis. In fact, evidence for the involvement of the ASPP proteins in tumour initiation and progression has come from many studies. Firstly, the crystal structure of the binding between 53BP2 and p53 revealed that several conserved contacts of p53 are involved in the binding between the two proteins, such as 178His, 181Arg, 243Met and 247Arg (IARC p53 mutation database). Importantly, two of the most frequently mutated p53 residues found in cancer (248Arg and 273Arg) are fundamental contacts in both p53 and ASPP2 (Gorina and Pavletich 1996). Secondly, Samuel and colleagues demonstrated that mutation of the contact residue 181Arg on p53 was observed in human cervical cancer. Again,

this mutation would prevent ASPP1 and ASPP2 from stimulating the apoptotic function of p53 (Samuels-Lev, O'Connor et al. 2001). ASPP2 has also been found to inhibit the transforming activity of RAS and E1A in rat embryonic fibroblasts (Bergamaschi, Samuels et al. 2003). Moreover, analysis of a panel of eleven tumour cell lines clearly demonstrated that the mRNA level of ASPP2 correlated with cellular sensitivity to the cytotoxic effects of UV and X-ray irradiation. Again, ASPP1 and ASPP2 protein levels were reduced in breast and lung carcinomas that retained wild type p53 (Mori, Ito et al. 2004; Liu, Lu et al. 2005). Finally, *in vitro* studies of various human tumors have confirmed the important role of ASPP1 and ASPP2 in tumour development. Using matching normal and tumour samples from a breast carcinoma panel, reduced expression of ASPP1 and ASPP2 was found in more than 60% of the samples that retained wild type p53 (Samuels-Lev, O'Connor et al. 2001). Consistent with these findings, ASPP2 expression was observed to be reduced in metastatic breast cancer (Sgroi, Teng et al. 1999). Furthermore, screening of several leukemia cell lines demonstrated a decrease in expression of ASPP1 and ASPP2 at the mRNA level (Agirre, Roman-Gomez et al. 2006). In addition, a study conducted in our laboratory using ASPP2 KO mice has suggested that ASPP2 plays a central role in tumour suppression (Vives, Su et al. 2006). ASPP2 heterozygous mice, in fact, have a 45% chance of tumour incidence in their life span, while wild type mice have only 15%. Compared to the wild type, ASPP2 heterozygous mice develop twice as many spontaneous lymphomas, rhabdomyosarcomas and squamous cell carcinomas (Vives, Su et al. 2006). These data clearly demonstrate that ASPP1 and ASPP2 have fundamental roles in tumourigenesis, suggesting a tumour suppressive role for the two proteins.

1.2.4.2 iASPP as an oncogene.

Given the tumor suppressive ability of ASPP1 and ASPP2 to inhibit cell growth, iASPP on the other hand functions as a specific inhibitor of the apoptotic function of p53 both *in vitro* and *in vivo*. This ability of iASPP to inhibit p53-mediated apoptosis suggests that iASPP could be an oncoprotein. Consistent with this hypothesis, iASPP is able to cooperate with RAS and E1A to transform rat embryonic fibroblasts *in vitro*, as elegantly demonstrated by Bergamaschi and

colleagues (Bergamaschi, Samuels et al. 2003). *In vitro*, oncogenes such as RAS, E1A and E7 have been shown to transform embryonic fibroblasts by overcoming the apoptotic function of p53. Bergamaschi et al. demonstrated that iASPP cooperates with RAS, E1A and E7, but not with mutant p53, to transform fibroblasts *in vitro* (Bergamaschi, Samuels et al. 2003). This finding demonstrates that iASPP enhances the transforming activity of RAS through its ability to inactivate p53. Furthermore, in the same study, exogenous expression of iASPP was shown to induce cellular resistance to apoptosis induced by both UV radiation and chemotherapeutic drugs, indicating the importance of iASPP in tumor development *in vitro* (Bergamaschi, Samuels et al. 2003). Inhibition of iASPP expression by small RNA interference molecules (snRNAi) results in increased rate of apoptosis in MCF-7 and U2OS cells, and in other tumour cell lines (Bergamaschi, Samuels et al. 2003). The idea that iASPP has oncogenic properties is further supported by evidence that it is frequently overexpressed in human tumours expressing wild type p53 (Trigiante and Lu 2006). In fact, our studies have demonstrated that iASPP expression is up-regulated in a panel of human breast carcinoma cell lines that express wild type p53. Moreover, iASPP mRNA levels were found to be significantly higher in acute leukemia (AL) patients when compared with normal donors or AL patients in complete remission (Zhang, Wang et al. 2005). Together, these findings strongly suggest that iASPP can act as an oncoprotein by interfering with the apoptotic function of p53.

1.2.5 The ASPP family in development.

1.2.5.1 ASPP1 and ASPP2 in development.

Although all of the studies conducted so far on the ASPP family strongly indicate that their main function is the control of malignancy and cellular responses by influencing p53-mediated apoptosis, the numerous binding partners identified suggest that they may have other novel functions. Recent studies have indicated a possible new role for the ASPP proteins in normal development, independent of p53's apoptotic activity. A study performed in our own laboratory indicated that ASPP2 has a fundamental role in embryogenesis as, in a mixed 129v/C57BL6 background, the

majority of ASPP2-null mice died around birth (Vives, Su et al. 2006). Those that did survive were runty with a dome-shaped head, and died a few days after birth of hydrocephalus, suggesting a role for ASPP2 in neural development. Unpublished data from our laboratory also indicates that ASPP2 mRNA transcripts detected by whole mount *in situ* hybridisation are strongly expressed in the brain, spinal cord and optic cup from E9.5 onwards (V. Vives, personal communication). Additional evidence of ASPP2 being a pivotal player in neural development comes from its identification as a binding partner and negative regulator of APP-BP1 amyloid precursor protein, and activator of the ubiquitin-like protein NEDD8 (neural precursor cell expressed, developmentally down-regulated 8) (Chen, Liu et al. 2003). Finally, last year our laboratory identified a novel function for ASPP2 in regulating and controlling cell polarity *in vivo*. Investigation of exon 3–ASPP2 deficient mice in a pure Balb/c background indicated impaired development of the neuroepithelium and defects in the proliferation of neural progenitors (Sottocornola, Royer et al. 2010). The organization of the mouse neuroepithelium is achieved by the maintenance of polarity complexes between neuronal cells, such as the apical-junctional complex (AJC) and the Par complex (Par3-atypical-PKC-Par6) (Hartsock and Nelson 2008). We showed that ASPP2 localises with Par3 and ZO1 in mouse neural epithelia, and that an absence of ASPP2 destabilises the tight junction complexes in the choroid plexus of the mouse brain, causing the hydrocephalus phenotype in ASPP2 exon-3 KO mice (Sottocornola, Royer et al. 2010).

Supporting evidence for this new function of the ASPP proteins also comes from a study conducted on ASPP1 KO mice. ASPP1 was identified to be an endothelial specific gene that functions during mouse embryogenesis (Hirashima, Sano et al. 2008). This study showed that ASPP1 is required for the initial assembly and function of the lymphatic vasculature, a function that is independent of p53 (Hirashima, Sano et al. 2008). Together these findings demonstrate a novel role of ASPP1 and ASPP2 that is independent of p53's apoptotic activity and their role in embryogenesis and organ development.

1.2.5.2 iASPP and wa3 mice: spontaneous mutation of PPP1R13L protein in mice.

David R. Beir and colleagues in 2005 identified a new strain of mice with wavy hair and open eyelids at birth (Herron, Rao et al. 2005). These mice, called Wa3 mice, carried a spontaneous mutation in their genome which resulted in reduced postnatal viability, abnormal coats and cardiovascular defects (Herron, Rao et al. 2005). Using positional cloning techniques, they located the causal gene in mouse chromosome 7. The putative gene encodes for the RelA associated inhibitor protein, also known as iASPP. In their investigation, they named this gene and its related protein Nkip-1, and briefly described two different phenotypes affecting the Wa3 progeny (Herron, Rao et al. 2005). Firstly, they reported that the fur abnormalities were similar to those found in waved 1 (Wa1) (Crew et al., 1933) and waved 2 (Wa2) mice (Keeler 1935), which carry respective mutations in the TGF-α and EGFR-α receptor genes. However, their only observation was that the "wave" hair phenotype was fully penetrant, and that the hair shafts derived from homozygous Wa3 mice were thinner but not shorter than those of normal control mice (Herron, Rao et al. 2005). Secondly, they analysed necropsies of Wa3 homozygous mice, following the observation that only 20% of transgenic homozygous mice reached adultness. They reported that the heart was of abnormal shape and size, with small white patches which were associated with myofiber degeneration (Herron, Rao et al. 2005). In addition, they only marginally explored the mechanism underlying the Wa3 phenotypes, suggesting a common mechanism for both hair follicles and heart abnormalities. Since the RAI protein, or the C-terminus of full length iASPP, was originally described as an NFkB-interaction partner using 2-hybrid screen analysis (Yang, Hori et al. 1999), and given the clear role of NFkB in the inflammation processes, they proposed that the absence of Nkip1 expression in Wa3 mice altered the expression profile of genes whose transcription is normally regulated by NFkB. They showed by immunoprecipitation analysis of whole skin protein extracts, from new born mutant and wild type pups, that Nkip-1 interacts with and binds NFkB. Next, they performed quantitative PCR analysis on newborn mouse hearts to asses the mRNA expressions of several genes regulated by NFkB (Herron, Rao et al. 2005). They observed

significantly higher ICAM-1 expression in Wa3 mouse hearts when compared to wild type controls, and concluded that an inflammatory process affecting Wa3 mutant hearts was the cause of the development of the lethal DCM in mice (Herron, Rao et al. 2005).

1.3 Mammalian cardiovascular system: an overview.

The cardiovascular system consists of the heart, blood and blood vessels, and is responsible for the transport of blood around the body. As the cardiovascular system moves the blood around, cells receive oxygen and nutrients, and carbon dioxide and other wastes are removed. The heart functions as a pump, forcing the blood to move through the body. In this brief overview, the function and biology of the heart and specific cardiac cell populations will be described. The main pathologies by which the heart can be affected, and known information regarding the underlying mechanisms will then be discussed. Finally, the cardiotoxic effect of anti-cancer drugs will be examined.

1.3.1 Heart: function, structure and development.

The heart is a muscular organ found in all animals with a circulatory system. It is responsible for moving the blood into two independent cardiovascular systems by regular and constant contractions. Mammalian hearts consist mainly of cardiac tissue, an involuntary striated muscle tissue specifically found in this organ, and connective tissue, which is compost of fibroblasts and extracellular matrix components that define the scaffold in which the cardiac tissue is embedded.

The murine heart originates from the embryonic mesoderm layer that divides and differentiates to form a bilateral pair of cardiogenic plates, 7.5 days into embryonic development (Brune, Bard et al. 1999). Adjacent to these plates, endothelial cells migrate to form the primordial heart tube (Kaufman and Navaratnam 1981), which subsequently loops to the right forming three distinct regions: the bulbus cordis (future right ventricle), primitive left ventricle and a common atrial chamber (Brune, Bard et al. 1999) *(figure 1.8)*. At the same time as this rightwards looping, lengthening of the cardiac tube and ballooning of the future four chambers takes place *(figure 1.8)*. The development of both the atria and ventricles is dependent on the growth, regression and swelling of the primordial chambers. The atrial chambers expand on both sides of the developing arterial pole, whereas the ventricular chambers form and expand along the outer curvature of the

cardiac tube as a result of intricate signaling pathways of proliferation and apoptosis (Anderson, Brown et al. 2006) *(figure 1.8)*. Between embryonic day 13.5 (E13.5) and 15.5 (E15.5), the final structure of the heart is complete and is composed of four different chambers, two superior atria and two inferior ventricles *(figure 1.8.)*. The atria are the receiving chambers with the function of collecting the blood from the two circulation systems; i.e. the right atrium accepts the blood from the systemic circulatory system, while the left atrium receives blood from the pulmonary circulatory system. In contrast, the ventricles are the discharging chambers, where blood is collected from the atria and pushed into the circulatory systems. During diastole (heart relaxation), blood flows to the atria through the ventricles.

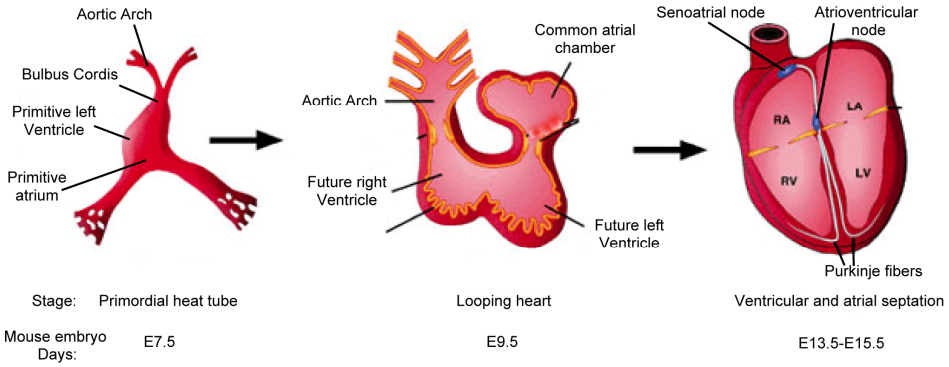


Figure 1.8: Schematic representation of the main stages of heart development. Murine cardiomyocyte progenitors become organised into a linear heart tube at day 7.5 *post coitum (left)*. Subsequently, looping and swelling of the heart gives rise to the ventricular and atrial chambers *(center)*. Between E13.5 and E15.5 the structure of the heart is complete and consists of: the right atrium (RA), left atrium (LA), right ventricle (RV) and left ventricle (LV). The sinoatrial node *(blue dot)* is the natural heart pacemaker, while the atrioventricular node *(blue dot)* delays the depolarisation wave in order for the atria to complete their discharge of blood into the ventricles. Purkinje fibers, where the depolarisation wave descends to the ventricles, are represented *(white line).*
(Figure reproduced and adapted from the medscape website, part of Nat Med © 2004 Nature publishing group)

During systole (heart contraction), instead, the right and left ventricles pump the blood into the pulmonary and systemic circulatory systems, respectively. In order to facilitate this, the cardiac muscle need to contract. Some cardiac cells are self-excitable, which means that they have the

ability to contract without any impulse from the nervous system: even if removed and placed in culture, they still retain the capacity to contract and can be analysed in great detail (Camelliti, Gallagher et al. 2006). The sinoatrial node, located at the top of the right atrium, can independently generate an electric impulse and self-contract *(figure 1.8)*. This region is of fundamental importance in setting the rate and timing at which all cardiac muscle cells contract. Because adjacent cardiac muscle cells are electrically coupled by components of the intercalated disc (ID) structures, the electric impulses can spread rapidly through the walls of the atria, causing both atria to contract in unison. The impulses then pass through a particular area of the heart, located between the right atrium and ventricle, called the atrioventricular node *(figure 1.8)*, where cells are specialised to delay the electric wave before it spreads to the ventricular walls. This delay ensures that the two atrial chambers are completely empty before the ventricles contract. Specialised muscle fibers called Purkinje fibers then conduct the electric impulse to the apex of the organ and throughout the ventricular walls ("Heart". MedicaLook. Medicalook.com. retrieve 2010-05-03).

The heart is effectively a syncytium: a meshwork of cardiac muscle cells interconnected by contiguous cytoplasmic bridges. This syncytium ensures the propagation of the electric impulse and the contraction of the myocardium. The electric impulse generated by the heart beat produces an electrical current which can be detected on the surface of the skin, and recorded as an electrocardiogram (ECG), which has provided the first diagnostic tool with which to detect heart dysfunctions.

1.3.2 Cardiomyocytes.

Mammals possess different types of muscle that are classified functionally as voluntary or involuntary, and structurally as striated or smooth muscle. Cardiac muscle is classified as striated involuntary muscle and is comprised of a unique type of cell population with some skeletal muscle features, such as a striated appearance, and some smooth muscle features, such as the central location of the single nuclei. However, it differs from both skeletal and smooth muscle mainly

because adjacent cells are joined to one another via ID complexes, and its contraction can occur without an initial nervous input.

The cells that comprise the cardiac muscle are called cardiomyocytes. As with all striated muscle, they are formed by various specialised protein complexes that are essential for the integrity and function of the myocardium. Sarcomeres are the functional units of all skeletal muscle and are responsible for the muscle's striated appearance. Cardiomyocytes also contain: numerous mitochondria to support their extensive use of ATP molecules; an enormous sarcoplasmic reticulum (SR), which compose most of the cytosol of the cardiomyocytes and functions as a reservoir of intracellular calcium ions (Ca^{2+}); a sarcolemmal membrane which contains the cardiomyocytes' contents; and T-tubules which are invaginations of the sarcolemmal membrane, to ensure the release of calcium from the SR in all of the myofibers (Brette and Orchard 2007) *(figure 1.9)*.

The sarcomere is an immense proteins complex that is organised into thin and thick filaments, which run transversely through the cardiomyocyte *(figure 1.9)*. Thick filaments are made up of myosin proteins which posses a rod like tail region and a head region compose of two globular subunits projecting out at approximately right angle with the filament. On the other hand, thin filament cointain three proteins: actin, troponin and tropomyosin. Actin is a small spherical molecule that it is arranged in the filament into two helical strands. Tropomyosin is a filamentous protein that is thought to form two strands that lie in the grooves formed between actin strands. Troponin is a globular protein that binds to tropomyosin at only one site, therefore is thought to sit astride the tropomyosin protein strand at regular interval. Troponin and tropomyosin are sometimes referred as regulator protein for their central role in regulating muscle contraction. During systolic contraction, the electrical excitation of the sarcolemmal membrane triggers an increase in the calcium level within the cardiomyocyte, resulting in movement between the thick (myosin) and thin (actin) filaments and inducing the cardiomyocyte to contract (Bers 2002). In particular, a small amount of Ca^{2+} enters the cytosol of the cardiomyocyte via specific Ca^{2+} channels and ionic exchange pumps during sarcolemmal depolarisation. This event triggers a major release of Ca^{2+} from the sarcoplasmic reticulum. The calcium level rapidly rises and binds to troponin *(figure 1.9)*.

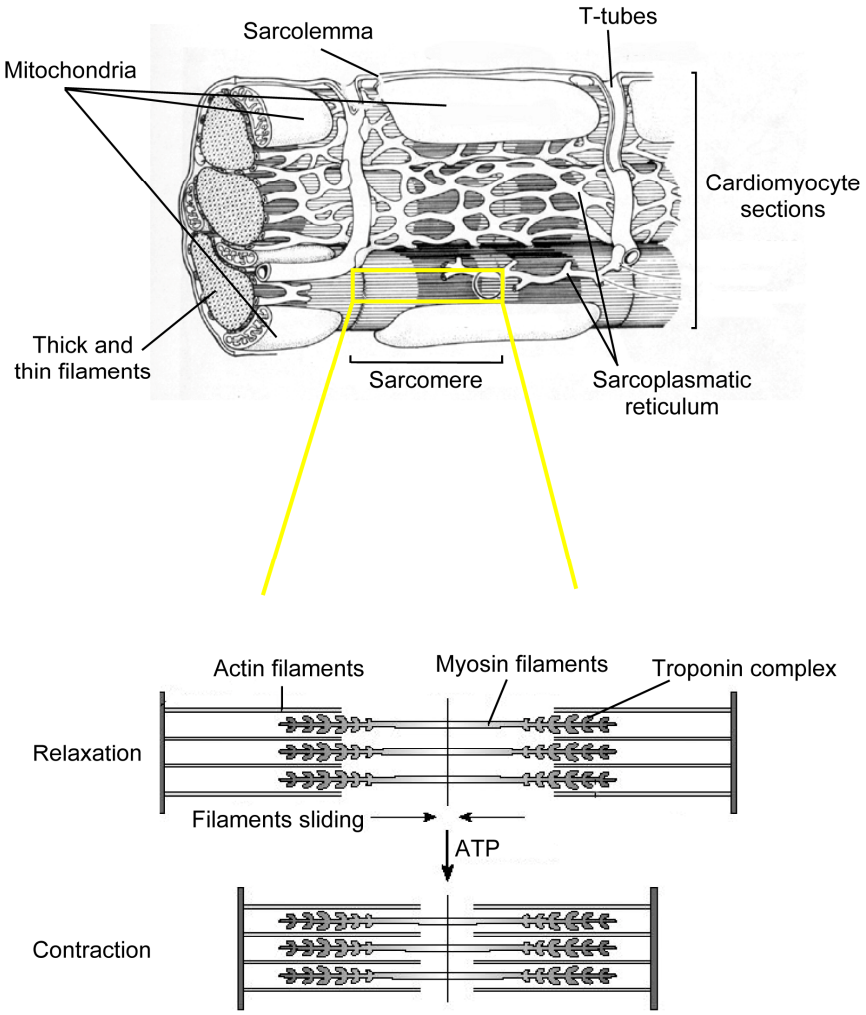


Figure adapted from Jennett, S. (1989). Human physiology. Churchill Livingstone, Edinburgh.)

Figure 1.9: Schematic representation of a cardiac myocyte. *(top)* Adult cardiomyocytes are rod-shape cells mainly compost of myofibrils, which constitute the contractile apparatus of the cardiomyocyte. Myofibrils are fascicules of thick (myosin) and thin (actin) filaments. The cardiomyocyte cytosol is composed of: the sarcoplasmic reticulum, which is the system for controlling the contraction of myofibrils through changes in calcium concentration; mitochondria; the sarcolemmal membrane; and T-tubes. The darker bands in the diagram represent overlap of the actin and myosin filaments. Yellow square represents the functional unit of the cardiomyocyte: the sarcomere. *(bottom)* Schematic representation of a single sarcomere. Actin and myosin filaments, and the troponin complex at the end of the myosin filament, are visible. The troponin complex allows the two filaments to "slide" and shortens the length of the sarcomere in the presence of ATP (contraction). The regular alignment of the light and dark bands of the sarcomeres across the whole muscle fiber accounts for the striped or 'striated' microscopic appearance of the myocardium.

Each myosin head is an ATPase, capable of hydrolyzing ATP to ADP, releasing energy. Now, ATP binds to myosin head and then in the presence of high Ca^{2+} level, troponin and tropomyosin expose a myosing binding site on the thin filament and a physical link between actin and myosin is formed. The ATPase activity of the myosin head is exterded causing a rotation of the head toward the tail, pulling the thin filament (Bers 2002) *(figure 1.9)*. Because the head of the myosin molecules are oriented in opposite directions at opposite ends of the thick filament, each pulls its adjacent thin filament toward the centre of the sarcomere and the sarcomere shortens. In contrast, during diastolic relaxation calcium is quickly removed from the cytosol of the myocyte by specialised ionic pumps located at the surface of the SR *(figure 1.10)*, ATP replace ADP on the myosin head and the myosin-actin bond is broken and the sarcomere will be restored to its resting length (Bers 2002). The mechanical force generated during contraction is propagated through a complex network of proteins called the cytoskeleton, which links the sarcomere to the sarcolemmal membrane and the extracellular marix. It is composed mainly of intermediate filaments (desmin), microfilaments and microtubules (non-sarcomeric actin) on top of sub sarcolemma components (Ahmad, Seidman et al. 2005) *(figure 1.10)*. Costameres are subsarcolemmal complexes that interconnect the bundle of filaments of the cytoskeleton with the sarcolemmal membrane, laterally *(figure 1.10)*. They locate at the surface of the striated muscle and their function is to link the sarcolemma regularly with nearby myofibrils, and transmit the contractile force laterally, through the membrane to the extracellular matrix. There are three types of costameres: focal adhesion complexes, mainly composed of vinculin, talin, tensin, paxillin and α and β integrins; spectrin based complex which are composed of actin, ankyrin and desmin and dysthrophin associated complexes composed by dystrophin, dystroglican and sacroglycan proteins (Bers 2002). Finally, the structural integrity of the heart is maintained by specific cardiac structures called intercalated discs (ID), which contain various junctional complexes such as adherens junctions, desmosomes and gap junctions *(figure 1.10)*. The IDs guarantee and mediate normal mechanical and electrical coupling between cardiomyocytes (Ferreira-Cornwell, Luo et al. 2002). In addition to supporting and maintaining the heart's

architecture by transmitting the contractile force between cells, they also participate in signal transduction pathways (Ahmad, Seidman et al. 2005).

In the adult heart, the intercalated discs are situated at the bipolar ends of the rod-shaped cardiomyocytes, and the myofibrils are anchored at this structure through the cytoskeleton. The myofibrils also make lateral contacts with the cardiomyocyte membrane, and there is a clear segregation between cell-cell contacts (ID) and cell-matrix contacts (costameres) in cardiac tissue (Perriard, Hirschy et al. 2003). At the intercalated discs desmosomes and adherens junctions the are intercellular adhesive junctions that anchor the desmin-based intermediate filaments and the actin cytoskeleton, respectively, with the sarcolemma membrane *(figure 1.10)* (Li and Radice 2010).

Desmosomes consist of three families of proteins: desmosomal cadherins, armadillo proteins and plakins (Franke, Borrmann et al. 2006). Desmosomal cadherins, desmocollins and desmogleins form extracellular connections by heterophilic binding between desmosomal cadherins *(figure 1.10)*. The cytoplasmic cadherin tail binds the armadillo protein plakoglobin and plakophilin, which in turn bind the plakin protein desmoplakin. Desmoplakin links desmosomes to the desmin-based intermediate filaments of the cytoskeleton (Franke, Borrmann et al. 2006). Adherens junctions, in contrast, contain the classical Ca^{2+}-dependent cadherins, of which N-cadherin is the most abundant in the heart. The extracytoplasmic domain of N-cadherin interacts homophilicly, mediating strong cell-cell junctions and plays a key role in the maintenance of the tissue's cyto-architecture. In the classical model for adherens junctions, the cytoplasmic tail of N-cadherin interacts in a mutually exclusive manner with either β-catenin or plakoglobin (Li and Radice 2010). β-catenin or plakoglobin then links N-cadherin to α-catenin, which regulates the cadherin's adhesive activity and links the adherens junction specifically to the actin-based cytoskeleton (Franke, Borrmann et al. 2006) *(figure 1.10)*. Gap junctions are the last junction found at the ID structures and are responsible for ion transfer between neighbouring cardiomyocytes. Each gap junction is composed of two hexameric structures called connexins that pass trough the sarcolemma membrane and form a permeable pore. Each connexin is formed by connexin proteins, of which connexin 43 is the most abundant in the heart (Franke, Borrmann et al. 2006) *(figure 1.10)*.

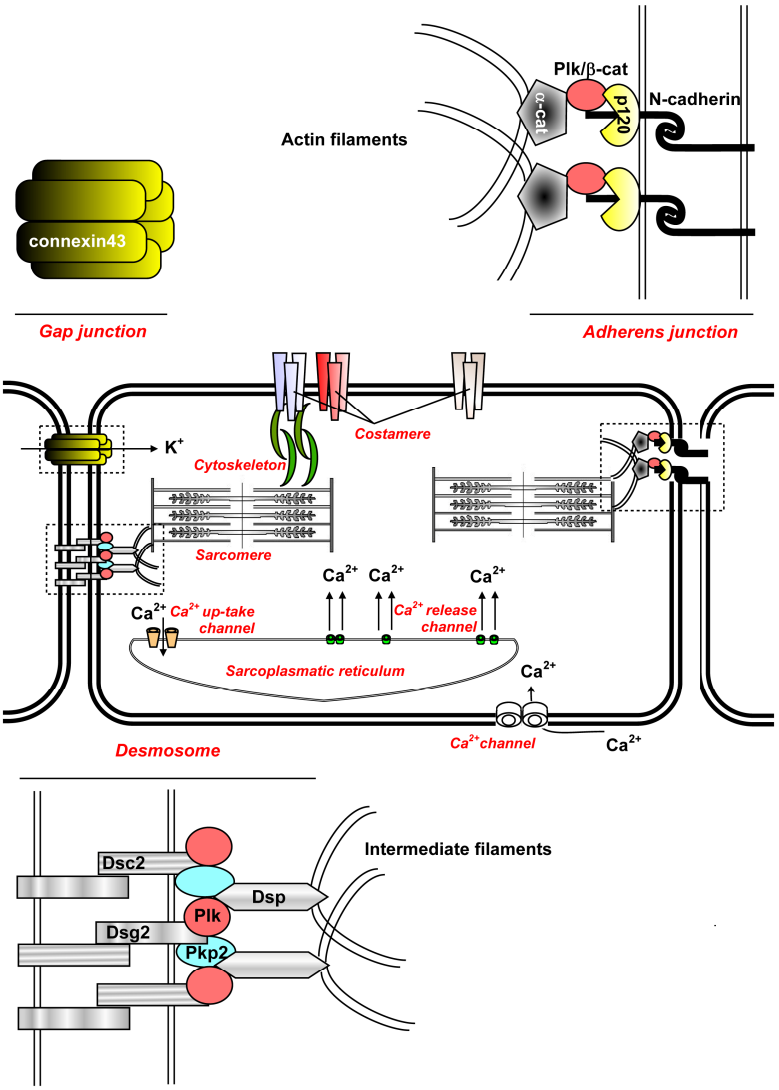


Figure 1.10: Cardiomyocyte intracellular components. Illustrated are the major protein complexes, cardiomyocyte architecture and intracellular organelles involved in cardiac excitation–contraction coupling. The initial event is the depolarisation of the sarcolemmal membrane, which occurs through ion entry from gap junctions *(top left)*. The depolarisation of the membrane results in the opening of Ca^{2+} channels and the entry of $Ca2^{+}$ molecules from the t-tubes *(bottom right)*. Entry of Ca^{2+} into the cell triggers the release of Ca^{2+} from the sarcoplasmic reticulum through Ca^{2+} release channels. Ca^{2+} then binds to the troponin complex in the sarcomere and activates the contractile apparatus. Cellular relaxation occurs on removal of Ca^{2+} from the cytosol by the Ca^{2+}-uptake pumps of the sarcoplasmic reticulum.
The molecular components that are required for normal electrophysiological activity and cell–cell adhesion are also shown. Gap junctions mediate the electrical coupling between cardiomyocytes. They are composed of various connexin proteins to form a channel where ions can be transferred. Among connexin proteins, the most important is connexin 43 *(top left)*. Adherens junctions and desmosomes mediate the mechanical continuity of the cardiomyocytes. Interactions between the desmosomal and adherens components at the intracellular and extracellular parts of the junctions are shown. Desmosome: transmembrane desmosomal cadherins desmoglein-2 (DSG2) and desmocollin-2 (DSC2) bind the armadillo family proteins plakoglobin (PLK) and plakophillin-2 (PKP), which in turn anchor to the plakin family member desmoplakin (DSP) *(bottom left)*. Adherens junctions: consist of the classical cadherin, N-cadherin, as the extracellular part of the complex that mediates contact with adjacent myocytes. The cytoplasmic end is formed by p120, PLK and β-catenin (β-cat), which in turn bind with α-catenin (α-cat), which mediates contact with actin filaments.

Desmosomal adhesion and adherens junction are essential between different cell types that must withstand high mechanical stress, such as skin keratinocytes and cardiac myocytes. Desmosomal and adherens junction components are differentially expressed in a tissue specific manner. Plakoglobin, also know as γ-catenin, and desmoplakin are the only plakin linker proteins present in both desmosomes and adherens junctions in epidermis and cardiac tissue (Cowin, Kapprell et al. 1986) *(table 1.1)*. Plakoglobin and desmoplakin are also the first components of the ID structures to be linked to the pathogenesis of two cardiocutaneous syndromes, characterised by arrhythmogenic right ventricular cardiomyopathy, keratosis and woolly hair (Protonotarios and Tsatsopoulou 2004). The different composition of desmosomes in the skin and heart is summarised in table 1.1.

	Skin	Heart
Desmosomal cadherins	Desmoglein 1-4 Desmocollin 1-4	Desmoglein 2 Desmocollin 2
Amadillo proteins	Plakoglobin Plakophilin 1-3	Plakoglobin Plakophilin 2
Plakins	Desmoplakin Plectin Envoplakin Periplakin	Desmoplakin Plectin

Table 1.1. The different composition of desmosomal components in skin and heart.

1.3.3 Diseases of the myocardium: cardiomyopathies.

Literally, “cardiomyopathy” means “heart muscle disease”, and is defined as a progressive disorder of the myocardium associated with abnormalities in organ morphology and structure (Richardson, McKenna et al. 1996). Morphological defects include alterations in organ shape, the thickness of the ventricular walls and the size of heart chambers. Structural defects, instead, are defined as

changes in the cyto-architecture and composition of the myocardium, associated with replacement of the cardiac tissue. Remodeling of the heart is defined as alteration in the structure (dimension, mass and shape) of the heart in response to hemodinamic changes or cardiac injuries in order to sustain the heart function (Opie, Commerford et al. 2006). Cardiac remodeling may be described as adaptive (physiological) or maladaptive (pathological). Physiological remodeling is a compensatory change in dimensions and function of the heart in response to physiological stimuli such as exercise or pregnancy. Pathological remodelling, instead, may occur with pressure and volume overload or following cardiac injury and itself is the major determinants of cardiac dysfunction and heart failure (Opie, Commerford et al. 2006). Heart failure is always a secondary effect, which occurs when the function of the heart is diminished by an underlying condition such as cardiomyopathy. The progression to heart failure is associated with a remodeling process of the heart, which manifests as gradual increases in left ventricular end-diastolic and end-systolic volumes, thickenning of the left ventricular wall and changes in chamber geometry to a more spherical, less elongated shape. The concept of cardiac remodeling was initially developed to describe changes which occur in the days and months following myocardial infarction. It has been extended to cardiomyopathies of non-ischemic origin, such as idiopathic dilated cardiomyopathy or chronic myocarditis, suggesting a common mechanism for the progression of cardiac dysfunction. Non-ischemic cardiomyopathies usually originate from congenital malformations of the heart's structure, such as alteration of the sarcomere complexes, cell-cell or cell-matrix junction dissolution or electrical conduction abnormalities, but can also arise from various environmental factors such as hypertension, diabetes or life style factors (Ahmad, Seidman et al. 2005). Cardiomyopathies are associated with specific cardiac alterations and have been traditionally classified based on anatomic findings in hyperthrophic or dilated cardiomyopathies. In particular, cardiac hypertrophy is characterised by an increase muscle mass, which results in increased wall thickness, mainly due to an enlarged myocardium and/or expansion of myocardial interstitial fibrosis (Hughes and McKenna 2005). In contrast, cardiac dilatation is characterised by an increase in the size of the organ, although this mainly relates to a dilatation of the ventricular and atrial chambers and not an increase in overall

cardiac mass. Although, anatomic findings and haemodynamic parameters make a clear distinction between hypertrophic and dilated remodeling, both can lead to severe cardiac dysfunction and subsequent heart failure. At this stage, morphological and haemodynamic differences between hypertrophic and dilated cardiomyopathy become less prominent, and both systolic and diastolic functions are severely impaired.

Cardiomyopathies can be classified by their haemodynamic characteristics and morphological abnormalities in:

- Hypertrophic cardiomyopathy (HCM) is the major heart disorder, caused mostly by genetic mutations affecting sarcomere proteins. Approximately 45% of mutations occur in the β-myosin heavy chain gene, while 35% occur in the cardiac myosin binding protein C gene, which encode two structural sarcomeric proteins. In HCM the heart muscle is thickened, which can obstruct blood flow and prevent the heart from functioning properly.
- Dilated cardiomyopathy (DCM) is one of the most common forms of heart disease and is characterised by enlarged ventricular chambers and impaired heart performance. Approximately 40% of cases are familiar, but the mechanisms are poorly understood compared with HCM.
- Arrhythmogenic right ventricular cardiomyopathy (ARVC) mostly affects the right ventricle and it is characterised by defects in the electrical wave in the heart. Areas of fibrotic tissues and replacement of cardiomyocites with adipocitic tissue are also common in ARVC.
- Restrictive cardiomyopathy (RCM) is an uncommon cardiomyopathy. The walls of the ventricles are stiff, but may not be thickened, and resist the normal filling of the heart with blood.

Clinical, haemodynamic and morphological characteristics of different cardiomyopathies are summarised in table 1.2.

	HCM	DCM	ARVC	RCM
Clinical				
Heart failure	occasional	frequent	frequent (RV)	frequent (BV)
Arrhythmias	atrial and ventricular	atrial and ventricular due to conduction defects	atrial and ventricular due to conduction defects	atrial fibrillation
Sudden death	< 10%	frequent	frequent	< 5%
Hemodynamic				
Systolic function	normal	reduced	reduced (RV or BV)	normal
Diastolic function	reduced	reduced	reduced (RV or BV)	severely reduced
Morphological				
Cavity size atrium	normal-enlarged	enlarged (LV or BA)	enlarged (BA)	enlarged (BA)
Cavity size Ventricle	reduced	enlarged (LV or BV)	enlarged (RV or BV)	normal-reduced (BV)
Wall Thickness	enlarged-asymmetric (LV)	normal-reduced (LV or BV)	normal-reduced (RV or BV)	normal (BV)

Adapted from Lancet, vol 358, Nov 10, 2001 *Cardiomyopathy, from genetics to the prospect of treatment*

Table 1.2 Characteristics of cardiomyopathies. Summary of the clinical, hemodynamic and morphological features relative to each cardiomyopathy. Abbreviations: LV=left ventricle. BV=both ventricles. RV=right ventricle. BA=both atria. LA=left atrium. RA=right atrium

1.3.3.1 Hypertrophic cardiomyopathy.

HCM is characterized by left ventricular hypertrophy, which is typically asymmetrically associated with occasional dilatation of the left ventricle (Maron, Olivotto et al. 2000). Typical histo-morphological abnormalities of HCM include myocyte hypertrophy and cardiac structure disarray. With HCM, the sarcomeres are increased in size, so the heart muscle becomes progressively thicker. In addition, the normal alignment of muscle cells is disrupted, a phenomenon known as myocardial disarray, which leads to disruption of the electrical coupling of adjacent cardiomyocytes and is most commonly due to a mutation in one of the sarcomeric genes (Ahmad, Seidman et al. 2005). Diagnosis is often by an abnormal ECG and by the analysis of two-dimensional echocardiography, which allows precise measurement of ventricular dysfunction, location and extension of the hypertrophy (Klues, Schiffers et al. 1995). HCM is an autosomal dominant familial disease in more than 50% of patients (Maron, Nichols et al. 1984). Genetic analysis has linked

hundreds of mutations with 11 different genes in the human genome, all of which encode for structural sarcomere proteins (Richard, Charron et al. 2003): β-myosin heavy chain, myosin binding protein C, cardiac troponin I and T, cardiac actin, cardiac troponin C and titin are only some of the proteins whose functions are inactivated by genetic mutations in familial HCM cases. Through extensive investigation, we now understand that these proteins have different roles in maintaining the contraction-relaxation cycle of myocytes. For example, α- and β- myosin heavy chain and, myosin binding protein-C are the main components that interact with actin filaments to generate the mechanical strength to contract the cardiomyocyte; troponin and myosin light chain proteins have structural roles in the sarcomere; while the largest cardiac protein titin helps to transmit force to the cytoskeleton. Nevertheless, cellular or molecular events triggered by non-functional sarcomere proteins that lead to HCM remain unclear. Engineered animal models have helped us understand in more detail the mechanisms by which mutant sarcomeric proteins activate pathways that result in hypertrophic remodeling. Although different signals might be activated by different non-functional proteins, calcium has emerged as a critical and common player in all the HCM mutations identified to date, and has been identified as the molecule that triggers the HCM remodeling response (Ahmad, Seidman et al. 2005). Hence, HCM arises from mutations in genes that encode proteins that are important for force generation (Franz, Muller et al. 2001). There is currently no cure for HCM and, due to its heterogeneity in clinical manifestations, no uniform treatment strategy is available (Maron 1997).

1.3.3.2 Dilated cardiomyopathy.

DCM is characterised by left or bi-ventricular chamber(s) dilatation, in association with impaired contraction and function of left or both ventricles. The reduced heart function progressively results in heart failure and sudden cardiac death, typically from ventricular arrhythmias (Elliott 2000; Franz, Muller et al. 2001). Histological and morphological changes in DCM are frequently associated with extensive areas of fibrosis as well as hypertrophic myocardium (“Heart”,

heartlook.com). The clinical appearance of DCM ranges from a symptomless condition to sudden death of patients. Fatigue, weakness and exercise intolerance are often the only phenotypes that affect DCM patients (Elliott 2000). About 35% of the adult patients affected by DCM also have first-degree relatives affected by the same pathology, indicating an important role for genetics in the establishment of the disease (Grunig, Tasman et al. 1998). Inherited DCM is most commonly transmitted as an autosomal recessive X-linked trait, but matrilineal (mitochondrial) inheritances also occur (Kurrelmeyer, Kalra et al. 1998). Furthermore, results from genetic studies have linked most familial DCM pathologies with mutations in chromosomal loci that encode for costamere proteins (Franz, Muller et al. 2001). For example, dystrophin, α-dystroglycan or the sarcoglycan complex of proteins are a few of the most mutated genes found in familial DCM (Franz, Muller et al. 2001). In particular, dystrophin protein is a rod-shaped protein involved in the maintenance of the sarcolemmal structure, and is encoded by a gene located on the X-chromosome. It is believed to function by stabilising the sarcomere by attaching actin filaments to the extracellular matrix, through the dystrophin-associated glycoprotein complex (Franz, Muller et al. 2000). α- and β-dystroglycans are part of the dystrophin-associated glycoprotein complex, and their inactivation by various genetic mutations leads to the development of DCM (Cox and Kunkel 1997). Finally, different mutations in the sarcoglycan gene have been linked with primary DCM (Tsubata, Bowles et al. 2000). These findings indicate that most DCM myopathies result from impaired anchoring of the sarcomere to the sarcolemmal membrane, as well as the disruption of the myocyte cytoarchitecture that links the nucleus to the sarcolemma (Franz, Muller et al. 2001). These findings support the hypothesis that familiar DCM results from impaired force transmission from the sarcomere to the lateral syncytium. However, electrical conduction abnormalities and altered energy production have also been found to be associated with familiar DCM (Cox and Kunkel 1997; (Santorelli, Mak et al. 1996; Arbustini, Diegoli et al. 1998). Specific treatments for DCM are not currently available, and the main therapeutic approach available is the control of the disease's progression to avoid sudden cardiac arrest (Franz, Muller et al. 2001).

1.3.3.3 Arrhythmogenic right ventricular cardiomyopathy/dysplasia.

ARVC is a heritable myopathy with typically autosomal dominant inheritance. The disease was first described by Fontaine in 1978 and was recognised as a distinct cardiomyopathy only eighteen years later (Maron and Louie 1986). Pathologically, ARVC is a dilated form of cardiomyopathy characterised by a fibro-fatty replacement of the myocardium that primarily involves the right ventricular chamber (Corrado, Basso et al. 1997). It is also characterised by impaired contraction of areas involving the free wall of the right ventricle, and is often associated with arrhythmia (Corrado, Basso et al. 1997). Patients affected by ARVC show also degenerative changes in the cardiomyocyte structure associated with severe disarray. The thickness of the right myocardial free wall is usually reduced. The disease's progression typically leads to dysfunction of the right ventricle, although the performance of the left ventricle can also be affected (Burke, Farb et al. 1998). In contrast with DCM, ARVC presents itself with disproportionate dilation of the right ventricle (Franz, Muller et al. 2001). Replacement myocardium with fibro-fatty deposits seems to be a degenerative process cause by the death of cardiomyocytes. Apoptosis and inflammation are often seen in the affected ARVC heart (Corrado, Basso et al. 1997). However, Runge et al. investigated eight ARVC human biopsy samples to determine the pattern of programmed cell death, and clearly demonstrated that replacement of the myocardium by fibro-fatty deposits is the result of excessive apoptosis with avoidance of local inflammation (Runge, Stouffer et al. 2000). As a genetic disorder, ARVC is usually an autosomal dominant manifestation and, by genetic linkage analysis, twelve genetic loci have been related to this myopathy (Azaouagh, Churzidse et al. 2011). Five of which encode for desmosomal proteins.: plakophilin-2, desmoplakin, plakoglobin, desmocollin-2 and desmoglein-2 are the desmosomal proteins mutated in ARVC patients (McKoy, Protonotarios et al. 2000; Rampazzo, Nava et al. 2002; Gerull, Heuser et al. 2004; Azaouagh, Churzidse et al. 2011). However, the basis of the predilection of ARVC for the right ventricle is still unclear, despite the identification of genetic mutations. In fact, expression analysis for plakophilin-2, desmoplakin and plakoglobin has revealed that all proteins are expressed in both ventricles (Ahmad, Seidman et al. 2005). It has been demonstrated that reduced integrity of the cell-cell

junctions between cardiomyocytes might promote myocardial degeneration and induce programmed cell death (Hakimelahi, Parker et al. 2000). Recently, Ali J. Marian's group suggested that displacement of plakoglobin from the ID complexes leads to the relocation of the protein into the nucleus, where it suppresses canonical Wnt/β-catenin-Tcf/Lef1 signalling (Garcia-Gras, Lombardi et al. 2006). The latter is a key regulator for the transcriptional switch between myogenesis to adipogenesis (Ross, Hemati et al. 2000).

- Naxos and Carvajal diseases.

ARVC is a hereditary disorder with autosomal dominant inheritance. However, families with recessive transmission have also been identified. In fact, in 1986 Protonotarios and colleagues reported a recessive cardiocutaneus syndrome in families from the Greek island of Naxos, with three clear clinical features of woolly hair, diffuse non-epidermolytic palmoplanar keratoderma and ARVC (Protonotarios, Tsatsopoulou et al. 1986). Since this disease was first reported in families from Naxos (Protonotarios, Tsatsopoulou et al. 1986) it was called "Naxos" disease, but was later also reported in other parts of the world (Tosti, Misciali et al. 1994; Bukhari and Juma'a 2004; Kilic, Babaoglu et al. 2007). The woolly hair that characterises this condition is present from birth and affects the scalp and eyebrows, as well as pubic hair, while palmoplanar keratoderma develops during the first year of life with no blistering or manifestations of skin erosion (Protonotarios, Tsatsopoulou et al. 2001; Protonotarios, Tsatsopoulou et al. 2001). Importantly, both the woolly hair and palmoplanar keratoderma phenotypes clinically precede the myopathy, which usually becomes symptomatic during adolescence. Over the course of the disease, affected hearts reveal substitutions of myocardial tissue with fibro-fatty accumulations and severe right ventricular dilation (McKenna, Thiene et al. 1994). In adults, almost 100% of people affected show ECG abnormalities, and sudden death is often due to ventricular tachycardia (Protonotarios, Tsatsopoulou et al. 2001).

A two base-pair (bp) deletion in the plakoglobin gene locus causes a frameshift in the ORF of the protein, which results in the truncation of the last 56 amino acids, and is now known to be the

genetic cause of Naxos syndrome (McKoy, Protonotarios et al. 2000). It is believed that the C-terminal truncated plakoglobin is expressed, but fails to localise into the ID complexes at the polar end of the cardiomyocyte (Kaplan, Gard et al. 2004). Moreover, expression of connexin 43 has been found to be severely reduced in Naxos and ARVC patients, possibly explaining the electrical and rhythm abnormalities observed in the heart (Kaplan, Gard et al. 2004). Moreover, changes in plakophilin-2 could affect the expression of connexin 43 (Oxford, Musa et al. 2007). It is, then, tempting to speculate that changes in adherens junctions or desmosomes could affect gap junctions indirectly, by the displacement of plakoglobin into the nucleus, where it could alter the Wnt signaling pathway which is also thought to be involved in the regulation of connexin 43 expression (Ai, Fischer et al. 2000). This also indicates an intimate correlation between all junctional components of the ID complexes. Moreover, a direct link between displacement of plakoglobin and its relocation to the nucleus, suppression of Wnt/β-catenin signaling and activation of the adipogenesis pathway in the context of ARVC has been unveiled (Garcia-Gras, Lombardi et al. 2006). However, more recently, Cabral et al. showed that a missense mutation into the plakoglobin gene induce skin fragility, diffuse palmoplantar keratoderma, and woolly hair with but no symptoms of cardiomyopathy (Cabral, Liu et al. 2010).

Mutations in the desmoplakin gene locus have also been reported to induced keratoderma, this time often associated with epidermolysis and skin blistering, woolly hair and a mainly left-side DCM, which in later stages become a biventricular dilatation, emphasises even further the parallels between DCM and ARVC (Carvajal-Huerta 1998; Norgett, Hatsell et al. 2000). Histopathology of affected patients has revealed skin fragility, follicular keratosis and clubbing of finger nails. Most of the patients experience blistering and psoriasis of the skin (Carvajal-Huerta 1998). Cardiac tissues biopsy from Carvajal patients has also revealed ventricular hypertrophy and enlargement of the left ventricular chamber, although the right ventricle and the atrium are clearly affected as well. Interestingly, the expression of both plakoglobin and connexin 43 was found to be reduced in association with a displacement of desmin protein, which failed to insert into the ID complexes. No

fibro-fatty deposition was observed in Carvajal patients (Kaplan, Gard et al. 2004). As mentioned before, Norgett and colleagues in 2000 found that Carvajal syndrome was caused by a homozygous mutation in the genetic locus that encodes for desmoplakin (Norgett, Hatsell et al. 2000). This mutation leads to a truncated form of the protein that lacks of C-terminus. Other mutations have also been described that are associated with cardiocutaneous clinical features of Carvajal disease, all of which occur in the desmoplakin locus (Bolling and Jonkman 2009).

1.3.3.4 Restricted cardiomyopathy.

RCM is the rarest of the cardiomyopathies. The World Health Organization (WHO) defines RCM as a myocardial disease characterised by restrictive filling and reduced diastolic volume of both ventricles, with normal or near-normal systolic function and wall thickness. It is characterised by increased stiffness of the heart muscle, usually due to fibrotic scar tissue, which prevents adequate filling of the ventricular chambers (Dornal's medical dictionary). Diastolic dysfunction is usually the most prominent abnormality and leads to atrial enlargement, elevated systemic and pulmonary venous pressures and subsequent heart failure (Ahmad, Seidman et al. 2005). Myocyte hypertrophy or ventricular dilatation are not typical hallmarks of RCM, in contrast with the more common types of cardiomyopathy. In fact, the pumping action and electrical coupling of the heart is generally normal. However, blood flow is reduced and the blood that would normally enter the heart is backed up in the circulatory system. In time, restrictive cardiomyopathy patients develop diastolic dysfunction and eventually die of cardiac arrest. The extremely low prevalence of the disease has limited the use of genetic linkage studies or mutation analysis (Ahmad, Seidman et al. 2005). However, studies performed on hereditary forms of familiar RCM have revealed structural alteration of desmin protein (Zhang, Kumar et al. 2001). Mutations in the cardiac troponin I gene were discovered in families with either RCM or HCG (Mogensen, Kubo et al. 2003). No cure is available to date for the treatment of RCM patients, and all current therapies mainly focus on the prevention of thromboembolism and sudden death (Franz, Muller et al. 2001).

1.3.2.5 Desmosomes and diseases

Adhesive intercellular junctions are an absolute requirement for the correct functioning of cells, tissues and entire organisms. As a consequence, disruption of desmosomal assembly, structure or integrity leads to diverse pathologies such as cardiomyopathy, epidermal and mucosal blistering, palmoplantar keratoderma, woolly hair, keratosis, epidermolysis bullosa, ectoderma dysplasia and alopecia (Brooke, Nitoiu et al. 2011). Several aspects of desmosomal biology can be implying from examinations of the clinical presentation of diseases in which desmosome components are altered. First, the primary role of the desmosome is to resist mechanical stress. As the two tissues subjected to major mechanical forces are the heart and the skin, inevitably, desmosomal alteration leads to compromised cardiac or cutaneous function. Second, different clinical presentations often arise when different desmosomal components are affected or even when region of the same molecule are mutated. Finally, the complex expression profiles of desmosomal genes are important for the differentiation program of tissues such as the epidermis (Brooke, Nitoiu et al. 2011).

In 1991, Amagai and colleagues reported that Desmoglein 3 (Dsg3) is the target of autoantibodies produced in the skin disease called pemphigus vulgaris (PV) (Amagai, Klaus-Kovtun et al. 1991). Pemphigus is a class of skin disorders characterized by the loss of cell-cell adhesion in the epidermis and mucous membranes (Payne, Hanakawa et al. 2004). The type of tissue affected depends on the isoform of Dsg targeted by autoantibodies. In pemphigus foliaceus (PF) Dsg1 is targeted which results in superficial blistering of the skins without effect on the mucous membrane, reflecting the expression profile of Dsg1 into the epidermis (Fig 1.13) By constrast, PV is characterized by anti-Dsg3 autoantibodies and clinical manifestations such as oral erosions and only occasionally blistering of the skin. However, approximately 50% of PV patients will develop additional antibodies against Dsg1. *Staphylococcus* scaled-skin syndromes and bullous impetigo are characterized by superficial blistering that is clinically and histologically identical to that seen in PF (Amagai, Matsuyoshi et al. 2000). Blistering in these patients is caused by exfoliate toxins which are bacterial proteases that target Dsg1 only (Amagai, Matsuyoshi et al. 2000). These autoimmune and infectious diseases provides striking evidence for a role of desmogleins in

epidermal cell adhesion (Payne, Hanakawa et al. 2004). Autosomal-dominant skin disease named striate palmoplantar keratoderma (SPPK) is caused by haploinsufficiency of Dsg1 gene (Rickman, Simrak et al. 1999). Patients with Dsg1 haploinsufficency display a thickening of the stratum corneum on the palms and the soles. Thickening of the stratum corneum over areas of repeat trauma is a normal response of healthy skin. However, SPPK represent this type of response occurring al low level of mechanical stress. This possibility is supported by the observation that SPPK can also result from mutations in genes encoding components of the desmosomal plaque like desmoplakin or plakoglobin (Norgett, Hatsell et al. 2000; Protonotarios and Tsatsopoulou 2004). Desmocollins (Dsc) also play a fundamental role in desmosomal adhesion but also in epidermal integrity and differentiation. Dsc1-null mice exhibit loss of cell-cell junction in the granular layer of the epidermis, hyperproliferative changes and increased expression of the wound keratins 6 (K6) and 16 (K16) (Chidgey, Brakebusch et al. 2001). By contrast, aberrant expression of Dsc3 results in altered keratinocytes differentiation and hair follicle changes (Hardman, Liu et al. 2005). These are consistent with the reciprocal localization of these cadherins in the differentiated (Dsc1) or proliferative (Dcs3) layer of the epidermis (Fig 1.13). Plakophillins (PKPs1-3), together with plakoglobin, are part of the armadillo family of protein which functions as adaptor proteins with important roles in facilitating the adhesion of desmoplakin to intermediate filaments. Patients exhibiting a severe autosomal recessive dysplasia and skin fragility were found to have mutations in PKP1 (McGrath, McMillan et al. 1997). In particular, their skin cannot withstand minor trauma, which support the notion that PKP1 plays a key role in desmosomal adhesion. *In vitro*, keratinocytes PKP1$^{-/-}$ showed aggregation of intermediate filaments in a perinuclear location rather than being attached to desmosomes (Hatzfeld, Haffner et al. 2000). Whereas PKP1 mutations are manifest only in the skin, human PKP2 mutations cause Arrhythmogenic right ventricular cardiomyopathy (ARVC) (Gerull, Heuser et al. 2004). Experiments ablating PKP2 gene in mice indicate that the cardiomyopathy in patients with PKP2 mutations is most likely to be the result of mechanical fragility. In common with mutations of human PKP1 gene, lack of PKP2 in mouse cardiomyocytes causes intermediate filament to retract from the membrane (Grossmann, Grund et

al. 2004). Thus both PKP1 and PKP2 play essential roles in mediating desmoplakin association with desmosomes in the epidermis and heart respectively.

Mouse KO studies have provided important clues on how important are plakoglobin or desmoplakin proteins in maintaining cell-cell adhesion in both epidermis and heart. Consistent with this, plakoglobin mutation in humans causes an autosomal recessive conditions named Naxos disease, characterize by a phenotypic triad of cardiomyopathy, palmoplantar keratoderma and "woolly hair" (McKoy, Protonotarios et al. 2000). Similarly, mutations into desmoplakin gene will cause an autosomal recessive disorder, called Carvajal syndrome, described by dilated cardiomyopathy, "woolly hair" and keratoderma (Norgett, Hatsell et al. 2000). Naxos and Carvajal syndromes will be described in more details in paragraph 1.3.3. Desmoplakin mutations can cause an array of human diseases which vary in severity (Lai Cheong, Wessagowit et al. 2005). Desmoplakin haplosufficency leads to striate palmoplantar keratoderma (Armstrong, McKenna et al. 1999), whereas a more severe keratoderma together with "woolly hair" results from compund heterozigosity of nonsense and missense mutations (Whittock, Wan et al. 2002). Moreover, a lethal condition named acantholytic epidermolysis bullosa was shown to raise from heterozigous mutation that truncate the desmoplakin C-terminus(Jonkman, Pasmooij et al. 2005). Summary of desmosomal disorders can be found in table 1.2.

1.3.4 Signaling pathways involved in the adaptive and maladaptive response in cardiomyopathy.

In contrast with the well described anatomical characteristics and genetics findings in the hypertrophy and dilated remodeling processes, the cellular mechanism(s) and signaling pathway(s) that trigger these compensatory responses in the heart are largely unknown. With the recognition that a single gene mutation can lead to dilated and/or hypertrophic cardiomyopathies, the strategies used to study these disorders has shifted towards molecular genetic methods (Chen and Chien 1999). In this section, the known pieces of the cardiomyopathy signaling pathway puzzle will be outlined.

1.3.4.1 Myocyte hypertrophy and the apoptotic pathway.

In response to a variety of stimuli that provoke both biochemical and mechanical stress to the heart, the myocardium responds by enlarging the individual myofibers, increasing wall thickness and increasing the ventricular cavity in order to sustain the heart's performance (Elliott 2000). The triggering mechanism for the progression from cardiac hypertrophy and/or ventricular dilation to heart failure and sudden death is not fully understood, but many observations indicate that programmed cell death could make a major contribution.Volume overload and increased diastolic pressure in the left ventricle have been described as initiating events for myocytic apoptosis (Cheng, Li et al. 1995), among other injuries such as ischemia, reperfusion and myocardial infarction (Kajstura, Cheng et al. 1996; Kajstura, Cheng et al. 1996). Due to the maladaptive process of sustained cardiac hypertrophy, and the lack of proliferation of adult cardiomyocytes (Beltrami, Urbanek et al. 2001), the biological signaling pathway leading to the enlargement of the cardiomyocytes remains at the center of attention for future therapeutic approaches. Traditionally, these processes have been indicated as biological circuits that are not mutually exclusive. An example of this line of interpretation comes from the analysis of the signal pathways mediated by the guanidine nucleotide-binding proteins G_q family, which transduce signals from a variety of membrane receptors to generate tissue specific responses (Simon, Strathmann et al. 1991). In cardiomyocytes, G_q receptor agonists such as catecholamine, angiotensin II or endothelin-1 bind the extracellular domain of the receptors and initiate the activation of specific cytoplasmic signals. M.G. Davis' group has shown that moderate overexpression of G_q receptors in cultured cardiomyocytes induces a stable form of hypertrophy with normal cardiac function, while substantial overexpression of these receptors induces a remarkable dilation of both ventricles, associated with a high incident of myocytic apoptosis in response to stress conditions (Adams, Sakata et al. 1998). The new identification of additional signaling pathways that are involved in the enlargement of the cardiomyocytes has provided a more accurate view of this model, in which initial signaling exerts an early hypertrophic remodeling phase, often characterised by stable and normal cardiac function. Failure of survival signaling to inhibit myocytic apoptosis ultimately

initiates a critical step towards severe cardiac dysfunction, ventricular dilation and finally a loss of contractile force associated with sudden death (van Empel and De Windt 2004). Cardiotropin-1 protein has been indicated as one of the most potent myocyte survival factors identified to date (Chen and Chien 1999). It functions through gp130/leukemia inhibitory factor LIF and STAT signaling to enhance the survival of myocytes during stress conditions. Using Cre/loxP gene targeting technology, mice deficient for cardiac gp130 showed normal cardiac function under baseline conditions, but rapid dilated cardiomyopathy associated with increased apoptotic index in response to the same mild stress conditions. On the other hand, wild type mice developed mild hypertrophy without compromise to the normal performance and function of the heart under the same conditions (Yoshida, Taga et al. 1996).

1.3.4.2 Cytoskeletal pathway and dilated cardiomyopathy.

Effective muscle contraction requires the generation of mechanical force by the sarcomere, and transmission of this force from the sarcomere to the cytoskeleton and extracellular matrix. In all striated muscle, mechanical force is in part transmitted to the extracellular matrix through lateral cell-matrix junctions (costameres) (Franz, Muller et al. 2001). Although early molecular findings suggest that unsuccessful force transmission is the essential cause for myocyte dysfunction in DCM patients (Chen and Chien 1999), more recent studies have revealed that abnormal sarcomere structure may lead to the development of DCM. The believed mechanism by which costamere alterations and sarcomere abnormalities diminished cardiac contraction is through ineffective force propagation from the sarcomere to the extracellular matrix. Deficits in force transmission would initiate compensatory responses in the myocardium that result in cardiac remodeling in an ultimate effort by the heart to sustain its systolic function (Ahmad, Seidman et al. 2005). It has been shown that weakened myocytes, derived from inactivation of structural sarcomeric or cytoskeletal proteins, are more susceptible to apoptosis. The premature death of these cells reduces the contractile function and triggers pathways for cardiac remodeling (Arber, Hunter et al. 1997). Moreover, genetic disruption of genes that encode for actin-associated cytoskeletal muscle protein (LIM) or

intermediate filament desmin, disrupted normal myocyte architecture causing cardiomyocyte degeneration and death (Milner, Weitzer et al. 1996). Although little is known about the inactivation of sarcomere proteins and the molecular pathways that associate with the remodeling response, evidence suggests that a fundamental role could be played by Ca^{2+} molecules. Investigations of non-genetic related cardiac hypertrophy and dilation indicate that angiotensin II mediates the expansion of cardiomyocytes in culture by causing changes in Ca^{2+} concentration (Ito, Kagaya et al. 1997). Recent studies on the expression and function of calcineurin A, a calcium dependent phosphate, also suggest that Ca^{2+} could may activate the cardiac hypertrophy signaling pathway. In fact, overexpression of calcineurin A in the murine heart specifically causes dephosphorylation and nuclear translocation of NF-AT3. NF-AT3 is a transcription factor that selectively induces the transcription of genes involved in cell growth, such as GATA4. Treatment with cyclosporine A, a calcineurin inhibitor, completely abrogates the hypertropic response observed in these transgenic mice (Molkentin, Lu et al. 1998). Additional evidence for the role of calcium in myocyte growth and hypertrophy pathways comes from genetic studies on myosin filaments. Normally, cardiomyocytes respond to calcineurin A inhibition by increasing their calcium levels (Fatkin, McConnell et al. 2000). Interestingly, a specific point mutation into the myosin head in position 403 fails to elevate free intracellular calcium within the myocyte's cytosol and, surprisingly, the hypertrophic process is markedly increased when cyclosporine is given to mutant mice (Fatkin, McConnell et al. 2000). Given the fundamental role of Ca^{2+} ions in the contraction-relaxation process of the myocardium, Fatkin and colleagues speculate that this mutation may increase calcium uptake into the sarcomere, hence, the depletion of this ion occurs in the sarcoplasmic reticulum. Calcium imbalance might then activates signals for hypertrophic growth (Fatkin, McConnell et al. 2000).

1.3.4.3 PI3K-Akt axis and TNF-α-NFk-B pathways.

The phosphoinositide 3-kinase (PI3K)-Akt pathway is implicated in many important *in vivo* biological responses such as growth, organ size, trafficking, cytoskeletal organisation and apoptosis

(Toker and Cantley 1997; Conlon and Raff 1999). In particular, insulin-like growth factor-1 (IGF-1) and its downstream effectors play an important role in controlling tissue proliferation and organ size (DeChiara, Efstratiadis et al. 1990). The PI3K pathway is a downstream effector of the IGF-1 receptor, and the best characterised targets of PI3K kinase are Bad and procaspase-9 (Alessi and Cohen 1998). Transgenic mice harboring constitutive expression of IGF-1 suffer cardiac hypertrophy, which gradually leads to a reduction in the heart's performance and sudden death of the mutant mice (Delaughter, Taffet et al. 1999). An example of the survival capacity of this pathway was shown by Wu et al. in 2000. Neonatal cardiomyocytes were infected with an adenoviral vector which carried a constitutively active form of PI3K. They were able to show that activation of the serine/threonine kinase Akt can directly phosphorylate both Bad and caspase-9 proteins, inhibiting their pro-apoptotic functions and therefore promoting the survival of cardiomyocytes (Wu, Lee et al. 2000). However, subsequent studies have suggested that the phosphorylation of Bad in cardiomyocytes upon Akt activation remains debatable; indicating that pro-survival functions of PI3K in the heart may not be restrained exclusively to Bad phosphorylation. Nevertheless, PI3K is intimately involved in the hypertrophic response of the myocardium *in vivo,* and also plays an important role in the cellular survival of myocytes.

Cytokines are deeply involved in the inflammation process, and tumor necrosis factor α (TNF-α) has been shown to accumulate in heart tissues after myocardial infarction (Meldrum 1998). TNF-α can induce both myocardial hypertrophy and apoptosis in neonatal rat cardiomyocytes *in vitro*. In particular, transgenic mice engineered to over-express a secreted form of TNF-α develop hypertrophy which progressively becomes a dilated cardiomyopathy over time (Kubota, McTiernan et al. 1997). TNF-α has been shown in different cell types to activate its receptor (TNFR) and directly provoke caspase 8 and NFk-B activation (Micheau and Tschopp 2003). Transgenic mice with restricted cardiomyocyte TNF-α over-expression, also develop cardiac inflammation, left ventricular dilation and heart failure (Sivasubramanian, Coker et al. 2001). Expression analysis of the pro-apoptotic target genes of NFk-B, such as FAS ligand, RIP and caspase-8, has revealed

activation of the programmed cell death signaling pathway in these animals (Sivasubramanian, Coker et al. 2001). However, activation of the NFk-B pathway has not been studied in detail in cardiovascular remodeling events. It is only recently that transgenic mouse models have been generated and they shown a fundamental role of NFk-B in cell growth and the survival of myocytes in cardiac remodeling processes (Sawa, Morishita et al. 1997; Purcell, Tang et al. 2001; Kupatt, Wichels et al. 2002). For instance, the Purcell group showed that a dominant negative form of NFk-B prevents several features of cardiac hypertrophy in response to $G\alpha_q$ agonists, indicating the involvement of NF-kB in the hypertrophic response (Purcell, Tang et al. 2001). However, *in vivo* transfection of molecules that selectively reduce NFk-B's function results in a reduction in reperfusion damage, suggesting a pro-apoptotic function for NFk-B. The ambivalent character of NFk-B in cellular survival signalling pathways complicates our understanding of this protein's role in the remodeling process of the heart.

1.3.4.4.Wnt/β-catenin signaling pathway in heart.

Signaling by the Wnt family of secreted glycoproteins is involved in diverse cellular responses such as cell proliferation, differentiation, apoptosis and polarity (Melkonyan, Chang et al. 1997; Smalley and Dale 1999). The Wnt signaling pathway has been also described as affecting cardiac development and morphogenesis, and several members of the Wnt pathways have been found to be abundantly expressed in adult heart (Schneider and Mercola 2001; Brade, Manner et al. 2006). Under pathological stress conditions, the heart reactivates a number of signaling pathways, which were originally activated only during embryogenesis. In fact, atrial nautrietic peptide (ANP), a widely established marker for the indication of cardiac hypertrophy and heart failure, is expressed during cardiomyopathies (Nikolova, Leimena et al. 2004). As Wnt signaling is primarily described as a cellular pathway involved during embryogenesis, it is possible that during cardiac remodeling Wnt/β-catenin signaling can be re-activated. In agreement with this hypothesis, it has been shown that the expression of co-receptor frizzled-2 (Fz-2), an important player to activate the canonical Wnt/β-catenin pathway, is upregulated during cardiac hypertrophy (Blankesteijn, Essers-Janssen et

al. 1996). However, it is not yet clear how Fz-2 can activate the canonical signaling pathway, as it has been shown to couple preferentially to the non-canonical pathway (Kuhl, Sheldahl et al. 2000; Haq, Michael et al. 2003). Furthermore, Malekar et al. demonstrated that cardiac-specific overexpression of dishevelled (Dsh-1), a scoffold protein fundamental for the activation of the pathway, in pressure overload conditions leads to severe cardiomyopathy, supporting the idea that Wnt signaling is involved in cardiac remodeling processes (Malekar, Hagenmueller et al. 2010).

Finally, in hypertrophic heart and in most cardiomyopathies, intercalated disc structures have been shown to be disorganised (Ahmad, Seidman et al. 2005). β-catenin is an key mediator of the Wnt/β-catenin signaling pathway, but it is also a major component of adherens junctions. Mauselli et al. demonstrated that an accumulation of β-catenin in the area of the intercalated discs upon hyperthropic conditions is due to changes in GSK-3β activity (Masuelli, Bei et al. 2003). Plakoglobin, also know as γ-catenin, has structural and functional similarities to β-catenin (Moon, Bowerman et al. 2002), and has been shown to interact and compete at different cellular levels with β-catenin in repressing the canonical Wnt/β-catenin signaling pathway (Ben-Ze'ev and Geiger 1998; Klymkowsky, Williams et al. 1999; Zhurinsky, Shtutman et al. 2000). Finally, Garcia-Gras and colleagues have elegantly shown a possible link between the pathogenesis of ARVC and the translocation of plakoglobin into the nucleus, where it can activate the transcription of genes important for adipogenesis, fibrogenesis and myocyte apoptosis (Garcia-Gras, Lombardi et al. 2006).

1.3.5 Cardiotoxicity of anticancer drugs.

Recent advances in chemotherapy and anticancer drug discovery have substantially improved the prognosis of patients affected by solid and non-solid tumours (Albini, Pennesi et al. 2010; Raschi, Vasina et al. 2010). Cancer treatments, nowadays, involve the combination of classic chemotherapeutic drugs such as anthracycline, antibiotics or radiotherapy with surgery, to provide a cure and to prolong the life of the patients. However, a new generation of anticancer agents and

specific targeted therapies have recently born fruit: the so-called “molecular-target drugs” (Minami, Matsumoto et al. 2010). Most of these new anti-neoplastic drugs are either antibodies against cell surface proteins or small inhibitor molecules that block protein kinase receptors (i.e. HER2 and HER1/EGFR antibodies or imatinib). A patient who undergoes cancer therapy today will be subject to inevitable side-effects, some of which exert specific effects on the cardiovascular system (Albini, Pennesi et al. 2010; Minami, Matsumoto et al. 2010; Raschi, Vasina et al. 2010). In the past, this risk was less evident because the life span of patients with cancer in an advance state was often too short to make the cardiovascular complication of the treatment a matter of concern. However, now that huge progress have been made in terms of early diagnosis, therapy and survival of cancer patients, cadiotoxicity is a fundamental issue, as highlighted in several recent reviews (Force, Krause et al. 2007; Schmidinger, Zielinski et al. 2008; Minami, Matsumoto et al. 2010).

Cardiotoxicity is defined in very general terms as “toxicity that affects the heart” by the National Cancer Institute (www.cancer.gov/dictionary). An evaluation committee supervising the side effects of new chemotherapeutic drugs defines cardiotoxicity as one of the following: a reduction of left ventricular ejection fractions (LVEF), heart failure (HF) and associated symptoms such as tachycardia and arrhythmias or both (Seidman, Hudis et al. 2002). Cardiovascular side-effects can develop in an acute or chronic manner. Acute cadiotoxicity manifestations range from the occurrence of abnormalities to the repolarisation of the ventricles, and thus alterations of the electrocardiographic QT-interval which leads to arrhythmias and tachycardia events. Acute coronary syndromes and pericardytis are also observed as acute effects within 2 weeks after termination of the treatment (Dolci, Dominici et al. 2008). Chronic cardiotoxicity signs appear later than one year after termination of the chemotherapy, and the most typical manifestation is asymptomatic systolic and/or diastolic left ventricular dysfunction, which leads to the establishment of a cardiomyopathy that ultimately leads to heart failure (Dolci, Dominici et al. 2008; Albini, Pennesi et al. 2010). Briefly, anthracyclines such as doxorubicin can generate HF and LVEF dysfunction in a dose-dependent manner (Shan, Lincoff et al. 1996), through the regulation of the ubiquitin-dependent pathways of p300 and p53. p300, by its ubiquitin ligase activity, is partially

involved in the ubiquitin-dependent degradation of p53 in cardiac myocytes (Morimoto, Fujita et al. 2008). Trastuzumab, a monoclonal antibody specific for the HER2 receptor protein, results in the establishment of dilated cardiomyopathy and heart failure (Popat and Smith 2008). Myocardial fibrosis, valvular heart disease and endothelial cell damage can occur following thorax radiation therapy. Finally, tyrosine kinase inhibitors such as imatinib, widely used to treat chronic myelogenous leukemia patients, shows both acute and chronic cardiotoxicity effects. In particular, patients treated with imatinib show congestive HF associated with left ventricular contractile dysfunction and cardiomyocyte loss (Kerkela, Grazette et al. 2006). However, the mechanisms of cardiotoxicity vary widely among diverse chemotherapeutics and are not clearly understood. Table 1.1 summarises the potential mechanisms and the cardiovascular damage induced by widely used solid and non-solid anticancer treatment.

Chemotherapeutics	Cardiovascular damage	Possible mechanism
Cytotoxic agents:		
Anthracyclines antibiotics *(Doxorubicin, daunorubicin, epirubicin)*	CHF, LVD, acute myocarditis, arrhythmia	Enhance apoptosis by DNA damage, ATP mitochondrial block, apoptosis protein release and ROS generation
(5-fluorouracil, capecitabine, cytarabine)	Ischemia, CHF, perycarditis, cardiogenic shock	Enhance DNA damage
(paclitaxes and taxes compounds)	Ventricular tachycardia, atrioventricular block, CHF and ischemia	Enhance DNA damage
Molecular-target agents:		
(HER2 and HER1/EGFR antibodies) *(Trastuzumab and bevacizumab)*	Arrthymias, CHF, angioedema and LVD	Possible cell signalling survival block and endothelial damage.
(HER2 and HER1/EGFR tyrosine kinase inhibitor) *(lapatimib, sorafenib, sunitinib)*	Arrthymias, hypertension, LVD	Possible cell signalling survival block and endothelial damage.
(imatinib)	CHF, LVD, arrythmias, periorbital and peripheral edema	ATP block, apoptosis enhancment and possible cell signalling survival block
Radiotherapy: *(thorox radiation)*	Myocardial fibrosis, LVD and valvular disease	Enhance DNA damage, ROS generation and possible apoptosis enhancement

Table 1.3. Cardiovascular damage and possible mechanisms induced by anticancer treatments. CHF= congestive heart failure, LVD=left ventricular dysfunction. For references see review (Minami, Matsumoto et al. 2010)

1.4 Mammalian skin: overview.

At the surface of the body, skin and its appendages form the soft outer layer that protects us from environmental insults of different natures. Because it interfaces with the environment, skin plays a key role in protecting organisms, mainly by keeping the microbes out and essential body fluids in. It is subject to mechanical, chemical and biological assaults everyday and confronts these attacks by undergoing a constant self-renewal process to repair damaged tissue or to replace old cells. It is composed of three different layers, and in this concise introduction the epidermal appendage of the hair follicle will first be described, before briefly introducing the structure and the regeneration process of mouse epidermis with particular emphasis on its key regulator p63.

1.4.1 Hair follicles: structure and development.

One of the typical features of mammals is that the outer surface of their bodies is covered with hair. This hair contributes to an extensive range of functions including thermal insulation, camouflage or sensory activity and, in the modern human world, even social interactions. Hairs are composed of an upper part and lower parts. The upper "permanent" part does not cycle, and is divided into the so-called infundibulum and isthmus *(figure 1.11)*. The infundibulum is the opening of the hair canal to the epidermis, while the isthmus is the region where the erector pili muscle is inserted (Paus and Cotsarelis 1999). The lower "cycling" part represents the actual hair shaft "factory" and consists of the suprabulbar region and the hair follicle bulb (Paus and Cotsarelis 1999). The lower part of the isthmus also harbours the bulge region which contains epithelial and melanocytic stem cells *(figure 1.11)*. It is thanks to this pool of cells that the hair follicle can undergo an almost unlimited cycles of degeneration and regeneration throughout life (Cotsarelis, Sun et al. 1990). The hair follicle bulb contains matrix keratinocytes and the hair follicle pigmentation unit. Matrix cells are referred as trans-amplifying cells, which migrate from the bulge area to colonise the lower part of the hair follicle bulb. They are the key players in the renewal capacity of the hair follicle

(Schneider, Schmidt-Ullrich et al. 2009). When matrix cells stop proliferating, they terminally differentiate into various cell lineages within the hair shaft and are disposed of, typically, in concentric layers *(figure 1.11)*. These cell lineages express different keratins as differentiation markers (Schneider, Schmidt-Ullrich et al. 2009). Finally, the derma papilla has a mesenchymal-derived origin that differs from the ectodermal origin of the bulge and hair follicle bulb (Stenn and Paus 2001). In fact, the derma papilla consists of densely packed fibroblasts and has a pivotal role in hair formation, growth and cycling, in particular on the length and duration of the growing phase of the hair follicles outlined below (Paus and Foitzik 2004).

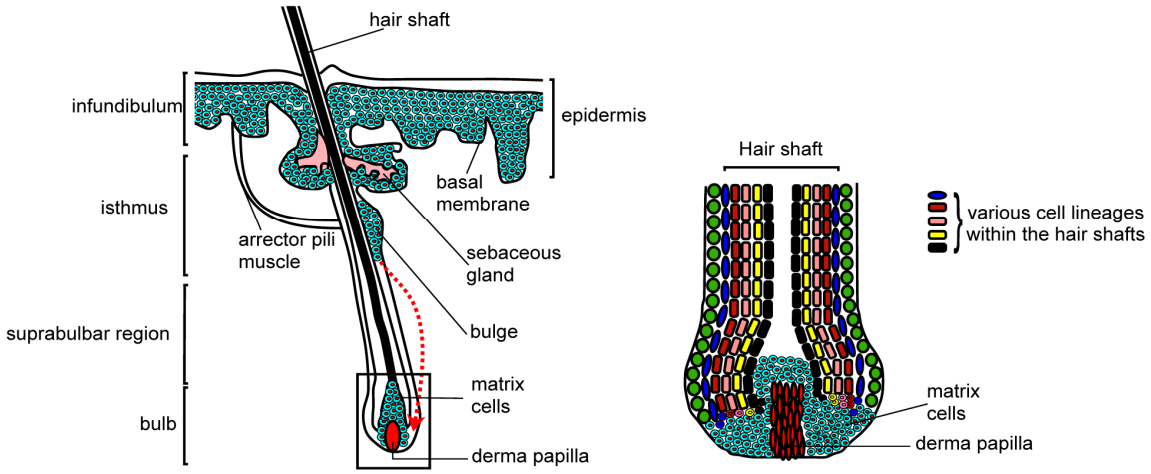


Figure 1.11. Hair follicle structure. Diagram (left) shows a cross-section of a hair follicle. The upper section of the diagram shows the "permanent" part of the hair follicle which consists of the so-called infundibulum and isthmus. The anagen-associated components instead (suprabulbar and bulb region) are the actual hair follicle factory. At the bottom of the follicle is the hair bulb, made from proliferating matrix cells which terminally differentiate to generate the various cell types of the hair follicle (right). Also shown is the bulge area, where epidermal stem-cells reside. Bulge stem cells migrate towards the hair follicle bulb where they proliferate and initiate a new hair follicle cycle (red dotted line). Schematic drawing (right) illustrating the different concentric cells layers of the hair shaft in within the bulb.

The hair follicle is, together with the epidermis, one of the few organs in the human body to undergo cyclic rounds of degeneration and regeneration. The different phases of the hair follicle cycle are summarised in figure 1.12. Briefly, the hair follicle cycle starts with the degenerative

phase, called catagen, during which matrix cells that populate the hair follicle bulb rapidly decline in numbers and the hair follicle undergoes apoptosis and regression. The catagen phase is a highly regulated event and the purpose of this part of the hair cycle is to delete the old hair shaft factory and influence the stem cell compartment of the bulge to set the stage for the formation of a new follicle (Fuchs 2007). Towards the end of the catagen stage, the dermal papilla condenses and moves upward, coming to a rest beneath the hair follicle bulge, and the hair follicles enters a phase of relative quiescence called the telogen phase. This part of the cycle can last several days after the first hair cycle, and more than three weeks in adults. After the resting phase, when a complicated threshold of different activating factors is reached, stem cells move from the bulge area of the hair follicle to reach the derma papilla and initiate the growing or so called anagen stage of the hair follicle cycle (Paus and Cotsarelis 1999). In the anagen phase, matrix keratinocytes present in the bulb area proliferate and differentiate into several different epithelial hair lineages (Legue and Nicolas 2005).

The molecular pathway that control the hair follicle cycle remains obscure, however, by characterising the gene expression profile of different transgenic mice that present abnormal fur phenotypes, multiple regulators have been recently identified (Lin, Chudova et al. 2004; Paus and Foitzik 2004). In fact, using KO technologies it has been demonstrated that Wnt/β-catenin and its downstream target effector sonic hedgehog (Shh), in association with Bone Morphogenetic Protein (BMP) antagonists such as noggin, are inducers of the anagen phase (St-Jacques, Dassule et al. 1998; Botchkarev, Botchkareva et al. 1999; DasGupta and Fuchs 1999). In addition FGF5, TGF-β1, TNF-α and BMP-2 and -4 have all been implicated in the induction of the catagen phase (Paus and Foitzik 2004). Recently, the interaction between TNF-α and keratin 17 has been demonstrated to be responsible, at least in part, for controlling some aspects of the regression phase by regulating the rate of apoptosis (Tong and Coulombe 2006). Finally, although described as the resting or quiescent phase of the hair follicle cycle, telogen phase coincides with major alterations in gene activity (Lin, Chudova et al. 2004). For instance, the estrogen receptor is markedly up-regulated during the telogen phase and Wnt/β-catenin signaling is switched on but reaches its optimal activity in the

anagen phase while, on the other hand, the BMP signaling pathway is turn off (Ohnemus, Uenalan et al. 2006; Plikus, Mayer et al. 2008).

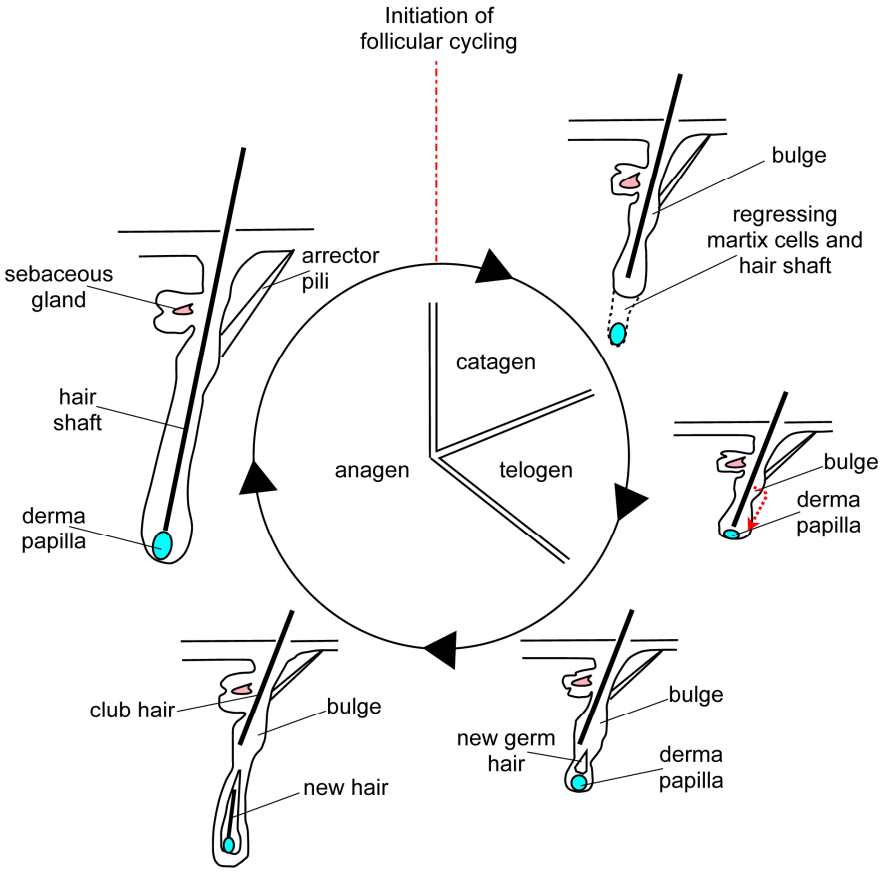


Figure 1.12. Different stages of the hair follicle cycle. The hair cycle is divided into three phases: anagen (growth phase), catagen (regression phase) and telogen (resting phase). Once the hair follicle has matured, it enters the regression phase *(initiation of the follicular cycle)* where two-thirds of the hair follicle rapidly regress, mainly due to apoptosis of matrix and hair shaft keratinocytes *(catagen)*. Eventually, the derma papilla comes into close proximity of the bulge area, where bulge stem-cells can re-populate the bulb *(red dot line)* and re-start the growing phase of the follicle. The proximity between the bulge area and derma papilla is maintained throughout the resting phase *(telogen)*. Only when a critical concentration of hair growth signals is reached, anagen phase is entered and a new hair is grown.

1.4.2 Epidermis and the stratification process.

The skin serves as protective armour for the body. Mammalian skin is composed of three different layers: the epidermis, which serves as a protective barrier from dehydration and from a variety of

different environmental insults; the dermis, which consists of connective tissue and provides the site for the skin organelles; and the hypodermis, which is the subcutaneous adipose layer.

The epidermis is the outer part of the skin and consists of multilayered stratified squamous epithelium, divided from the underlying dermis by a basal lamina *(figure 1.13)*. The epidermis must be sturdy and resilient in order to oppose the physical and chemical traumas of each passing day. It must keep pathogens and microorganisms out and important fluids in, and receives daily injuries including UV radiation from the sun or mechanical attacks such as wounds or scratches. It copes with these insults by undergoing self-regeneration cycles, thanks to a pool of epidermal stem cells located in the portion of the hair follicle known as the bulge (Fuchs 2007). These stem cells can give rise not only to the epidermis, but also to the hair follicle and other skin appendices (Taylor, Lehrer et al. 2000; Oshima, Rochat et al. 2001). Progeny of the stem cells exit the bulge area and migrate upwards to populate the inner-most layer (basal layer) of the epidermis. However, a subset of epidermal stem cells seems to directly populate the basal layer (Lechler and Fuchs 2005).

Most cells within the basal layer are rapidly proliferating cells, referred to as transamplified cells, which undergo a limited number of divisions before they withdraw from the cell cycle and commit to terminal differentiation (Fuchs 2007). In fact, the epidermis is mainly composed of self-renewing keratinocytes, which detach from the inner basal layer and migrate towards the outer cornified layer, where they became terminally differentiated and provide a physical barrier to the organism's external environment (Candi, Cipollone et al. 2008; Descargues, Sil et al. 2008). During the stratification process, keratinocytes change their morphology to an association of flattened (squamous) dead cells, which remains in the most outer layer of the skin, where they will be sloughed off and replaced by inner cells that continuously move outwards (Barrandon and Green 1987) *(figure 1.13)*.

This constant replacement of cells is due to a tight balance between proliferation and differentiation signals. In particular, the existence of epidermal stem cells and transient amplifying cells in the basal layer of the epidermis allows the epidermis to stratify into various differentiated layers until it forms the stratum corneum (SC) (Candi, Cipollone et al. 2008). Basal layer (BL) keratinocytes form

the mitotically active layer of the epidermis, characterised by the expression of proliferation markers such as keratin 14 (K14) and keratin 5 (K5) (Tomic-Canic, Komine et al. 1998). As cells leave the basal layer, they change their protein expression profile from K14 and K5 to keratin 1 (K1) and keratin 10 (K10) (Fuchs et al., 1980), and commit themselves to become terminally differentiated keratinocytes. This switch in transcription profile was discovered more than 20 years ago, and remains the most reliable signal that a keratinocyte will undergo terminal differentiation and move towards the SC (Fuchs and Green 1980). The first suprabasal differentiation layer is called the spinous layer (Sp) and is where keratin filaments start to bundle together to initiate a robust cell-cell junction network, which not only provides the intracellular framework for their migration, but also regulates cell proliferation by activating different signal pathways that include p63, mTor/akt and notch (Fuchs 2007). As the spinous layer progresses towards terminal differentiation, keratinocytes start producing electron-dense keratin granules together with profilagrin which, when activated, starts processing bundle of intermediate filaments into microfibrillar “cables” (Fuchs 2007). Given the particular look that the granular keratin gives to this layer, it takes the name of the granular layer (Gr). The final step of differentiation involves the elimination of all cellular organelles, including the nucleus and the activation of transaglutaminase, to create the hydrophobic scaffold of the cornified layer. The dead stratum corneum produces the physical seal that is constantly replaced by keratinocytes, which moves forward from the basal layer of the epidermis.

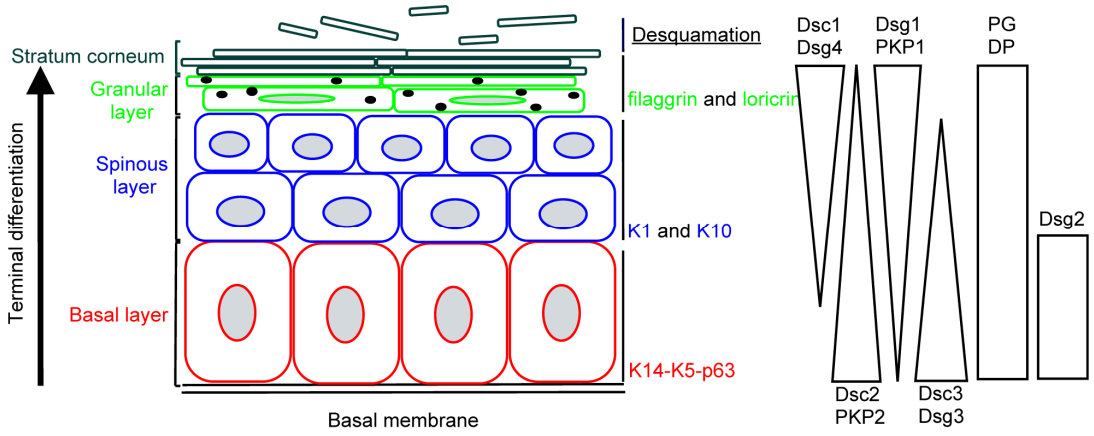


Figure 1.13. Schematic representation of the different cellular layers in the epidermis and the expression pattern of desmosomal components.
The epidermis is a stratified squamous epithelium that is composed of several different cell layers. Each layer is characterised by expression of different molecular markers. Cells of the basal layer (red) are attached to the basal membrane. They are mitotically active cells which express K14, K5 and p63. The basal layer stratifies into the spinous layer (blue), where transit-amplifying cells exit the cell cycle and proceed towards keratinocyte terminal differentiation by changing their keratin expression profile from K14-K5 to K10-K1. The granular layer (green) consists of terminally differentiated keratinocytes that produce electron-dense keratin granules together with profilagrin which, when activated, starts to process bundles of intermediate filaments into microfibrillar "cables" in order to gain resilience against mechanical stress. Granular layer markers are loricrin and fillagrin. Finally, cells that reach the body surface (gray) are dead, enucleated and flattened, and consist of the cornified protective epidermal layer. These cells are constantly sloughed off and are continually replaced by inner cells that move outwards. The profile and relative expression level of various desmosomal proteins in the epidermal layers are depicted on the right.

1.4.2.1 p63 expression is essential for epithelial development.

To coordinate the changes in gene expression that occur in the basal/spinous and terminally differentiated layers, important transcription factors have been identified. p63 has been demonstrated to play a fundamental role in regulating the self-renewal and long-term proliferative capacity of the basal layer of the epidermis. The idea that the *TP63* gene is involved in the formation and establishment of multilayer stratified epithelia first arose from two pieces of evidence. First, the genetic deletion of the *TP63* gene from the mouse genome resulted in late embryonic lethality caused by deficiency of all squamous epithelial organs, including the skin and prostate. In addition, mice lacking the *TP63* gene did not develop epithelial appendices such as salivary, lachrymal and mammary glands. Pups lacking p63 expression also showed truncated limbs

and abnormal craniofacial development due to the absence of the functional ectodermal ridge, which is of fundamental importance for epithelial-mesenchymal interactions (Mills, Zheng et al. 1999; Yang, Schweitzer et al. 1999). Secondly, particular type of ectodermal dysplasia (ED) find in humans result from mutations in the *TP63* genetic locus, however nearly 200 different conditions have been described under the term ED and not all show p63 gene alterations (Mikkola 2009; Koster 2010). These finding indicate that p63 is essential for maintaining the regenerative cell populations necessary to sustain epithelial development and stratification in stratified epithelia (Candi, Cipollone et al. 2008). However, how p63 contributes to epidermal formation and the underlying signalling pathway(s) is still under investigation (Candi, Cipollone et al. 2008). The presence of six different p63 isoforms is one of the reasons why the puzzle is not yet been solved. As previously mentioned, the human and mouse *TP63* gene can be transcribed from two different promoters *(figure 1.2)* to create two different subsets of p63 proteins with different properties and functions (Yang and McKeon 2000). However, it has already been noted that both isoforms are able to regulate the transcription of different target genes important for proliferation, differentiation and cell adhesion (Carroll, Carroll et al. 2006). The DBD and the OD are the key domains for the activity of all p63 isoforms. Is not yet possible to assign a specific function to particular p63 isoforms (Candi, Cipollone et al. 2008), however, messenger RNA for both TAp63 and ΔNp63 has been detected in both human and mouse epithelial tissues, with an almost exclusive presence of ΔNp63 isoforms at the protein level (Laurikkala, Mikkola et al. 2006). Quantitative studies performed on various mouse epidermal tissues, using different p63 antibodies raised against diverse protein domains, have demonstrated that ΔNp63α is strongly expressed in proliferating keratinocytes in the basal layer and that its expression is reduced in the terminally differentiated layer of the epidermis (Nylander, Vojtesek et al. 2002). On the other hand, whether TAp63 expression contributes to the correct formation of stratified epithelia remains under debate. Indeed, mRNA encoding a full-length TAp63 isoform has been detected both in mouse embryos at E13.5 and in mature skin, although it only accounts for 1% of the total mRNA presence at that embryonic stage (Laurikkala, Mikkola et al. 2006). An elegant approached used by Candi and colleagues, in

2007, tried to solve this controversy. They complemented p63-null mice by expressing both TA- and ΔN- isoforms under the control of a K5 promoter. In this way, they generated mice that expressed only one p63 isoform in the epidermis. Analyses of the transgenic mice complemented with ΔNp63 ($p63^{-/-}$;ΔN) revealed substantial epidermal basal layer formation, while transgenic mice complemented with TAp63 ($p63^{-/-}$;TA) did not differ much from p63 KO mice (Candi, Rufini et al. 2006). The authors of this study suggested that TA's contribution to epidermal formation is only concomitant or subsequent to the function of ΔNp63 (Candi, Rufini et al. 2006). In the same study, transcriptional analysis of p63 target genes in Saos-2 cells demonstrated that TA isoforms mainly regulates the expression of terminal differentiation markers such as K1, K10, envoplakin or involucrin, while ΔN- mainly regulates basal layer markers such as K14 (Candi, Rufini et al. 2006). These data suggest that ΔNp63 isoforms play a pivotal role in maintaining the proliferative capacity of the basal layer, while TA- isoforms are mainly involved in the terminal differentiation program (Candi, Rufini et al. 2006). Recently, using KO technology, Su et al. demonstrated that mice that lose TAp63 expression develop blisters, ulcerated wounds and surprisingly accelerated ageing (Su, Paris et al. 2009). This phenotype was linked with the depletion of the epidermal stem-cell compartment that resides into the hair follicle bulge. Hence, loss of TAp63 led to hyperproliferation, senescence, genomic instability and premature senescence, indicating that TA isoforms could serve to maintain adult tissue stem cells (Su, Paris et al. 2009). In addition, another report proposed TAp63 to be a potent tumour suppressor *in vivo* (Guo, Keyes et al. 2009). Using a specific inducible KO mouse model for TAp63 expression, they demonstrated that an absence of TAp63 increases proliferation and enhances Ras-mediated oncogenesis. Moreover, they showed that TAp63 is required to induce cellular senescence and thus to halt tumourigenesis in epithelial tissues (Guo, Keyes et al. 2009). For a long time, it was thought that ΔNp63 was not able to transactivate gene expression since it does not posses the TA domain needed for p53 family members to activate transcription. Its accepted activity was only to act as a dominant negative protein on TAp63 isoforms (Yang, Kaghad et al. 1998), although, ΔN-isoforms could also activate transcription due to a second transactivation domain found in their C-termini (Dohn, Zhang et al.

2001; King, Ponnamperuma et al. 2003). Several approaches have been used to identify p63 target genes including microarray analyses (Carroll, Carroll et al. 2006; Testoni, Borrelli et al. 2006), *in vivo* complementation systems (Candi, Rufini et al. 2006) or chromatin immunoprecipitation analyses (ChIP) (Perez, Ott et al. 2007). However, only a few of the genes identified to date have been validated as mediating an effect on epithelial stratification. In proliferating primary keratinocytes, 14-3-3σ and $p21^{waf1/CIP1}$ have been shown to be directly down-regulated by ΔNp63 (Westfall, Mays et al. 2003), while K14 expression is maintained by the presence of ΔN isoforms (King, Ponnamperuma et al. 2003). IkB kinase-α (IKK-α) is also a p63 target gene, and it is essential for the correct development of stratified epithelia (Sil, Maeda et al. 2004). In some *in vitro* experimental assays, TAp63 and ΔNp63 can regulate IKK-α, directly (for TAp63) or indirectly (for ΔNp63) (Candi, Terrinoni et al. 2006), complicating even more the understanding of the different roles of TA- or ΔN- isoforms.

An additional signaling pathway crucial for epidermal stratification and keratinocyte differentiation is the Notch signaling pathway. Notch received its notoriety as a result of analyses of lethal loss-of-function mutations in embryos. These mutations produced a "neurogenic" phenotype, where cells destined to become the epidermis switched fate and instead gave rise to neural tissue. This was the first evidence that notch signaling is important for keratinocyte differentiation. Notch signaling has been implicated in late stages of epidermal differentiation, in particular, Blanpain and colleagues demonstrated using a loss and gain of function approaches that notch signaling is required at the basal/suprabasal juncture to induce the differentiation of basal keratinocyte into spinous layer cells, hence to down-regulate basal fate (Blanpain, Lowry et al. 2006). Moreover, other evidence indicates that p63 functions as a modulator of notch-1 and its ligand Jagg-1 (Sasaki, Ishida et al. 2002). However the role of p63 in the regulation of notch is not clear.

1.5 Aim of the study.

The aim of this thesis is to elucidate the molecular details of the biological role of iASPP *in vivo* using a conditional knockout (KO) mouse model system focusing, in particular, on the heart and epidermal biology. Our approach differs from the natural iASPP-deleted Wa3 mouse by the presence of two loxP sequence within iASPP genetic locus which can be excise in a precise spatial/temporal manner. Our mouse model system also provides the opportunity to generate primary cell lines from different mouse tissues in order to investigate the molecular mechanism(s) that iASPP deletion may affect.

Firstly, the generation of the iASPP conditional KO mouse is described and verified by employing both *in vitro* cellular systems and *in vivo* expression studies. Using primary mouse embryonic fibroblasts (MEFs) originating from iASPP transgenic embryos, we have been able to understand whether our Cre/loxP inducible system for the excision of iASPP exon 8 results in a substantial reduction of iASPP protein expression *in vitro* and *in vivo*.

Secondly, as iASPP was known to be involve in the pathogenesis of cardiocutaneous-like disorders such as Naxos and Carvajal syndromes in humans or in the cardiomyopathy and woolly haircoat syndrome (CWH) of Poll Hereford cattle, details analysis of the cardiomyopathy and the epidermal phenotype development showed by iASPP KO progeny will be investigated both in embryonic, young and adult mice, in order to elucidate a potential molecular mechanism.

Finally, as one of the most well-known functions of iASPP is to interact with and inhibit the apoptotic function of p53 and its family members, the molecular contribution of p53- or p63 alleles to the iASPP null phenotype will be investigated.

Chapter 2
Materials and Methods

2.1 Animals.

Mice were bred and housed in the British Heart Foundation functional genetics facility in the Henry Wellcome Building of Genomic Medicine. They were kept in IVC cages which had a sealed lid that acts as second part of the two-barrier system. Procedures were carried out following the Home Office Animals (Scientific Procedures) Act 1986 (PIL: 70/20068; PPL: 70/06380) guidelines. iASPP$^{flox/flox}$ mice were generated by inGenius laboratory. CMV-Cre^{+} mice were previously described (Schwenk, Baron et al. 1995) and were a kind gift from Dr Bart Vanhaesebroeck. All mice used in the present study were on a C57BL/6 (B6) and 129Sv mixed genetic background. In all experiments, littermates of each conditional knockout mouse were used as a wild type control for that line, and are simply referred to as wild type.

2.2 Breeding.

The mating strategy to obtain iASPP$^{flox/flox}$;Cre^{+} mice is summarised in Fig. 2.1. The first round of crossing gave rise to an F1 progeny heterozygous for the iASPP "flox" locus, and either negative or positive for the presence of the Cre expression gene (iASPP$^{flox/wt}$;Cre$^{\pm}$). Progeny were genotyped to confirmed heterozygosity at the iASPP "flox" locus and to identify Cre^{+} mice. iASPP$^{flox/+}$;Cre^{+} were renamed iASPP$^{\Delta 8/+}$ and back-crossed together in order to obtain iASPP$^{flox/flox}$;Cre^{+} progeny which were investigated and renamed iASPP$^{\Delta 8/\Delta 8}$.

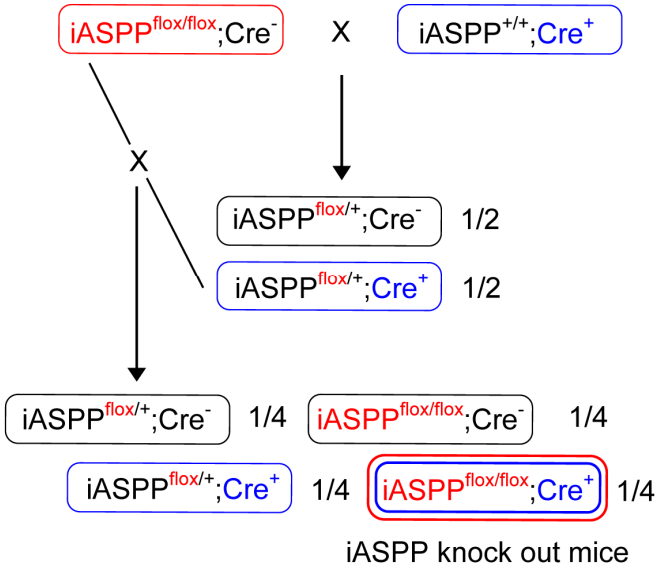


Figure 2.1. Schematic representation of breeding strategy of iASPP$^{flox/flox}$ with CMV-Cre^{+} mice. iASPP$^{flox/flox}$ (iASPP$^{flox/flox}$;Cre^{-}) were crossed with CMV-Cre+ mice (iASPP$^{+/+}$;Cre^{+}) in order to obtain iASPP$^{flox/wt}$;Cre$^{\pm}$ mice. iASPP$^{flox/wt}$;Cre^{+} were renamed iASPP$^{\Delta 8/+}$ and back-crossed together to obtain iASPP$^{flox/flox}$;Cre^{+} progeny, which were investigated and renamed iASPP$^{\Delta 8/\Delta 8}$.

2.3 Genotyping.

2.3.1 DNA extraction from ear biopsies.

Mice were ear-punched for identification and the resulting tissue was used for genotyping. Ear tissue was digested overnight at 55ºC in 100µl of extraction buffer GNT and 7.8 mg/ml of proteinase K (Qiagen). The digested tissue was boiled for 10 min at 97ºC and 0.5µl used for polymerase chain reaction (PCR) analysis.

2.3.2 iASPP$^{flox/flox}$ genotyping.

DNA extracted from iASPP$^{flox/flox}$;Cre^{+} and iASPP$^{wt/wt}$;Cre^{+} mice was routinely amplified with Promega TAQ DNA polymerase (Promega, UK) using the following primers:

- FRNT9 5'-GGGTAGGAAAAAGGGCTGAG-3'
- FLP2 5'-CCGAATTGGAGAAGTGAAGC-3'

The products obtained were ~400 base pairs (bp) for iASPP$^{wt/wt}$ and 68 bp longer for iASPP$^{flox/flox}$. The thermal cycling conditions used were:

1. 94ºC, 5 min
2. 94ºC, 30 sec
3. 62ºC, 1 min
4. 72ºC, 30 sec
5. back to step 2. 30 cycles
6. 72ºC, 5 min

2.3.3 iASPP$^{\Delta 8/\Delta 8}$;Cre^{+} genotyping.

DNA extracted from iASPP$^{\Delta 8/\Delta 8}$ Cre^{+} and iASPP$^{wt/wt}$ Cre^{+} mice was routinely amplified with Promega TAQ DNA polymerase (Promega, UK) using the following primers:

- FLP2 5'-CCGAATTGGAGAAGTGAAGC-3'
- E8-2 5'-AGAGCAGCCTCAGAGCATGG-3'
- I8-2 5'-ACAGGCAGCTACTGGTATTC-3'

The products obtained were 600 bp for iASPP$^{wt/wt}$ and 800 bp long for iASPP$^{\Delta 8/\Delta 8}$. The thermal cycling conditions used were:

1. 94ºC, 5 min
2. 94ºC, 30 sec
3. 62ºC, 1 min
4. 72ºC, 30 sec
5. back to step 2. 30 cycles
6. 72ºC, 5 min

The Cre transgene was detected using specific primers:

- Cre-Fw 5'-CATTTGGGCCAGCTAAACAT-3'
- Cre-Rev 5'-ATTCTCCCACCGTCAGTACG-3'

PCR conditions used were:

1. 94ºC, 5 min

2. 94ºC, 30 sec

3. 62ºC, 30 sec

4. 72ºC, 1 min

5. back to step 2. 30 cycles

6. 72ºC, 5 min.

2.4 Materials.

2.4.1 Reagents.

All chemicals, unless otherwise stated, were obtained from Sigma (Sigma, MO, USA) or BDH Chemicals (UK). All autoradiography films (Hyperfilm) and ECL (Enhanced Chemical Luminescence) reagents were purchased from Amersham Pharmacia Biotech (UK). Nitrocellulose membrane was purchased from Whatman, Germany. All restriction enzymes, and their buffers, were purchased from New England Biolabs (UK). All tissue culture dishes and flasks were obtained from Geiner (UK).

The RNeasy midi kits were purchased from Qiagen (UK).

5X Agarose Sample Buffer

50% (w/v)	Sucrose
100mM	EDTA, pH 8.0
0.1% (w/v)	Bromophenol Blue
0.1% (w/v)	Xylene

Agarose Gel for DNA Electrophoresis

Agarose powder (Gibco BRL, UK) was weighed and dissolved in 1X TAE buffer at the appropriate concentration. The mixture was heated in a microwave oven to dissolve the agarose and the solution allowed to cool to 40°C. Ethidium Bromide was added to a final concentration of 20μg/ml. The agarose solution was poured into a casting tray with the required comb and left to solidify at room temperature.

Ammonium Persulfate

10% (w/v) stock solution was prepared in water and store at -20°C in single use aliquots.

Ampicillin Stock

0.5g of the antibiotic was dissolved in 10ml of sterile distilled water, creating a 50mg/ml solution. This was stored at -20°C in single use aliquots.

Blocking solution

10% (w/v) fat-free milk (Marvel, UK) was prepared in 1X TBS-T.

Calcium Chloride

A 2.5M solution was made by dissolving 36.75g $CaCl_2.2H_2O$ in distilled water. The solution was then filter-sterilised and stored at room temperature, to be used for calcium phosphate transfection.

COmplete™ protein inhibitor cocktail

One COmplete™ protein inhibitor (Boehringer Mannheim, UK) tablet was dissolved in 2ml of sterilised distilled water as a 25X stock solution.

DNA Marker

100bp and 1000kb DNA ladders were purchased from New England Biolabs and were used as a size standard for agarose gel electrophoresis.

EDTA Solution

A 0.5M $C_{10}H_{14}N_2O_2Na_2.2H_2O$ (EDTA) stock solution was made by dissolving 186g of EDTA in 700ml of distilled water. The pH was then adjusted to pH 8.0 with NaOH and the volume made up to 1L with distilled water.

Ethidium Bromide

A 10mg/ml stock was prepared by dissolving 0.2g ethidium bromide in 20ml of distilled water and then stored at 4°C in the dark.

Freezing Medium

50% (v/v) Foetal Calf Serum (FBS)

45% (v/v) Complete Medium (DMEM, RPMI 1640 or EMEM)

5% (v/v) DMSO

Stored at 4°C.

GNT buffer

50 mM KCL

1.5 mM $MgCl^{2+}$

10 mM Tris-HCl (ph: 8.5)

0.01% gelatine

0.45% NP-40 (Sigma-Aldrich)

0.45% Tween-20 (Fisher)

20X HBS (HEPES buffered saline) for 100ml (in water):

9.29g Hepes

0.745g KCl

16.36g NaCl

0.213g Na_2HPO_4 (anhydrous)

2.16g Glucose

Four different 2X solutions were made and their pH adjusted with NaOH to 6.7, 6.9, 7.1, and 7.3 respectively. Each solution was sterilised for transfection assays. These were stored in 50ml aliquots at -20°C for long term storage, or at 4°C for short term storage.

Mowiol Solution

6ml Glycerol

2.4g Mowiol 4-88 (Calbiochem)

12ml Tris-HCL 200 mM (pH 8.5)

The solution was made up to 50ml final volume, heated to 60°C overnight to dissolve all components, filtered through a 0.45μm filter and stored in aliquots at -20°C.

Oil Red O

0.5g Red Oil O

100 ml 1, 2-Propanediol (Sigma-Aldrich)

The solution was prepared by adding a small amount of propylene glycol to Oil Red O powder. After crushing larger pieces of Oil Red O with a stirring bar, the remainder of the propylene glycol was gradually added while stirring. The solution was gently heated until it solution reached 95-100 ^oC, then filtered through 3MM filter paper and allowed to stand overnight at room temperature.

Paraformaldehyde Solution (4%)

A 20% paraformaldehyde stock solution was made by dissolving 20g of paraformaldehyde powder in 700 ml of PBS. The solution was heated to dissolve the powder and the volume made up to 1L with PBS. The solution was diluted to 4% with PBS and stored at -20°C in aliquots.

Phosphate Buffered Saline

12.5 mM NaCl

1 mM Sodium dihydrogen phosphate, NaH_2PO_4

1.6 mM Disodium dihydrogen phosphate, Na_2HPO_4

The pH was adjusted to 7.0 and autoclaved.

Ponceau S Staining solution (10X)

5% (v/v) Acetic acid

2% (v/v) Ponceau S (sodium salt) (Sigma, MO, USA)

30% (w/v) Trichloroacetic acid $CCl_3.COOH$

30% (w/v) 5-sulfosalicyclic acid $C_7H_6O_6S.2H_2O$ (Sigma, MO, USA)

The solution was dissolved in distilled water to a 1X dilution before use.

Protein molecular weight markers

The prestained protein markers were purchased from New England Biolabs and were used as a size standard for SDS-polyacrylamide and tris-acetate gel electrophoresis.

Qiagen Solution -1- ATL buffer - animal tissue lyses

The solution contained SDS and was stored at room temperature

Qiagen Solution -2- AL buffer

The solution contained SDS and was stored at room temperature

Qiagen Solution -3- AW1 and AW2- Washing Buffer

The solution was stored at room temperature

1 M NaCl

50 mM MOPS, pH 7.0

15% Isopropanol

Qiagen AE (Elution Buffer for DNA samples)

10 mM Tris-Cl

0.5 mM EDTA; pH 9.0.

RIPA Lysis Buffer

150 mM NaCl

1 % (v/v) NP40 (or equivalent)

0.1% (w/v) SDS

50 mM Tris-HCl, pH 8.0

1/25 COmplete® Protein Inhibitor cocktail

Ribonuclease A (RNase A)

50mg of ribonuclease A (Sigma, MO, USA) was dissolved in 1ml of 10mM Tris-HCL pH 7.5, 15mM NaCl to make a 10mg/ml stock solution which was stored in single use aliquots at -20°C.

SDS Solution

A 10% (w/v) sodium dodecyl sulfate (SDS) was dissolved in water and stored at room temperature.

6X SDS-PAGE Sample Buffer (Laemmli buffer)

750 mM 0.5M Tris-HCl pH, 6.8

30% (v/v) Glycerol

6% (w/v) 10% SDS

0.03% (w/v) Bromophenol blue

60 mM 2-mercaptoethanol

10X SDS-PAGE Running Buffer

720g Glycine

150g Tris

50g SDS

Final volume was adjusted to 5L with distilled water.

10X SDS-PAGE Transfer Buffer

725g Glycine

145g Tris

Final volume adjusted to 5L with distilled water. The buffer was then used with 20% ethanol as a 1X solution.

Stripping Buffer

Provided by Chemicon International, USA

50X TAE (Tris-Acetate-EDTA) buffer

242g Tris

57.1ml Glacial acetic acid

100 ml 0.5M EDTA

The final volume was adjusted to 1L with distilled water and the pH adjust to 8.5, before using at 1X concentration. To make an agarose gel, 2µl of 10mg/ml Ethidium bromide solution per 100ml was added to the 1X TAE.

TE Buffer

10mM 5ml of 1M Tris-HCL, pH 8.0

1 mM 1ml of 0.5 M EDTA, pH 8.0

The final volume was adjusted to 500ml with distilled water.

Tris Stock Solution

Tris base was dissolved in water to provide 0.5M, 1M and 1.5M solutions, which were pH adjusted with concentrated HCl to the desired pH.

10X Tris Buffered Saline Tween-20 (TBS-T)

121g Tris base

36.53g NaCl

250ml Tween-20 (Sigma, MO,USA)

The pH was adjusted to 7.6 with around 60ml HCl in a total volume of 5L. Used at 1X concentration.

Urea Buffer

8M Urea

1M Thiourea

0.5% (w/v) CHAPS (3-[3-Cholaminodopropyl)dimethylammonio]-1-propanesulfonate)

50mM DTT (Dithiothreitol)

24mM Spermine

Primers Used in PCR

All primers were synthesised by Operon, Germany.

Water

Nanopure (typeI) generated from the MilliQ water system was used for all procedures

2.4.1 SDS-polyacrylamide Gels.

	Resolving Gels				**Stacking**
	6%	**8%**	**10%**	**12%**	**4%**
Acrylamide/Bisacrylamide	2ml	2.7ml	3.3ml	4.0ml	1.3ml
1.5M Tris-HCL, pH 8.8	2.5ml	2.5ml	2.5ml	2.5ml	--
1.0M Tris-HCL, pH 6.8	--	--	--	--	2.5ml
10% SDS	100µl	100µl	100µl	100µl	100µl
10% Ammonium Persulfate	100µl	100µl	100µl	100µl	50µl
TEMED	10µl	8µl	5µl	5µl	10µl
Distilled Water	5.3ml	4.6ml	4.0ml	3.3ml	6.1ml
Total Volume	10ml	10ml	10ml	10ml	10ml

All resolving and stacking gels were prepared using 30% acrylamide/bisacrylamide 29:1 (NBL, UK). Values given are per 10ml of gel required. Abbreviations; N,N,N',-tetramethy-ethylenediamine (TEMED), Tris (Tris-hydroxymethyl-aminomethane, sodium dodecyl sulphate (SDS). Tris acetate gel and gradient gels were purchased from Invitrogen.

2.4.2 Primary antibodies and their working conditions:

Name	Antigen	Host	Type	Source (catalogue #)	Working condition	
					WB	IHC-Pr
LX128.5	iASPP	mouse	monoclonal	Ascite	1:2000	1:500
LX049.3	iASPP	mouse	monoclonal	Ascite	1:2000	1:500
Cre	Cre	rabbit	polyclonal	Novagen (69050-3)	1:1000	
GAPDH	GAPDH	rabbit	polyclonal	Assay designs (905-734-100)	1:1000	
ANP (FL-153)	Atrial natriuretic peptide	rabbit	polyclonal	Santacruz (sc-20158)		1:250
Collagene IV	Collagene IV	rabbit	polyclonal	Abcam (ab6586)		1:500
Collagene I	Collagene I	rabbit	polyclonal	Calbiochem		1:250
Laminin I+II	Laminin I+II	rabbit	polyclonal	Abcam (ab7463)		1:500
Desmin	Desmin	rabbit	polyclonal	Abcam (ab15200)		1:250
Vimentin	Vimentin	mouse	monoclonal			1:100
Vimentin	Vimentin	rabbit	polyclonal			1:100
Ki67	Ki67	mouse	monoclonal			
P53 (CM-5)	P53	rabbit	polyclonal	Ascite		1:200
Caspase-3 (Asp175)	Caspase-3	rabbit	polyclonal	Cell signaling (9661)		1:200

Name	Antigen	Host	Type	Source (catalogue #)	Working condition	
					WB	IHC-Pr
N-cadherin	N-cadherin	rabbit	polyclonal	Abcam (ab12221)	1:1000	1:500
α-catenin	α1-catenin	rabbit	polyclonal	Abcam (ab11346)	1:1000	1:500
β-catenin	β-catenin	mouse	monoclonal	BD (610154)	1:1000	1:250
p120	P120 (15D2)	mouse	monoclonal	SantaCruz (sc-23872)	1:250	
Plakoglobin	γ-catenin	rabbit	polyclonal	Abcam (ab15153)	1:1000	1:250
Connexin 43	connexin-43	rabbit	polyclonal	Abcam (ab11370)		1:500
Keratin 5	Keratin 5	rabbit	polyclonal	Covance (PRB-160-P)	1:500	1:500
Keratin 14	Keratin 14(AF 64)	rabbit	polyclonal	Covance (PRB-155-P)	1:1000	1:500
Keratin 1	Keratin 1	rabbit	polyclonal	Covance (PRB-149-P)	1:1000	1:500
Loricrin	Loricrin	rabbit	polyclonal	Covance (PRB-145-P)	1:1000	1:500
P63	P63 (4A4)	mouse	monoclonal	SantaCruz (sc-8431)	1:500	1:250
E-cadherin	E-cadherin	mouse	monoclonal	BD (610182)	1:1000	1:250
N8	ASPP1	rabbit	polyclonal	serum	1:1000	
LX054.2	ASPP2	mouse	monoclonal	Hybridoma	1:1000	
β-1 Integrin	β-1 Integrin	mouse	monoclonal	Millipore (MAB1997)		1:500

Secondary antibody and their working condition:

Name	Source	Application	Working condition
Mouse IgG	mouse secondary, (Dako)	Western blotting	1:3000
Rabbit IgG	rabbit secondary, (Dako)	Western blotting	1:3000
Alexa Fluor® 488 F(ab')$_2$ goat anti-mouse IgG	mouse secondary, (Invitrogen)	Immunofluorescence (tissue)	1:400
Alexa Fluor® 546 F(ab')$_2$ goat anti-mouse IgG	mouse secondary, (Invitrogen)	Immunofluorescence (tissue)	1:400
Alexa Fluor® 488 F(ab')$_2$ goat anti-rabbit IgG	rabbit secondary, (Invitrogen)	Immunofluorescence (tissue)	1:400
Alexa Fluor® 546 F(ab')$_2$ goat anti-rabbit IgG	rabbit secondary, (Invitrogen)	Immunofluorescence (tissue)	1:400

2.4.3 Cell lines.

Primary Cell Lines

- Mouse embryonic fibroblast (MEFs) generating form E13.5 mouse embryos.
- Mouse keratinocyte (KCs) generating by dissecting the epidermis from P0-P1 (newborn) mice

2.5 Methods.

2.5.1 Tissue Culture.

Basic Media

RPMI 1640 and Dulbecco's Modified Eagle's Medium (DMEM) were purchased from Gibco-BRL, UK and stored at 4°C.

Eagle's Minimum Essential Medium (EMEM) with Earlie's balanced salts solution (EBSS), non-essential amino acids and L-Glutamine without Calcium Chloride was purchased from Lonza, MD USA.

Media supplements

Foetal calf serum (FCS) was purchased from PAA Laboratories and tested for its ability to support the growth of various cell lines, It was heat inactivated for 30 minutes at 55°C and stored at -20°C in 50ml aliquots.

L-Glutamine was purchased from Gibco-BRL at 200mM concentration, stored at -20°C, and used at a final concentration of 2mM.

Penicillin / Streptomycin was purchased from Gibco-BRL at 10,000 units/ml, stored at -20°C and used at a final concentration of 200 units/ml.

Maintenance of cell lines

All cell lines listed in 2.4.3 section were cultured in Complete Medium (DMEM, RPMI 1640 or EMEM) supplemented with L-Glutamine, penicillin / streptomycin and 10% (v/v) foetal calf serum, in flasks or dishes maintained in a Heraeus incubator at 37°C in the presence of 10% CO_2. Medium was change every 2-4 days depending on the cell line. Upon reaching confluence, the cells were washed once with 1X PBS and incubated with 2-4ml pre-warmed Trypsin-EDTA 0.05% (Gibco-BRL) at 37°C until the cells detached from the flasks or dishes. Trypsin was inhibited by addition of the appropriate volume of fresh grown medium and this culture was then seeded onto fresh flasks or dishes at the desired density.

Undifferentiated primary keratinocyte cell lines were cultured in Eagle's Minimum Essential Medium (EMEM) without Calcium Chloride, supplemented with 0.05mM $Cacl_2$, L-Glutamine, 1X Antibiotic Antimycotic Solution (Sigma, MO,USA) and 8% $CaCl_2$ chelate foetal calf serum. When needed, undifferentiated primary keratinocyte cell lines were differentiated by the addition of $CaCl_2$ to a final concentration of 1.2mM.

Cells in the exponential phase of growth were used for analysis.

Freezing / Thawing of cells

Cells were seeded the day before freezing at a density such that they would be 70% confluent on the day of freezing. Cells from the growing culture were detached by trypsinising with 0.5ml trypsin-EDTA 0.05%, then resuspended in 2 ml of freezing media at a concentration of around 1-5 x 10^7 cells per ml. 1ml aliquots of the cell suspension were transferred into 2ml freezing ampoules (Nunc). The vials were then labeled and cooled at the rate of 1°C per minute in a Nalgen Cryo 1°C freezing container or in a tissue-insulated polystyrene box, when placed in a -80°C freezer (NEW

Brunswick Scientific) for at least 24 hr, before being transferred to a liquid nitrogen tank for long term storage.

To thaw cells from the liquid nitrogen stack, vials were placed in a 37°C water bath for 2-4 minutes and then transferred to a 6cm or 10cm dish with an appropriate amount of pre-warmed fresh complete growth medium, and kept in the 37°C incubator overnight to recover.

Ca^{2+} depletion

Chelating resin was designed for the removal of metal cations at appropriate pH values, and this was used to deplete calcium cations from FBS. Briefly, 80g Chelx 100 resin (Bio Rad) was added into 1 liter of double Nanopure water (ddH_2O). The pH value was adjusted to 7.5 by adding HCl drop-wise into the stirring solution. When the pH value reached 7.5, the resin was filtered through 1MM Whatman circular filter papers. 500 ml of thawed FBS was mixed with the Chelex resin pH 7.5 by continual stirring for at least 2 hours in a glass beaker. After that, FBS was filter sterilised first through a 0.45μM filter, and then a 0.22 μM filter in a cell culture hood. The Ca^{2+}-depleted FBS was aliquoted and stored at -20°C.

Mouse primary keratinocytes were purified from newborn mice and exposed to Ca^{2+} free medium DMEM (Gibco, UK), supplemented with 10% prepared Ca^{2+}-depleted FBS to maintain their undifferentiated/proliferating nature (Hennings, Holbrook et al. 1980). 1.2 mM Ca^{2+} was added into the Ca^{2+}-depleted complete medium to induce the terminal differentiation of primary keratinocytes (Hennings, Holbrook et al. 1980).

2.5.2 DNA techniques.

Agarose gel electrophoresis

DNA samples were mixed with 5X DNA loading buffer to a final concentration of 1X, before being run on an agarose gel of the appropriate percentage, according to the size of the DNA bands to be visualised. The gels were made with TAE buffer containing ethidium bromide and run at 60-80 V

with DNA markers. The ethidium bromide-stained DNA bands were then visualised under UV-irradiation.

DNA extraction from ear biopsies

Mice were ear-punched for identification and the resulting ear tissue used for genotyping. Ear tissue was digested overnight at 55ºC in 100µl of extraction buffer GNT and 7.8 mg/ml of proteinase K (Quiagen). The digested tissue was boiled for 10min at 97 ºC and 0.5µl used for polymerase chain reaction (PCR) analysis.

DNA extraction from embryonic yolk sack

Embryos were carefully dissected from the uterus of the pregnant female, and a small part of the yolk sack (<25 mg) was excised from individual embryos and digested overnight at 55ºC in 200µl ATL buffer supplemented with 20µl of proteinase K (7.8 mg/ml, Quiagen). After the overnight incubation, 200µl of AL buffer and 200µl of ethanol (96-100%) were add to the mixture and vortexed from 15 sec. The mixture was then applied to a DNeasy Mini spin column and placed into a 1.5 ml microcentrifuge tube. The column was then centrifuged at 8000 rpm for 1 min. The flow-through was subsequently discarded and the column washed twice with 500µl of AW1 buffer first, then with 500µl of AW2 buffer. The column was placed into a new microcentrifuge tube and 200 µl of AE buffer added to the centre of the column. After 1 min, the column was centrifuged at 8000 rpm for 1 minute to elute the DNA. The obtained DNA was then used for PCR analysis.

2.5.3 Protein manipulation.

Sample preparation

Cells grown in monolayers in a 10 cm dish were washed three times with 1X PBS and incubated with 2-4ml of pre-warmed Trypsin-EDTA 0.05% (Gibco-BRL) at 37°C, until the cells detached from the dish. Trypsin was inhibited by addition of the appropriate volume of fresh growth medium

and the cells were pelleted at 400g for 5 minutes. The pellet was the resuspended in the appropriate volume of lysis buffer (150-250µl per 10 cm dish). The mixture was cleared by centrifugation at 14.000rpm, at 4°C or room temperature depending on the lysis buffer, for 20 minutes (eppendorf 5417R). The resulting lysate was removed to a fresh microcentrifuge tube and the cell debris discarded.

Adult mouse organs were frozen in liquid nitrogen and crushed into a fine powder. The powder was mixed with urea buffer (8M urea, 1M thiourea, 0.5% CHAPS, 50mM DTT, 24mM spermine) and sonicated 3 times in ice. Tissue lysates were then clarified by centrifugation (13'000 rpm) for 20 min at 4°C. Supernatants were collected and centrifuged again under the same conditions to ensure that no cellular debris was transferred. Protein concentration was estimated via Bradfords assay. 40µg of tissue lysate was loaded per lane (plus 5X loading buffer (100mM Tris HCl ph 6.8, 4% SDS, 20% glycerol, 0,2% bromophenol-blue) was added to all samples, boil and loaded) on SDS-polyacrylamide gels. Gels were electrophoresed at 100V and protein transferred onto nitrocellulose membrane at 55V for 3h or 20V at RT, or O/N at 4°C. Membranes were blocked in 5% milk in Tris Buffer Saline, TBS (125mM Tris and 200mM NaCl), containing 5% Tween-20. Primary antibody was added for 3h at RT or O/N at 4°C. Secondary antibody was added for 1h at RT. Membranes were washed 3 times for 10min with TBS-Tween in between antibody incubations. The results were visualised by enhanced chemoluminescent detection (ECL, Amersham Biosciences) using X-ray films (Fujifilm).

Protein concentration determination

The protein concentrations of cell extracts were determined using the BioRad protein assay reagent system. 1µl of cell lysate was mixed with 200µl of 1X BioRad assay reagent and then measured at 595nm in a spectrophotometer. Five dilutions of known concentrations of bovine serum albumin (BSA; Sigma-Aldrich) were prepared at the same time to generate the standard curve. 200µl of 1X BioRad reagent was added to each well and incubated at room temperature for 5 minutes. The

absorbance at 595nm was then measured using a microplate reader (TECAN, sunrise microplate reader). All samples were measured in duplicate and the absorbance was compared against the standard curve.

Preparation of SDS-polyacrylamide gels

All plates were washed with distilled water and detergent, dried and assembled in the casting tray (Pharmacia Biotech, UK). The acrylamide content of the gels varied between 6%-12% depending on the size of the protein of interest. The acrylamide gels were overlaid with 70% isopropanol solution and left to polymerise at room temperature. After polymerisation, the isopropanol solution was removed and a 4% stacking gel was set with the appropriate number and size of wells.

SDS-polyacrylamide gel electrophoresis (PAGE)

Know concentrations of protein were mixed with appropriate volumes of 5X SDS-PAGE Sample Loading Buffer and boiled for 5 minutes. Equal amounts of protein were loaded in respective wells cast in the stacking gel. The resolving gels were made with 6%-12% of polyacrylamide, depending on the size of the protein to be resolved. The gels were run at 135V for 1 hour in 1X SDS-PAGE running buffer using the Mighty Small II system (Amersham), with prestained protein markers purchased from New England BioLabs and used as a size standard.

Immunoblotting

Cells lysates and protein markers were diluted in 5X SDS-PAGE Sample buffer, loaded onto SDS-polyacrylamide gels in a 1X SDS-PAGE running buffer, and electrophoresed at a constant voltage of 100-250V. Equal amounts of protein were loaded in each lane as determined by the BioRad assay system, unless otherwise stated. After the samples were separated through the gel, the gel was transferred to a wet transfer unit containing 1X SDS-PAGE transfer buffer. The proteins were the electrophoretically transferred onto nitrocellulose membrane for 1-3 hours at a constant voltage of 55V, or overnight, in a Hoefer Transphor Electrophoresis unit. The membrane was then stained

with Ponceau Solution to determine the success of the transfer of proteins and equal loading of the lanes. The membrane was then washed in distilled water and incubated in 5% of non-fat milk solution at room temperature for 1 hour. The membrane was then ready to be probed with primary antibody at the recommended concentration for 1-3 hours at room temperature or overnight at 4°C. The membrane was then washed with large amounts of 1X TBS-T solution, three times for 15 minutes each, and the secondary HRP-antibody added at the recommended concentration (usually 1:2000) at room temperature for 1 hour. After incubation with the secondary antibody, the membrane was extensively washed with 1X TBS-T, with repeated changes of TBS-T. ECL was then performed according to manufacturers' instructions (Amersham Life science). The result was the visualised using X-ray film (Fujifilm). If reprobing with another primary antibody was required, stripping of membranes was performed as follows. Membranes were incubated with a commercial stripping buffer (Chemicon International) for 15 minutes at room temperature. The membranes were extensively washed with 1X TBS-T and then blocked in 5% non-fat milk solution for 1 hour at room temperature. The blot was then reprobed with primary antibody as before.

For quantification of the signal, the BioRad GS densitometer was used to digitally capture the image and quantify the intensity of the signal using Quantity One software (BioRad).

2.5.4 Cell-based assay.

Cell Infection

Adherent cells were grown to a confluence of approximately 70-80% in fresh medium. Typically, a 60mm dish was started with 8 x 105 Saos-2 cells, plated 24 hours before the transfection procedure. 1 hour prior to transfection, the medium on the dishes was replaced with 2 ml of fresh Complete Medium. 2X HBS buffer was diluted with sterile water to a final concentration of 1X, and 200µl per 60mm dish was place in an autoclaved micro centrifuge tube. The necessary quantity of plasmid DNA was added to the solution and mixed thoroughly together with 30µl of 2.5M $CaCl_2$ to form a precipitate. The mixture was then left at room temperature for 15 minutes. After this time, plasmid

DNA suspension was added to each 60mm dish drop-wise under a tissue culture hood, and the dishes placed in the incubator for an additional 6 hours. The medium was then removed, the cells were washed once with pre-warmed fresh DMEM, and 3ml growth tissue culture medium was finally added to each dish and the cells were left for 48 hours, for a transient assay. If a lipotransfection method (Fugene® 6, Roche) was required, the manufacturers' procedure was followed.

Immunocytochemistry

Cells were grown in 24 well sterile plates (Corning, USA) at 70-80% confluence. Once experimental procedures were completed, cells were fixed with 200µl of 4% paraformaldehyde solution for 15 minutes, then permeabilised with 0.1% Triton X-100 for 4 minutes on ice. Different antibodies were diluted in PBS containing 5% of normal goat serum and utilised to cover the cells for 40 minutes. Protein expression was detected by using Alexa® (1:400, Molecular Probes) for 20 minutes. TO-PRO (Invitrogen) was used to stain nucleic acids (1:1000).

2.5.5 Mouse work.

Mouse colonies

iASPP$^{+/\Delta 8}$ and iASPP$^{\Delta 8/\Delta 8}$ mutant and wild type mice were maintained at the Wellcome Trust Centre on a C57BL/6 (B6) and 129Sv mixed genetic background. All animals were handled according to IACUC approved guidelines. A conditional allele of iASPP, iASPP$^{flox/flox}$, has 2 lox P sites that surround exon 8. Deletion of exon 8 resulted in a null allele, designated iASPP$^{\Delta 8/\Delta 8}$. Genotyping was performed by PCR analysis using primers FLP2 (5'-CCGAATTGGAGAAGTGAAGC-3'), I8-2 (5'-CCGAATTGGAGAAGTGAAGC-3') and E8-2 (5'-AGAGCAGCCTCAGAGCATGG-3'). Detection of Lox P sites was performed using specific primers FLP2 and FRTAN9 (5'-GGGTAGGAAAAAGGGCTGAG-3').

BrdU injection and cell cycle analysis

Pregnant females were injected with a dose of 100 mg/Kg of BrdU and sacrificed after 1 hour. Embryos were dissected and processed as described above for paraffin sections.

Electrocardiogram (ECG)

ECG is a non-invasive, transthoracic interpretation of the electrical activity of the heart over time, captured and externally recorded by skin electrodes. The ECG works mostly by detecting and amplifying the tiny electrical changes on the skin that are caused when the heart muscle "depolarises" during each heartbeat. Depolarisation of the myocytic membrane activates the cascade of events that leads to the contraction of the myocardium and the “heartbeat” (Chapter I, section 1.3.2). During each heartbeat, a healthy heart will have an orderly progression of waves of depolarisation that are detected as tiny rises and falls in the voltage between two electrodes placed either side of the heart *(figure 4.9A)*. These rising and falling peaks can be displayed as a wavy line either on a screen or on paper, and can be analysed. The resulting wavy line has characteristic patterns that indicate the overall rhythm of the heart and weaknesses in different parts of the cardiac muscle. Anaesthetised surface ECG recordings were obtained under light isoflurane general anaesthesia (1.25%) on a heating pad. Fine needle electrodes were positioned in a lead II configuration, with recordings obtained at a sampling rate of 1kHz, with filtering and amplification of signals using a BioAmplifier (ADInstruments). Mice were allowed to equilibrate after anaesthetic induction prior to rhythm recordings. All traces were manually inspected off-line for arrhythmia. Specific ECG intervals were measured by off-line analysis of signal-averaged waveforms using PowerLab software (ADInstruments) blind to genotype.

High Resolution Episcopy Microscopy (HREM)

Episcopic image analysis is a technique that has been extensively used to create 3D computer-generated models of the cavernous sinus region of human infants (Weninger, Meng et al. 1998;

Weninger and Mohun 2002), and to study the anatomy of mouse embryonic hearts in *Cited2*-null mice (Weninger, Lopes Floro et al. 2005). The technique is based on the use of histologically prepared and embedded samples, which are imaged during sectioning rather than after the sections have been obtained from the microtome. The advantage of capturing images in this way is the maintenance of the alignment of each section, and the resulting image stack can be simply transformed into 3D volume data for the visualisation of the organ using appropriate software tools. Episcopic analysis can be generated in a variety of different ways (Weninger, Meng et al. 1998; Weninger and Mohun 2002). In the high-resolution episcopic microscopy (HREM) method, samples are imbedded in a methacrylate resin (JB4) that contains a florescent dye, which sustains the tissue while the florescent dye provides a homogenous background, different from the tissue below the block surface, which will be important for visualising the specimens. Images are captured from the surface of the block, and the visualisation of the tissue results from the suppression of the fluorescent signal wherever tissue is present at the surface of the block. Computer imaging software collects the images and reconstructs a 3D picture of the organs.

Histology and immunohistochemistry

Embryos of various developmental stages were fixed in 4% paraformaldehyde solution overnight and then dehydrated in an ethanol series, cleared in histoclear and embedded in paraffin wax. Sections were cut at 4μm thickness and either stained for hematoxylin & eosin or processed for immunostaining. Rehydrated paraffin-sections were immersed in 10mM sodium citrate buffer, pH 6 for 7 minutes, then left to cool to room temperature on the bench. Sections were incubated in 3% hydrogen peroxide in methanol, washed in PBS, and incubated overnight with the primary antibody at 4°C, followed by biotinylated secondary antibody for 1 h at room temperature. Staining was visualised using the peroxide substrate solution DAB (diaminobenzidine, Vector). Indirect immunofluorescence was performed on heart and skin paraffin sections. After blocking with 5% Goat serum in PBS for 1h at RT, the sections were incubated with primary antibody against β-

catenin, N-cadherin, connexin 43 and plakoglobin, followed by FITC-anti-rabbit secondary antibody incubation for 40min at RT (1:400, Molecular Probes). The sections were mounted, viewed and photographed with a confocal microscope.

Organs of various stages were fixed in 10% buffer formalin overnight and then dehydrated in an ethanol series, cleared in histoclear and embedded in paraffin wax. Section were cut at 4μm thickness and handled as before.

Masson trichrome staining

Masson trichrome staining was performed on deparaffinised heart sections from mutant or control mice. Sections were fixed in preheated Bouin's solution at 56°C for 15 min. After washing the sections in cold tap water, they were incubated for 5min with Weigert's iron hematoxylin solution, then with phosphotungstic/phospholimbic acid solution, and finally with aniline blue solution. Sections were washed for 5min with deionised water in between incubations. Slides were then dehydrated with alcohol, cleared in xylene and mounted.

MR imaging of cardiac function *(in vivo)*

MRI is an excellent method with which to image the anatomy, or measuring the functional performance, of an organ *in vivo* (Weissleder and Mahmood 2001). The MRI technique is based on the magnetic moment of hydrogen atoms. Since mammals' bodies contain a large amount of water, this technique is extremely good at imaging water-rich soft tissue like the heart. One of the biggest advantages of MRI is the versatility of the technique compared to other imaging modalities such as X-rays, Computer Tomography (CT), ultrasound and nuclear techniques like Single Photon Emission Computed Tomography (SPECT) or Positron Emission Tomography (PET). In fact, MRI does not use ionising radiation or radio-active isotopes to generate high quality anatomical or functional images of the heart; hence it is more user-safe. MRI is also a non-invasive technique and can, therefore, play a vital role in reducing the total number of animal experiments, in agreement

with animal welfare restrictions. However, the main disadvantage of MRI is the resolution of the images generated, as they cannot be resolved at the cellular or molecular level.High-resolution cine magnetic resonance (MR) imaging was carried out using a 40-mm ^{1}H-imaging probe in a vertical bore 500 MHz, 11.7 T MR system with a Bruker console running Paravision 2.1.1 as previously described (Schneider *et al*, *J. Magn. Reson. Imaging* **18** (2003), pp. 691–701). Mice were anaesthetised with isoflurane, positioned supine in a purpose built holder and maintained at 2% isoflurane in 1.5 l/min oxygen flow throughout the MRI experiments. Short-axis slices were acquired to cover the whole heart using a cardiac-triggered and respiration-gated fast low-angle shot (FLASH) sequence. The end diastolic and systolic volumes (EDV and ESV) were measured for each slice using Image J (Rasband WS (1997-2009) ImageJ, U. S. National Institutes of Health, Bethesda, Maryland, USA,. http://rsb.info.nih.gov/ij/) and totalled over the whole heart. Left ventricular mass was calculated by multiplying the left ventricular wall volume by the specific gravity of the myocardium (1.05 g/cm^3). Stroke volume (SV = EDV − ESV), ejection fraction (EF = SV/EDV) and cardiac output (CO = SV × heart rate) were calculated from the EDV and ESVs.

Oil Red O Staining *(in vivo)*

10 μm thick frozen myocardial sections were fixed in 10% neutral formalin buffer (Sigma-Aldrich), washed 3 times in distilled water and placed in 100% propylene glycol for 2 minutes to ensure no water was carried on to the next step. Slides were immersed in Oil Red Solution for 1 hour at 60°C, rinsed in distilled water and counterstained with Mayer's haematoxylin (Sigma-Aldrich).

TUNEL assay

Terminal deoxynucleotidyl transferase biotin-UTP nick end labelling (TUNEL) assay was carried out on paraffin-embedded heart sections from mutant and control hearts. TUNEL assay was performed according to the manufacturer's instructions (Chemicon Luninescence).

Generation of murine embryonic fibroblasts (MEFs)

MEFs were prepared from E13.5 embryos. A 13.5 days old pregnant female mouse was sacrificed by cervical dislocation, the uterus was removed and washed in PBS. The embryos were then isolated from the uterus in sterile conditions and the head and internal organs carefully removed and disposed. The remaining tissue was disaggregated by fine mincing followed by treatment with 4 ml of trypsin-EDTA (Invitrogen) for 10 minutes at 37°C. The cell suspension was subsequently transferred into 15 ml Falcon tubes, to which 10ml of complete DMEM media was added. After 5 minutes, the cell suspension was cautiously removed without disturbing the precipitated debris and plated into T75 cell culture flasks (Corning, USA). The cells were left to attach to the flask by overnight incubation and the media and unattached cells were removed the next day. Cells were named P1 to indicate the passage number, and split every time they reached 90% confluency.

Generation of murine primary keratinocytes

Newborn mice were sacrificed in a CO_2 chamber and all steps were performed in aseptic condition in a laminar-flow hood. The entire skin was dissected from the newborn pup and left float overnight over 0.25% Trypsin-EDTA. The next day, the epidermis was detached from the dermis and place in a 10cm petri dish with 10 ml of Ca^{2+}-depleted complete media. The epidermis was subsequently minced with scissors into fine pieces and resuspended with a 10 ml pipette. Finally, the resulting suspension was transfer to a 50ml falcon tube through a 100-µm cell strainer (BD Falcon n°352360), to get rid of most of the stratum corneum and debris. Cells were centrifuged at 700 rpm for 7 mins, and the resulting pellet resuspended in low calcium media. Primary keratinocytes were plated on different sized petri dishes or glass cover slips which had been coated with collagen prior to use.

2.5.6 Computer images.

All autoradiographs were scanned using an Epson perfection 1660 Photo scanner and an Adobe Photoshop 8.0 software. Images were manipulated only as a whole for size, brightness and contrast. No signal was modified in relation to the whole image.

2.5.7 Statistics.

Kaplan-Meier survival analysis was performed with prism 4 software (GraphPad software, San Diego). Differences were considered significant at a value of $P \leq 0.05$. The T-test was used to calculate the statistical significance between two measurements.

Chapter 3
RESULTS

Generation of iASPP$^{flox/flox}$ mice: a conditional knockout system for the depletion of iASPP protein *in vivo*.

3.1 Introduction.

iASPP is a member of the ASPP family of proteins, which specifically regulate the apoptotic function of p53 and its homologues p63 and p73 (Bergamaschi, Samuels et al. 2004). In particular, ASPP1 and ASPP2 synergise with p53 to induce the transcription of pro-apoptotic genes, whereas iASPP impairs only p53-mediated apoptosis (Sullivan and Lu 2007). To further understand the biological function of iASPP *in vivo,* we generated a transgenic mouse model in which the expression of iASPP is controlled by the presence of Cre recombinase enzyme. This system, therefore, allows the specific deletion of iASPP in a spatio-temporally controlled manner.

In this chapter the targeting vector used to alter *PPP13R1L* (iASPP gene) genetic locus in embryonic stem (ES) cells and the mice used throughout this study will be investigated. In addition, the expression pattern of iASPP in different mouse organs will be described to understand where a loss of iASPP expression may impact on the structure/function of mouse organs.

3.1.1 Traditional knockout technology vs. conditional knockout technology.

Gene targeting technologies in embryonic stem (ES) cells have allowed scientists to replace genes of interest with a selectable marker in the mouse germline, in order to create a mammalian model in which the final product of the targeted genes is destroyed (Capecchi 1989). Normally, KO mice contain one gene that has been altered, mutated or simply deleted to investigate its biological

functions *in vivo*. Since these transgenic mice are usually homozygous for the deleted gene, they provide a valuable system for the investigation of hereditary diseases. However, a major limitation of this system is an inability to alter genes that are essential for the correct development of the mouse embryo (Mak T. W. *The gene knockout facts book.* Academic San Diego, CA). In fact, the inactivation of a gene that leads to embryonic lethality in the uterus of the pregnant female makes the animal almost impossible to use in scientific studies. Nevertheless, KO technologies are a formidable device with which to understand and appreciate the importance of a gene *in vivo*, by connecting specific molecular genetic alterations with tissue phenotypes (Hooper, Hardy et al. 1987).

The discovery of the site-specific recombinase family of enzymes, which includes the bacterial Cre recombinase, refined the "traditional" KO mouse system (Rajewsky, Gu et al. 1996). Conventional KO systems do not represent the best technical approach with which to study the function of a gene *in vivo*. Inducible KO systems, in contrast, surmount the traditional problems of conventional KO technologies, allowing scientists to inactivate specific genes only in a particular organ or at specific developmental stages (Zou, Muller et al. 1994). Normally, inducible KO systems systems are based on the ability of one or more enzymes to recognise and "cut" the specific recognition sequences. The disruption of the target gene is achieved by the insertion of a bacterial recombinase (Cre or FLP) into the mouse germ line in association with two recombinase recognition sequences (loxP or FRT recognition motive), usually cloned on either side of the target gene. This method, thus, requires the use of two strains of mice, one carrying the loxP or FRT flanked gene sequence introduced into its genome by gene targeting technologies in ES cells, and a second strain of mice harboring constitutive Cre recombinase enzyme or the enzyme under the control of a inducible promoter (Sauer and Henderson 1988) *(figure 3.1)*. These two strains of transgenic mice can then be crossed to generate, as a final product, a mutant mouse harboring both the target gene in between the two recognition sequences, and the recombinase enzyme in its genome *(figure 3.1)*. Also, loxP-

containing mice can be converted into "conventional" KO mice by a single cross with a so-called 'deleter' strain of mice, in which the Cre recombinase is constitutively expressed *(figure 3.1)*.

The Cre enzyme, or cyclic recombinase, is a 38 kDa protein discovered and purified from the bacteriophage P1, which can bind and specifically "slice" a segment of DNA whenever it recognises a loxP sequence. The loxP recognition sequence is a 34 base pair (bp) series, containing two 13 bp inverted repeats flanking an 8 bp core sequence *(figure 3.2)*. The outcome of the recombination depends on the orientation of the recognition sequences: two loxP sequences in opposite orientation to each other invert the intervening piece of DNA; whereas two sites in direct orientation determine the excision of the intervening DNA between the two sites, leaving one loxP site behind. When loxP sites are present in the genome of a cell that expresses the bacterial Cre protein, a recombination event can occur between the two loxP sites, leading to the excision of the DNA fragment in between the loxP sites *(figure 3.2*).

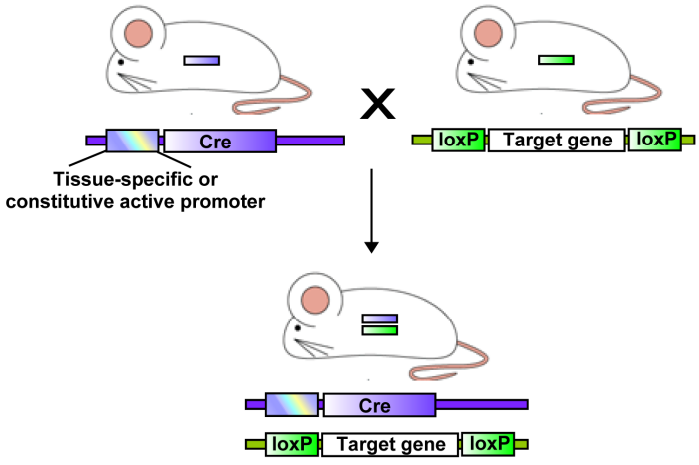


Figure 3.1. Schematic representation of conditional gene knockout (KO) technology using the Cre/loxP recombination system in transgenic mice. Transgenic mice harboring the Cre recombinase gene in a specific tissue, or ubiquitously in all mouse organs, are bred with mice containing a target gene surrounded by two loxP sites. When the mice are bred together, some of the resulting progeny will carry the Cre enzyme together with the target gene, according to Mendelian segregation.

We know from previous work completed in our laboratory that iASPP can bind and inhibit the apoptotic function of p53 and its family members p63 and p73 (Bergamaschi, Samuels et al. 2004), but little is known about its role in development or its biological function *in vivo*. To better understand the role of iASPP *in vivo*, and the conditions under which it functions through p53 and its family members, we generated a transgenic mouse model system to study iASPP function(s) both *in vivo* and in a primary cell culture system. We decide to use the inducible Cre/loxP system to overcome the potential problem of embryonic lethality already encountered with mdm2 and mdm4 transgenic mice (Jones, Roe et al. 1995) (Montes de Oca Luna, Wagner et al. 1995).

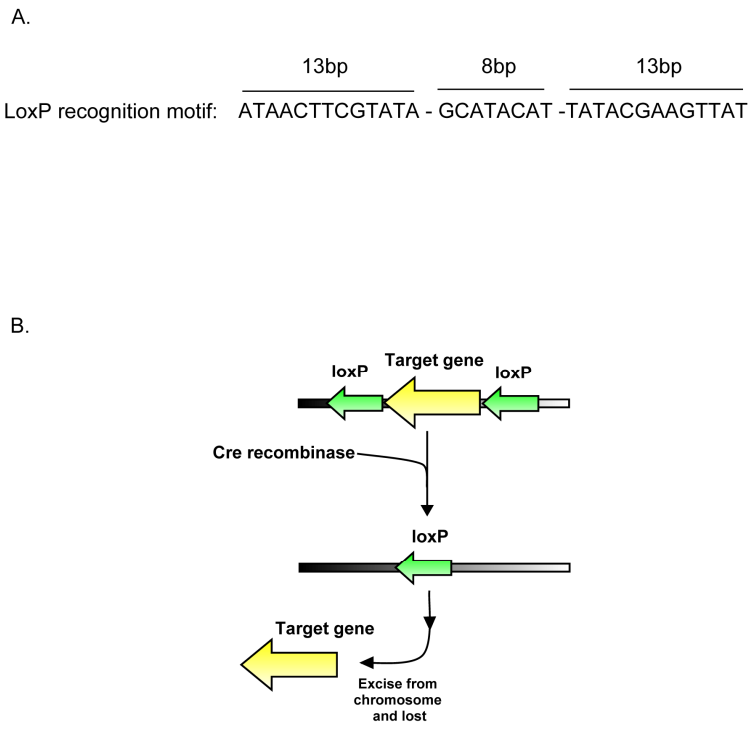


Figure 3.2. LoxP recognition motif and schematic mechanism of excision of the target loxP-flanked gene. (A) The loxP recognition sequence is a palindromic sequence of 34 bp, containing two 13 bp inverted repeats flanking by an 8 bp core sequence. (B) Simplified representation of the Cre/loxP recombination system. A pair of loxP sites *(green arrows)* flanking the target DNA sequence *(yellow)* to be deleted are shown in the same orientation. After the Cre recombination event has excised the target DNA, one loxP site is left behind which is the result of the remains of the two loxP recognition motifs spliced together. The target DNA is excised and degraded.

3.2 Results

3.2.1 Generation of iASPP$^{flox/flox}$ mice.

In order to obtain a KO system to investigate the biological functions of iASPP *in vivo*, a transgenic mouse was generated in which iASPP's expression was controlled by the bacterial site-specific DNA recombination system Cre/loxP. The approach is summarised in figure 3.3. The *PPP1R13L* genomic locus was modified to generate a mouse which carried, in its germ line, two loxP recognition motifs (iASPP$^{flox/flox}$), one at either end of exon 8 of the *PPP1R13L* gene. The alteration of the *PPP1R13L* genomic locus was been made by inGenious Targeting Laboratory, Inc. (NY, USA). Briefly, to inactivate the iASPP gene, a targeting vector was constructed that contained the genomic DNA fragment encoding exons 8 to 13 of the mouse *PPP1R13L* gene (NM_001010836). The targeting vector consisted of a short arm that spanned the iASPP gene, from 2.5 kb to 0.9 kb upstream of exon 8. This part of the vector was inserted 5' into the Neomycin resistant cassette which was flanked by both loxP and FRT sites *(figure 3.3)*. The second part of the vector was constructed by cloning a 1.2 kb DNA fragment containing the modified sequence of *PPP13R1L*-exon 8, and was inserted 3' of the Neo gene cassette. Finally, the third part of the vector contained the DNA fragment of *PPP1R13L* gene from the Swa I site to the end of the clone, which included exons 8 to 13 *(figure 3.3)*. The 3rd Lox P site, together with a newly introduced EcoRI site, was located between exon 9 and the Swa I site *(figure 3.3)*. Ten micrograms of targeting vector was linearised and transfected by electroporation into 129Sv/Ev embryonic stem cells. After selection in G418 antibiotic, surviving colonies were analysed using PCR amplification to identify positive recombinant clones. The correctly targeted ES cell lines were microinjected into C57BL/6J blastocysts to give rise to germline transmitting chimaeric mice that contained the conditional iASPP gene. The conditional iASPP mice were mated with FLPe mice from the Jackson Lab to remove the Neo cassette (*figure 3.3).*

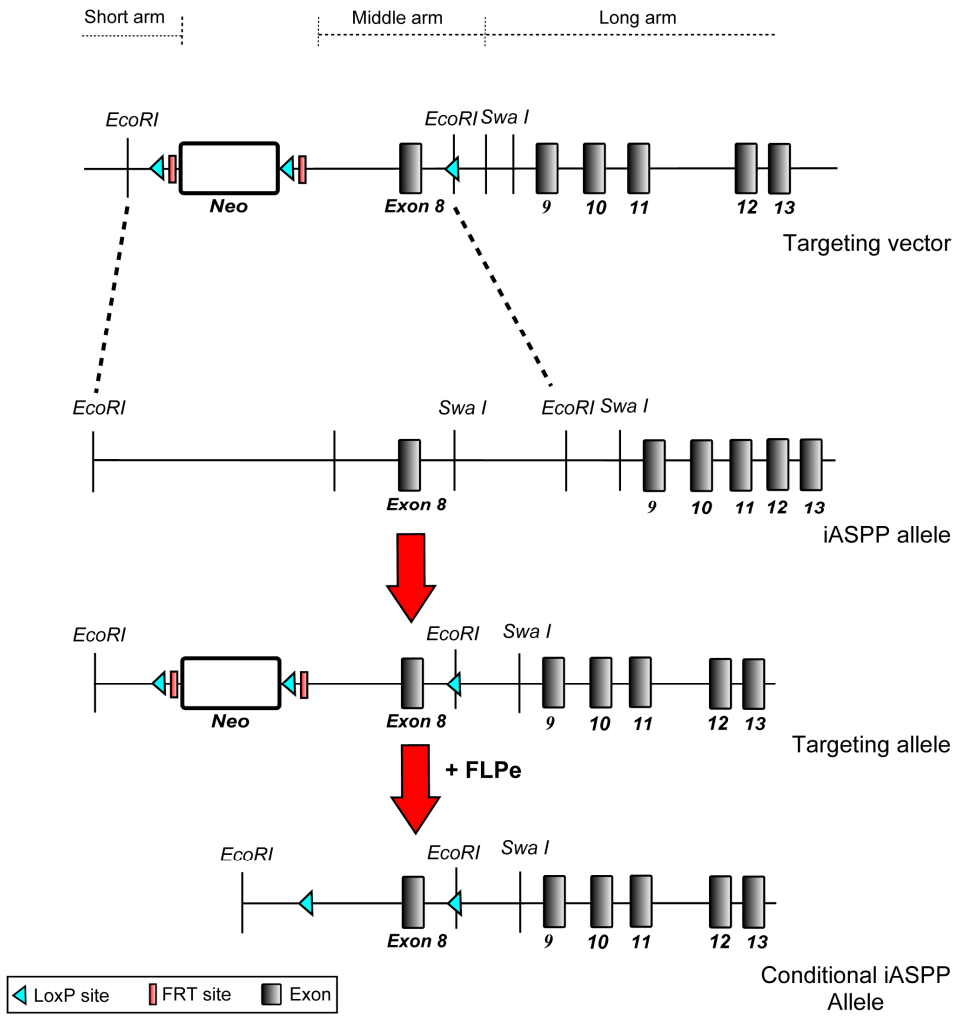


Figure 3.3. Construction of "flox" iASPP mice. In the targeting vector (*top*), loxP recognition sequences *(light blue arrows)* were positioned surrounding the exon 8 of the *PPP1R13L* gene. A neomycin resistance gene (Neo) was also cloned in between two FLP recombination target (FRT) sequences *(red bars)* within intron 7. After the recombination events into ES cells, the targeting iASPP conditional allele was generated *(targeting allele)*. Mice containing the "targeting allele" were mated to an FLPe recombinase expressing mouse line to excise the Neo resistance cassette and originate the conditional iASPP allele (iASPP$^{flox/flox}$) in which the exon 8 is surrounded by two loxP sites *(bottom)*.

After the iASPP$^{flox/+}$ mice were obtained, positive for one *PPP13R1L* "flox" allele, the correct insertion of the two loxP sites was verified. For this purpose, DNA was extracted from mice ears by biopsy and PCR analyses were performed using specific primers for the detection of the loxP motifs. In particular, the recognition sequences were detected using specific primers named FRNT9 and FLP2, which spanned the 3' intronic region between exon 8 and exon 9, at both ends of the loxp site *(figure 3.4, right).* The presence of the recognition motif (exon 8 "flox") would generate a band 34 base pairs (bp) longer than the wild type exon 8 (exon 8 WT), as shown in figure 3.4. The detection of both bands would indicate heterozygous mice, while the detection of a single band would indicate, respectively, the homozygous iASPP$^{flox/flox}$ mice if the only upper band was detected band iASPP$^{+/+}$ mice if the lower band was detected *(figure 3.4, left).* To detect the loxP site located 5' to exon 8, specific primers called E8-2 and I-82 were used. Again, positive PCR for the presence of the recognition sequence would generate a DNA fragment 68 bp longer that that from the wild type (data not shown).

Since we could not exclude the possibility that the insertion of loxP sites at both ends of exon 8 would impair iASPP gene transcription, whether the iASPP$^{flox/flox}$ allele had any outcome on normal viability and fertility of the mutant mice was initially studied. Of the 55 pups born from heterozygous iASPP$^{+/flox}$ pairs; we did not detect any variation from the normal Mendelian segregation *(figure 3.4).* All litters analysed were of normal size and the pups looked as healthy as the WT control. This indicated that the alteration of the *PPP13R1L* gene did not have any effect on mouse embryonic development or viability. Breeding together homozygous iASPP$^{flox/flox}$ couples again generated normal sized litters, and pups had normal post-natal development with genotype frequencies according to the Mendelian ratio (data not shown). Therefore, this conditional knockout mouse model is a useful tool for studying the functional importance of iASPP *in vivo*.

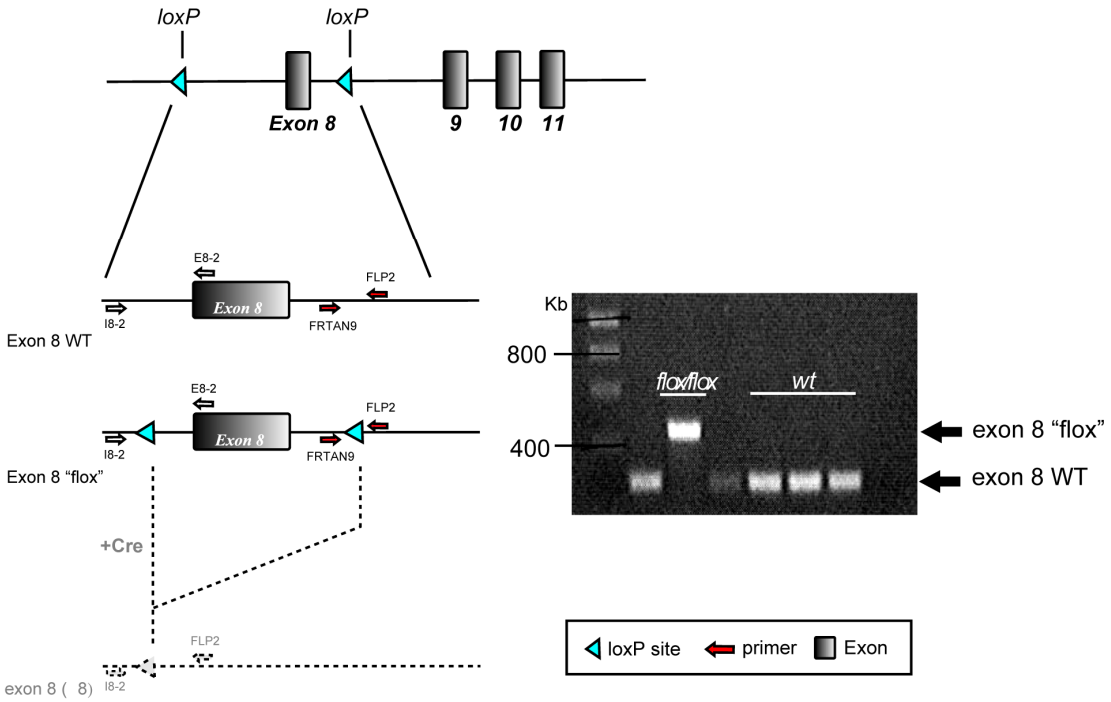


Figure 3.4. Schematic representation of the primers used to verify the insertion of the loxP sites around the PPP13R1L gene, and PCR analysis. *(left)* Diagram shows part of the wild type iASPP exon 8 allele (Exon 8 WT) and the conditional iASPP exon 8 "flox" allele (Exon 8 "flox"), with the respective location of the primers *(red arrows)* utilised to genotype iASPP$^{flox/flox}$ mice for the presence or absence of loxP sites. *(right)* PCR analysis of DNA isolated from iASPP$^{flox/flox}$ and iASPP$^{+/+}$ mice shows a delay in the run of the exon 8 "flox" PCR product, due to its increased size. PCR products were run on 1.5% agarose gel and visualised using Ethidium Bromide (EtBr).

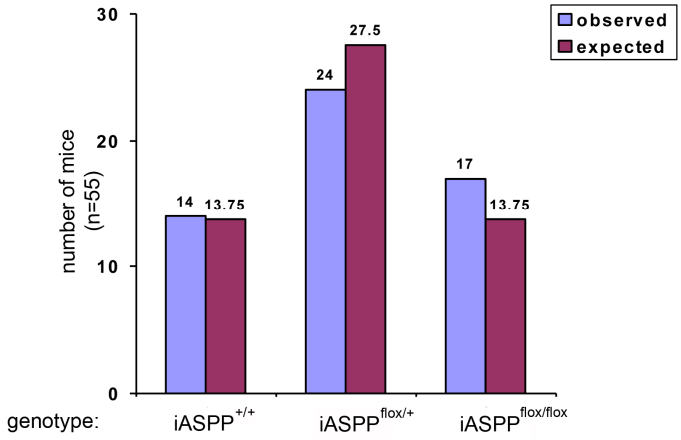


Figure 3.4. Mendelian segregation of iASPP "flox" allele. Genotyping of offspring from breeding heterozygous for iASPP$^{+/flox}$ using specific primers FRTAN9 and FLP2, and I8-2 and E8-2. Figure shows the post-natal segregation of the iASPP "flox" gene recorded for the breeding scheme *(blue)* and the expected segregation *(red)* according to Mendelian inheritance.

3.2.1.1 Validation of Cre-loxP for the deletion of iASPP exon 8 *in vitro*.

After successfully determining the presence of loxP sites around *PPP13R1L* exon 8 in iASPP$^{flox/flox}$ mice, the next step was to validate whether the Cre enzyme could induce the excision of the loxP-flanked DNA region. To investigate this, we generated primary mouse embryonic fibroblasts (MEFs) from iASPP$^{+/+}$, iASPP$^{flox/+}$ and iASPP$^{flox/flox}$ E13.5 embryos. MEFs stop dividing after only a few passages (7-10), so need to be frequently, freshly isolated from pregnant mice. These cells are of great value because they have the same genetic abnormalities of the transgenic mice, giving scientists the opportunity to link tissues phenotypes with *in vitro*-based cell systems, to study the underlying molecular mechanism. MEFs generated from iASPP$^{+/+}$ and iASPP$^{flox/flox}$ E13.5 embryos were infected with a recombinant adenovirus expressing the Cre enzyme. After different concentrations of adenovirus infection (moi: multiplicity of infection) were tested, solid expression of the Cre recombinase enzyme was achieved with 500 moi (*figure 3.5A).* This multiplicity of infection was selected as the best condition for effective expression of the Cre enzyme in MEFs. Subsequent quantification analyses of protein extracts generated from iASPP$^{+/+}$ and iASPP$^{flox/flox}$ cells infected with Cre-expressing adenovirus vector were performed, using specific monoclonal antibodies for iASPP (LX049.3) *(see figure 3.7A)* and the Cre enzyme. Figure 3.5B revealed that consistent expression of the Cre enzyme was accompanied by an almost 80% reduction of iASPP protein expression (*figure 3.5, lane 4.)*. The remaining signal detected by the LX049.3 antibody could be due to a small percentage of non-infected MEF cells, or the half-life of the iASPP protein. Nevertheless, these data clearly demonstrated that the Cre/loxP system in iASPP$^{flox/flox}$ mice worked efficiently, and that a substantial reduction of iASPP expression was achieved upon Cre expression *in vitro*.

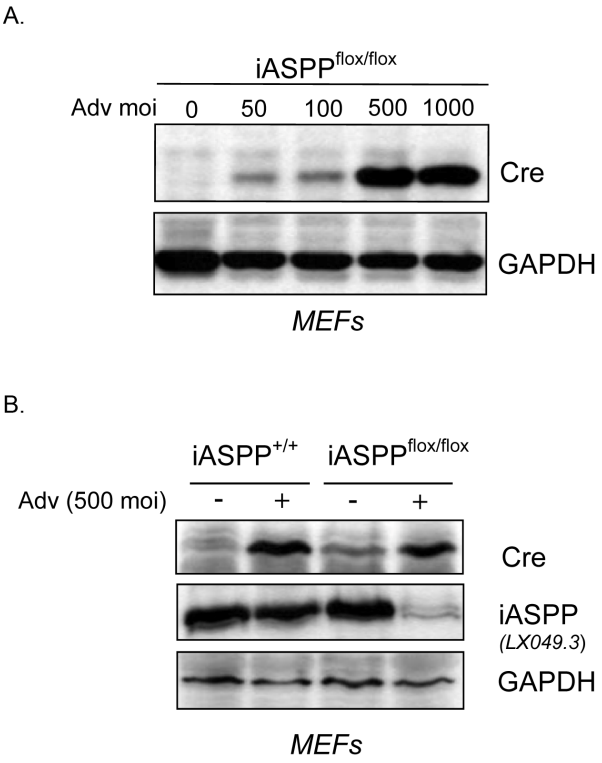


Figure 3.5. Cre expression induces the reduction of iASPP expression in iASPP $^{flox/flox}$ MEFs. *(A)* iASPP$^{flox/flox}$ MEFs were infected with Cre-expressing adenovirus with indicated multiplicity of infection (moi). Proteins lysates were prepared using UREA buffer solution and proteins were analysed by SDS-PAGE electrophoresis and Western blot technique. Membranes were immunoprobed using Cre primary antibody. GAPDH was used as a loading control. *(B)* iASPP $^{+/+}$ and iASPP$^{flox/flox}$ MEFs were infected with 500 moi of Cre-expressing adenovirus. Proteins lysates were prepared in UREA buffer and proteins analysed by SDS-PAGE and Western blot. Membranes were immunoprobed for iASPP (LX049.3) and Cre expression. GAPDH was used as a loading control.

3.2.2 Generation of iASPP$^{\Delta 8/\Delta 8}$ mice.

3.2.2.1 Confirmation of genomic excision of loxP-flanked sites in Cre-expressing mice.

Mice carrying the heterozygous conditional iASPP allele (iASPP$^{flox/+}$) were crossed with CMV-Cre^{+} transgenic miceto obtain iASPP$^{\Delta 8/+}$progeny. The resulting heterozygous iASPP$^{\Delta 8/+}$ mice were mated together to breed iASPP homozygous mutant mice (iASPP$^{\Delta 8/\Delta 8}$), in which exon 8 of the iASPP gene was eliminated in both alleles. The deletion of exon 8 from the *PPP13R1L* gene was confirmed by

PCR amplification analysis using DNA templates extracted from ear biopsies of iASPP$^{+/+}$, iASPP$^{\Delta 8/+}$ and iASPP$^{\Delta 8/\Delta 8}$ mice. Ablation of exon 8 was confirmed using two iASPP-specific primers, which gave a fragment of 0.8 Kb: I8-2 located 570 base pairs (bp) upstream of exon 8 and FLP2 located 1080 base pairs (bp) downstream of exon 8 (*figure 3.6, left)*. The amplification of wild type exon 8 was confirmed by the presence of a PCR product of 0.6 Kb, generated using the iASPP-specific primers I8-2 and E8-2, and located at the start of exon 8. The detection of both bands indicated that the mice were heterozygous (*figure 3.6, right).* The genomic presence of Cre recombinase was determined, again, by PCR using specific primers designed to recognise the Cre genetic locus. Mice positive for Cre recombinase gave rise to a 400 bp product as shown in figure 3.6 *(left).* This analysis demonstrated that Cre successfully excised the loxP-flanked DNA region of the *PPP13R1L* locus from the mouse genome, and that the Cre/loxP system is capable of working both *in vivo* and *in vitro*.

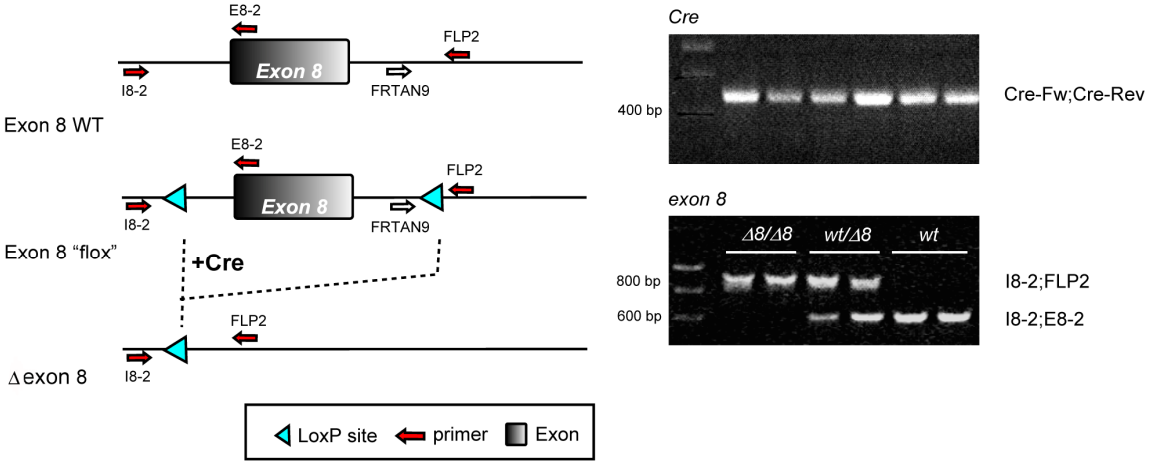


Figure 3.6. Schematic representation of the primers used to verify the deletion of exon 8 from the *PPP13R1L* gene, and PCR analysis of the loxP-flanked region in genomic DNA from iASPP$^{\Delta 8/\Delta 8}$;Cre^{+}, iASPP$^{\Delta 8/+}$;Cre^{+} and iASPP$^{+/+}$;Cre^{+} mice. *(left)* Diagram shows part of the wild type iASPP allele (Exon 8 WT), part of the conditional iASPP allele (Exon 8 "flox") and part of the conditional iASPP allele where exon 8 has been excised by Cre recombinase (Δexon 8). The respective locations of the primers *(red arrows)* utilised for genotyping iASPP$^{\Delta 8/\Delta 8}$ and iASPP$^{+/+}$ mice are also shown. *(right)* PCR analyses using Cre specific primers confirmed the presence of the Cre gene *(top right)*. Amplification of exon 8 from ear biopsy DNA obtained from iASPP$^{+/+}$(wt), iASPP$^{\Delta 8/+}$(wt/Δ8) and iASPP$^{\Delta 8/\Delta 8}$(Δ8/Δ8) mice confirmed the recombination event and the excision of exon 8 from the *PPP1R13L* gene. 1.5% agarose gel, 70V for 20min.

3.2.2.2 Confirmation of iASPP deficiency in iASPP$^{\Delta 8/\Delta 8}$ tissue and primary cells.

Despite the confirmation that *PPP13R1L* exon 8 had been excised by Cre recombinase, it was vital that the genomic recombination event in the *PPP13R1L* locus ultimately resulted in the absence of full length iASPP protein from tissues and primary cells originating from iASPP$^{flox/flox}$ mice upon expression of the Cre enzyme. Moreover, the design of the inducible KO system, which allowed the excision of only one exon from the PPP13R1L genetic locus, could not exclude the production of different truncated forms of the iASPP protein after the recombination event. In order to clarify this point, protein lysates were extracted from iASPP$^{+/+}$, iASPP$^{+/\Delta 8}$ and iASPP$^{\Delta 8/\Delta 8}$ MEFs and resolved by SDS-gel electrophoresis. Protein detection analysis was then conducted using two different antibodies raised against iASPP protein fragments from the N- (residues 1-240) and C-termini (residues 459-639) *(figure 3.7A).* Full length iASPP expression was efficiently extinguished in protein extracts from iASPP$^{\Delta 8/\Delta 8}$ MEFs *(figure 3.7B).* Of note, the heterozygous mouse had a half dose of iASPP expression. In addition, it was confirmed that no production of different truncated iASPP isoforms was detected upon the expression of Cre recombinase. The extra band detected using LX049.3, which resolved around the 70 KD mark, is not a truncated form of iASPP generated by the exon 8 deletion as it appeared also in control protein extracts *(figure 3.7B).*

Majors organs were dissected from iASPP$^{+/+}$, iASPP$^{+/\Delta 8}$ and iASPP$^{\Delta 8/\Delta 8}$ mice. After proteins had been extracted using a UREA buffer solution, immunoblot analysis was performed to confirm the loss of full length iASPP, or the presence of any truncated isoforms. Figure 3.7B shows the complete absence of full length iASPP protein from iASPP$^{\Delta 8/\Delta 8}$ organs. Furthermore, confirmation of whether the Wa3 mice were a true KO system for iASPP protein was desired. For that reason, protein exacts from iASPP$^{+/+}$ and iASPP$^{\Delta 8/\Delta 8}$ mice we resolved by SDS-page next to protein extracts from WT and Wa3 mice. As shown in figure 3.7B, iASPP protein disappeared in protein extracts from iASPP$^{\Delta 8/\Delta 8}$ hearts, but was still present in organs from control animals. Similarly, iASPP was

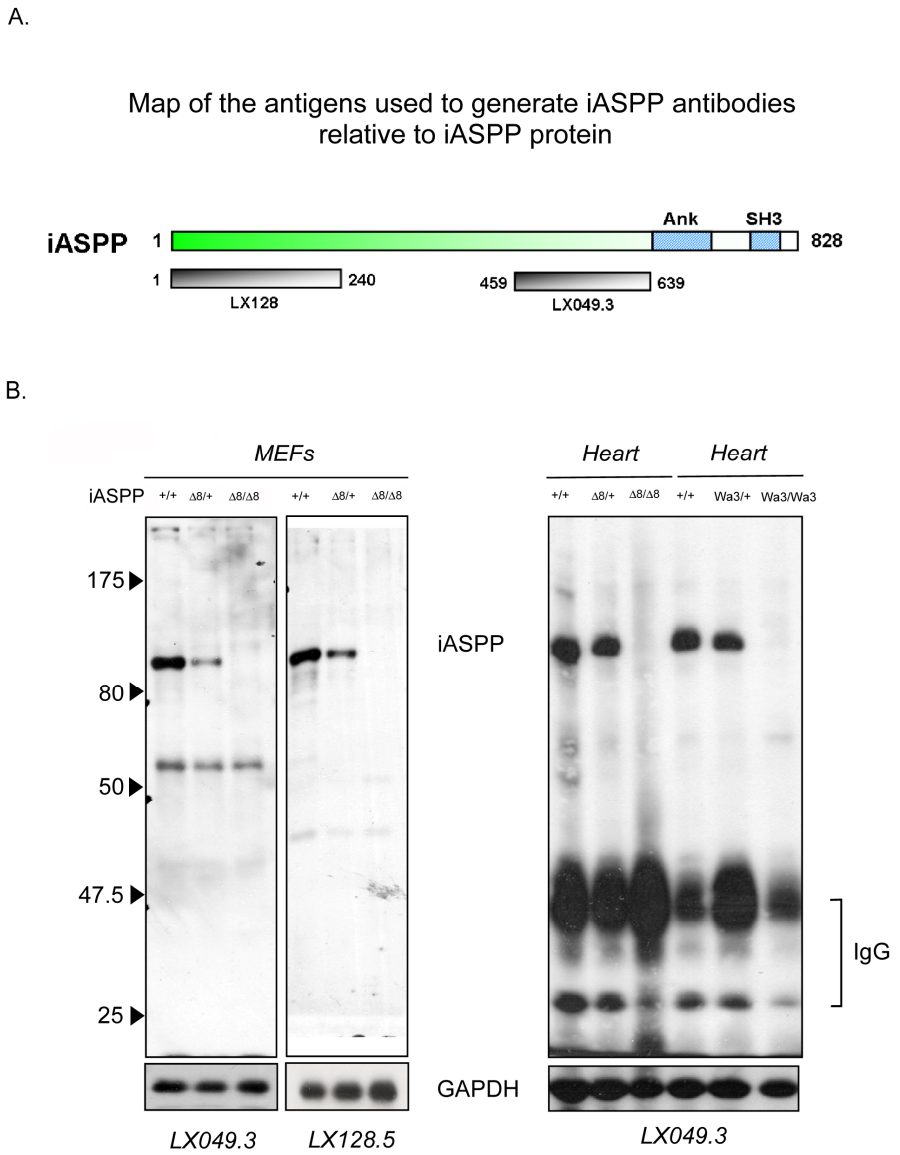


Figure 3.7. Confirmation of iASPP loss in iASPP$^{\Delta 8/\Delta 8}$ tissue and primary cells. (A) Diagram shows the location of the antigens used to generated LX128.5 and LX049.3 iASPP antibodies relative to full length iASPP protein. (B) MEFs were generated from iASPP$^{+/+}$, iASPP$^{\Delta 8/+}$ and iASPP$^{\Delta 8/\Delta 8}$ embryos. Proteins were extracted using UREA buffer solution and resolved by SDS-PAGE electrophoresis. iASPP expression was analysed by Western blot by immunoprobing the membrane with LX049.3 and LX128.5 monoclonal antibodies. GAPDH was used as a loading control *(right).* Hearts were dissected from iASPP$^{+/+}$, iASPP$^{\Delta 8/+}$, iASPP$^{\Delta 8/\Delta 8}$, wild type (+/+), Wa3/+ and Wa3/Wa3 mice. Proteins were extracted using UREA buffer solution and separated by SDS-PAGE. iASPP expression was analysed by Western blot by immunoprobing the membrane with LX049.3. GAPDH was used as a loading control *(left).*

absent in Wa3 protein extracts compare to control littermates, indicating that Wa3 mice are indeed KO mice for iASPP expression *(figure 3.7B)*.

Taken together, these results demonstrate that iASPP$^{\Delta 8/\Delta 8}$ mice and primary cells derived from them do not express the full length iASPP protein, thus, a conditional KO mouse model for the depletion of iASPP protein has been generated.

3.2.3 iASPP deficiency leads to high mortality rates in mice.

iASPP expression was shown to be abrogated in iASPP$^{\Delta 8/\Delta 8}$ mice after the introduction or expression of Cre enzyme in the mouse genome. In order to investigate the biological importance of iASPP *in vivo,* we first analysed the survival rate and Mendelian segregation of the iASPP$^{\Delta 8/\Delta 8}$ allele. Of 197 post-natal offspring derived from a heterozygous iASPP$^{\Delta 8/+}$ mating, only 25 were homozygous iASPP$^{\Delta 8/\Delta 8}$ (13%) *(figure 3.8 top panel)*. Hence, the post-natal survival rate of iASPP deleted mice was below the expected Mendelian frequency of 25%. To investigate at which stage of embryonic development the iASPP$^{\Delta 8/\Delta 8}$ embryos failed to survive, we performed a timed mating study in which we harvested embryos from iASPP$^{\Delta 8/+}$ breeding pairs at different embryonic days, and calculated the Mendelian ratio for each time-point. This study revealed that the expected number of iASPP null embryos could survived up to embryonic day 13.5 (E13.5) (*figure 3.8 lower panel)*. In fact, of the 96 E13.5 embryos analysed, 19 (20%) carried the homozygous allele iASPP$^{\Delta 8/\Delta 8}$, suggesting that most of them failed to develop properly between days E13.5 and E18.5. Although the number of embryos is not statistically relevant, the analysis of 48 E18.5 embryos born from heterozygous iASPP$^{\Delta 8/+}$ mice further supports this hypothesis. Of the 48 embryos studied, just 5 were PCR positive for the deletion of *PPP13R1L* exon 8, which was more than a 50% reduction from the expected Mendelian segregation of 11 (25%) *(figure 3.8 middle panel)*. These data strongly indicate a pivotal role for iASPP during mouse embryogenesis.

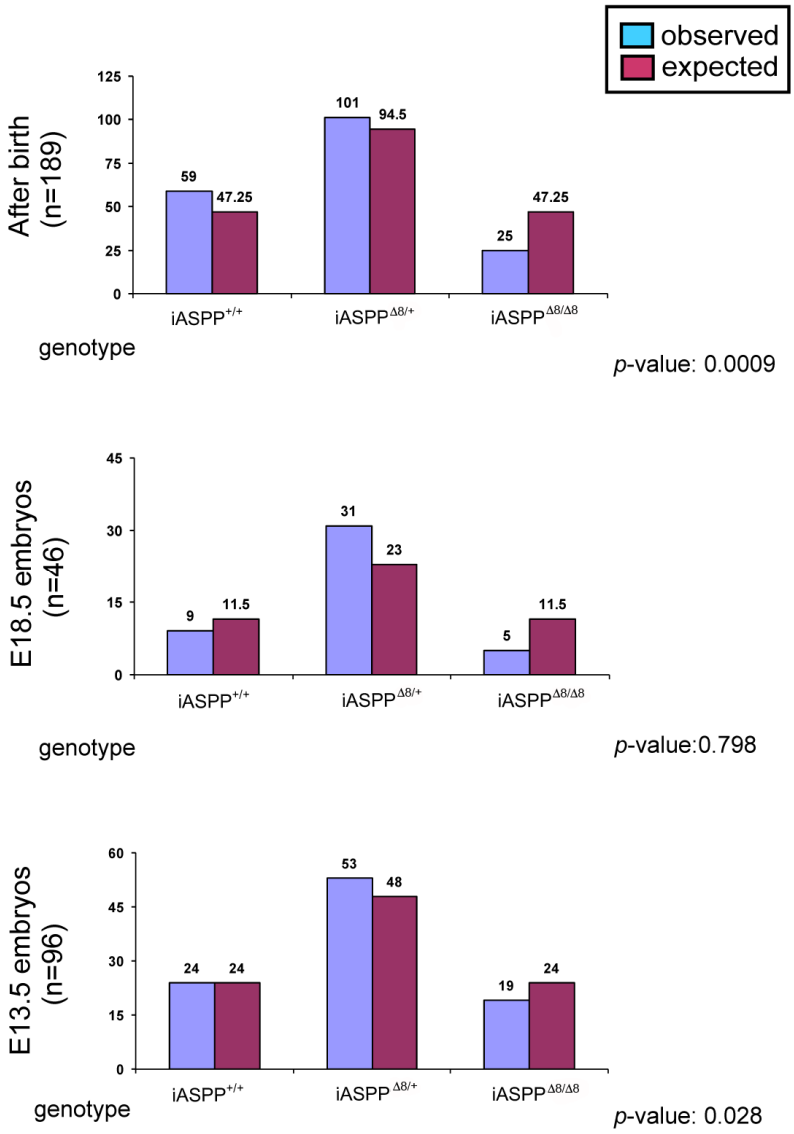


Figure 3.8. Mendelian segregation of iASPP$^{\Delta 8/\Delta 8}$ alleles at different embryonic stages and after birth. Figure shows the post-natal and embryonic lethality of iASPP-null mice. *(top)* In a cohort of 189 pups born from iASPP$^{+/-}$ intercrosses, the Mendelian expected frequency *(red)* and the observed frequency *(blue)* were compared in mice born with different iASPP genotypes. *(middle and bottom)* The Mendelian expected frequency *(red)* and the observed frequency *(blue)* were compared in embryos generated with different iASPP genotypes at different stages. p-values are shown at the bottom right corner of each bar graph.

3.2.4 Investigation of expression and cellular localisation of iASPP in vivo.

To study iASPP's expression pattern, and confirm the absence of iASPP protein in different mouse organs, we dissected and analysed a number of appendages derived from iASPP$^{+/+}$ and iASPP$^{\Delta 8/\Delta 8}$ mice. Tissues were freshly dissected from animals with different genotypes, snap frozen in liquid N_2 and reduced to fine powder using a pesto and mortar. Proteins were extracted using 9M urea buffer and resolved on a SDS-polyacrylamide gel. Investigation of iASPP expression was performed by western bolt technique using a specific antibody against the N-terminal part of iASPP (LX128.5). As shown in figure 3.9, lysates from various wild type organs indicated that heart, testis and skin were the mouse appendices in which iASPP was expressed the most. Under the same conditions, iASPP was not detected in the spleen and liver (*figure 3.9)*. The bar graph shows the actual expression of iASPP in different organs, normalised with loading control expression (GAPDH), which confirmed our observation that iASPP is heavily expressed in both the heart and skin.

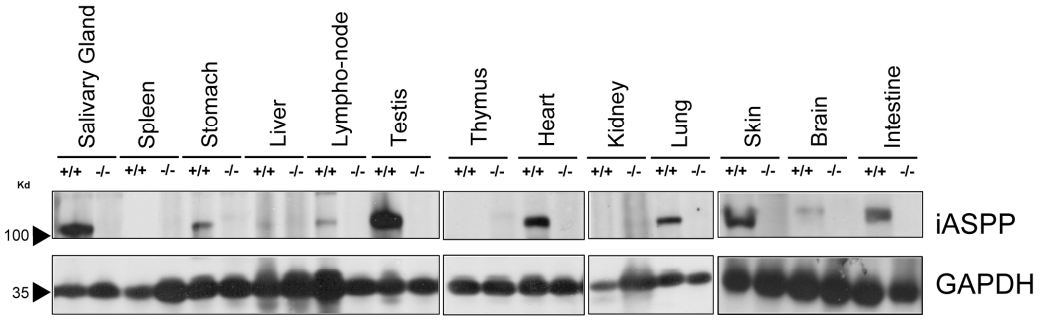


Figure 3.9. iASPP expression levels in different mouse organs. *(top)* The indicated mouse organs were dissected and snap frozen in liquid N_2. The tissues were reduced to a fine powder and protein extracted using UREA buffer. Three round of sonication were performed to disintegrate any DNA residue. Proteins were resolved by SDS-PAGE electrophoresis and, after western blotting, the membrane immunoprobed for iASPP (LX0.49.3) expression. GAPDH was used as a loading control.

Next, we examined the cellular location of full length iASPP in adult mouse organs expressing high levels of iASPP, in order to obtain vital information on the possible biological role of iASPP *in vivo*. Visualisation of proteins by immunofluorescence is the gold standard for the investigation of their cellular localisation. Previously, iASPP/RAI protein overexpressed in HeLa cells had been reported to have only a nuclear localisation, predominantly in the nucleoplasm (Yang, Hori et al. 1999). However, full length iASPP locates mainly in the cytoplasm and nucleus of cells *in vitro* (Slee, Gillotin et al. 2004). To study the location of iASPP in heart and skin tissues, immunohistochemistry and immunofluorescence analysis were performed on adult heart and skin tissue section dissected from iASPP$^{\Delta 8/\Delta 8}$ and WT littermates. First, immunohistochemistry on heart paraffin sections dissected from iASPP$^{+/+}$ was performed using both monoclonal antibodies LX049.3. Fully differentiated cardiomyocytes have a characteristic rod-shaped morphology and intercalated discs at the polar end, which link the complex myocyte's cytoskeleton to the sarcolemmal membrane (Franke, Borrmann et al. 2006). Interestingly, positive staining obtained with both specific monoclonal iASPP antibodies was observed at the polar end of the cardiomyocyte in correspondence with the intercalated disc (ID) complex *(figure 3.10A)*. Of note, no signal was detected in iASPP mutant heart, confirming the specificity of the iASPP antibody used. This experiment showed for the first time a novel location of iASPP specific for adult heart tissue, and its possible involvement in cell-to-cell contacts.

Second, we analysed iASPP's location in adult skin *in vivo*. The epidermis was dissected from the back skin of iASPP$^{+/+}$ and iASPP$^{\Delta 8/\Delta 8}$ mice. We observed that iASPP was predominantly expressed in the basal layer of the epidermis *(figure 3.10B)*. The specificity of the anti-iASPP antibody used (LX049.3) was confirmed, again, by the lack of iASPP expression from iASPP$^{\Delta 8/\Delta 8}$ epidermal specimens *(figure 3.10B)*.

Together these results revealed that different organs expressed iASPP at different levels, suggesting a differential role of the protein in various organs. Testis, salivary glands, heart and skin are the

tissues in which iASPP is expressed the most. In addition, a novel location of iASPP in myocardial tissue revealed a possible involvement for iASPP in cell-to-cell contacts *in vivo*.

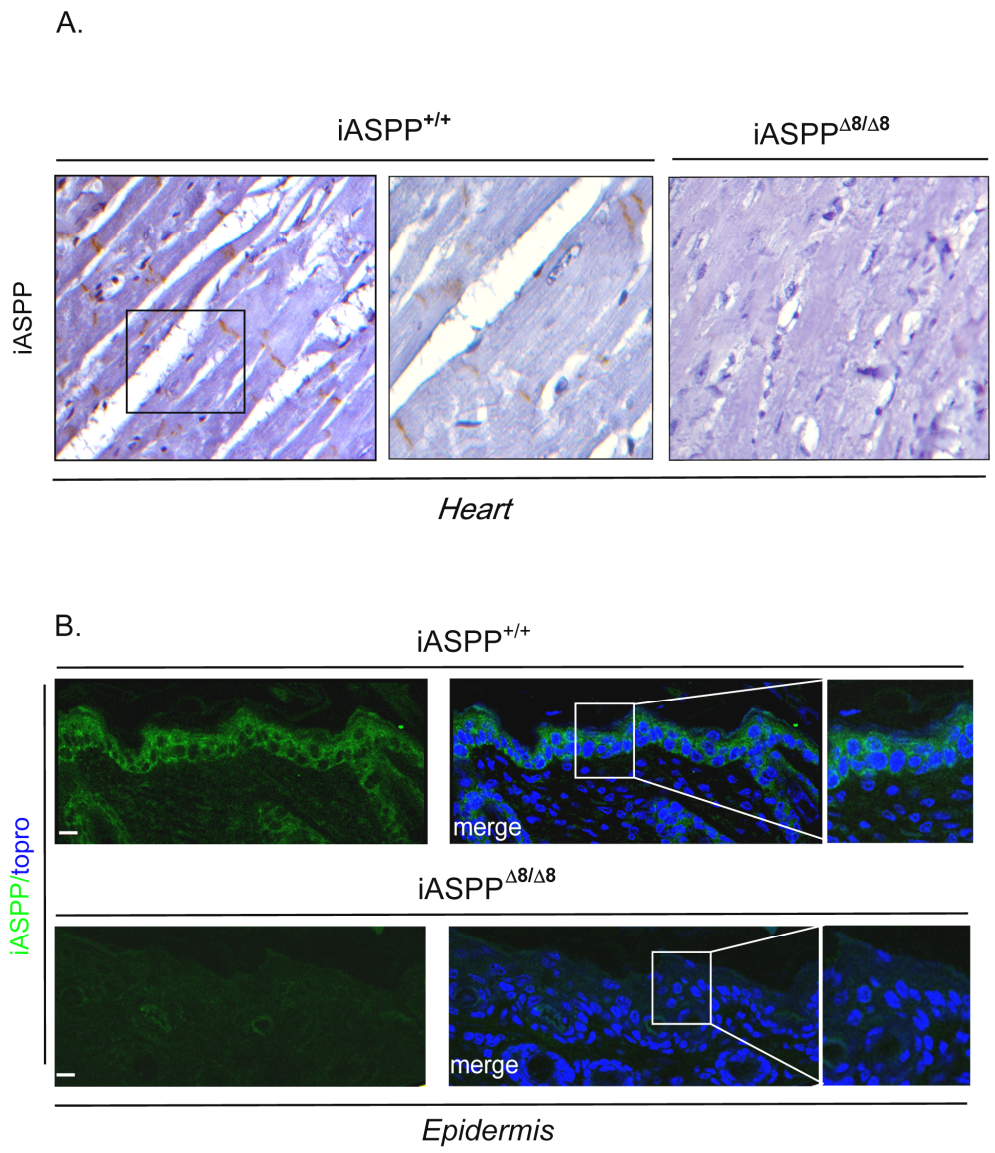


Figure 3.10. iASPP immunostaining pattern in wild type and KO myocardial and epidermal sections. (A) Ventricular myocardial sections from wild type (iASPP$^{+/+}$) and iASPP mutant (iASPP$^{\Delta 8/\Delta 8}$) adult hearts were immunostained using LX049.3 antibody *(left)*. Immunohistochemistry shows the characteristic location of iASPP at the polar-end of the rod-shape cardiomyocytes. Black square represents area of higher magnification of wild type myocardial tissue *(middle)*. Specificity of the LX049.3 antibody was confirmed by the lack of signal from iASPP$^{\Delta 8/\Delta 8}$ myocardial sections *(right)*. (B) Immunofluorescence of dorsal skin sections from iASPP$^{+/+}$ mice shows iASPP's location. iASPP expression was not detected in iASPP$^{\Delta 8/\Delta 8}$ sections, confirming the specificity of the antibody. Squares represent higher magnification of the epidermal region.

3.3 Discussion and conclusion.

In order to study the biological functions of iASPP *in vivo*, the *PPP1R13L* genetic locus was modified to achieve the generation of a conditional mammalian system for the depletion of iASPP protein upon expression of the Cre recombinase enzyme. The work described in this Chapter was conducted mainly to confirm the creation of the conditional iASPP KO transgenic mouse line. First of all, we demonstrated that two loxP sites were successfully inserted at both ends of exon 8 of *PPP13R1L* in the mouse germline. This was made possible by Ingenius Targeting Laboratory (NY, USA), which constructed the targeting vector for the insertion of the loxP recognition sequences at both ends of iASPP exon 8. Importantly, the addition of two extra pieces of DNA into *PPP13R1L* did not affect the normal transcription of the iASPP gene. This is consistent with *in vivo* conditional KO systems developed by other laboratories and described in the literature. In fact, we showed that iASPP$^{flox/flox}$ mice are healthy, fertile and behave normally when compared to wild type controls. In addition, the segregation of the iASPP "flox" allele followed the normal Mendelian segregation of 25% in the resulting progeny. The genomic excision of the DNA region between the two loxP sites in the iASPP$^{flox/flox}$ allele was confirmed *in vitro* using MEFs upon infection of Cre-expressing adenovirus. PCR amplification analyses proved the complete excision of exon 8 from the *PPP13R1L* genomic locus upon Cre adenovirus infection, only in iASPP$^{flox/flox}$ primary cell lines. Although exon 8 excision efficiency was around 100%, the relative amount of iASPP protein expression found in iASPP$^{flox/flox}$ MEFs after Cre-expressing adenovirus infection needed to be investigated. Remarkably, iASPP expression levels were decreased by ~80% in protein extracts from iASPP$^{flox/flox}$ primary cells 48 hours after Cre adenovirus infection. The decrease in iASPP protein expression is consistent with previously published data regarding the efficiency of Cre/loxP systems, however, we were unable to demonstrate a total absence of iASPP protein in primary "flox/flox" Cre-infected cell lines due to a small portion of cells being either not infected or, since we analysed iASPP expression 48 hours after infection, due to the half-life of iASPP. Nevertheless, our Cre/loxP system was demonstrated to achieve a good reduction of iASPP protein expression,

therefore we accepted the iASPP$^{flox/flox}$ mice as a high-quality conditional iASPP KO system for the investigation of iASPP function *in vivo*.

To investigate the possibility that the conditional *PPP13R1L* exon 8 KO approach might generate truncated iASPP RNA messengers, which could be translated into shorter isoforms of the iASPP protein, iASPP immunoblotting was undertaken using on MEF lysates with two different antibodies raised against iASPP protein fragments from the N- and C-termini. Remarkably, no truncated forms of iASPP were detected in iASPP$^{flox/flox}$ Cre-infected protein lysates, indicating that the elimination of exon 8 from the iASPP gene did not lead to the generation of an alternative stop codon or truncated iASPP proteins which could interfere with the analysis of the biological role of iASPP *in vivo*.

Next, iASPP$^{flox/flox}$ mice were bred together with a transgenic mouse line harbouring a constitutive and ubiquitously expressed Cre recombinase enzyme (CMV-Cre^{+}), in order to generate a "conventional" KO system for iASPP expression. Surprisingly, the resulting iASPP$^{\Delta 8/\Delta 8}$ offspring were viable, although they were recovered at lower frequencies than the normal expected Mendelian segregation. This was in contrast to previous reports about a KO system for the abrogation of proteins important in inhibiting p53's activity *in vivo* (Jones, Roe et al. 1995; Montes de Oca Luna, Wagner et al. 1995). In fact, loss of mdm2 or mdm4 resulted in mouse embryonic lethality while, surprisingly, loss of iASPP did not. One possible explanation for the absence of complete embryonic lethality in iASPP$^{\Delta 8/\Delta 8}$ could be the genetic background of the animals employed in the experiment. Our iASPP$^{\Delta 8/\Delta 8}$ mice were generated in a mixed C57BL/6J and 129Sv/Ev background, and it is known that different genetic backgrounds can influence or completely change the phenotype of a particular strain of mice (Mak T. W. *The gene knockout facts book.* Academic San Diego, CA). However, Wa3 mice have a pure C57BL/6J background and similarly did not show complete embryonic lethality (Herron, Rao et al. 2005).

So far, various p53 inhibitors have been identified, demonstrating how tightly p53's activity must be regulated in order to avoid cell death. This is reinforced by an *in vivo* system with a

constitutively active form of p53, which showed resistance to spontaneous tumours (Tyner, Venkatachalam et al. 2002). Alternatively, loss of expression of p53 inhibitors results in embryonic lethality which is entirely p53 dependant (Jones, Roe et al. 1995; Finch, Donoviel et al. 2002; Migliorini, Lazzerini Denchi et al. 2002). Among them, loss of iASPP might not increase the apoptotic index enough to drive an embryo to premature death. However, the decreased ratio of iASPP$^{\Delta 8/\Delta 8}$ newborns compared to the normal Mendelian segregation suggests a possible important role for iASPP in controlling tissue homeostasis during embryogenesis. It is exciting to speculate that iASPP has a new role, independent by p53, in mouse development, as recently shown for ASPP2 (Sottocornola, Royer et al. 2010). This study has led to the development of the first conditional model that allows the assessment of iASPP's functions in a tissue/cell-specific manner. Since embryonic lethality in iASPP mutant progeny is not fully penetrant, investigation of the function of iASPP in adult animals also is needed to fully understand the cause of the embryonic lethality. Interestingly, heart and skin are two organs in which iASPP protein is expressed the most. This could imply an important role for iASPP in maintaining the integrity, structure or function of these organs. Therefore, both immunohistochemistry and immunofluorescence analysis were performed to provide information on the cellular localisation of iASPP. Preliminary data indicates a potential function of iASPP in maintaining the integrity of the heart junctions, and direct or indirect involvement in epidermis formation, as iASPP was found in the actively proliferating layers of the skin.

To conclude, in this chapter the deletion of iASPP protein from all major organs in iASPP-deficient mice was confirmed, as was the fact that the inducible *PPP13R1L* exon 8 excisions could indeed result in the ablation of iASPP protein. The importance of iASPP in the heart, together with the embryonic lethality and the skin phenotype will be the topics of, respectively, Chapters IV and V of this study.

Chapter 4
RESULTS

iASPP is required for normal functioning of the heart and its development *in vivo*.

4.1 Introduction.

In Chapter III, the efficiency of an inducible KO system for the removal of iASPP expression in both *in vivo* and *in vitro* systems was established, by demonstrating that the excision of exon 8 of the *PPP13R1L* gene was obtained after the expression of Cre enzyme. As a consequence, the expression of full length iASPP was suppressed in both mouse tissues and primary cell populations. Subsequent investigation of iASPP expression in mouse wild type organs indicated that the heart, testis and skin are the tissues in which iASPP is abundantly expressed. In order to reveal a potential biological role for iASPP *in vivo*, these organs were analysed for any abnormalities in their morphology, structure or function. The work described in this Chapter therefore aims to investigate the biological function of iASPP in the adult and developing mouse myocardium, focussing on the identification of heart abnormalities, the description of the phenotype and correlation with known human pathologies. Finally, the dependency of the heart phenotype on the expression of p53 and its family members will be investigated.

4.2 Results

4.2.1 Loss of iASPP leads to a shorter life span *in vivo*.

As illustrated in Chapter III, iASPP expression seems to be required for the normal development of mouse embryos as showed by the reduced Mendelian segregation of iASPP$^{\Delta 8/\Delta 8}$ embryos *(figure 3.8)*. However, 13% of iASPP-null mice can survive up to the weaning age, and reach adulthood with no obvious signs of abnormal behaviour. Despite appearing healthy, many of these iASPP$^{\Delta 8/\Delta 8}$ mice were observed to die suddenly. Therefore, a cohort of iASPP KO mice, as well as a matched control group, was followed for more than 1 year in order to confirm the shorter life expectancy of the iASPP mutant progeny. Interestingly, the survival rates of the iASPP$^{\Delta 8/\Delta 8}$ and iASPP$^{\Delta 8/+}$ mice were significantly shorter when compared to their control littermates, with median survival of 40 weeks and 57 weeks, respectively. Beginning at 10 weeks of age, iASPP-null mice displayed a more rapid mortality that the wild type controls. Notably, iASPP$^{+/+}$ mice survived up to 2 years of age *(figure 4.6)*. It is also noteworthy that the experiment were performed on age-matched animals, with males and females used equally throughout the study and that iASPP$^{\Delta 8/\Delta 8}$ male and female mice were equally susceptible to early death. The earliest sudden death, which occurred in the iASPP-deficient cohort, was observed 10 weeks into the study. Moreover, all of the iASPP mutant mice employed in the study were affected by severe cardiomyopathy and died suddenly without any prior sign of illness, a situation resembling the human pathology of cardiomyopathy. This data clearly demonstrates that mice lacking iASPP expression have a shortened life span when compared to wild type littermates.

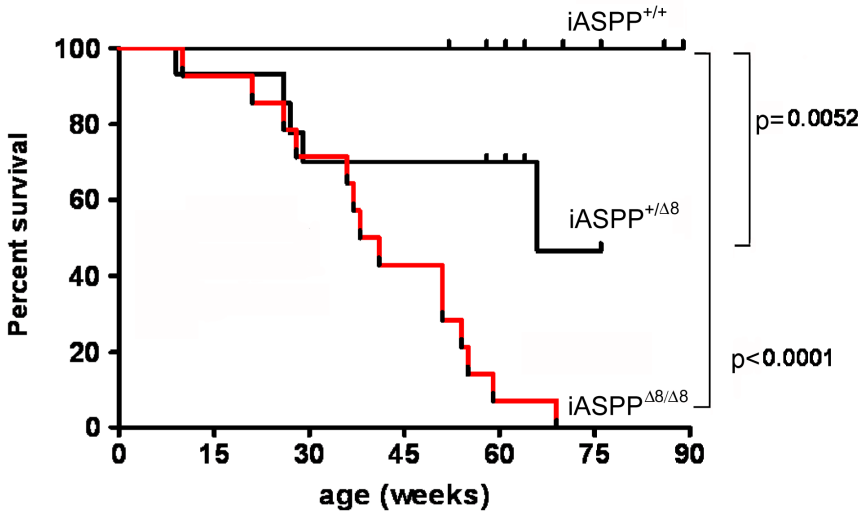


Figure 4.6. iASPP loss causes high mortality rates in iASPP$^{\Delta 8/\Delta 8}$ mice. Kaplan-Meier survival curve of iASPP$^{+/+}$ (n=20), iASPP$^{\Delta 8/+}$ (n=20) and iASPP$^{\Delta 8/\Delta 8}$ (n=22) mice. Gender does not affect the mortality rate of iASPP$^{\Delta 8/\Delta 8}$ mice. By 37 weeks of age, only 50% of iASPP$^{\Delta 8/\Delta 8}$ mice survived. All of the iASPP-depleted mice died suddenly without prior signs of illness. Gross analyses of the iASPP$^{\Delta 8/\Delta 8}$ hearts revealed that all of the iASPP mutant mice had developed dilated cardiomyopathy (n=22).

4.2.2 iASPP-deficient mice display Arrhythmogenic Right Ventricular Cardiomyopathy (ARVC).

4.2.2.1 iASPP-depleted mice exhibit morphological and molecular evidence of cardiac dysfunction.

Given the elevated expression of iASPP in whole heart protein extracts, and its location at the polar end of adult mouse cardiomyocytes, three hearts were dissected and studied from iASPP$^{\Delta 8/\Delta 8}$ mice, which die of sudden death at approximately 20 weeks of age. Using different histological techniques in association with light or fluorescence microscopy, we analysed and compared iASPP mutant hearts with organs matching in age and gender dissected from wild type mice. The organs were freshly removed and prepared for histological examination. Interestingly, at the macroscopic level, all mutant mice displayed a significantly enlarged heart, both in shape and size, accompanied

by the presence of white patches (fibrotic scars) on the exterior walls of both ventricles *(figure 4.1)*. The hearts dissected from iASPP-null animals showed a moderately increased heart weight/body weight wet ratio when compared to their WT controls (+23% versus controls; n=3). Next, the organs were processed in order to remove water from the tissues and replace it with a solid medium to allow thin sections to be cut for light microscopy analysis. For images originating from histological sectioning, it is vitally important to map and compare the corresponding planes of sections from the same organs obtained from two different specimens. For this reason, first of all haematoxylin and eosin staining (H&E) was performed on a series of heart sections from control and iASPP-null mice, and the resulting stainings were analysed with the help of a mouse atlas, to search for the same plane of section between $iASPP^{+/+}$ and $iASPP^{\Delta 8/\Delta 8}$ hearts. Only matching sections were used throughout this study. In order to define and examine the overall structure of the heart and the architecture of the myocardium in $iASPP^{\Delta 8/\Delta 8}$ mice, H&E staining was performed on 8 μm thick matching myocardial sections dissected and processed from iASPP mutant and wild type mice.

Histological analysis of the iASPP-null hearts demonstrated a severe dilatation of both ventricular and atrial chambers, in association with thinner ventricular and septal walls *(figure 4.2A)*. Microscope analysis revealed that the overall architecture of the myocardium of iASPP KO mice appeared to be severely compromised; both ventricles showing extensive regions of myocyte loss associated with disarray of the myocardial tissue *(figure 4.2A-B)* and increased intercellular spaces between myocytes *(figure 4.2B)*. Moreover, cross-sections of iASPP-depleted hearts showed the presence of enlarged and obviously hypertrophic cardiomyocytes *(figure 4.2C, right panel)*. Immunohistochemical staining of atrial natriuretic peptide (ANP), a molecular marker extensively used to demonstrate cardiomyocyte hypertrophy and abnormal heart function (Nikolova, Leimena et al. 2004), was performed. Positive signals were only detected in iASPP mutant myocardial sections *(figure 4.2C, left panel)*. Since positive markers for myocytic hypertrophy and heart failure were

observed in iASPP mutant hearts, immunostaining for extracellular matrix components was performed. Enhanced deposition of extracellular matrix between cardiomyocytes is known, in heart

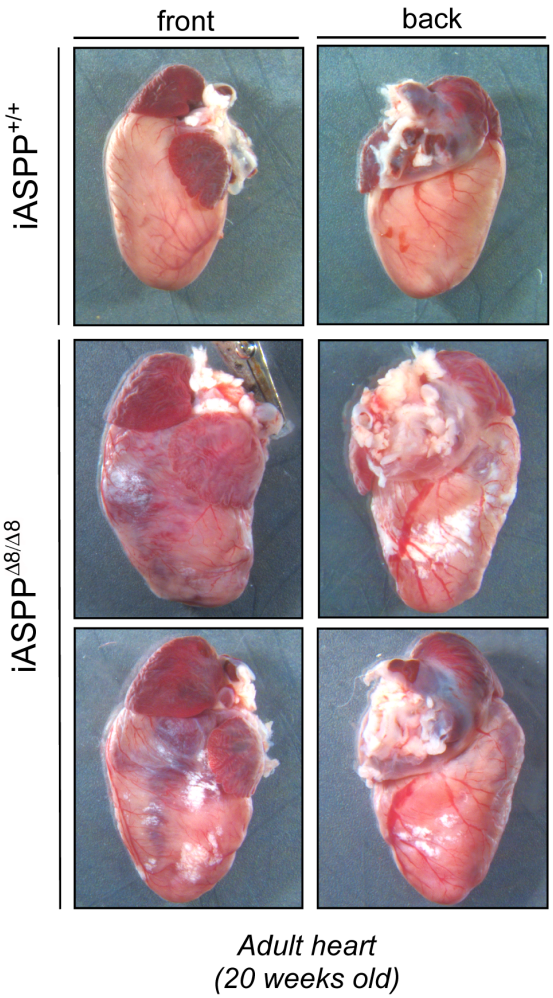


Figure 4.1. Gross abnormalities in iASPP$^{\Delta 8/\Delta 8}$ hearts. Hearts were dissected from "found dead" iASPP KO mice, placed in 10 cm dishes contained PBS buffer solution and photographed using a dissection microscope. Magnifications 2X. Matching age and sex wild type mice were sacrificed, and the hearts dissected and used as controls. Hearts from iASPP$^{\Delta 8/\Delta 8}$ mice show enlarged size of the organ, associated with white, focal lesions on the exterior of the ventricular wall.

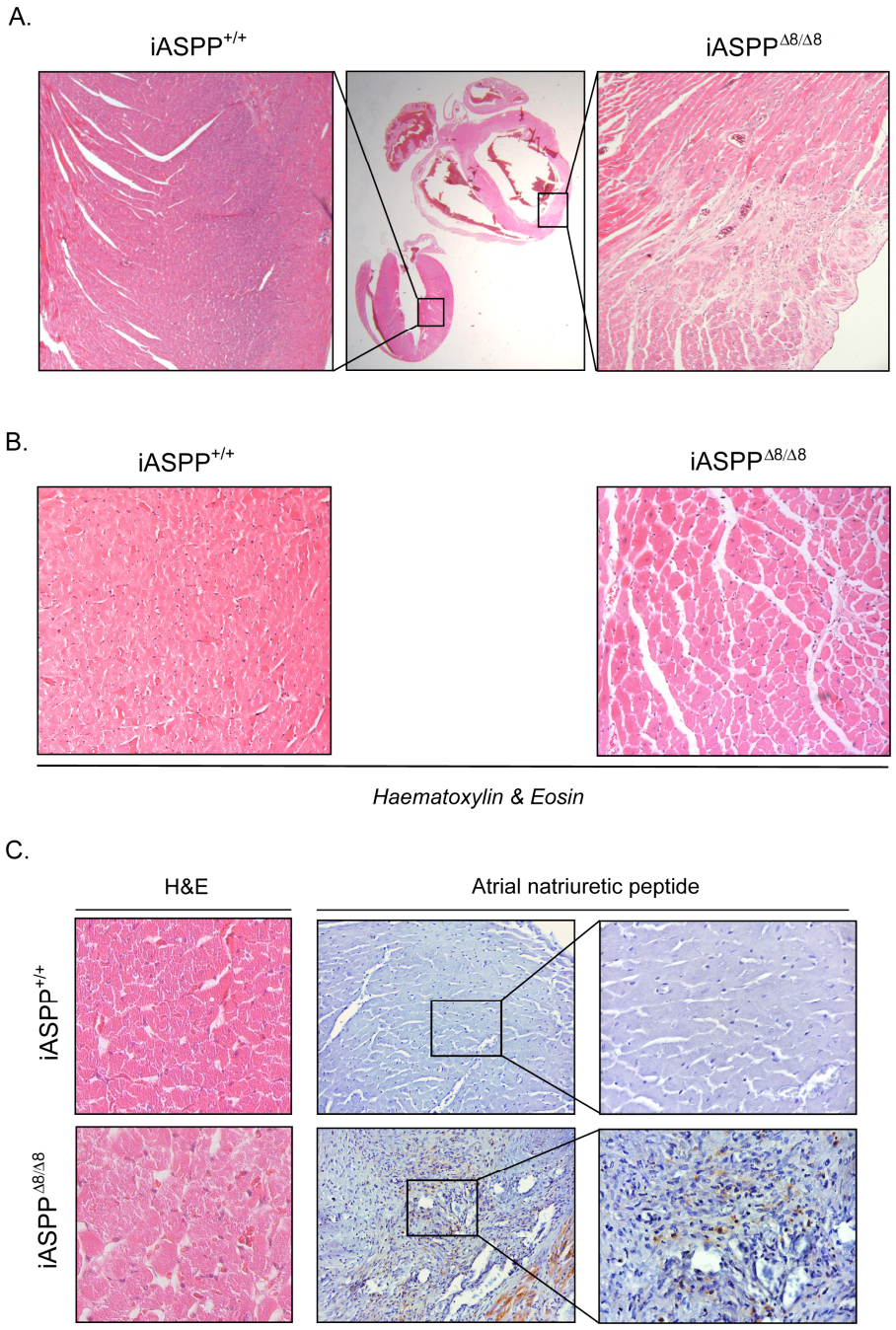


Figure 4.2. Histological analysis of iASPP$^{\Delta 8/\Delta 8}$ mice. (A) Transverse heart sections from 20 week old iASPP$^{+/+}$ and iASPP$^{\Delta 8/\Delta 8}$ mice were stained using the haematoxylin & eosin (H&E) technique. Note the dilated ventricles in the iASPP$^{\Delta 8/\Delta 8}$ heart and the thin right ventricular wall *(middle panel).* Loss of cardiomyocytes in the iASPP$^{\Delta 8/\Delta 8}$myocardium was also evident *(right panel).* (B) Higher magnification of a random area of myocardium from H&E stained wild type and iASPP KO mice. Abnormal myocardial arrangement and increased intercellular space was observed in iASPP$^{\Delta 8/\Delta 8}$ samples. (C) *(left panel)* H&E stain of myocardial cross-sections from iASPP$^{+/+}$and iASPP$^{\Delta 8/\Delta 8}$ mice show moderate cardiac hypertrophy in iASPP KO sections and positive immunostaining for the ANP marker.

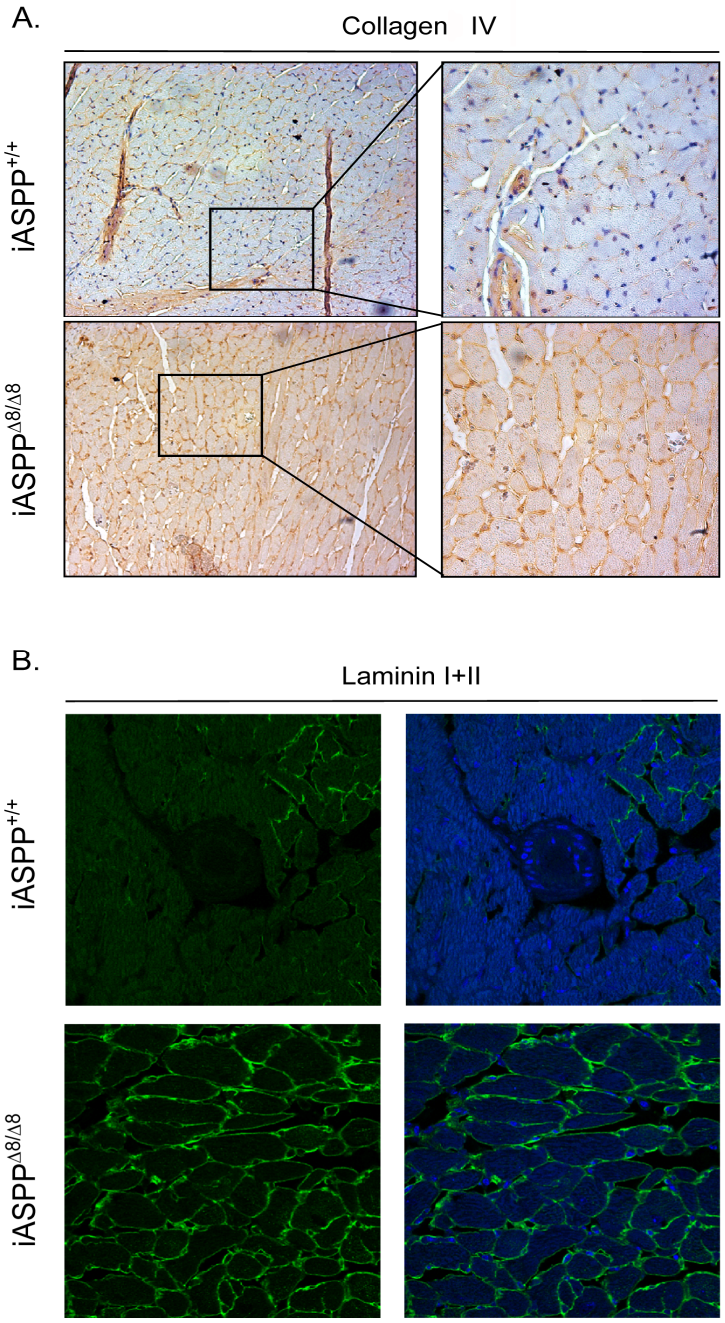


Figure 4.3. Increased extracellular matrix components in iASPP$^{\Delta 8/\Delta 8}$ hearts. (A) Heart sections from 20 week old iASPP$^{+/+}$ and iASPP$^{\Delta 8/\Delta 8}$ mice were used to perform immunohistochemistry using a collagen IV primary antibody. A positive signal was detected using peroxidise substrate (ABC kit). Picture shows accumulation of collagen IV in between cardiomyocytes. (B) Heart sections from 20 week old iASPP$^{+/+}$ and iASPP$^{\Delta 8/\Delta 8}$ mice were immunostained using a specific antibody, which recognises both laminin I and II. On this occasion, a secondary antibody linked to a fluorescent fluorochrome was used to reveal a positive signal. Accumulation of laminin I and II was obvious in iASPP$^{\Delta 8/\Delta 8}$ hearts.

pathology, as a compensatory mechanism of a failing heart to sustain the mechanical stress and performance of the heart's contraction (Ahmad, Seidman et al. 2005).

The staining shown in figure 4.3 demonstrated that the intercellular space between the iASPP$^{\Delta 8/\Delta 8}$ cardiomyocytes was filled with collagen type IV, laminin-1 and -2 (*figure 4.3)*. Ventricular dilatation, extensive fibrosis and loss of myocardial organisation are the key cellular features that define the presence of dilated cardiomyopathy, hence we asked the question whether fibrotic areas were present in iASPP mutant myocardia. Localised areas associated with lighter H&E staining and disorganised structures of the myocardia were evident in iASPP$^{\Delta 8/\Delta 8}$ hearts *(figure 4.2A).* Hence, in order to investigate whether these areas are fibrotic deposits, Masson trichrome staining was performed. The Masson trichrome technique is routinely used for the detection of collagen fibres in biological tissues. As shown in figure 4.4, positive blue staining was clearly evident in specific areas of the iASPP KO myocardium that correspond with the areas of cardiac disarray seen in figure 4.2 *(figure 4.4 compared with figure 4.2).*

To conclude, this section of the study showed that loss of iASPP expression alters the normal morphology of the heart and the organisation of the myocardium. iASPP-deficient hearts exhibited an obvious dilatation of both ventricular chambers associated with moderate myocytes hypertrophy and increased extracellular matrix deposition. In addition, iASPP-null hearts showed focal areas in which the normal cardiac structure was lost and myocytes had been replaced by fibrotic deposits. Hence, iASPP$^{\Delta 8/\Delta 8}$ progeny appear to be affected by a severe primary or secondary dilated cardiomyopathy. These data also suggest a potential role for iASPP in maintaining the structural and functional integrity of the heart.

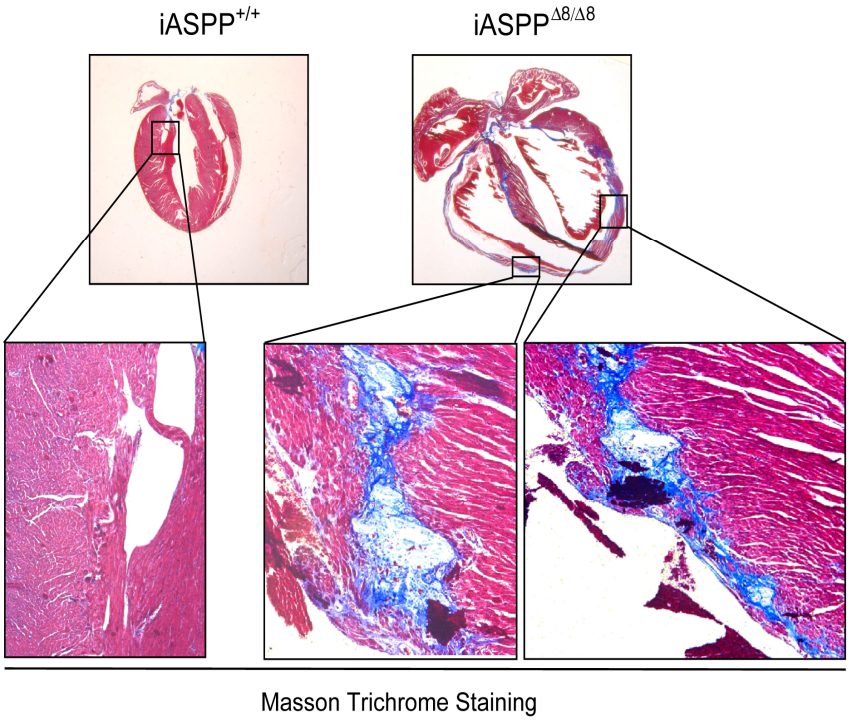


Figure 4.4. Histological analysis of iASPP$^{\Delta 8/\Delta 8}$ mice using Masson Trichrome staining. Thin myocardial sections from 20 week old iASPP$^{+/+}$ and iASPP$^{\Delta 8/\Delta 8}$ mice were investigated for fibrotic deposits. iASPP$^{\Delta 8/\Delta 8}$ mice showed extensive positive areas (blue staining) of fibrotic deposits. Increased interstitial fibrosis was also noted.

4.2.2.2 *In vivo* MR imaging reveal impaired function and performance of the cardiac muscle of iASPP$^{\Delta 8/\Delta 8}$ mice.

The severe cardiomyopathy observed in iASPP-deficient mice *post mortem* encouraged us to further investigate the cardiac phenotype. To confirm the observations from the histological analysis described above, and obtain new insights into the cardiac performance of iASPP-deficient mice, cardiac-gated magnetic resonance imaging (MRI) was performed on matching age and gender mutant and wild type mice, in collaboration with Carolyn Carr at the Department of Physiology, Anatomy and Genetics department, University of Oxford under the supervision of Prof. Kieran Clarke. Wild type (iASPP$^{+/+}$) and iASPP transgenic mice (iASPP$^{\Delta 8/\Delta 8}$) (n = 3 each group) of 12 weeks of age were anaesthetised with isoflurane, positioned supine in a purpose-built holder and

maintained unconscious at 2% isoflurane in 1.5 l/min oxygen flow throughout the MRI experiments. Cardiac function of iASPP$^{\Delta 8/\Delta 8}$ mice was severely impaired in both the left and right ventricles, as the calculated parameter in table 4.1 shows.

In summary, the mutant hearts were found to be hypertrophic with a moderate increase in the ventricular mass *(table 4.1)*. Interestingly, iASPP$^{\Delta 8/\Delta 8}$ hearts displayed a consistent banana-shaped morphology within the chest cavity (f*igure 4.5A)*. In particular, reduced thickness of the right ventricular free wall was evident, associated with a more distended shape of the ventricular cavity (f*igure 4.5A)*. Left (LV) and right ventricular (RV) diastolic short-axis cavities (end-diastolic lumen) were measured at basal, mid-ventricular and apical locations to demonstrate an overall larger diameter of the two ventricle cavities in the mutant heart. Consistent with a more elongated and enlarged circumference of iASPP mutant hearts, MRI of iASPP KO hearts confirmed the dilatation of both ventricular chambers *(table 1, end-diastolic & end-systolic lumen and figure 4.5B)*. Contraction of the myocardium in iASPP-depleted hearts was minimal, resulting in a significant increase in the end-systolic volume and a consistent decrease in stroke volume and blood ejection fraction *(table 4.1 and figure 4.5B)* as showed by two mid-papillary slices for each heart at diastole. Shown in black is the area covered by the lumen of the left ventricle of the same slice at systole, indicating the extent of contraction of the myocardium. These results undoubtedly demonstrate that young adult iASPP-null mice have profoundly impaired cardiac function consistent with the histological evaluation of their hearts. Interestingly, given the sudden death of iASPP-null mice used for histological examination, and the impaired heart performance showed by iASPP mutant hearts at 12 weeks of age, it is tempting to speculate that iASPP mutant progeny could die of cardiac failure.

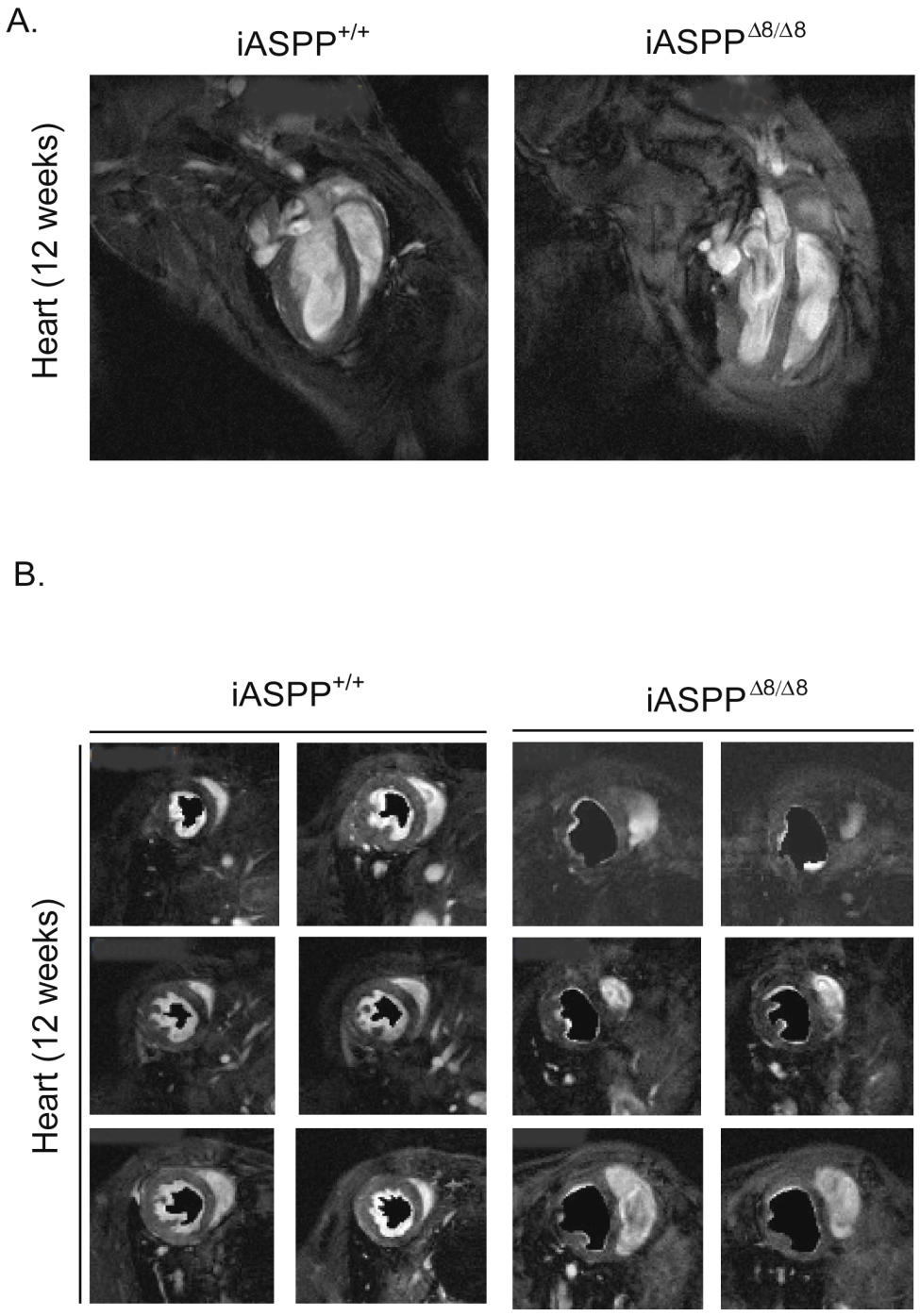


Figure 4.5. *In vivo* MR imaging of cardiac function in iASPP$^{+/+}$ and iASPP$^{\Delta 8/\Delta 8}$ mice. (A) Representative long axis MRI images of wild type and transgenic iASPP mouse hearts, showing the distended right ventricle in the KO mouse heart. (B) Two mid-papillary slices are shown for each heart (n=3) at diastole. The area covered by the lumen of the left ventricle of the same slice at systole is shown in black, indicating the extent of contraction of the myocardium.

	iASPP$^{+/+}$ Left Ventricle	iASPP$^{\Delta 8/\Delta 8}$ Left Ventricle	iASPP$^{+/+}$ Right Ventricle	iASPP$^{\Delta 8/\Delta 8}$ Right Ventricle
Average Mass (mg)	93 ± 3	107 ± 3 *		
End Diastolic Lumen (µl)	53 ± 6	70 ± 7	51 ± 6	74 ± 5 *
End Systolic Lumen (µl)	19 ± 6	60 ± 9 *	20 ± 6	63 ± 6 **
Stroke Volume (µl)	34 ± 0.2	10 ± 3 **	30 ± 2	11 ± 2 **
Ejection Fraction (%)	65 ± 8	14 ± 5 **	61 ± 8	15 ± 3 **
Heart Rate (bpm)	367 ± 38	411 ± 7		
Cardiac output (µl/min)	13 ± 1	4 ± 1 **	11 ± 1	5 ± 1 **
Body weight (g)	22 ± 2	23 ± 0.4		

Table 4.1. Echocardiographic characteristics of iASPP$^{+/+}$ and iASPP$^{\Delta 8/\Delta 8}$ mice. Cardiac function and heart morphology were measured using cine MRI in iASPP$^{+/+}$ (n=3) and iASPP$^{\Delta 8/\Delta 8}$ (n=3) mice of 12 weeks of age. Significant difference: * $p < 0.05$, ** $p < 0.01$ compared with iASPP$^{+/+}$.

4.2.2.3 iASPP-null hearts display typical features of ARVC.

Cardiomyopathies are primary disorders of the myocardium, with a varying array of phenotypic expression that range from altered morphology of the heart to its impaired performance. However, they all encompass heart failure and sudden cardiac death (Ahmad, Seidman et al. 2005). At this point in the study, the evidence suggested that iASPP-depleted mice suffered of an underlying cardiac myopathies, which phenotypically resemble the human pathologies of DCM or ARVC (see introduction section 1.3.3.1 and 1.3.3.2). In fact, enlargement of the ventricular cavity, reduced ventricular function and fibrotic deposits are characteristics of both DCM and ARVC (Franz, Muller et al. 2001). Specifically, ARVC is an uncommon cardiomyopathy with some pathological and clinical features that are distinct from DCM (Sen-Chowdhry, Syrris et al. 2005).

In order to establish whether iASPP$^{\Delta 8/\Delta 8}$ mice were affected by ARVC, the morphological characteristic of ARVC were investigated. First, H&E staining was performed on heart sections obtained from young adult mice (12 weeks of age) to analyse the thickness of the right ventricular wall. Figure 4.7 shows two matching cross-sections from wild type and iASPP-null hearts. Interestingly, a reduced size of the right ventricular wall was obvious in iASPP-depleted hearts, suggesting that the cardiomyopathy is disproportional towards the right ventricle *(figure 4.7)*. In particular, the area of the ventricular wall that showed the more severe reduction in thickness was located at the front of organ *(figure 4.7)*. In addition, iASPP mutant hearts showed dilation of the right ventricular chamber only, while the cavity size of the left ventricle was comparable with iASPP$^{+/+}$ mice *(figure 4.7, bottom panel)*. However, while the thickness of the ventricular wall on the back of the organs was not as dramatic as the one observed on the front, a clear phenotypic effect on the right ventricle was evident.

Loss of the myocardium and replacement with connective tissue is also typical of DCM, but adipocyte infiltration of fibrotic deposits is restricted to ARVC patients only (Corrado, Basso et al. 1997). To better understand whether iASPP-deficient mice were affected by ARVC, accumulation of fat droplets was investigated using the Red Oil staining technique. Oil Red O compound is a fat

soluble dye used for staining neutral triglycerides and lipids on frozen histological thin sections, as alcohol fixation or dehydration of paraffin wax specimens usually removes lipids. Oil Red O staining of thin frozen myocardial sections prepared from iASPP-null mice showed an accumulation of fat droplets only at the site of the fibrotic deposits *(figure 4.8, white arrows)*. Although the accumulation of adipocytes was not of a great magnitude, it was at least considerably higher when compared to wild type control myocardial sections, where no adipocyte droplets were found *(figure 4.8).* In summary, the abnormalities described within the cardiac tissue of iASPP-null mice recapitulate the pathological characteristics of ARVC. The myopathy seems to be focussed in the right ventricle, with dilation of the chamber and reduced thickness of the ventricular wall. In addition, adipocyte droplets were found at the sites of fibrotic deposits only in iASPP-depleted hearts, strongley suggesting that the process of fibrosis also comprises fat accumulations. Together, these results suggest that iASPP mutant mice could indeed be affected by ARVC.

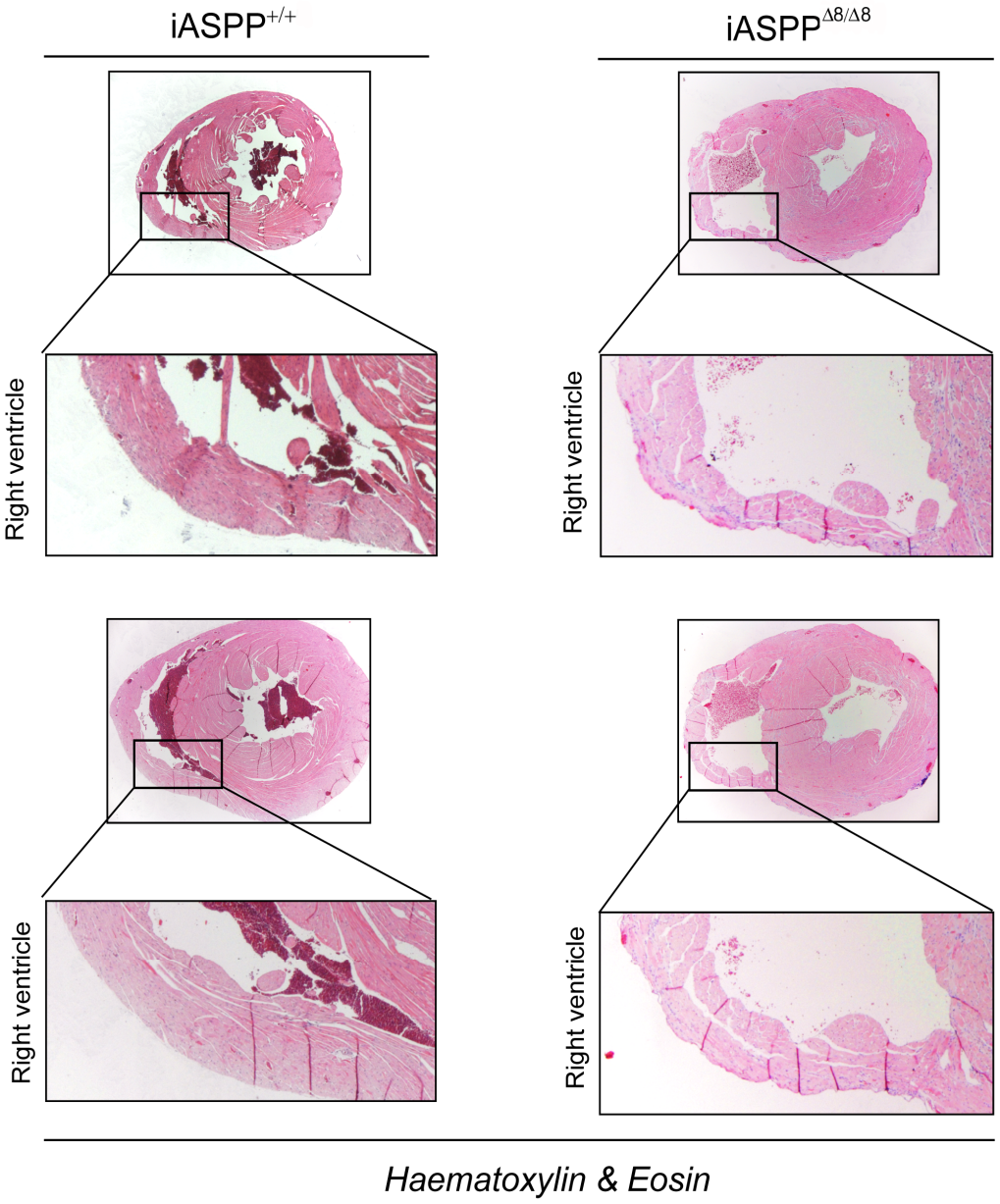


Figure 4.7. Hearts of 12 week old iASPP$^{\Delta 8/\Delta 8}$ mice showed reduced thickness of the right ventricular wall and dilatation of the right ventricular chamber. Histological analysis of myocardial tissue from 12 week old control (iASPP$^{+/+}$) and iASPP KO (iASPP$^{\Delta 8/\Delta 8}$) mice stained with H&E showed right ventricular dilatation and thinning of the right ventricular free wall. Hearts were dissected and embedded in paraffin-wax. Organs were cut in sequential sections from the apex towards the atrium of the organs. One in every 25 slides were stained with H&E and analysed, comparing iASPP$^{+/+}$ versus iASPP$^{\Delta 8/\Delta 8}$.

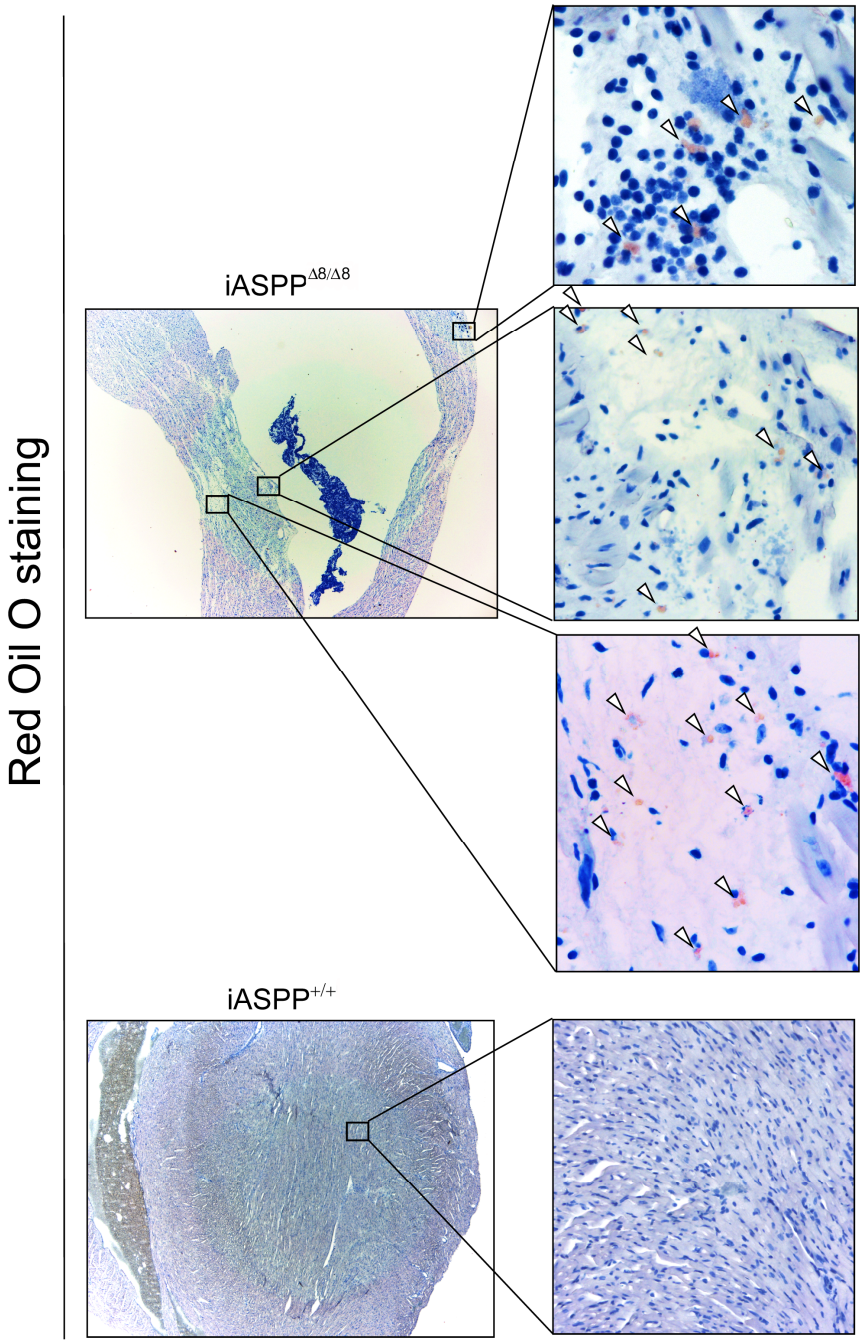


Figure 4.8 Fibroadipocytic replacement of myocytes in iASPP$^{\Delta 8/\Delta 8}$ hearts. Oil Red O-stained thin myocardial sections obtained from 20 week old iASPP$^{+/+}$ and iASPP$^{\Delta 8/\Delta 8}$ mice that died of sudden death. Organs were dissected and immediately frozen in liquid N_2. Sections were cut 15µm thick and stained with Oil Red O solution. iASPP$^{\Delta 8/\Delta 8}$ sections showed extensive areas of fibrotic deposits infiltrated with fat droplets and adipocytes *(white arrows)*.

4.2.2.4 Spontaneous ventricular arrhythmias in iASPP-deficient mice.

Clinical diagnosis of ARVC is usually achieved by the simultaneous demonstration of structural, functional and electrophysiological abnormalities, which reflect the mechanical and electrical alteration of the right ventricle (McKenna, Thiene et al. 1994). Since it had been established that iASPP KO mice died suddenly in association with impaired heart performance, dilatation of the ventricular chambers (with clear disproportion towards the right ventricle) and the presence of fibro-fatty deposits, we examined whether conduction abnormalities were also present in iASPP-null hearts. In order to investigate whether iASPP$^{\Delta 8/\Delta 8}$ mice are also affected by electrophysiological abnormalities, we performed electrocardiograms (ECGs) on young adult mice of 12 weeks of age.

As arrhythmias indicate a large number of heterogeneous heart pathologies in which there are abnormal conductivies of the heart, ECG is the perfect tool to investigate whether iASPP-null mice suffer from arrhythmias (McKenna, Thiene et al. 1994).

In collaboration with Prof Hugh Watkins' laboratory at the John Radcliffe hospital, we performed at the unconscious telemetric monitoring of electrocardiograms in wild type (n=6, 3 males and 3 females) and iASPP$^{\Delta 8/\Delta 8}$ (n=6, 3 males and 3 females) young adult mice of 12 weeks of age. As shown in figure 4.9A *(magnification square)* control mice displayed normal sinus rhythms with P waves preceding each QRS complex. On the other hand, all iASPP-null mice investigated manifested some degree of cardiac electrical abnormality. These manifestations ranged from subtle intraventricular contraction delay or atrial bigeminy, to multifocal ventricular ectopy, inverted T waves and junctional tachycardia *(figure 4.9 B-C-D-E)*. In particular, iASPP KO mice showed frequent evidence of heart delay/block in which the wave of cardiac excitation from the sinoatrial node (sinus rhythm) to the ventricle, via the conduction pathway, was delayed or blocked *(figure 4.9B)*. iASPP KO ECGs also showed spontaneous ventricular ectopic beats (VEB) and ventricular couplets (ventricular bigeminy). Ectopic beat (or cardiac ectopy) is a disturbance of the cardiac rhythm frequently related to the electrical conduction system of the heart, in which beatsarise from a fiber or group of fibers outside the region, in the heart muscle, ordinarily

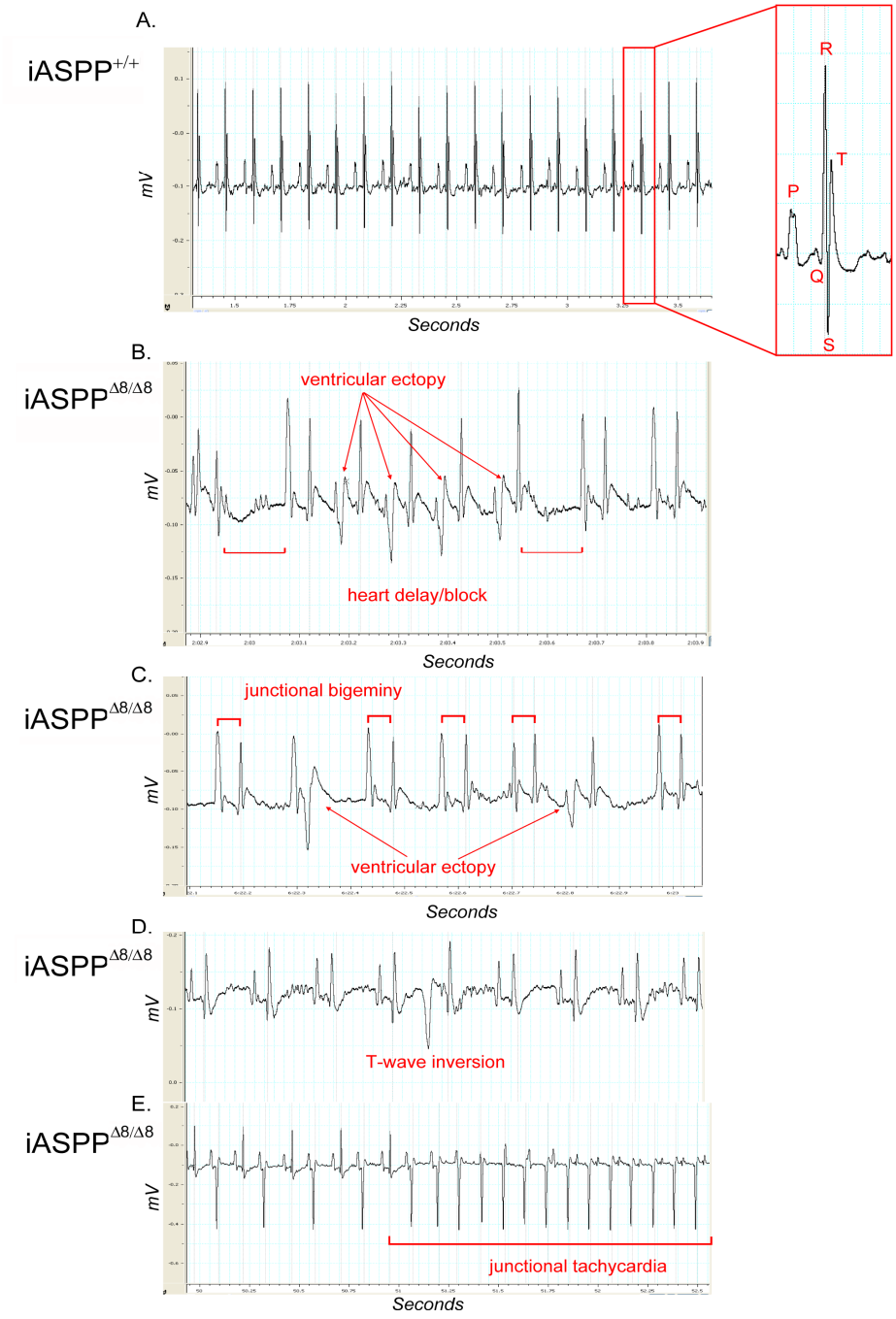


Figure 4.9. Cardiac conduction abnormalities are present in iASPP$^{\Delta 8/\Delta 8}$ mice. Figure shows rhythm strips from unconscious telemetry obtained from iASPP$^{+/+}$ and iASPP$^{\Delta 8/\Delta 8}$ mice. (A) Normal sinus rhythms were recorded in iASPP$^{+/+}$ (n=6) mice associated with normal QRS waves. (B-E) Instantaneous ECG traces from iASPP$^{\Delta 8/\Delta 8}$ (n=6) mice represent the major conduction abnormalities present in iASPP mutant mice. (B) 24 week old iASPP$^{\Delta 8/\Delta 8}$ mice showed four consecutive events of ventricular ectopy, preceded and followed by a heart delay. (C) Repetitive events of junctional bigeminy were recorded in iASPP-depleted mice. This particular trace, from a 24 week old iASPP mutant female, shows three consecutive junctional bigeminys proceeded and followed by ventricular ectopy events. (D-E) 12 weeks old male iASPP$^{\Delta 8/\Delta 8}$ ECG tracings demonstrate a prolong episode of T-wave inversion (D) and junctional ventricular tachycardia (E).

responsible for impulse formation (i.e., the sinus node) *(figure 4.9B)*. VEB is an extra heartbeat originating in the lower chamber of the heart. VEB is a form of cardiac arrhythmia and may be followed by ventricular tachycardia and fibrillation, which can lead to sudden death (source eMedicine). Ventricular bigeminy instead describes a form of arrhythmia in which abnormal heartbeats occur every other concurrent beat. In particular, iASPP-null mice suffered bigeminal premature ventricular beats, also known as premature ventricular contractions/complexes (PVC) *(figure 4.9C)*. Finally, two iASPP transgenic mice showed signs of junctional tachycardia, which is defined as the occurrence of an intermittent tachycardia, provoked by an anomaly of the conduction of the nervous impulse in the heart, but most importantly which can lead to a sudden cardiac death *(figure 4.9 D)*.

These data, importantly, indicate that loss of iASPP induces a severe cardiomyopathy associated with arrhythmias, ventricular ectopy and junctional tachycardia. iASPP-deficiency, thus, severely disrupts the electrical conduction of the heart with clear signs of no sinus rhythm and wider QRS complexes, indicating a clear electrical conduction abnormalities in iASPP deficent hearts.

4.2.3 Alteration of the intercalated disc complexes is associated with loss of iASPP in vivo.

The intercalated discs (IDs) are cardiac structures which link the complex myocyte cytoskeleton to the sarcolemmal membrane at the polar end of the myocytes maintaining the structural integrity of the heart (Franke, Borrmann et al. 2006). In normal mice, the location of iASPP in cardiomyocytes matches that of other proteins known to be involved in the integrity of the ID complexes *(figure 4.10A)*. Since recent findings in human cardiology indicate that a loss of “intercalated disc-related proteins” results in early and usually lethal dilated cardiac myopathy (Gerull, Heuser et al. 2004; Kostetskii, Li et al. 2005; Antoniades, Tsatsopoulou et al. 2006), we investigated whether loss of iASPP could have an effect on the integrity of IDs. Intercalated discs are forms by various junctional complexes including adherens junctions, desmosomes and gap junctions (Bolling and

Jonkman 2009). The importance of maintaining cell junction integrity was highlighted by the findings that mutations in plakoglobin, as well as non-functional desmoplakin protein, lead to ARVC or DCM respectively in humans (McKoy, Protonotarios et al. 2000; Norgett, Hatsell et al. 2000).

Immunofluorescence analysis was performed in order to examine the expression and cellular localisation of several ID components in hearts of adult iASPP transgenic mice. As shown in figure 4.10B, ID structures were readily visible in normal wild type hearts. N-cadherin, the major component of adherens junctions, localised at the ID with a characteristic expression pattern. Plakoglobin, which belongs to the catenin family of proteins and regulates the adhesion activity of N-cadherin (Gumbiner 2000), and connexin 43, a major component of gap junctions, normally localise to the ID structures in the mature myocardium, as shown in wild type hearts *(figure 4.10B)*. On the other hand, in iASPP transgenic myocardial sections, ID complexes were completely lost. N-cadherin staining was severely reduced, together with plakoglobin and connexin 43. In contrast, β-catenin staining was found at its typical location (i.e. at the polar end) in iASPP KO heart slices *(figure 4.10B)*. Subsequent protein expression analysis was conducted to confirm the loss of IDs in mutant hearts. Adult hearts were dissected from 20 week old mutant and wild type mice, and proteins extracted using UREA buffer. Western blot analysis was performed to assess the expression of major ID constituents and, as shown in figure 4.10C, a severe down-regulation of all major components of the adherens junctions, desmosomes and gap junctions were observed. Surprisingly, β-catenin was not affected by iASPP depletion, suggesting an important role of iASPP on specific ID components *(figure 4.10B)*. Displacement of plakoglobin and severe reduction of its expression was the most striking and interesting evidence, because it directly linked the cardiac pathology affecting the iASPP mutant mice with a gene that has already been found to be mutated or inactivated in ARVC patients (Corrado, Basso et al. 1997). Furthermore, Asimaki and colleagues recently suggested a new diagnostic test for ARVC patients based on the immunoreactive signal level of plakoglobin, and demonstrated that its signal was specifically diffusely reduced in ARVC

samples but not in HCM or DCM myocardial sections (Asimaki, Tandri et al. 2009). However, while the expression and distribution of several ID components is often perturbed in cardiomyopathies, it is unclear whether these changes are involved in the aetiology of the disease or are a secondary event subsequent to the heart pathology. The question was therefore asked whether the dissolution of IDs could also be observed in young adult iASPP transgenic mice. To verify this hypothesis, N-cadherin, plakoglobin and connexin 43 were examined by immunofluorescence analysis on myocardial sections obtained from 12 week old mutant and control wild type mice.Analyses of the location and integrity of the IDs revealed that junctional complexes in the left ventricular walls were visible and intact in both iASPP wild type and KO hearts *(figure 4.11)*. Junctional structures were also visible at their typical polar end location in iASPP-depleted cardiomyocytes, with adherens, desmosomes and gap junctions represented by the characteristic positive signal shown in figure 4.11. Positive staining can be also seen in the iASPP-null heart associated only with an increase in the size of the myocytes *(figure 4.11)*. However, a small but evident reduction in plakoglobin staining was observed in left ventricular myocardial iASPP$^{\Delta 8/\Delta 8}$ sections. In contrast, analysis of the integrity of the IDs in the right ventricular wall revealed severe defects in the expression of adherens junctions. In fact, as shown in figure 4.11, a significant reduction in the expression of both N-cadherin and plakoglobin was evident, suggesting impaired integrity of the ID complexes in the right ventricle. Immunofluorescence analysis of desmoplakin, a constituent of the desmosomal plaque which binds the intermediate filament desmin and connects the cytoskeleton to the sarcolemmal membrane in myocytes *in vivo* (Leung, Green et al. 2002; Ahmad, Seidman et al. 2005) was also examined. Interestingly, desmoplakin largely failed to locate at the intercalated discs in iASPP-deficient cardiomyocytes in both 12 and 20 week old heart tissues *(figure 4.12, left panel)*. Similarly, in iASPP$^{\Delta 8/\Delta 8}$ cardiomyocytes, desmin also failed to localize at the intercalated discs even though it was readily detected at the locations of Z-discs *(figure 4.12, middle panel)*. These defects are unlikely to be caused by a reduction in protein expression, as equal

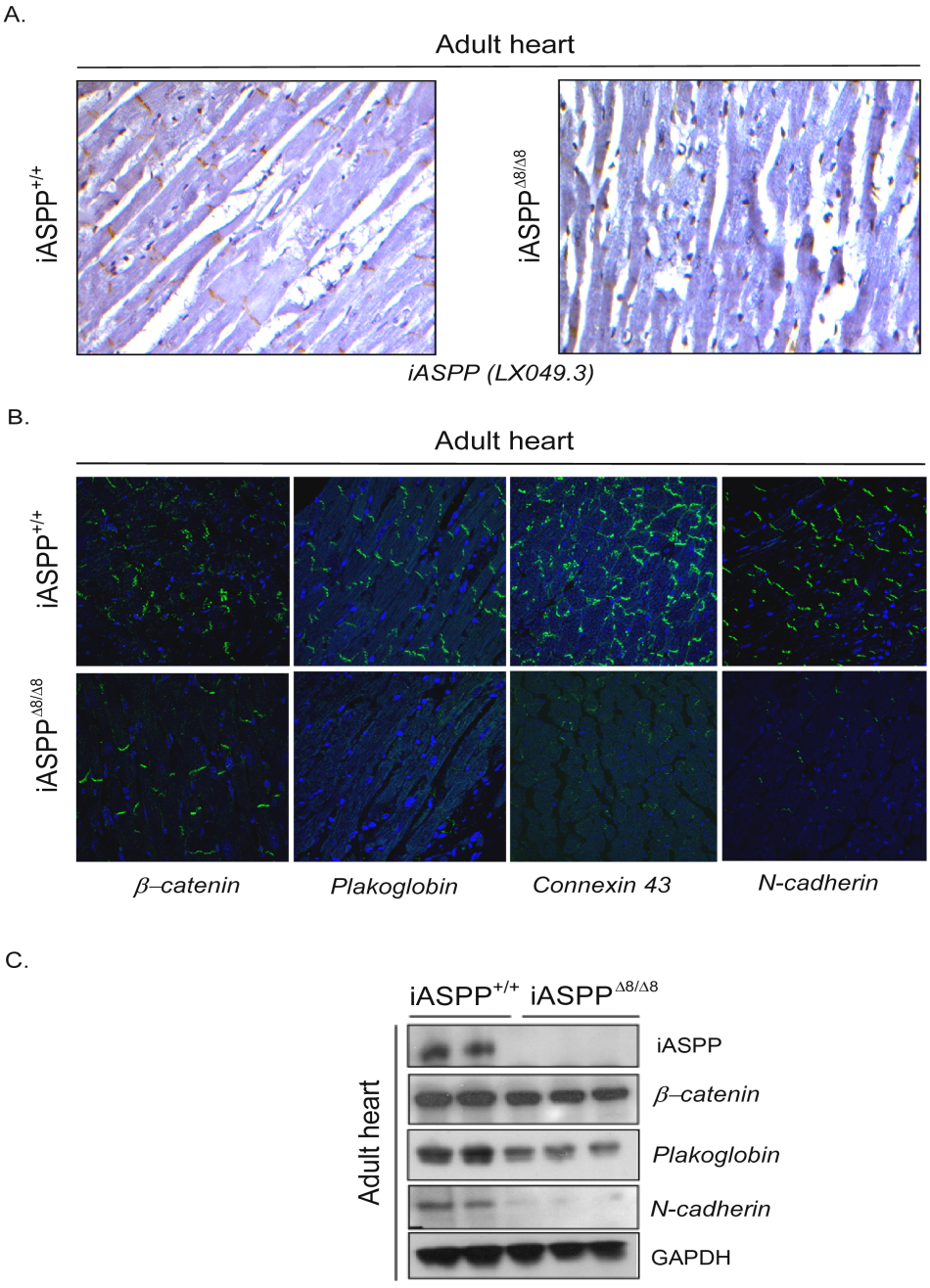


Figure 4.10. Cardiac myocytes null for iASPP show a lack of intercalated disc (ID) components. (A) Myocardial paraffin wax thin sections obtained from adult iASPP$^{+/+}$ and iASPP$^{\Delta 8/\Delta 8}$ mice were immunostained using LX049.3 monoclonal antibody. *(left)* Picture shows positive staining in the intercalated disc region of the cardiomyocytes. *(right)* No signal was detected using iASPP$^{\Delta 8/\Delta 8}$ heart sections. (B) Myocardial paraffin wax sections obtained from adult iASPP$^{+/+}$ and iASPP$^{\Delta 8/\Delta 8}$ mice were immunostained using a series of antibodies representing all three major junctions of IDs. β-catenin, plakoglobin, connexin 43 and N-cadherin staining was localised normally along the ID region in control sections (iASPP$^{+/+}$) but was almost completely absent in iASPP$^{\Delta 8/\Delta 8}$ mice. (C) Whole heart lysates from adult iASPP$^{+/+}$ and iASPP$^{\Delta 8/\Delta 8}$ mice were prepared using Urea buffer solution and resolved by SDS-PAGE electrophoresis. Membranes were immunoblotted using LX049.3, β-catenin, plakoglobin and N-cadherin antibodies. GAPDH was used as a loading control

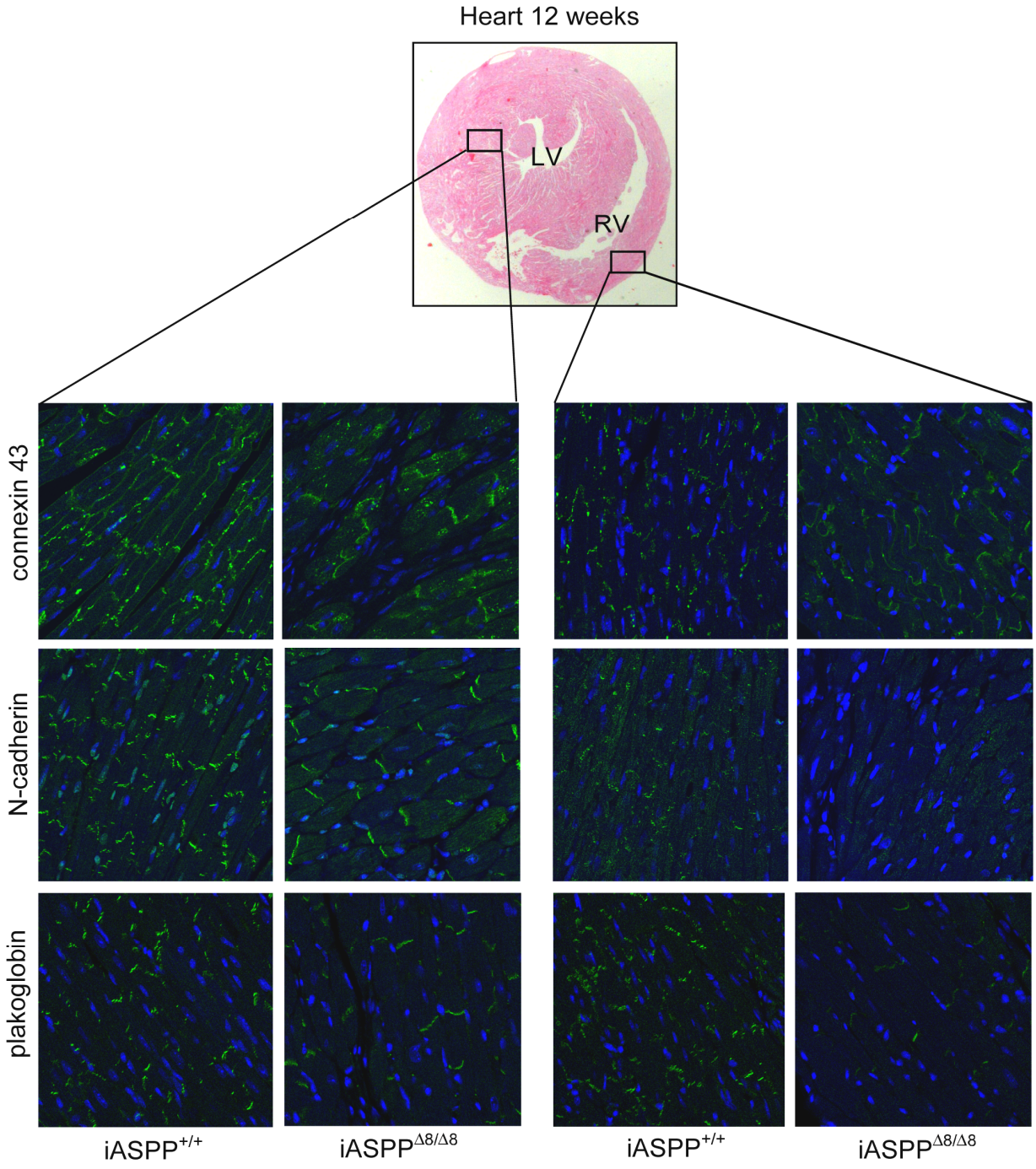


Figure 4.11. Differential expression of intercalated disc components between the left and right ventricles in iASPP$^{+/+}$ and iASPP$^{\Delta 8/\Delta 8}$ mice. Hearts dissected from 12 week old iASPP$^{+/+}$ and iASPP$^{\Delta 8/\Delta 8}$ mice were processed for histological examination and embedded in paraffin wax medium. Transverse sections were obtained and immunostained using connexin 43, N-cadherin and plakoglobin antibodies. The picture shows that ID components are only marginally affected in the left ventricular wall, where only plakoglobin staining was reduced. Staining on the right ventricular wall, instead, reveals that all three junctional components in the ID are affected. RV: right ventricle; LV: left ventricle.

amounts of desmoplakin and desmin were detected using heart lysates derived from iASPP$^{\Delta 8/\Delta 8}$ and wild type littermates *(figure 4.12)*.These results demonstrate that a loss of iASPP specifically impairs the location of desmin at the intercalated discs, but not the interactions between desmin and sarcomeric proteins at the Z-discs, in cardiomyocytes *in vivo*. On the contrary, no obvious sign of reduction of the positive connexin 43 signal was observed, only an abnormal location was detected.

IDs are also extremely important to attach both intermediate-based filament desmin and the microtubules-based actin to the sarcolemma membrane (Ahmad, Seidman et al. 2005). Non functional desmosomes are observed in desmoplakin null embryos and fail to attach to intermediate filaments. These observations support the importance of the desmoplakin in linking intermediate filaments to the plasma membrane (Bornslaeger, Corcoran et al. 1996). Desmin is known to bind to Z-disks of sarcomeres in addition to localize at intercalated disks through its interaction with desmoplakin (Smith and Fuchs 1998). Since iASPP$^{\Delta 8/\Delta 8}$ mouse shows defects in the integrity of IDs, the distribution of the intermediate filament protein, desmin, was analyzed in both failing heart (adult heart) and 12 weeks old iASPP KO hearts. As showed in figure 4.12 desmin signal was distributed in a distinct sarcomeric pattern from both WT and KO iASPP heart tissues, indicating that interactions between desmin and Z-disks are not affected *(figure 4.12)*. However, in normal heart tissue, desmin signal was readily seen at the intercalated disks while in KO heart sample desmin failed to localize at the IDs, suggesting that interactions between desmin and desmoplakin are disrupted in iASPP null heart *(figure 4.12)*.

Together, these data suggest a possible role for iASPP in maintaining the integrity of the IDs, with particular emphasis on the right ventricle. Moreover, failure of the desmin protein to relocate at the IDs junction suggest a possible link between iASPP, desmoplakin and desmin in strengthen the link between the cytoskeleton and the sarcolemma membrane in order to have an efficient force transmission. In light of this evidence, it is tempting to speculate iASPP may be a new molecular player in the pathology of ARVC.

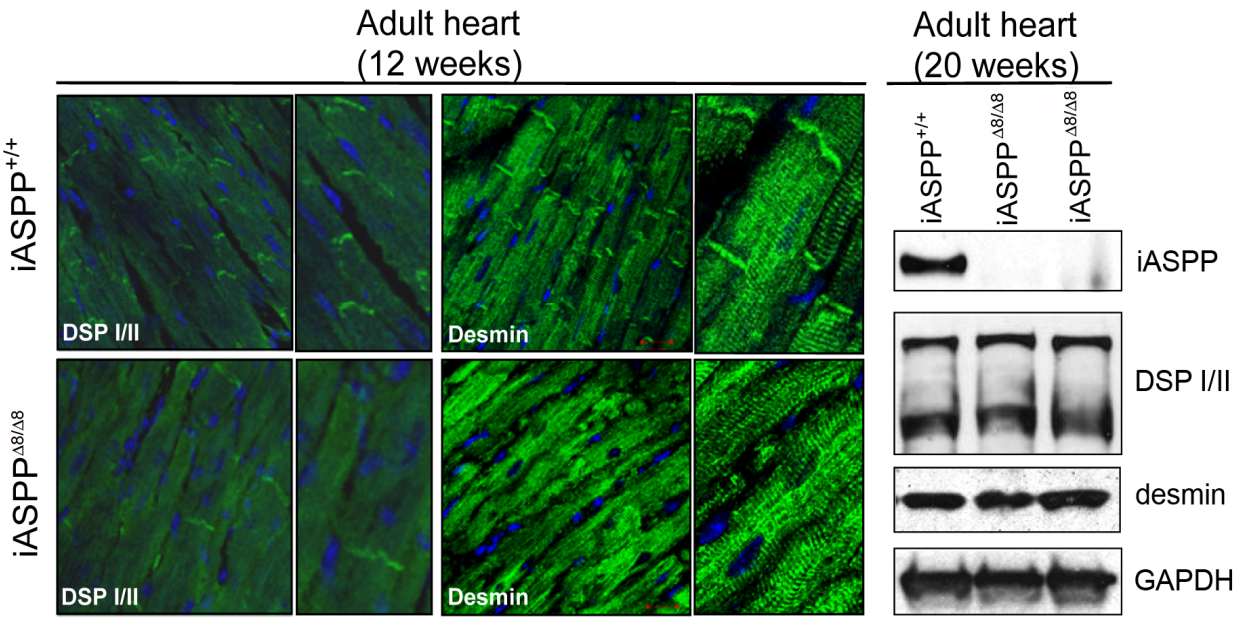


Figure 4.12. Distribution of desmin in iASPP$^{\Delta 8/\Delta 8}$ and control heart (iASPP$^{+/+}$). Hearts dissected from 12 week old iASPP$^{+/+}$ and iASPP$^{\Delta 8/\Delta 8}$ mice were processed for histological examination and embedded in paraffin wax medium. Transverse sections were obtained and immunostained using desmin polyclonal antibody was obtained. Desmin is distributed in a sarcomeric pattern in both iASPP$^{\Delta 8/\Delta 8}$ and control heart. Desmin signal is also concentrated at IDs in control tissue *(arrows)*. In contrast, desmin signal is absent at IDs in iASPP$^{\Delta 8/\Delta 8}$mice.

4.2.4 Loss of iASPP expression is the direct cause of the ARVC phenotype in iASPP$^{\Delta 8/\Delta 8}$ mice.

4.2.4.1 Young iASPP$^{\Delta 8/\Delta 8}$ mice showed morphological and molecular evidence of a remodelling process in the heart.

Fascinatingly, the combined data from the structural and functional analyses of iASPP$^{\Delta 8/\Delta 8}$ hearts suggested that iASPP-deficiency in mice leads to the establishment of a cardiomyopathy that resembles ARVC clinical presentation in humans. It was therefore important to investigate whether loss of iASPP expression was the direct cause of the myocardial phenotype. The best scientific approach to answer this question was to generate mice with specific abrogation of iASPP expression only in the myocardium. This could be achieved by crossing our iASPP$^{flox/flox}$ mice with

mice expressing the Cre recombinase enzyme under the control of a cardiac specific promoter. Nevertheless, we decide to first investigate the stage of mouse development at which clear evidence of a remodelling process of the myocardium could be observed. Discovery of early cardiovascular abnormalities in iASPP-null progeny would then give strong evidence that the ARVC observed in iASPP$^{\Delta 8/\Delta 8}$ progeny was primarily induced by a lack of iASPP.

To establish whether loss of iASPP expression was the major cause triggering a maladaptive remodelling process in the heart, iASPP$^{\Delta 8/\Delta 8}$ pups generated from heterozygous breeding pairs were sacrificed 5, 10 and 15 days after birth and their hearts dissected and prepared for histological analysis. The earliest heart abnormalities observed in iASPP$^{\Delta 8/\Delta 8}$ mice were detected 5 days after birth by macroscopic analysis of the dissected hearts *(figure 4.13)*. At days 5, most of the mutant hearts showed an enlarged organ associated with abnormal shape and size, with different levels of severity in between the dissected hearts (n=3). The first abnormality was a single white area on the exterior part of the ventricle walls, in the same location in all mutant hearts analysed. Consistently, this small lesion appeared on the anterior-upper part of the heart and extended into the intraventricular septum *(figure 4.13 A-C)*. Interestingly, in support of the hypothesis that iASPP$^{\Delta 8/\Delta 8}$ mice are affected by ARVC, two reports indicate that the replacement of the ventricular myocardium by fibro-fatty deposits initiates at the epicardium and gradually extends through the myocardium towards the subendocardium (Munclinger, Patel et al. 2000; Nava, Bauce et al. 2000).

H&E staining on matching p5 myocardial sections confirmed a loss of the architecture and organisation of the cardio-fibres in the iASPP$^{\Delta 8/\Delta 8}$ myocardium and the abnormal shape of the organ (*Figure 4.12B*). In particular, the most affected area in which the myocytes had been lost was the front part of the organ between the right ventricle and the septal wall (*Figure 4.13B).* Cardiac myocyte rearrangement was evident, and clear fibrotic deposits were noted using the Masson staining technique (*figure 4.7C)*. Of note, day 10 and day 15 old mice showed dilatation of the ventricles and fibrotic deposits similar to day 5 specimens (data not shown). Together, these results

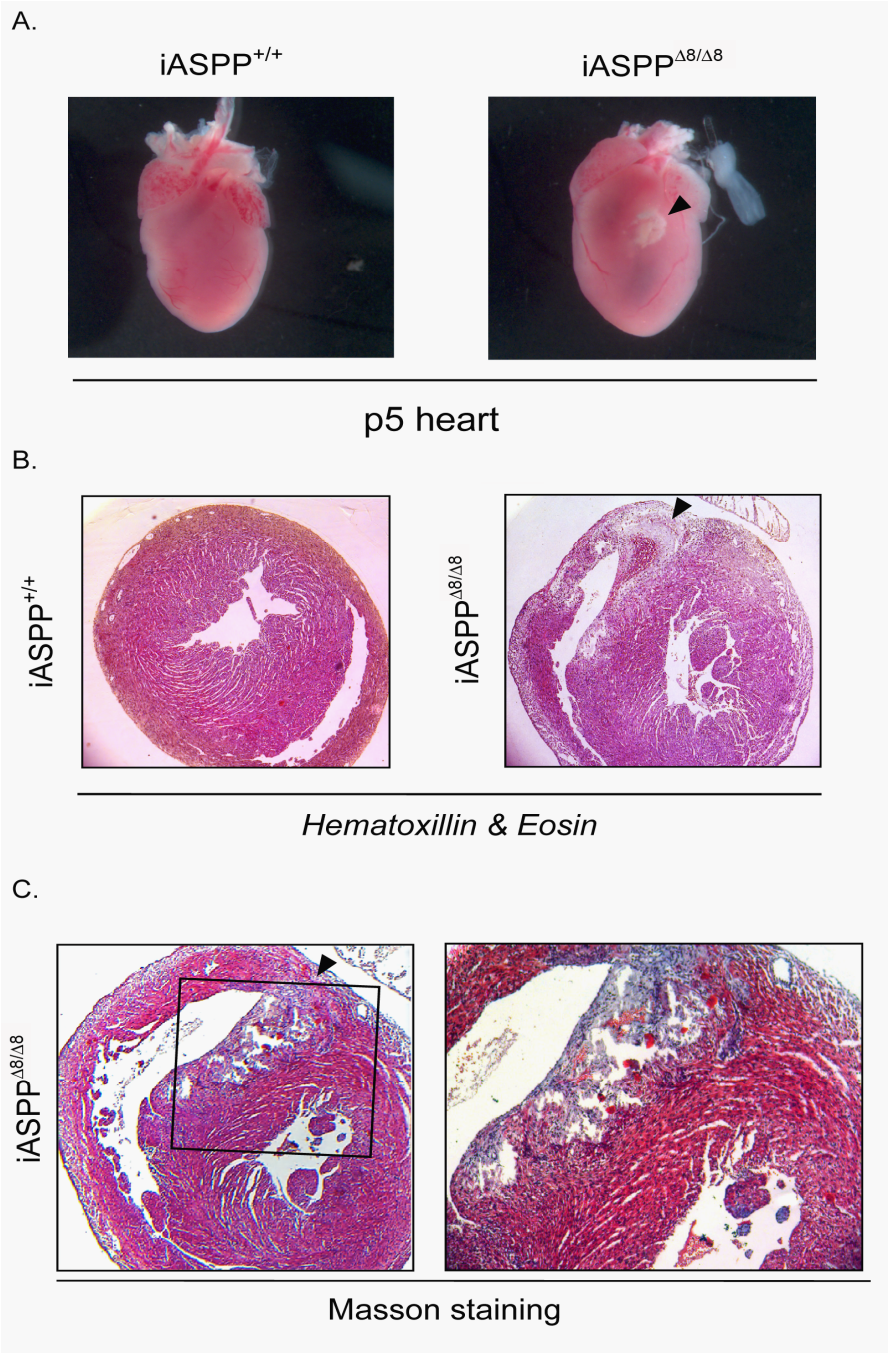


Figure 4.13. P5 heart abnormalities in iASPP$^{\Delta 8/\Delta 8}$ mice. (A) Hearts from homozygous mutant iASPP mice develop a single pale, focal lesion that first appears on the top anterior part near the outflow tract of the right ventricle *(black arrow)*. Note that iASPP$^{\Delta 8/\Delta 8}$ p5 hearts show an already enlarged shape and size of the organ. Hearts were dissected from control and mutant littermates, placed in a 10 cm dish containing PBS and photographed using a dissection microscope. Magnifications 2.6X. (B-C) Cross-myocardial sections of p5 iASPP$^{+/+}$ and iASPP$^{\Delta 8/\Delta 8}$ littermates' hearts. Paraffin wax matching sections were obtained and H&E (B) and Masson trichrome-staining were performed (C). Note that the area in which the white patch appears in (A) corresponds to the area in which loss of myocytes is evident in (B) *(arrow)*, and stains positive for fibrotic deposits in (C) *(arrow)*.

suggest that a remodelling process of the heart, in the form of ventricular dilation, is already active at day 5 after birth in mice that have lost iASPP expression, suggesting a direct role of the protein in maintaining the normal structure and function of the heart.

4.2.4.2 Embryonic iASPP$^{\Delta 8/\Delta 8}$ hearts demonstrate defects in the morphology and structure of the myocardium.

Histological analysis of 5 day old iASPP$^{\Delta 8/\Delta 8}$ mouse myocardial tissue demonstrated that structural abnormalities were already evident in iASPP-null hearts, suggesting that iASPP expression is of fundamental importance in maintaining the normal structure and function of the cardiovascular system. To further explore whether iASPP deficiency is the primary cause of the establishment of ARVC pathology in adult iASPP$^{\Delta 8/\Delta 8}$ mice, we collaborated with T.J. Mohun and his laboratory at the MRC National Institute for Medical Research in London to obtain three-dimensional (3D) episcopic images of iASPP-null hearts from mouse embryos at 14.5 (E14.5), 16.5 (E16.5) and 18.5 (E18.5) *post coitum*. In this way, we hoped to visualise defects in heart structure at the embryonic stage. Such investigations of iASPP mutant hearts at the embryonic level would give us strong evidence to support our hypothesis that iASPP is essential for the correct development of the heart *in vivo*. iASPP heterozygous couples were mated together and pregnant females were sacrificed at 14.5, 16.5 and 18.5 days *post coitum* (number of embryonic hearts analysed: E14.5 iASPP$^{+/+}$ n=1, iASPP$^{\Delta 8/\Delta 8}$ n=6; E16.5 iASPP$^{+/+}$ n=3, iASPP$^{\Delta 8/\Delta 8}$ n=3; E18.5 iASPP$^{+/+}$ n=7, iASPP$^{\Delta 8/\Delta 8}$ n=4). Embryo genotyping was obtained by PCR amplification using specific primers I8-2, E8-2 and FLP2 for the presence of exon 8 (data not shown). Only embryos positive for the presence or absence of iASPP expression were employed into the study. Hearts were then dissected from the embryos, fixed in 4% paraformaldehyde (PFA) and sent to be analysed by episcopic imaging. At E14.5, there was no obvious difference between the iASPP mutant hearts when compared with their wild type littermates, looking at ventricular wall thickness, trabeculation and ventricle chamber structure, valve formation or great vessel organisation. Only one of the six hearts analysed revealed a small

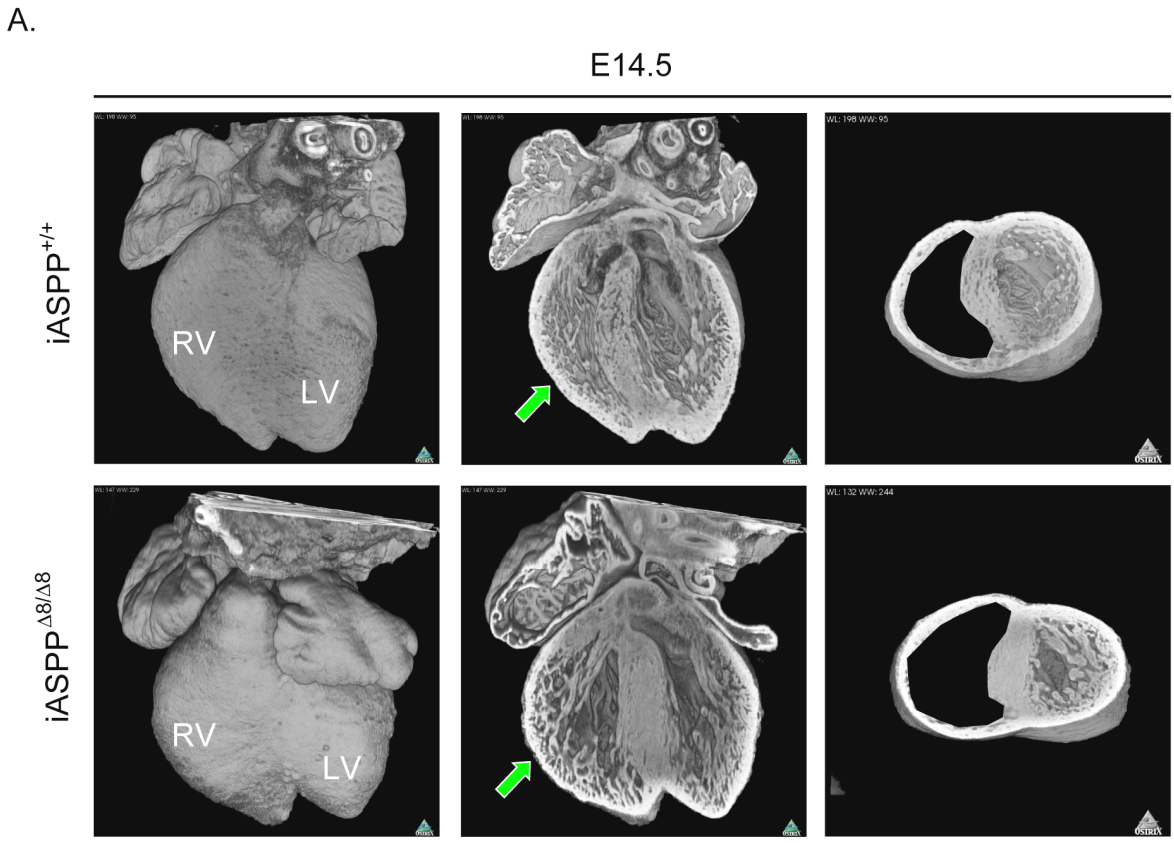


Figure 4.14. Three–dimensional reconstruction of E14.5 iASPP$^{\Delta 8/\Delta 8}$ and iASPP$^{+/+}$ hearts from high-resolution episcopic microscopy data. (A) E14.5 iASPP$^{\Delta 8/\Delta 8}$ and iASPP$^{+/+}$ hearts showing progressive erosion (from the front of the organ, front-erode) of data first revealing the entire heart structure *(left)* then revealing the ventricular and atrial chambers *(middle)*. Right ventricle (RV) and left ventricle (LV) are indicated. Note the dilation of the right ventricle in iASPP$^{\Delta 8/\Delta 8}$ specimens compared with iASPP$^{+/+}$ mice. Green arrows indicate the reduction of the right ventricular walls and increase in the trabeculation ridges in iASPP$^{\Delta 8/\Delta 8}$ hearts. Pictures on the right show E14.5 iASPP$^{\Delta 8/\Delta 8}$ and iASPP$^{+/+}$ heart erosions from the top of the organs (top-erode). The area shown in black is covered by the lumen of the right ventricle indicating modest dilation.

but detectable dilation of the right ventricle associated with a modest increased in trabeculation and thinning of the right ventricular wall *(figure 4.14A).* As this was the only case, we concluded that at this stage of embryonic development there were no obvious signs of cardiac abnormalities. However, at both E16.5 and E18.5 there was clear evidence of abnormal size and shape of the heart in all iASPP mutant embryos analysed. Looking at the gross morphology, the most profound effect

was the erosion of the right ventricular wall associated with severe disruption of the myocardial structure, which also extended into the intraventricular region of the heart septum *(figure 4.15)*. The tissue disruption was visualized as uneven with characteristic blotchy patterns which are probably most easily seen in the "front-erode" part of the images. The right ventricle of the E16.5 mutant heart in figure 4.14 was almost completely filled with a blood clot *(red arrow)* and had a very thin right ventricular wall *(green arrow)* which has lost almost all of its muscle. Note the extreme dilation of the right ventricle when compared to the wild type controls, or even when compared to the left ventricle *(figure 4.14)*, indicating that the primary site of the myopathy is the right ventricle. In one of the E18.5 hearts analysed (sample 19, not shown), cardiac tissue disruption was so extreme that most of the superior structure of the right ventricle was lost during dissection and processing. In all the other samples, the heart was complete but the effect of the depletion of iASPP's expression could be seen simply from the overall distorted morphology of the heart *(figure 4.16)*.

Together, 3D episcopic reconstruction analysis demonstrated that cardiac abnormalities were already evident in late stages of embryonic development in iASPPΔ8/Δ8 progeny. In all E18.5 and E16.5 hearts, loss and damage of the myocardium was only associated with thinner right ventricular walls and dilation of the right ventricular chambers, thus, iASPPΔ8/Δ8 embryos suffer from cardiac pathology that mainly involves the right ventricle. Finally, these data strongly suggest that cardiomyocytes are lost, and rearrangement of the myocardium with subsequent deposition of fibrotic deposits, is already an active process in iASPP embryonic mutant hearts. This supports our theory of iASPP as being the direct and primary cause of heart abnormalities.

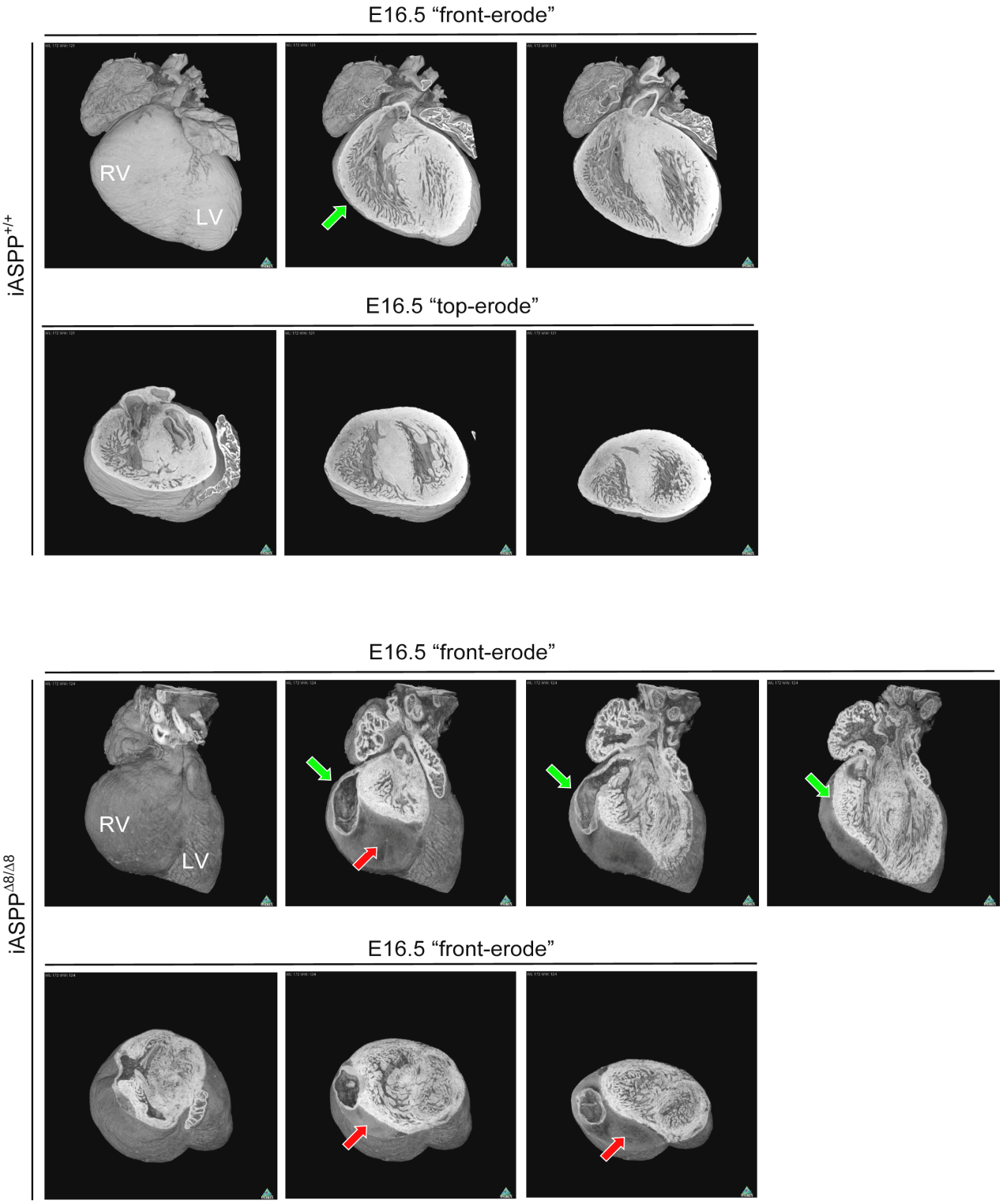


Figure 4.15. Three–dimensional reconstruction of E16.5 iASPP$^{\Delta 8/\Delta 8}$ and iASPP$^{+/+}$ hearts from high-resolution episcopic microscopy data

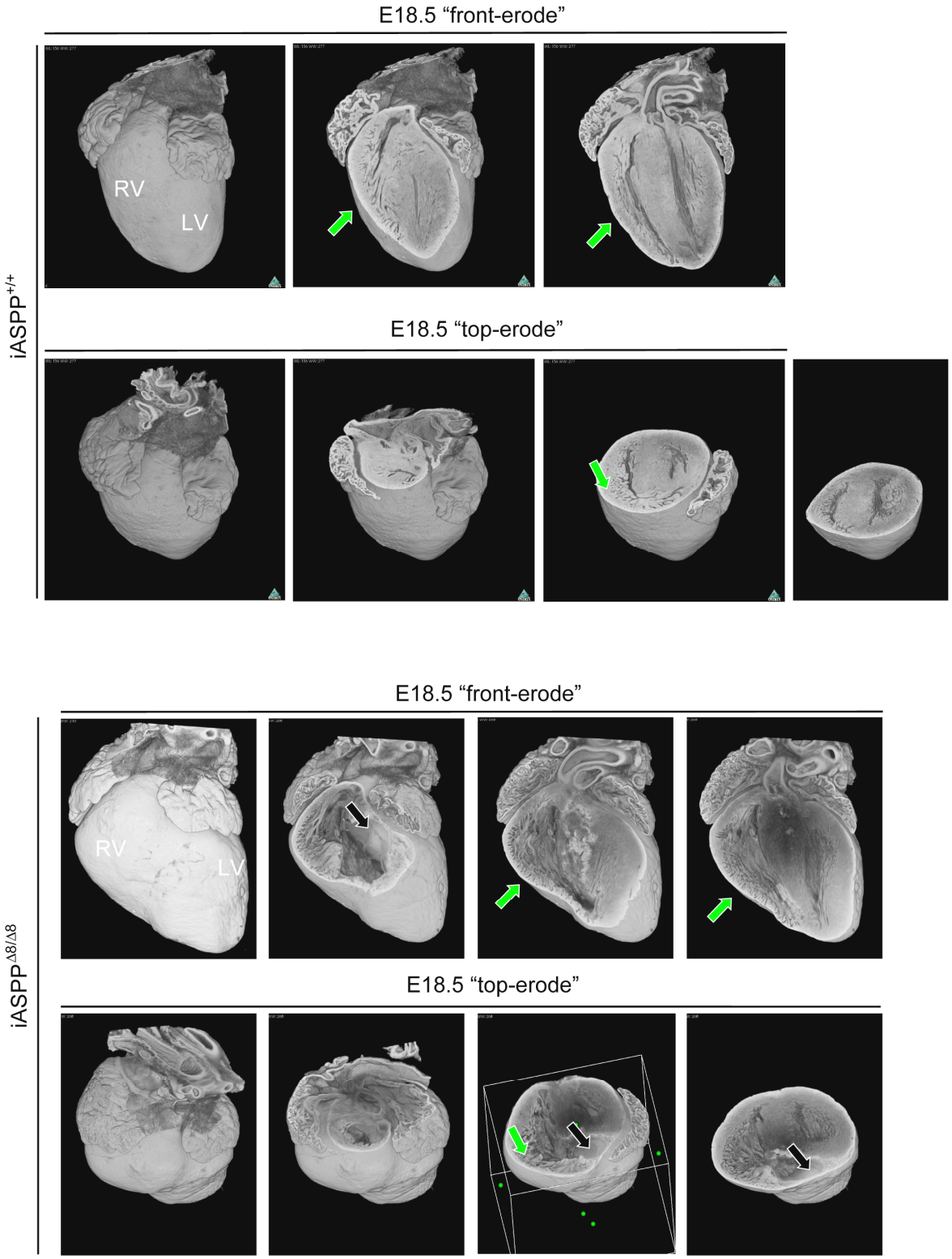


Figure 4.16. Three–dimensional reconstruction of E18.5 iASPP$^{\Delta 8/\Delta 8}$ and iASPP$^{+/+}$ hearts from high-resolution episcopic microscopy data.

Figure 4.15. Three–dimensional reconstruction of E16.5 iASPP$^{\Delta 8/\Delta 8}$ and iASPP$^{+/+}$ hearts from high-resolution episcopic microscopy data. E16.5 iASPP$^{\Delta 8/\Delta 8}$ and iASPP$^{+/+}$ hearts showing progressive erosion from the front of the organ "front-erode" and from the top "top-erode". Right (RV) and left (LV) ventricles are indicated. Green arrows indicate right ventricular wall thickness. Note the clear dilation of the right ventricle in iASPP$^{\Delta 8/\Delta 8}$ mice, which was almost completely filled with blood clot *(red arrows)* indicate an area of the right ventricle in which the cardiac muscle is almost entirely lost.

Figure 4.16. Three–dimensional reconstruction of E18.5 iASPP$^{\Delta 8/\Delta 8}$ and iASPP$^{+/+}$ hearts from high-resolution episcopic microscopy data. E18.5 iASPP$^{\Delta 8/\Delta 8}$ and iASPP$^{+/+}$ hearts showing progressive erosion from the front of the organ "front-erode" and from the top "top-erode". Right (RV) and left (LV) ventricles are indicated. Note the distorted morphology of the iASPP-null organ where loss of myocardial tissue is shown by a "blotchy" pattern. Green arrows indicate thickness of the right ventricular walls. Black arrow indicates a large blood clot on the superior right ventricular free wall and intraventricular septa. Variegated pattern shows muscle damage.

4.2.4.3 Validation of episcopic analyses by cellular and molecular investigation of iASPP-null embryonic hearts.

As episcopic analysis of iASPP KO embryonic hearts suggested, severe morphological and structural abnormalities were visible by E16.5 but not at E14.5. However, the possibility that molecular mechanism(s), which could drive the remodelling process, could already be activated in iASPP mutant embryonic hearts at E14.5 could not be excluded. Unfortunately, the specimens used to produce the 3D reconstruction images were not suitable for molecular analysis, therefore we generated E14.5 and E16.5 embryos from an iASPP heterozygous mating to validate the episcopic data. As noted previously, histological investigation has the advantage of providing extraordinary cellular resolution, with the ability to use a variety of cellular and molecular techniques to highlight different cellular structures or components.

After PCR analyses on DNA templates purified from each embryonic yolk sack, three different E14.5 iASPP$^{\Delta 8/\Delta 8}$ embryos were identified and analysed. Given the slightly reduced size of two out of three of the embryos (*figure 4.17A)*, the specimens were processed, embedded in paraffin and sliced into sequential sections. The overall structure, wall thickness, cell numbers and fibrotic deposit were analysed on matching sections between iASPP$^{\Delta 8/\Delta 8}$ and iASPP$^{+/+}$ embryonic heart. Surprisingly, all three E14.5 iASPP mutant hearts already had abnormal shapes, sizes and distorted morphologies, with increased trabeculation ridges and dilation of both ventricular cavities (*figure 4.17B)*. Interestingly, two out of the three mutant iASPP hearts also showed a clear reduction in the thickness of both ventricular walls, however, the right free wall was noted to be the most affected (*figure 4.17B, black arrow)*. Controversially, the remaining iASPP-deficient heart had an increased thickness of the ventricular walls (*figure 4.17B, white arrow)*. However, given the reduced thickness of the right ventricular walls in two out of the three mutant hearts, which suggested a loss of cardiomyocytes in the mutant hearts, we investigated whether a lack of iASPP expression caused the loss of cardiomyocytes in the embryonic myocardium. Right ventricular cell numbers from mutant and control E14.5 cross-sections of embryonic hearts were determined.

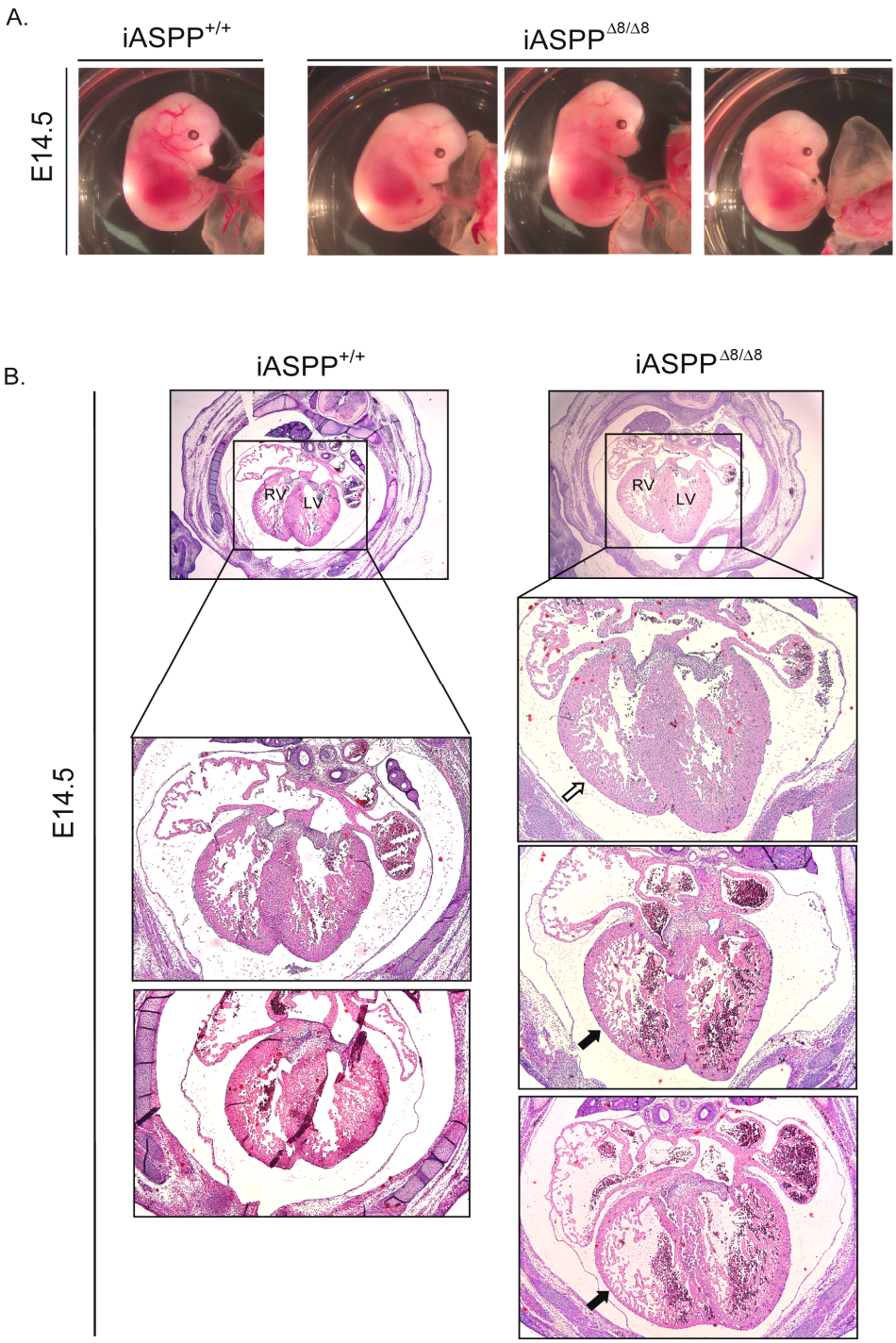


Figure 4.17. Histological analysis of E14.5 iASPP$^{+/+}$ and iASPP$^{\Delta 8/\Delta 8}$ embryonic hearts. (A) Embryos were dissected from pregnant iASPP$^{\Delta 8/+}$ females 14.5 days *post coitum*. Embryos were placed in 24 well plates and photographed using a dissection microscope. Magnifications 1.2X. (B) Transverse sections of two control (iASPP$^{+/+}$) and three mutant (iASPP$^{\Delta 8/\Delta 8}$) E14.5 embryos stained with H&E. Note the already enlarge right ventricular (RV) cavity and the reduced thickness of the right ventricular wall *(black arrow)* in two out of three iASPP$^{\Delta 8/\Delta 8}$ embryonic hearts.

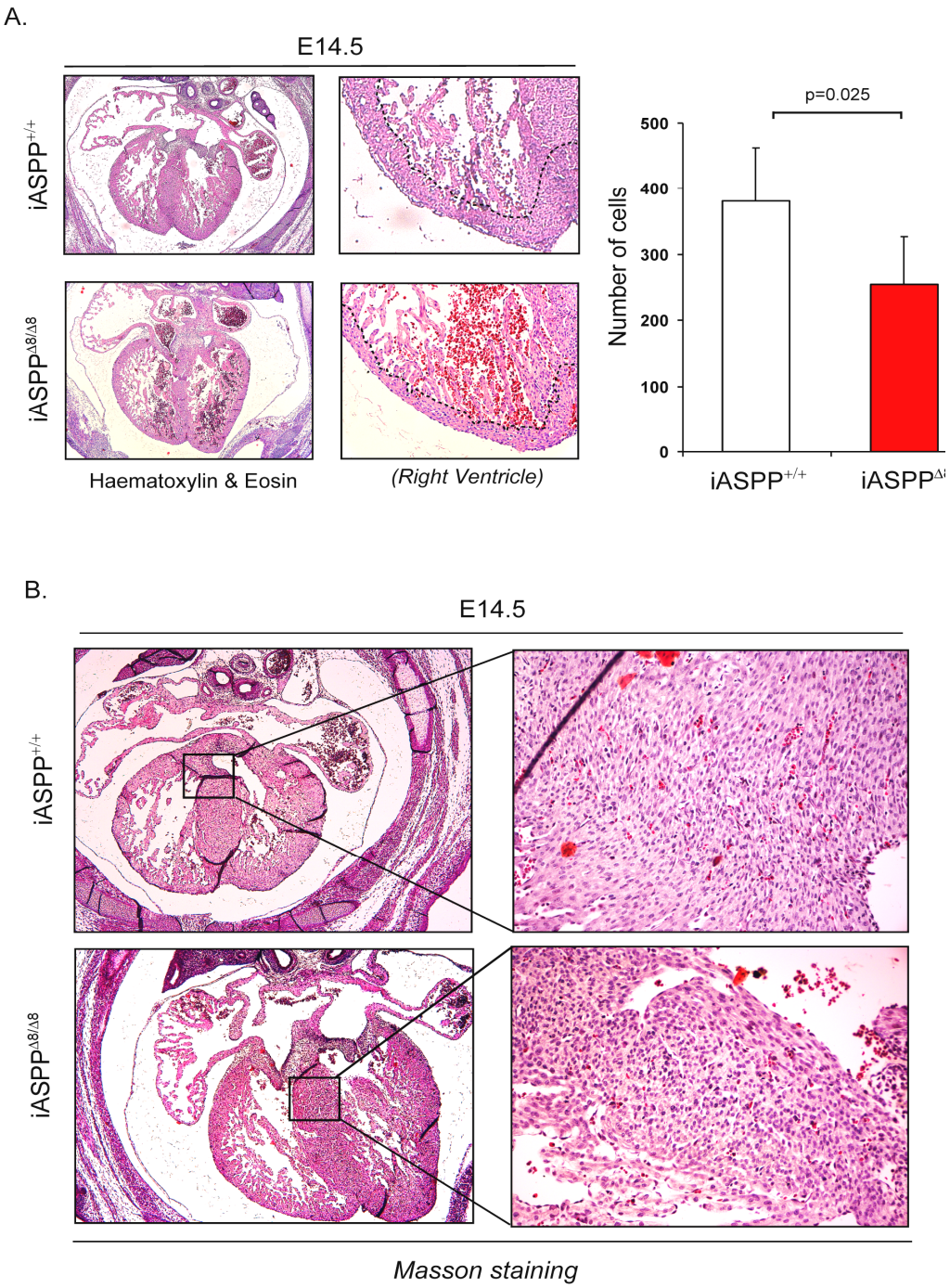


Figure 4.18. Reduced thickness of the right ventricular walls associated with loss of cardiomyocytes, but not with fibrotic deposits. (A) Cross-section of E14.5 hearts obtained from iASPP$^{+/+}$ and iASPP$^{\Delta 8/\Delta 8}$ mice shows reduced right ventricular wall thickness *(right).* Bar graph represents the quantification of cell number in the right ventricle, obtained by counting the blue nuclei from three random fields in three iASPP mutant specimens (n=3). (B) Masson staining of iASPP$^{+/+}$ and iASPP$^{\Delta 8/\Delta 8}$ E14.5 hearts revealed no fibrotic deposits.

The hearts of iASPP$^{\Delta 8/\Delta 8}$ embryos had a moderate, but statistically significant decrease in cardiomyocyte numbers compared to iASPP$^{+/+}$ (*figure 4.18A)*. Masson trichrome staining was performed to investigate the possible replacement of cardiomyocytes with fibrotic deposits. As in figure 4.18 shown, no fibrotic deposits or interstitial fibrosis were noted in iASPP-depleted embryonic hearts at day 14.5, supporting the results of the 3D episcopic analysis (*figure 4.18B)*.

On the other hand, histological analyses performed on E16.5 embryo hearts revealed the presence of severe heart defects in only one of the three specimens positive for iASPP absence (*figure 4.19A*). In particular, one sample showed severe structural re-arrangement of the myocardium associated with no chamber specification and unorganised myocardial tissue *(figure 4.19A)*. Red blood cells were noted into the pericardial sac, indicating a leakage of blood from the heart *(figure 4.19A, arrow)*. Furthermore, Masson trichrome staining was performed on heart sections from mutant and control hearts, in order to highlight fibrotic deposits. Interestingly, positive blue areas were only evident in the right ventricle and the septum between the two ventricular chambers in iASPP$^{\Delta 8/\Delta 8}$ (*figure 4.19B*). Of note, control myocardial tissue did not show any positive staining (*figure 4.19B*).

These data suggested that cardiomyocytes loss and replacement of the myocardium with fibrotic deposits begins at the anterior-top part of the right ventricular wall, consistent with the analyses of p5 hearts. Histological analysis of E14.5 and E16.5 iASPP-null hearts demonstrated that heart abnormalities are evident in the late embryonic stage of heart development, although they differ in degree of severity. Specifically, at E14.5 no clear abnormalities could be seen, with only a mildly distorted morphology and thinning of the right ventricular wall associated with a reduced number of myocytes. Interestingly at E16.5, fibrotic deposits could already been seen in the myocardium, indicating that myocytes had been lost and replaced with fibrotic deposits *(figure 4.19).* To conclude, these data validate the episcopic study and suggest that iASPP expression is required for the correct development of the mouse heart. It is evident that a remodelling process is re-shaping the iASPP KO heart with particular enphasis on the right ventricle.

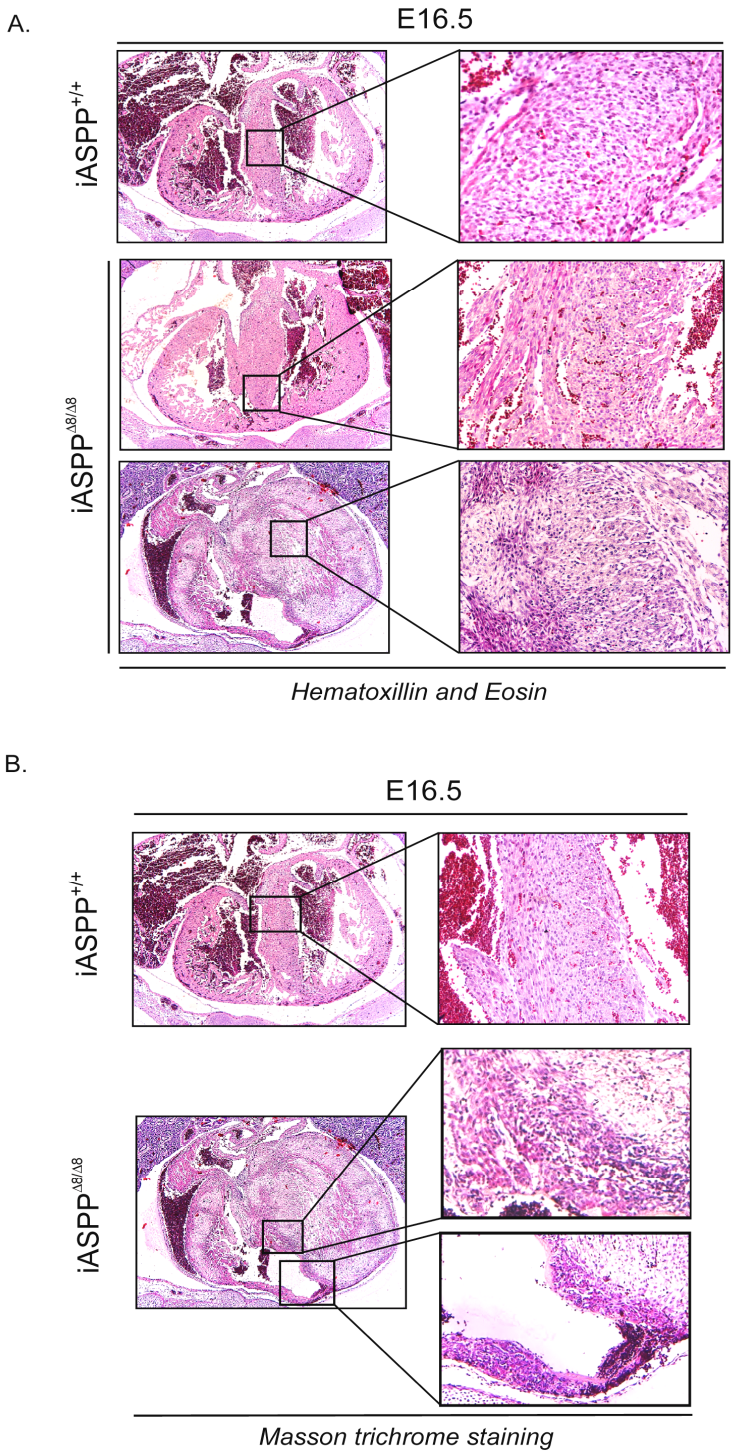


Figure 4.19. Histological analysis of E16.5 iASPP$^{+/+}$ and iASPP$^{\Delta 8/\Delta 8}$ embryonic hearts. (A) Transverse sections of E16.5 iASPP$^{+/+}$ and iASPP$^{\Delta 8/\Delta 8}$ hearts stained with H&E. Figure shows two of the three iASPP mutant hearts analysed. Note that rearrangement of the myocardial fibres was only seen in one of the mutant hearts *(bottom)*. (B) Transverse sections of E16.5 iASPP$^{+/+}$ and iASPP$^{\Delta 8/\Delta 8}$ hearts stained with Masson-trichrome staining. One mutant heart showed fibrotic deposits in the anterior part of the right ventricular walls, with some extending inside the intraventricular septum.

4.2.5 Investigation of the molecular mechanism(s) underlying the ARVC pathology in iASPP$^{\Delta 8/\Delta 8}$ mice.

4.2.5.1 Loss of iASPP induces apoptosis in young and embryonic mouse hearts.

As iASPP$^{\Delta 8/\Delta 8}$ mice showed histopathological features of ARVC and a remodelling process was clearly activated by loss of iASPP in the later stages of mouse embryonic development, we investigated why a loss of iASPP resulted in the establishment of an abnormal structure, morphology and function of the myocardium *in vivo*, similar to the human pathology of ARVC.

iASPP is known to be a potent inhibitor of p53-mediated apoptosis, and conserved from *C. elegans* to humans (Bergamaschi, Samuels et al. 2003). Furthermore, loss of mdm2 and mdm4, two well-known negative regulators of p53 expression (Marine and Jochemsen 2004), has been reported to cause embryonic lethality in mice due to an excess of apoptosis (Montes de Oca Luna, Wagner et al. 1995; Parant, Chavez-Reyes et al. 2001). The embryonic lethality phenotype is completely rescued by the concomitant loss of p53 alleles (Jones, Roe et al. 1995; Montes de Oca Luna, Wagner et al. 1995; Parant, Chavez-Reyes et al. 2001), indicating a genetic link between the two proteins. In addition, studies performed on human ARVC patients suggest that the loss of myocytes and their replacement with fibro-fatty deposits results from an excessive, and inappropriate, apoptotic process (Runge, Stouffer et al. 2000). Hence, it is reasonable to speculate that the ARVC phenotype observed in iASPP mutant progeny could be caused by enhanced cellular apoptosis in the myocardium.To test this hypothesis we examined myocyte proliferation and apoptosis using, respectively, Ki67 staining and terminal deoxynucleotidyl transferase dUTP nick end labelling (TUNEL) on matching myocardial sections of mutant and wild type littermate mice from *post natal* day 5. Ki67 is a cell-cycle related nuclear protein, expressed by proliferating cells in all phases of the active cell cycle (G1, S, G2 and M phase), but absent in resting (G0) cells. As shown by quantification analysis, no significant difference was observed between mutant iASPP and wild

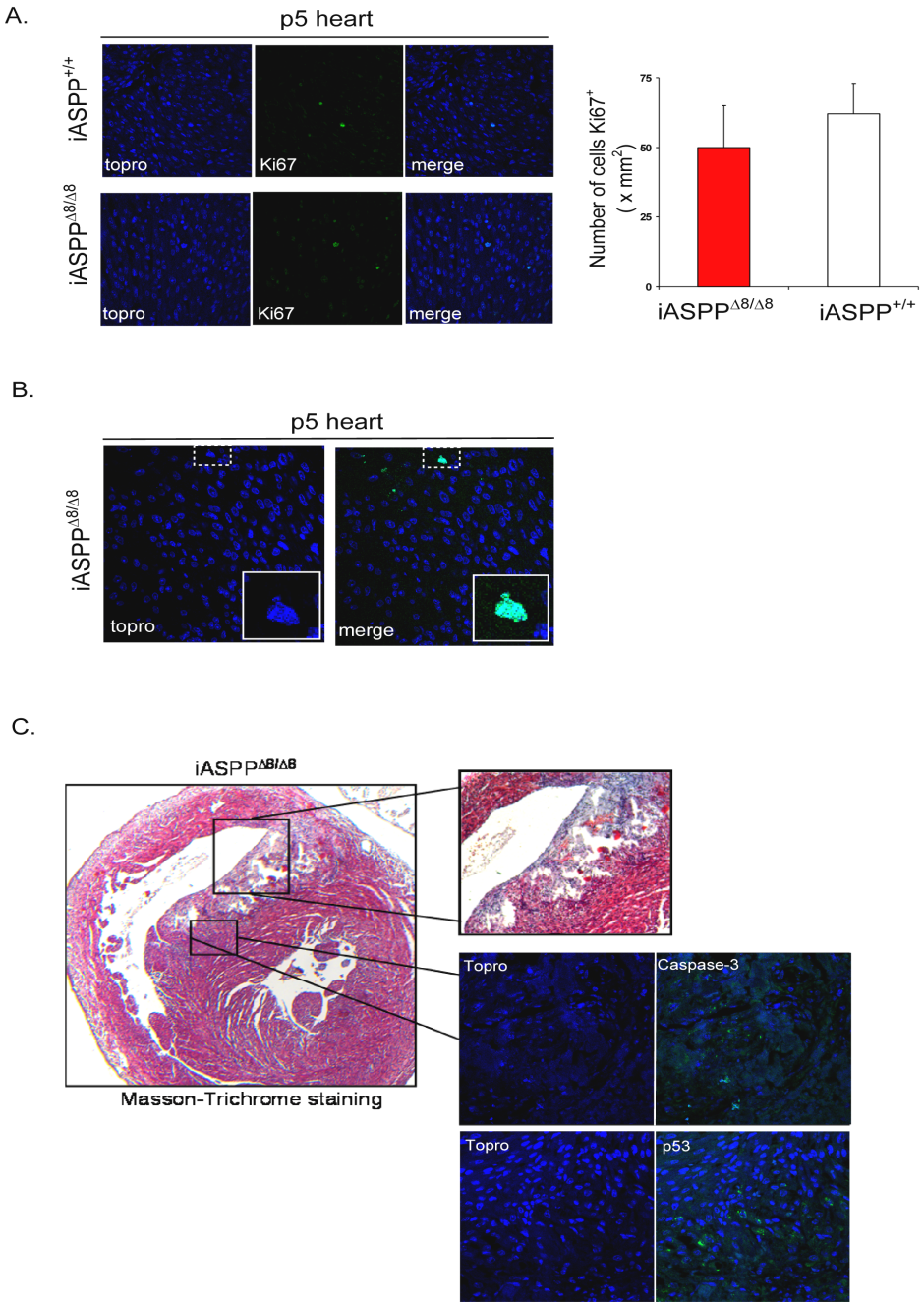


Figure 4.20. Enhanced apoptotic activity in p5 iASPP$^{\Delta 8/\Delta 8}$ hearts. (A) Paraffin wax ventricular sections from p5 iASPP$^{+/+}$ and iASPP$^{\Delta 8/\Delta 8}$ hearts were immunolabeled using a Ki67 monoclonal antibody *(right).* Topro was used as a nuclear stain. Bar graph represents the number of positive Ki67 cell counts in three different p5 mutant hearts (n=3). (B) TUNEL-stained thin myocardial sections showing positive DNA nicks only in iASPP mutant hearts. Topro was used as a nuclear stain. (C) Transverse myocardial sections of p5 iASPP$^{\Delta 8/\Delta 8}$ hearts, which show positive Masson trichrome staining, were used to immunostain p53 using rabbit polyclonal CM-5 antibody. Topro was used as a nuclear stain.

type control hearts *(figure 4.20A)*, indicating a normal cardiomyocyte proliferation rate in iASPP mutant hearts. The TUNEL assay is a common method for detecting DNA fragmentation that results from apoptotic signaling cascades. The assay relies on the presence of "nicks" within the DNA strings, which can be identified by terminal deoxynucleotidyl transferase, an enzyme that will catalyse the addition of dUTPs to the DNA "nicks". Then, the dUTPs can be visualised by a secondary antibody labeled with a detection marker. Apotosis was compared in heart tissue sections (n=3) from 5 day old mice. The number of TUNEL-positive cells was higher in the ventricles and septa of mutant mice when compared to the wild type *(figure 4.20B)*. This suggested a higher rate of apoptotic events in the mutant hearts compared with the controls. To understand whether the apoptotic process was an active component of the fibrotic deposits, p5 mutant myocardial areas neighbouring positive Masson trichrome staining areas were analysed for apoptotic markers. Immunofluorescence staining using polyclonal antibodies against p53 or active caspase-3 were performed. Positive nuclear signals were detected in the region adjacent to fibrotic deposits in p5 iASPP mutant hearts *(figure 4.20C)* strongly indicating that cardiac myocytes are lost by p53-induced apoptosis. In embryonic heart development, proliferation and apoptosis must be finely balanced to allow the correct expansion and differentiation of myocytes (Jacobson, Weil et al. 1997). Apoptosis plays a fundamental role in ventricular morphogenesis (Abdelwahid, Pelliniemi et al. 1999) and it is known that aberrant apoptotic patterns can cause cardiac malformation, ventricular dilatation and coronary abnormalities (Poelmann and Gittenberger-de Groot 2005). In order to examine the proliferative and apoptotic rates in embryonic iASPP-null hearts, 14.5 day pregnant iASPP heterozygous females were injected with a single pulse of bromodeoxyuridine (BrdU), 1 hour before being sacrificed. BrdU is a synthetic thymidine analogue that is incorporated into newly synthesised DNA during S- phase of the cell cycle. At E14.5, most of the $BrdU^+$ cells were recorded on the compact layer, in agreement with the literature (Ieda, Tsuchihashi et al. 2009), but no difference in the number of $BrdU^+$ cells was noticed between mutant and control heart sections, indicating a normal proliferation rate in iASPP-deficient cardiomyocytes *(figure 4.21A)*.

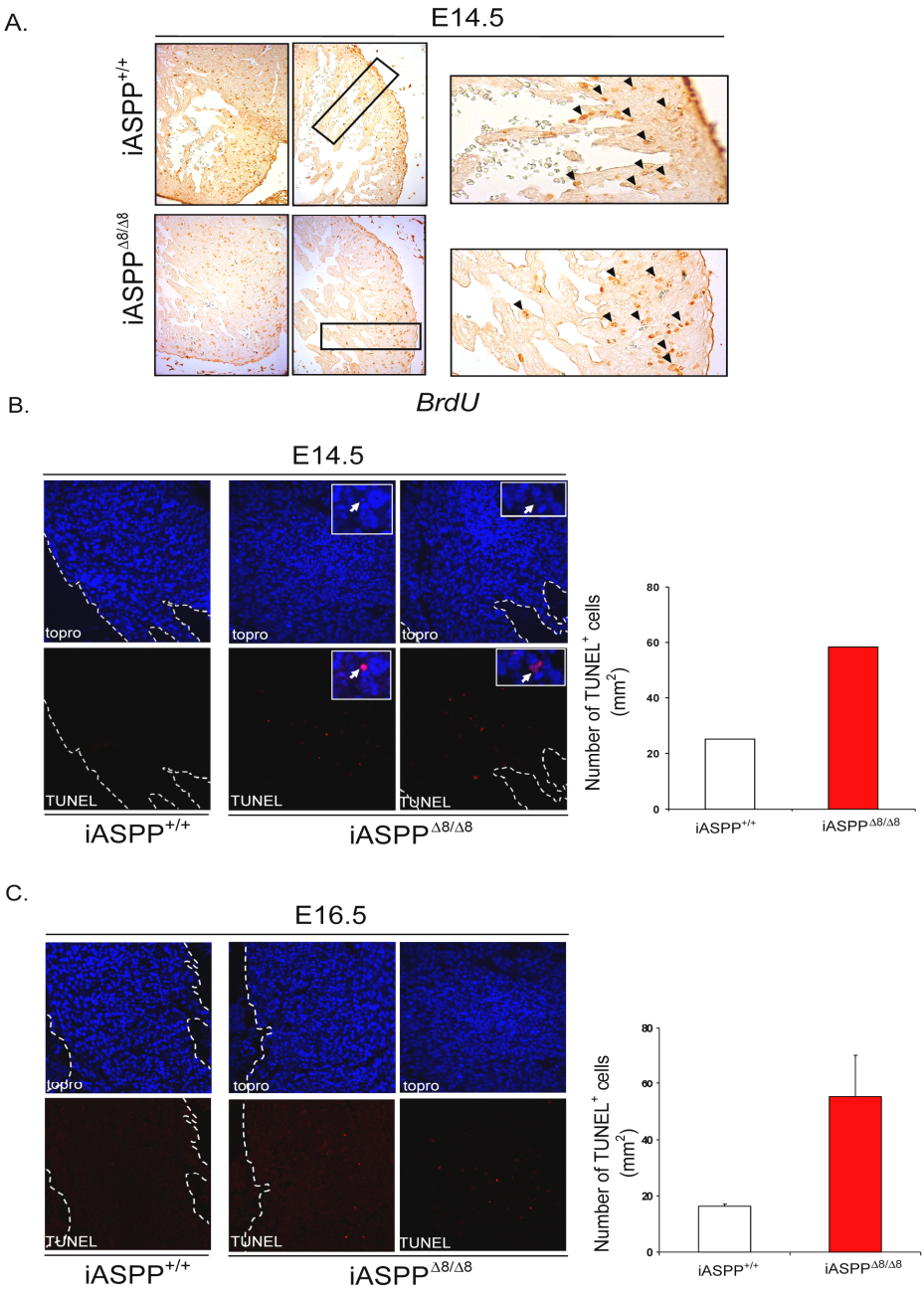


Figure 4.21. Enhanced apoptotic activity in E14.5 and E16.5 iASPP$^{\Delta 8/\Delta 8}$ hearts. (A) Paraffin wax ventricular sections from E14.5 iASPP$^{+/+}$ and iASPP$^{\Delta 8/\Delta 8}$ hearts were immunolabeled using a bromodeoxyuridine (BrdU) monoclonal antibody. Pregnant females were injected with one dose of BrdU 14.5 days *post coitum*, sacrificed one hour later and embryos were processed for histological examination. Picture shows junction between the right and intraventricular septum *(left)* and left ventricular wall *(middle)*. The right panel shows higher magnification of the black square area. Black arrows show positive BrdU myocytes. (B-C) TUNEL-stained paraffin wax embedded thin myocardial sections show positive DNA "nicks" in only iASPP mutant hearts. (B) Right ventricular and septal walls were the areas with the highest amounts of TUNEL-positive myocytes. Picture shows Topro was used as a nuclear stain. Bar graph represents the quantification analysis of TUNEL-positive cells per mm^2 (E 14.5 n=2; E16.5 n=3).

On the other hand, $TUNEL^+$ cells were clearly evident in mutant hearts *(figure 4.21B)*. In particular, the right ventricle and the septal wall were the places where higher numbers of $TUNEL^+$ cells were noticed. Even though the rate of apoptosis was relatively low in absolute number, it was significantly higher when compared to normal hearts *(figure 4.21, bar graph)*. These results indicate that iASPP deficiency leads to an increase in apoptotic events within the myocardium of $iASPP^{\Delta 8/\Delta 8}$ mice, while no signs of abnormal proliferation were detected. In addition, the surrounding fibrotic areas were shown to stain positive for apoptotic markers, suggesting that apoptosis is indeed involved in the biology of the scar tissue, in accordance with the literature. We therefore hypothesised that a lack of iASPP expression enhances the rate of apoptosis in embryonic and young iASPP-depleted hearts, and may drive the dilated remodelling process.

4.2.5.2 $iASPP^{\Delta 8/\Delta 8}$ ARVC is not dependent on p53 or its family members.

4.2.5.2.1 $iASPP^{\Delta 8/\Delta 8}$;$p53^{-/-}$ mice: loss of p53 alleles only rescues the local fibrotic deposits, and not the dilated cardiomyopathy in $iASPP^{\Delta 8/\Delta 8}$ mice.

Five days old iASPP-null mice showed focal fibrotic deposits, indicating a severe loss of cardiac myocytes. Clear stabilisation of p53 protein and positive nuclear staining of cleaved caspase-3 was also observed in areas neighbouring the fibrotic deposits, suggesting that $iASPP^{\Delta 8/\Delta 8}$ myocytes were lost due to activation of p53-mediated apoptosis. In addition, analysis of iASPP mutant hearts at late embryonic stages of development confirmed that myocytes had been lost from the myocardium when iASPP was absent. In fact, TUNEL-positive cells were observed in iASPP mutant hearts, in particular in the right ventricular and septal walls, validating the idea that cardiomyocyte loss is due to an increase in apoptosis. Since inactivation of mdm2 and mdm4 had previously been shown to induce p53-dependant cardiomyopathy *in vivo* (Parant, Chavez-Reyes et al. 2001; Grier, Xiong et al. 2006), it was possible that iASPP-dependent cardiomyopathy could also be caused by an enhanced level of programmed cell death, specifically activated by p53 activity.

total number: 168		male: 87		female: 81	
genotype	N. of mice (observed/expected)	genotype	N. of mice (observed/expected)	genotype	No of mice (observed/expected)
$iASPP^{+/+}$ $p53^{+/+}$	21/10.5	$iASPP^{+/+}$ $p53^{+/+}$	14/5.43	$iASPP^{+/+}$ $p53^{+/+}$	7/5.06
$iASPP^{+/+}$ $p53^{+/-}$	30/21	$iASPP^{+/+}$ $p53^{+/-}$	11/10.875	$iASPP^{+/+}$ $p53^{+/-}$	18/10.125
$iASPP^{+/+}$ $p53^{-/-}$	8/10.5	$iASPP^{+/+}$ $p53^{-/-}$	5/5.43	$iASPP^{+/+}$ $p53^{-/-}$	4/5.06
$iASPP^{+/-}$ $p53^{+/+}$	24/21	$iASPP^{+/-}$ $p53^{+/+}$	13/10.875	$iASPP^{+/-}$ $p53^{+/+}$	12/10.125
$iASPP^{+/-}$ $p53^{+/-}$	51/42	$iASPP^{+/-}$ $p53^{+/-}$	27/21.75	$iASPP^{+/-}$ $p53^{+/-}$	25/20.25
$iASPP^{+/-}$ $p53^{-/-}$	20/21	$iASPP^{+/-}$ $p53^{-/-}$	12/10.875	$iASPP^{+/-}$ $p53^{-/-}$	7/10.125
$iASPP^{-/-}$ $p53^{+/+}$	5/10.5	$iASPP^{-/-}$ $p53^{+/+}$	2/5.43	$iASPP^{-/-}$ $p53^{+/+}$	3/5.43
$iASPP^{-/-}$ $p53^{+/-}$	6/21.5	$iASPP^{-/-}$ $p53^{+/-}$	1/10.875	$iASPP^{-/-}$ $p53^{+/-}$	4/10.125
$iASPP^{-/-}$ $p53^{-/-}$	3/10.5	$iASPP^{-/-}$ $p53^{-/-}$	2/5.43	$iASPP^{-/-}$ $p53^{-/-}$	1/5.06

Table 4.2. Genotypes of mice produced by a breeding scheme in which $iASPP^{\Delta 8/+}$;$p53^{+/-}$ mice were used as breeding pairs. Genotype analysis of offspring at weaning age from double heterozygous couples for iASPP and p53 showed that all of the possible genotype combinations were obtained. However, offspring in which iASPP expression was deleted showed a reduce number of progeny from the expected Mendelian segregation.

In order to test this hypothesis, the p53-null alleles were introduced into iASPP-null mice. In a cohort of 168 pups birthed from $iASPP^{+/-}$;$p53^{+/-}$ couples, the expected combination of genotypes was obtained, except for the genotype in which iASPP alleles were deleted, confirming the partial embryonic lethality of iASPP-null progeny *(table 4.2)*. Although the number of the cohort needs to be increase to reach statistical significance, this data shows that the loss of p53 does not rescue the embryonic lethality typical of the iASPP KO progeny *(table 4.2)*. $iASPP^{\Delta 8/\Delta 8}$;$p53^{-/-}$ mice, which survived up to weaning, died within 32 weeks of age. Hearts were dissected and analysed in order to understand the impact of p53 expression on the establishment of the dilated myopathy in iASPP-null mice. Double KO mice for both iASPP and p53 alleles were analysed *post mortem*, and the heart dissected and prepared for histological examination.

Surprisingly, macroscopic examination of double mutant hearts revealed that the organ was obviously dilated, and that this was associated with a distorted morphology and increased size, similar to that of $iASPP^{\Delta 8/\Delta 8}$;$p53^{+/+}$ hearts *(figure 4.22)*. On the other hand, $iASPP^{+/+}$;$p53^{-/-}$ hearts presented were comparable in shape and size when compared with wild type controls *(figure 4.22)*.

Gross examination highlighted clear signs of dilatation of both ventricular and atrial chambers. However, fibrotic scars on the exterior of the ventricular walls and the focal areas of myocyte loss were reduced in size and number, indicating a partial rescue of the myopathy by loss of p53 expression *(figure 4.22)*.

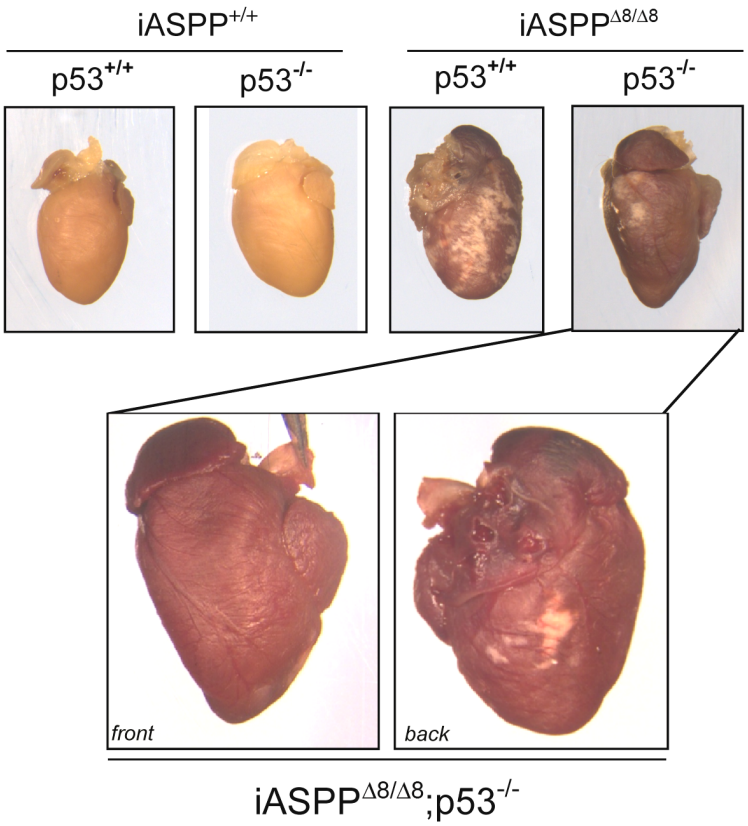


Figure 4.22. Gross abnormalities in iASPP$^{\Delta 8/\Delta 8}$;p53$^{-/-}$ hearts. Hearts were dissected form matching age and sex, adult iASPP$^{+/+}$;p53$^{+/+}$, iASPP$^{+/+}$;p53$^{-/-}$, iASPP$^{\Delta 8/\Delta 8}$;p53$^{+/+}$ and iASPP $^{\Delta 8/\Delta 8}$;p53$^{-/-}$ mice, placed in 10 cm dishes containing PBS buffer solution and photographed using a dissection microscope. Magnification is 2X. Double KO hearts for the iASPP and p53 alleles show the enlarged size of the organ, associated with only few white focal lesions on the exterior of the ventricular wall.

Histological analyses were performed in order to investigate the structure of the double mutant myocardium and the presence of fibrotic deposits. First, H&E staining confirmed the dilatation of both ventricles and clear defects in the myocardial architecture of iASPP$^{\Delta 8/\Delta 8}$;p53$^{-/-}$ mice. The histology of myocardial tissue from double KO hearts was very similar to that of iASPP$^{\Delta 8/\Delta 8}$;p53$^{+/+}$

myocardial sections *(figure 4.23A)*. iASPP and p53 double mutant hearts showed expansion of the intercellular spaces between myocytes, and a disarrayed arrangement of the myofiber architecture. The right ventricular free wall looked severely compromised *(figure 4.23A)*. Masson staining revealed mild interstitial fibrosis in the iASPP$^{\Delta 8/\Delta 8}$;p53$^{-/-}$ mice when compare with wild type controls *(figure 4.23A)*. Interestingly, in accordance with the reduced number of fibrotic scars, Masson staining showed that fibrotic deposits into the myocardium were reduced both in number and extension, throughout the myocardium of double KO mice. In fact, only a few focal fibrotic deposits were evident when compared with iASPP–null mice *(figure 4.23B)*. However, interstitial fibrosis was still evident *(figure 4.23B, black arrows)*. In conclusion, these data indicate that loss of p53 in iASPP mutant hearts did not rescue the embryonic lethality in iASPP$^{\Delta 8/\Delta 8}$ embryos, and only partially recovered the ARVC pathology induced by iASPP deficiency *in vivo*. Both the shape and size of the p53-iASPP double mutant hearts were comparable with what was previously observed for iASPP-null hearts. Severe dilation of both ventricles and disorganisation of the myofibril architecture of the right ventricular wall was evident. Local areas of fibrosis observed in iASPP$^{\Delta 8/\Delta 8}$ mice were the only abnormalities partially rescued by loss of p53 expression in iASPP null hearts, strongly indicating a genetic link between enhanced apoptosis and fibro-fatty deposits. This result is consistent with the mechanism underlying the fibro-fatty deposits in ARVC heart (Corrado, Basso et al. 1997; Runge, Stouffer et al. 2000). Hence, iASPP could function as an inhibitor of p53-mediated apoptosis in the developing heart. However, interstitial fibrosis between myocytes was still present, suggesting that ECM had been deposited in order to sustain heart performance. Hence, iASPP should also has a structural role in maintain myocardium structure. Together, these data suggest that the elevated apoptotic activity observed in iASPP-depleted hearts is the genetic cause of the development of the focal areas of fibro-fatty deposits. However, it is not sufficient for the establishment of the iASPP-dependent cardiomyopathy. iASPP must, then, have an additional role in maintaining cellular homeostasis within the myocardium, *in vivo*.

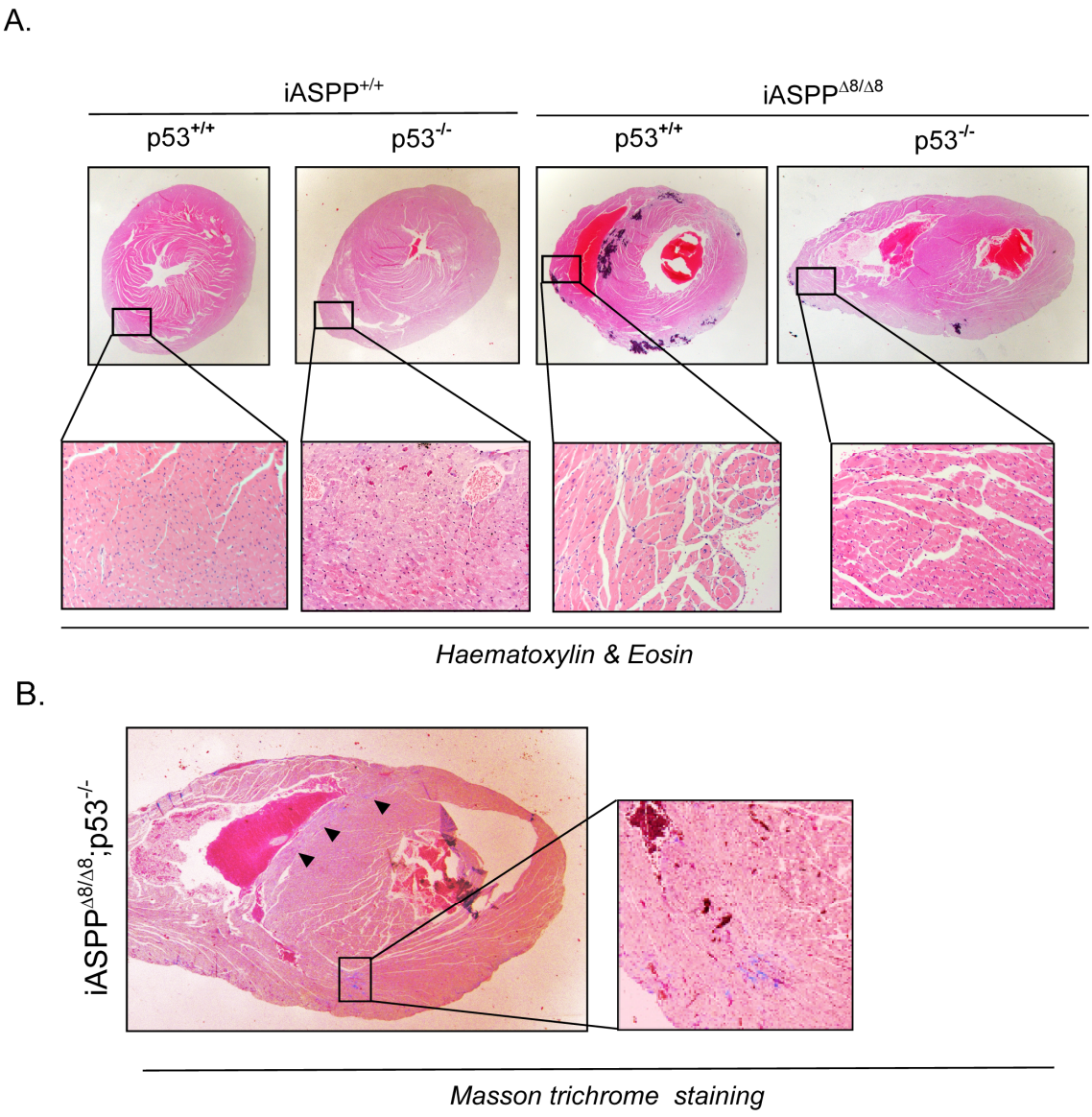


Figure 4.23. Histological analysis of iASPP$^{+/+}$;p53$^{+/+}$, iASPP$^{+/+}$;p53$^{-/-}$, iASPP$^{\Delta 8/\Delta 8}$;p53$^{+/+}$ and iASPP $^{\Delta 8/\Delta 8}$;p53$^{-/-}$ hearts. (A) Transverse sections of myocardial iASPP$^{+/+}$;p53$^{+/+}$, iASPP$^{+/+}$;p53$^{-/-}$, iASPP$^{\Delta 8/\Delta 8}$;p53$^{+/+}$ and iASPP $^{\Delta 8/\Delta 8}$;p53$^{-/-}$ hearts were stained with H&E. Dilation of both ventricular cavities was noted in double KO mice for the iASPP and p53 alleles *(top)*. Higher magnification represents detailed structure of the myocardial tissue from different iASPP;p53 genotypes *(bottom)*. Note the myocardial disorganisation and the increased intracellular space in iASPP$^{\Delta 8/\Delta 8}$;p53$^{+/+}$ and iASPP $^{\Delta 8/\Delta 8}$;p53$^{-/-}$ sections. (B) Masson trichrome staining of thin myocardial iASPP $^{\Delta 8/\Delta 8}$;p53$^{-/-}$ sections revealed a decreased number of focal fibrotic deposits *(black arrows)*, but interstitial fibrosis is still evident.

4.2.4.2.2 $p63^{+/-}$;$iASPP^{\Delta 8/\Delta 8}$ does not alleviate $iASPP^{\Delta 8/\Delta 8}$-dependent ARVC.

p63 is a member of the p53 family, and its role in epithelial development has been extensively investigated using both KO technologies and *in vivo* and *in vitro* studies. It is now clear that its expression and function is required for the correct development of all stratified epithelia and its derivates in mammals (Millis et al., 1999; Yang et al., 1999). However, little is know about its role in other organs or tissue types. Mutations in the *TP63* gene have been identified in five different types of ectodermal dysplasia (ED) in humans (Chan, Harper et al. 2004). Controversially, heart defects in ED patients have only occasionally been described and, to date, hypertrophic or dilated cardiomyopathies have never been observed in patients affected by p63-related mutations.

	27/07/2009						
total number of mice:	96		male: 42			female: 54	
genotype	N. of mice (observed/expected)		genotype		N. of mice (observed/expected)	genotype	No of mice (observed/expected)
$iASPP^{+/+}$ $p63^{+/+}$	13	./06	$iASPP^{+/+}$	$p63^{+/+}$	6/2.65	$iASPP^{+/+}$ $p63^{+/+}$	7/3.375
$iASPP^{+/+}$ $p63^{+/-}$	13	./12	$iASPP^{+/+}$	$p63^{+/-}$	6/5.25	$iASPP^{+/+}$ $p63^{+/-}$	7/6.75
$iASPP^{+/+}$ $p63^{-/-}$	0	./06	$iASPP^{+/+}$	$p63^{-/-}$	0/2.65	$iASPP^{+/+}$ $p63^{-/-}$	0/3.375
$iASPP^{+/-}$ $p63^{+/+}$	19	./12	$iASPP^{+/-}$	$p63^{+/+}$	10/5.25	$iASPP^{+/-}$ $p63^{+/+}$	9/6.75
$iASPP^{+/-}$ $p63^{+/-}$	38	./24	$iASPP^{+/-}$	$p63^{+/-}$	18/10.5	$iASPP^{+/-}$ $p63^{+/-}$	20/13.5
$iASPP^{+/-}$ $p63^{-/-}$	0	./12	$iASPP^{+/-}$	$p63^{-/-}$	0/10.5	$iASPP^{+/-}$ $p63^{-/-}$	0/6.75
$iASPP^{-/-}$ $p63^{+/+}$	4	./06	$iASPP^{-/-}$	$p63^{+/+}$	0/2.65	$iASPP^{-/-}$ $p63^{+/+}$	4/3.375
$iASPP^{-/-}$ $p63^{+/-}$	9	./12	$iASPP^{-/-}$	$p63^{+/-}$	3/5.5	$iASPP^{-/-}$ $p63^{+/-}$	6/6.75
$iASPP^{-/-}$ $p63^{-/-}$	0	./06	$iASPP^{-/-}$	$p63^{-/-}$	0/2.65	$iASPP^{-/-}$ $p63^{-/-}$	0/3.375

Table 4.3. Genotype analysis of offspring of mice produced by breeding from $iASPP^{\Delta 8/+}$;$p63^{+/-}$ couples. Genotype analysis of offspring at weaning age from mice double heterozygous for the iASPP and p63 alleles showed that all possible genotype combinations were obtained, except for the p63-null combination, which is embryonically lethal (Yang, Schweitzer et al. 1999). Offspring were observed to sho

However, the function of p63 in the heart has never been investigated. Previous studies conducted in our laboratory have identified iASPP as an inhibitor of p63 *in vitro* (Bergamaschi, Samuels et al. 2004). By structural analysis, it was shown by Robinson and colleagues that the C-terminus of iASPP can bind the DBD of p63 *in vitro* (Robinson, Lu et al. 2008). Given the already known

interaction between iASPP and p63, the possibility that the introduction of only one functional copy of the p63 allele could rescue, or just alleviate, the myopathy observed in iASPP-null progeny was investigated. In order to test this hypothesis, mice double heterozygous for p63 and iASPP were bred together. In a cohort of 96 pups obtained from the p63-iASPP heterozygous couples, the expected combinations of genotypes were obtained, except for the p63-iASPP double knockout which was never observed *post natally*, because p63 KO mice are embryonically lethal (Mills, Zheng et al. 1999; Yang, Schweitzer et al. 1999). Moreover, the percentages of iASPP-null pups obtained within a $p63^{+/+}$ or $p63^{+/-}$ background were only slightly reduced, but still in line with our previous observation that iASPP loss causes partial embryonic lethality *(table 4.3)*. This indicates that a single functional p63 allele does not rescue the embryonic lethality of $iASPP^{\Delta 8/\Delta 8}$. In order to understand the effect of p63 on the iASPP cardiomyopathy *in vivo,* double p63-iASPP heterozygous mice were mated together and iASPP-null mice in a $p63^{+/-}$ background were obtained. Their hearts were dissected and investigated for any sign of abnormal structure or morphology, fibrotic scars or disorganised architecture of the myocardial tissue. Macroscopic investigation demonstrated that loss of iASPP expression and one copy of the p63 allele did not rescue the morphological abnormalities already described for iASPP-null mice *(figure 4.24A)*. Once more, the shape and morphology of the double mutant hearts were obviously abnormal, with dilation of both ventricular chambers, implying a non-essential or secondary role for p63 in controlling iASPP-null mediated ARVC. Furthermore, fibrotic deposits on the exterior of the ventricular walls were still evident and extended throughout the myocardium of $iASPP^{\Delta 8/\Delta 8}$;$p63^{+/-}$ mice. H&E and light microscopy Taken together, this preliminary evidence demonstrates that a half dose of the p63 allele does not rescue the cardiomyopathy induced by a loss of iASPP. Abnormal morphology, severe dilation of ventricular chambers and extended fibrotic deposits were still present in $iASPP^{\Delta 8/\Delta 8}$;$p63^{+/-}$ hearts, indicating that p63 is not important in the aethiology of iASPP dependent ARVC analyses revealed that iASPP-null and $p63^{+/-}$ hearts showed extensive rearrangement of the cardiac tissue associated with local fibrotic deposits *(figure 4.24B)*

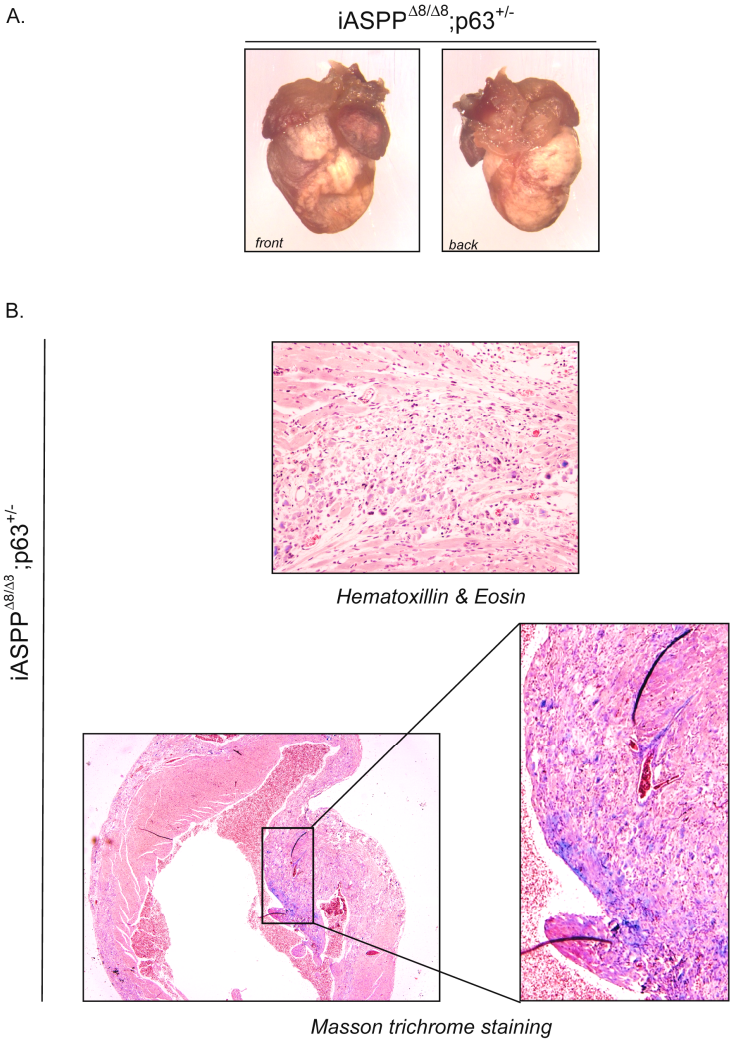


Figure 4.24. Histological analysis of iASPP$^{\Delta8/\Delta8}$;p63$^{+/-}$ hearts. (A) Hearts dissected from adult iASPP$^{\Delta8/\Delta8}$;p63$^{+/-}$ mice were placed in a 10 cm dish containing PBS, and photographed using a dissection microscope. Magnification 2.0X. White lesions were observed on the exterior of the ventricular walls. (B) Myocardial sections from iASPP$^{\Delta8/\Delta8}$;p63$^{+/-}$ mice stained with H&E showed rearrangement of the myofibrils *(top)*. Masson trichrome staining of iASPP$^{\Delta8/\Delta8}$;p63$^{+/-}$ myocardial sections showing extensive areas of fibrotic deposits.

.

4.3 Summary and discussion

The loss of iASPP's expression in mice resulted in three clear phenotypes that affected iASPP$^{\Delta 8/\Delta 8}$ progeny. The abnormalities were identified by gross analysis as affecting eyes, skin/hair follicles and heart tissues *(figure 4.25)*. Our tissue expression analyses also indicate that skin and heart abundantly express iASPP, suggesting an important role for the protein into the biology of these organs. In this Chapter, we provided evidence that inactivation of the iASPP gene results in severe heart dysfunction, which leads to the transgenic mice having a shorter life span. iASPP-null mice died suddenly, with no previous sign of

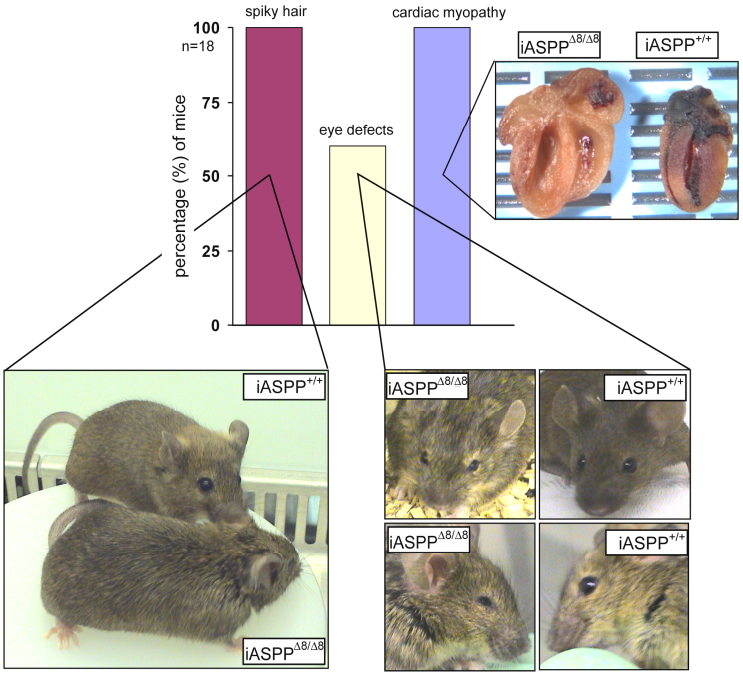


Figure 4.25. Percentage of iASPP$^{\Delta 8/\Delta 8}$ mice showing different phenotypes. A cohort of iASPP-depleted mice (n=18) were analysed for gross abnormalities in different tissues. Dilated cardiomyopathy and the "wavy" hair phenotype were noted to be fully penetrant in the cohort. Only 60% of iASPP-null mice showed eye phenotypes, which ranged from cataracts to complete blindness.

illness, due to heart failure. Interestingly, histopathological analyses of iASPP$^{\Delta 8/\Delta 8}$ hearts revealed surprising similarity with the clinical outcomes of ARVC disease in patients.

The findings described in this Chapter reveal, for the first time, a possible role for iASPP in controlling myocardial homeostasis and heart performance. Preliminary data are provided on the mechanism underlying the establishment of iASPP-dependent ARVC *in vivo*. First, iASPP-depleted mice were shown to have a shorter life expectancy. In fact, iASPP$^{\Delta 8/\Delta 8}$ mice that reached weaning age (13%) appeared initially healthy, but died suddenly with no obvious sign of prior illness. This outcome is in agreement with the sudden cardiac death observed in patients affected by various types of cardiomyopathies (Franz, Muller et al. 2001). Histological examination, together with MRI of young adult (12 weeks of age) iASPP-null mice, demonstrated that iASPP$^{\Delta 8/\Delta 8}$ mice suffered severe heart abnormalities associated with distorted morphology of the organ, dilation of both ventricles (with particular emphasis on the right ventricular chamber), focal and interstitial fibrosis and reduced systolic and diastolic performance. These data indicate impaired heart function and an inability of the organ to supply enough blood to the two major circulatory systems. Finally, ECG analysis revealed that iASPP deficiency severely disrupts electrical coupling in the heart, associated with frequent multifocal VEB, as well as spontaneous runs of non-sustained ventricular tachycardia (NSVT). In addition to NVST, older iASPP$^{\Delta 8/\Delta 8}$ mice exhibited a variety of other spontaneous rhythm and conduction abnormalities raging from atrial and junctional bigeminy to heart blockade. The presence of multiple spontaneous rhythm abnormalities –particularly episodes of NSVT- in association with sudden death is strongly suggestive of an arrythmias mode of the death in iASPP$^{\Delta 8/\Delta 8}$ mice. Interestingly, heart failure and sudden cardiac death are observed in human patients affected by various types of cardiomyopathy. In particular, ARVC patients are associated with the highest frequency of arrhythmias and sudden cardiac death (Thiene, Nava et al. 1988; Dalal, Nasir et al. 2005).

Since heart failure, sudden death, dilatation of the ventricular chambers and globally reduced systolic and diastolic function are shared features between the clinical presentation of DCM and ARVC in humans (Franz, Muller et al. 2001), detailed histopathological examination was carried out in order to elucidate which cardiac myopathy iASPP-null progeny were affected by. Primary cardiomyopathies are classified based on the morphological patterns of the remodelling process that the myocardium undergoes upon stress stimuli: hypertrophy or dilated remodelling (Ahmad, Seidman et al. 2005). However, disease progression often leads to an overlap of some of the typical morphological features of different cardiomyopathies, making it difficult to specifically recognise and define the precise myocardial disease. For instance, ARVC progression often leads to effects on both ventricles and subsequent heart failure, therefore mimicking DCM pathologies (Corrado, Basso et al. 1997), although bi-ventricular ARVC generally presents a characteristic disproportion towards the right chamber of the heart (Franz, Muller et al. 2001; Ahmad, Seidman et al. 2005; Garcia-Gras, Lombardi et al. 2006). Replacement of the myocardium by fibro-fatty deposits in association with ventricular arrhythmias and sudden cardiac death are specific attributes of ARVC (Corrado, Basso et al. 1997; Sen-Chowdhry, Morgan et al. 2010). In myocardial sections obtained from iASPP-null mice, the accumulation of fat droplets was evident only at the site of the fibrotic deposits, as shown by Oil Red O staining, indicating a fibro-adipocytic replacement of myocytes in iASPP-null hearts. Furthermore, baseline resting electrocardiograms of iASPP$^{\Delta 8/\Delta 8}$ mice demonstrated spontaneous ectopic beats, ventricular couplets and signs of tachycardia, further supporting the hypothesis that iASPP loss causes ARVC *in vivo*. Finally, Asimaki and colleagues demonstrated that reduced expression of plakoglobin could be used as a new diagnostic tool for the diagnosis of ARVC in humans (Asimaki, Tandri et al. 2009). Consistent with this report, immunofluorescent investigation of plakoglobin expression from heart biopsies dissected from adult iASPP$^{\Delta 8/\Delta 8}$ hearts revealed a severe reduction in plakoglobin staining, but not β-catenin, in failing hearts and an alteration of major ID components only in the right ventricle of young adult hearts, strongly indicating that iASPP-null mice could suffer of ARVC. It is also noteworthy that the

apoptotic region where the majority of $TUNEL^+$ cells were detected in iASPP-deficient hearts was in the right ventricle and interventricular wall. The molecular mechanism for this side-specific ventricular effect is currently unknown. However, the fact that iASPP deletion appears to be so specifically right-sided differentiates our iASPP mice from other mouse models, in which other desmosomal components such as desmoplakin were deleted. It also explains why iASPP transgenic mice exhibit most, if not all, features of human ARVC. iASPP transgenic mice could, therefore, be an ideal model for ARVC. It is, thus, tempting to speculate that iASPP is a novel protein involved in the pathogenesis of ARVC. To our knowledge, this is the first report which directly associates iASPP expression with the rise and development of a particular type of dilated myopathy *in vivo* (Corrado, Basso et al. 1997; Delmar and McKenna 2010). Thus, our $iASPP^{\Delta 8/\Delta 8}$ mouse model could help understand the molecular pathways underlying the progression of ARVC, shedding new light on the molecular and functional mechanisms of the disease. In addition, looking at the variety of the phenotypic expression within families affected by the same cardiomyopathy, it is exciting to speculate that iASPP's presence or absence could define different subtypes of pathological features or a more severe outcome of the cardiomyopathy. According to this idea, iASPP may act as a modifier gene for a specific set of syndromes, and the study of its role may lead to novel therapeutic regimes with which to tackle the disease. Moreover, it is possible that patients with idiopathic cardiomyopathies may carry a mutation(s) in the iASPP genomic locus. Hence, genetic screening for iASPP mutation in patients with idiopathic family histories of lethal cardiac arrhythmias or cardiac dysfunction could be helpful in uncovering a genetic link with ARVC (Sen-Chowdhry, Syrris et al. 2005).

Whether or not iASPP loss was the direct caused of cardiac dysfunction was extensively investigated. The best approach with which to answer this question was to generate mice with a tissue-specific deletion of iASPP expression in the myocardium only (i.e. α-light myosin chain) (Agah, Frenkel et al. 1997). This could be achieved by crossing $iASPP^{flox/flox}$ mice with mice

expressing the Cre recombinase enzyme in cardiac tissue only. Several Cre^{+} mouse lines have been established, all biologically engineered to express the recombinase enzyme gene under the control of tissue specific promoters (Miwa, Koyama et al. 2000). For this study, specific deleter mice which carried the recombinase enzyme under the control of cardiac promoters will be the mice of choice, to investigate whether iASPP depletion was the cause of ARVC. These transgenic mice had previously been used to inactivate a heart muscle gene that did not share expression in the skeletal muscle or *vice versa* (Heidt and Black 2005). However, different cell populations can be targeted within cardiac muscle, making it difficult to decide which cell sub-populations to target. Furthermore, the obvious problem of obtaining the Cre^{+} cardiac-deleter mice, in addition to the cost of maintaining the mouse colony, made us decide to first investigate whether early cardiac alterations were present in $iASPP^{\Delta 8/\Delta 8}$ progeny, in order to demonstrate that cardiac myopathy is indeed iASPP dependent. For this purpose, 5, 10 and 15 day old hearts were dissected from mutant and wild type mice and extensively investigated using different cellular and molecular techniques. Even at 5 days after birth, all of the hearts analysed showed, with differing severity, cardiac defects in size, morphology, thickness of ventricular walls and myocardial structure. Abnormal organ morphology and replacement of the myocardium with fibrotic deposits were the two most striking aspects of $iASPP^{\Delta 8/\Delta 8}$ at day 5. Moreover, episcopic 3D reconstruction analyses of embryonic iASPP-null hearts suggested that the abnormalities originated in the right ventricular chamber between E14.5 and E16.5 with myocytes loss, expansion of the right ventricular chamber and thinning of the ventricular wall. Hence, the right ventricle seems to be the location where the myopathy begins, re-enforcing the idea that ARVC is the pathology that iASPP-null progeny are affected by. Furthermore, histological and molecular analyses of E14.5 and E16.5 embryonic hearts supported this hypothesis, confirming the episcopic analyses and demonstrating severe heart abnormalities. In particular, areas of fibrosis and thinning of the right ventricular walls associated with reduced numbers of cells were evident. Although, cardiac abnormalities can be a secondary consequence of other physiological abnormalities in the body, the evidence presented here is

sufficient to indicate that iASPP deficiency is the primary event that triggers molecular pathways which lead to myocardial remodelling and heart failure.

In line with this, *in vivo* preliminary results using an inducible system to control iASPP expression by the presence or absence of 4-hydroxyltamoxifen (4-OHT) resulted in cardiac abnormalities associated with enlargement of the organ and rearrangement of the myocardial structure together with sudden death (data not shown). These data further indicate that the absence of iASPP expression is the direct and primary cause of impaired heart function *in vivo*. Collectively, these findings provide what we believe to be the first report that associates iASPP loss with ARVC, and this mouse model could be useful for the study of the establishment of the disease or, given the different range of phenotypes in familiar cardiomyopathies, could also be used to study the implications of iASPP as a modifier gene for the clinical severity of the outcome of the disease. However, further studies are needed, including the generation of iASPP$^{\Delta 8/\Delta 8}$ progeny with inducible cardiac-specific Cre expression, to conclude this study.

Histological analyses of iASPP$^{\Delta 8/\Delta 8}$ myocardia demonstrated characteristic areas of myocardial rearrangement, in which myocytes were replaced by fibro-fatty deposits. According to the literature fibrotic deposits are cause by myocyte death, which triggers an increase in the extracellular matrix collectively called cardiac fibrosis, in order to sustain the impaired heart's contraction (Ahmad, Seidman et al. 2005). In ARVC patient biopsies, fibro-fatty replacement of the myocardium helps the diagnosis of the disease (McKenna, Thiene et al. 1994). Two types of fibrosis are clearly present in iASPP$^{\Delta 8/\Delta 8}$ hearts, focal and interstitial fibrosis, and they both deserve to be discussed. Firstly, focal fibrosis deposits seem to begin on the exterior part of the ventricular walls in a distinctive location, at the top-front part of the heart, as showed by the analysis of p5 mutant hearts. Interestingly, this is also the region where iASPP KO hearts showed the most reduced thickness of the ventricular walls at E14.5, and fibrotic deposits at E16.5. Previous report have demonstrated that the anterior right ventricular outflow tract, the apex and the inferior-posterior wall are the most

frequent locations to be affected by fibro-fatty deposits in ARVC patients (Munclinger, Patel et al. 2000; Nava, Bauce et al. 2000). Consistently, the anterior outflow track could be the area in which the single white scar appears in new born iASPP$^{\Delta 8/\Delta 8}$ mice, supporting the hypothesis that iASPP is a novel protein involved in the establishment of ARVC. Secondly, as the fibrotic scar becomes progressively larger over time, it extends into the myocardium making the cardiac muscle floppy, stiff and unable to contract efficiently, as shown by the MRI investigation. In ARVC patients, this process is believed to initiate at the epicardium and slowly extends through the myocardium towards the subepicardium (Ahmad, Seidman et al. 2005), consistent with our investigation in iASPP-null mice. Third, focal fibro-fatty deposits appeared to be dependant on the presence of p53 alleles. Interestingly, genetic ablation of p53 protein reduced focal areas of fibrosis both in size and numbers. In fact, in agreement with this observation, apoptotic events were more evident in embryonic myocardial sections from iASPP$^{\Delta 8/\Delta 8}$ mice when compare with wild type littermates, and apoptotic markers were noted in neighbouring areas positive for Masson staining in p5 iASPP-null hearts. In addition to the embryonic survival studies performed in Chapter III, these data could suggest a contribution of iASPP in modulating p53-mediated apoptosis in the developmental stages of the heart or under stress conditions, such as a remodelling process to sustain heart performance *in vivo.* On the other hand, areas of the myocardium in which focal fibrotic deposits were absent showed altered myofibril organisation, with hypertrophic cardiomyocytes and increased intercellular space between myocytes. This intercellular space is filled with extracellular matrix components (interstitial fibrosis), required to sustain the mechanical stress of the heart beats (Ahmad, Seidman et al. 2005). When myocytes are hypertrophic, there is an increase in the number of longitudinally arranged sarcomeric structures, as demonstrated by the cross section of myocardia from iASPP-null mice, and the positivity of ANP (Xiong, Van Pelt et al. 2007). In the absence of p53, interstitial fibrosis is still present among the cardiomyocytes, indicating that the heart's function is still diminished and that the remodelling response of the heart to impaired heart performance is not only due to abnormal p53 activity.

In order to establish why loss of iASPP impaired heart structure and function, we investigated two possible mechanisms. First, since the loss of mdm2 (Barboza, Iwakuma et al. 2008) and mdm4 (Xiong, Van Pelt et al. 2007) had already been demonstrated to induce heart abnormalities and sudden cardiac death in a p53-dependent manner, a possible p53-dependent mechanism was investigated. To date, the best known function of iASPP is to bind p53, p63 and p73, and inhibit their apoptotic functions (Bergamaschi, Samuels et al. 2003; Bergamaschi, Samuels et al. 2006). Embryonic hearts that lack iASPP expression seem to progress from an adaptive cardiac remodelling process to the establishment of an ARVC myopathy and, finally, to heart failure. The early detection of fibrotic deposits in young hearts indicates a loss of cardiomyocytes and activation of p53 in areas neighbouring the fibrotic deposits, indicating that programmed cell death makes a major contribution to the deposition of collagen and fibrotic tissue. It is therefore possible that iASPP might serve as an apoptotic regulator involved in maintaining the fine balance between proliferation and apoptosis in developing hearts. However, the introduction of the p53-null alleles only partially rescued the iASPP$^{\Delta 8/\Delta 8}$ heart phenotype. Interestingly, only the fibrotic scars on the exterior of the ventricular walls, or the focal areas of cardiomyocyte loss in the myocardia, were reduced in size and number suggesting partial rescue of the phenotype caused by the loss of iASPP.

The molecular pathogenesis of ARVC is still not entirely understood (Corrado, Basso et al. 1997; Sen-Chowdhry, Syrris et al. 2005). Descriptive studies have suggested that loss of myocardia and replacement with fibro-fatty deposits results from excessive and inappropriate apoptotic processes (Runge, Stouffer et al. 2000). In agreement with this, enhanced apoptotic events were demonstrated here in iASPP-null mice, indicating a role for apoptosis in the establishment of ARVC, in accordance with the literature (Corrado, Basso et al. 1997; Ahmad, Seidman et al. 2005; Garcia-Gras, Lombardi et al. 2006). However, it is not the primary molecular event that establishes the myopathy. In fact, absence of p53 does not entirely rescue the cardiomyopathy in iASPP-deficient mice but only alleviates the fibro-fatty deposits, indicating that iASPP could act as a regulator of the apoptotic response in stress conditions such as pressure or volume overload. These observations

also suggest that iASPP might be involved, partially or under stress conditions, in the tight regulation of p53 in different mouse tissues.

Given the severity of the cardiac phenotype in our inducible iASPP KO system, and the finding that the loss of p53 alleles rescues the fibro-fatty deposits but not the overall myopathy, it is tempting to speculate that iASPP might have a new role above that of modulating the p53-response to cell death. This hypothesis has been supported by the following evidence. Firstly, iASPP has been found located at the polar end of the rod-shape cardiomyocytes, where the junctional complexes of the intercalated discs are found (Franke, Borrmann et al. 2006). Secondly, loss of many components of the cell-to-cell junctions have been linked with the development of either hypertrophy or dilated cardiomyopathies (Ahmad, Seidman et al. 2005). Finally, recent findings from our laboratory have revealed a novel function for ASPP2 in regulating cell polarity in the CNS, and proliferation of neuronal progenitors *in vivo* (Sottocornola, Royer et al. 2010). By demonstrating that ASPP2 clearly locates at the cell-cell junctions, Sottocornola and colleagues showed that ASPP2 is required to maintain the integrity of tight junctions by interacting with Par-3 (Sottocornola, Royer et al. 2010). For these reasons, we can speculate that a p53-independent mechanism for the establishment of ARVC exists in iASPP depleted mice. Desmosomes are specialised adhesive junctions that support the mechanical stress of heartbeats and also participate in the cross-talk between adherens and gap junctions (Delmar and McKenna 2010). A recent paper demonstrated that suppression of canonical Wnt/β-catenin signalling is important in the pathogenesis of ARVC (Garcia-Gras, Lombardi et al. 2006), suggesting that the absence of desmoplakin from the desmosomal complexes could free plakoglobin, also known as γ-catenin, to translocate into the nucleus and suppress the canonical Wnt/β-catenin pathway (Garcia-Gras, Lombardi et al. 2006). Suppression of Wnt/β-catenin signalling induces adipogenesis, fibrogenesis and apoptosis (Ross, Hemati et al. 2000; Chen, Guttridge et al. 2001; Longo, Kennell et al. 2002) the typical features of ARVC. In view of the above, we tested major components of the ID complexes and showed that they were severely

reduced in association with a complete loss of intercalated disc structures in iASPP mutant hearts. These data indicate that dissolution of the intercalated discs can be the primary mechanism for the establishment of ARVC. Analysis of young adult (12 weeks of age) iASPP KO mice surprisingly revealed that the ID complexes were still intact. However, investigation of the right free ventricular walls of the iASPP-null mice revealed reduced expression and dislocation of plakoglobin and N-cadherin, indicating deregulation of these proteins in the right ventricle. Adherens junctions and desmosomes mediate cell–cell couplings at the IDs via linkage to the actin cytoskeleton and intermediate filament system (i.e. desmin), respectively. Adherens junction formation is a prerequisite for gap junction assembly in cultured adult rat cardiomyocytes, as demonstrated by Kostin S. et al (Kostin, Hein et al. 1999), which could explain the serious abnormalities of iASPP-null ECGs. Consistent with this, the junctional localisation of iASPP is crucial for desmin to locate at the intercalated discs in cardiomyocytes. This newly identified property of iASPP provides a molecular insight into why iASPP deficiency causes the disorders that spontaneously occur in Wa3 mice and CWH Poll Hereford calves.

Hence, it is interesting to hypothesize that iASPP could be involved in strengthening or maintaining adherens junctions or desmosomes integrity and would be even more fascinating to study this possibility with a functional assay involving cardiomyocytes that have been freshly isolated from iASPP wild-type or -null hearts.

Chapter 5
RESULTS

iASPP loss results in impaired epidermal formation.

5.2 Results

5.2.1 iASPP$^{\Delta 8/\Delta 8}$ mice showed abnormal hair follicle organisation.

iASPP$^{\Delta 8/\Delta 8}$ mice could be recognised soon after birth by their peculiarly "curly" or "spiky" coats. At the macroscopic level, the fur on the back of iASPP$^{\Delta 8/\Delta 8}$ adult mice is less shiny, and the hairs look thinner and less in number when compared to their wild type control littermates *(figure 5.1)*.

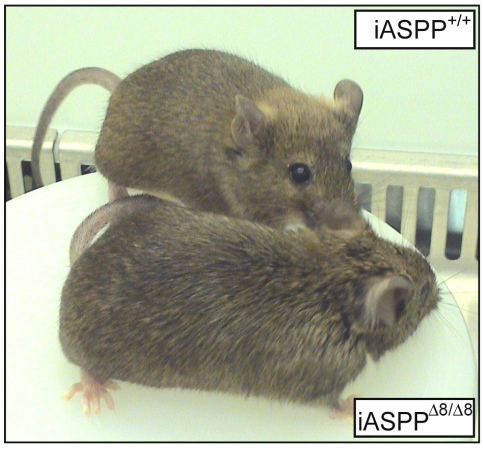


Figure 5.1. Phenotype affecting the hair follicles in iASPP$^{\Delta 8/\Delta 8}$ mice. iASPP mutant mice can be identified by their characteristic "wavy" hair at days 15 after birth. Pictures shows WT (iASPP$^{+/+}$) and transgenic (iASPP$^{\Delta 8/\Delta 8}$) adult mice. Note the abnormal fur on the back of the iASPP-null mouse.

Hair follicles and the epidermis are among the few mammalian organs that undergo repetitive cycles of disruption and regeneration (Fuchs 2007). The initiation of the follicular cycle starts with a growth phase called the "anagen" phase, where trans-amplifying cells proliferate to increase the

size and length of the hair shaft (Fuchs 2007). Follicles then simultaneously progress towards the degenerative phase called "catagen", during which the bottom part of the follicle undergoes programmed cell death and regression. The last phase of the cycle is the "telogen" or resting phase, where the derma papilla within the hair follicle bulge rests until a complicated number of molecular factors re-activate the stem cell compartment to re-grow the hair shaft (Fuchs 2007).

In order to establish the number and organisational pattern of the hair follicles in iASPP-null mice, dorsal skin samples were dissected from iASPP-depleted mice at different time points throughout the first anagen-catagen phases of the hair follicle cycle, and prepared for histological analysis. H&E staining, in association with light microscopy, revealed abnormalities in the number and position of the follicles in the dermis by *post natal* day 5 (p5). Hair follicles from iASPP$^{\Delta 8/\Delta 8}$ skin sections looked less organised *(figure 5.2A)*. This was also evident in samples from *post natal* day 7 (p7) and 10 (p10) mice, where the hair follicles had a diminished organisational pattern, when compare with the wild type control *(figure 5.2A)*. A closer look at the hair shafts in late anagen phase (p10) also revealed abnormalities in the pigmentation of the melanocytes *(figure 5.2A middle part, arrow)*. Quantification analysis of the number of hair follicles from epidermal cross-sections showed an increased number of follicles in skin samples from p5, p7, p10 and adult iASPP mutant mice, when compared with control mice *(figure 5.2, bar graph)*, suggesting an increased number of hair follicles in iASPP-deficient mice. Next, we investigate whether iASPP is expressed within the hair follicle shaft. To identify the cellular location of iASPP, immunofluorescence of dorsal skin sections was performed using specific monoclonal antibody LX049.3. Interestingly, the iASPP signal was particularly strong at the bottom of the hair follicle, corresponding with the hair bulb, which is composed mainly of proliferating matrix cells *(figure 5.2B)*. Since there are seven different "rings" of terminally differentiating cells within each hair follicle, all derived from matrix cells (Fuchs 2007), this data indicated a possible role for iASPP in the proliferation or differentiation processes of the hair follicle matrix cells. These findings suggested that the hair cycle could be

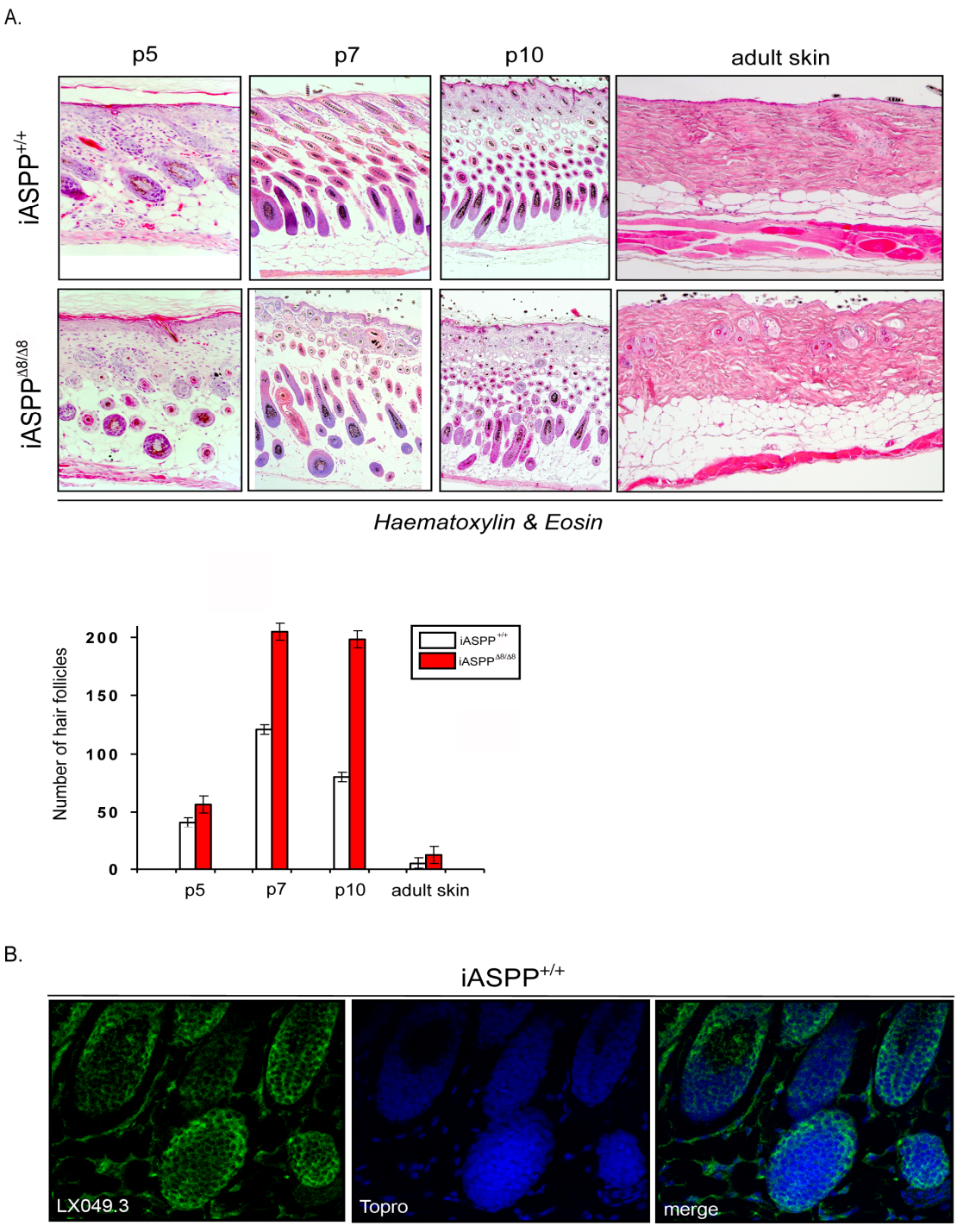


Figure 5.2. Loss of iASPP induces a 'spiky' hair phenotype in mice. (A) Skin histology showed abnormalities in the shape and orientation of hair follicles in p5, p7, p10 and adult skin samples from iASPP$^{+/+}$ and iASPP$^{\Delta 8/\Delta 8}$ mice. Hair follicles were elevated in number and the organisational pattern was lost in iASPP$^{\Delta 8/\Delta 8}$ epidermal sections. Histograms show quantification of hair follicle numbers counted from three different skin locations, generated from iASPP$^{+/+}$ (WT) and iASPP$^{\Delta 8/\Delta 8}$ (KO) mice. (B) Immunofluorescence analysis using iASPP monoclonal antibody LX049.3 revealed a predominant location of iASPP in the hair follicle bulb.

influenced by the loss of iASPP *in vivo*. In particular, the number of hair follicles was noted to be elevated in iASPP-depleted skin samples, and defects in the shape and position of the follicles in the dermis were also noted, suggesting an impairment of the hair follicle cycle.

5.2.2 iASPP is an important regulator of epithelial stratification in vivo.

iASPP is abundantly expressed in whole skin lysates in wild type mice *(figure 3.10)*. In addition, iASPP KO mice showed evident fur abnormalities associated with a disorganisation pattern and increased number of hair follicles in the dermis. Considering the link between cardiomyopathy and hair phenotypes in both Naxos and Carvajal syndromes (Chapter I, section 1.3.3.3), it is reasonable to speculate that iASPP could also have an important role in epidermal stratification.

To verify this hypothesis, we first analysed the morphology and structure of dorsal epidermal samples from young (p10) iASPP mutant mice and compared them with wild type littermates. Histological analyses of iASPP$^{\Delta 8/\Delta 8}$ epidermis revealed profound morphological abnormalities in various layers of the epidermis *(figure 5.3A*). In fact, in contrast to wild type epidermal specimens, the three layers of terminal differentiation – spinous (Sp), granular (Gr) and stratum corneum (SC) - were all noticeably thicker in iASPP$^{\Delta 8/\Delta 8}$ skin samples *(Figure 5.3A)*. In ordered to investigate whether the histological abnormalities observed in iASPP$^{\Delta 8/\Delta 8}$ mice were associated with altered expression of various epidermal markers, we performed immunofluorescence analyses using different keratin antibodies, as the epidermal layer can be recognised by different keratin markers. iASPP$^{\Delta 8/\Delta 8}$ epidermis showed displacement in the location of both spinous (K1) and granular (loricrin) markers *(figure 5.3B)*. As judged by immunolabeling of iASPP-null epidermal samples, K1 expression was not confined between the basal layer and stratum corneum, as found with wild type samples *(Figure 5.3B).* Instead, a positive signal could be clearly seen in the basal layer, and even more so in the terminally differentiated layers of the epidermis. Moreover, loricrin expression positively stains the granular layer and typically forms a smooth line on top of the spinous layer in

wild type specimens *(figure 5.3B)*. In contrast, skin sections of iASPP-depleted mice showed loricrin-positive staining in the spinous layer, suggesting an abnormal differentiation process *(figure 5.3B)*. Since basal layer keratinocytes express both keratin 5 and keratin 14, and are attached to the basal membrane, the number of cells expressing keratin 5 that sit on the basal membrane of the epidermis was compared with those that express K1 and do not locate there. The results in figure 5.3C showed that although iASPP deficiency affected the number of basal layer cells, its impact was not statistically significant *(figure 5.3C, bar graph basal layer, p=0.1066)*. However, iASPP deficiency caused an expansion in the number of suprabasal keratinocytes which expressed K1 *(figure 5.3C, bar graph suprabasal layer, p=0.054)*. As shown in figure 5.3C, the total number of cells in the epidermis was significantly increased in iASPP-deficient mice compared to their wild type counterparts, indicating an expansion of the differentiated layers in the epidermis of iASPP transgenic mice.

These observations suggested that epidermal stratification is impaired in iASPP-deficient mice. Based on the displacement of early differentiation markers and the increased thickness of the iASPP-null epidermis, it is possible that iASPP plays a role in the inhibition of the stratification process in mouse epidermis, as more cells detach from the basal membrane and start their journey towards the cornified envelop.

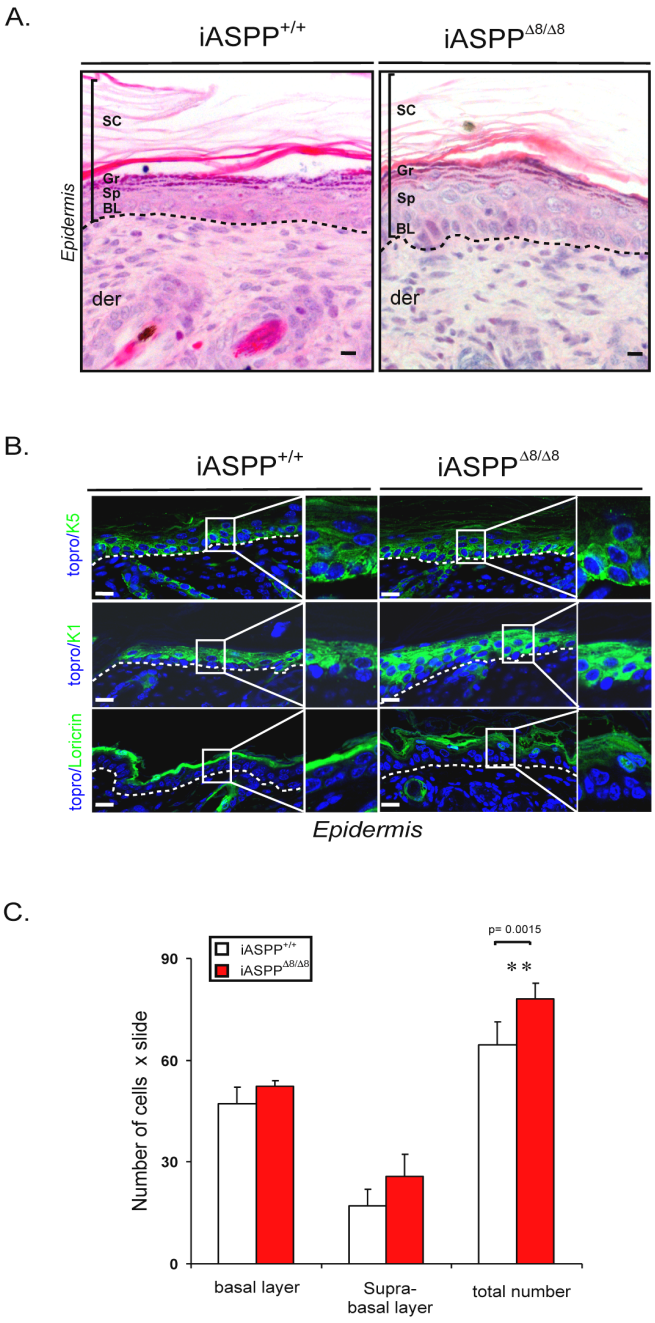


Figure 5.3. Loss of iASPP increase epidermal thickness *in vivo*. (A) Haematoxillin and eosin (H&E) staining of back skin sections obtained from iASPP$^{+/+}$ and iASPP$^{\Delta 8/\Delta 8}$ mice. BL, basal layer; SP, spinous layer; SG, stratum granulosum; and SC, stratum corneum. Vertical bars represent epidermal thickness. Dotted line represents the separation between the dermis and epidermis. (B) Immunolocation of various epidermal markers in iASPP$^{+/+}$ and iASPP$^{\Delta 8/\Delta 8}$ epidermal sections. Displacement of early (K1) and late (loricrin) differentiation markers is evident. Squares represent higher magnifications of the areas in the picture. Dotted white line represents dermo-epidermal boundary. (C) Bar graph represents mean ± SD of cell numbers in the basal, suprabasal or entire epidermal layer of mouse epidermis (n=3).

5.2.3 iASPP is predominantly expressed in the basal layer of stratified epithelia in vivo.

As previously shown in this study, iASPP is heavily expressed in mouse skin epidermis. Herron et al., previously reported that they detected an elevated quantity of iASPP messenger RNA in skin samples from wild type mice at embryonic day E19.5 (Herron, Rao et al. 2005). However, little is know about the *in vivo* cellular location of iASPP in the mouse epidermis. To provide supporting evidence that iASPP is an inhibitor of epidermal differentiation, we analysed iASPP's location *in vivo*. Immunofluorescence analysis was performed using LX049.3 on $iASPP^{+/+}$ and $iASPP^{\Delta 8/\Delta 8}$ dorsal skin sections. We observed that iASPP was predominantly expressed in the basal layer of the epidermis *(figure 5.4A)*. The specificity of the anti-iASPP antibody used (LX049.3), was confirmed by the lack of iASPP expression from $iASPP^{\Delta 8/\Delta 8}$ epidermal specimens *(figure 5.4A)*.Since iASPP expression was particularly strong at the basal layer of the epidermis, we investigate whether iASPP co-localised with the keratin K14 marker, a well known marker for basal epithelial keratinocytes (Fuchs and Green 1980). Using double immunofluorescence staining, we observed that the majority of iASPP-expressing cells also expressed K14 *(figure 5.4B)*. Importantly, iASPP expression was mutually exclusive to keratin K1 or loricin, two markers that identify differentiated cells from the spinous and granular epidermal layers (Fuchs and Green 1980) *(figure 5.4B)*. Together, these data provide the first *in vivo* evidence that iASPP protein is expressed in basal epithelial cells, and this expression pattern agrees with its ability to maintain the proliferative potential, and inhibit the differentiation, of basal epidermal keratinocytes.

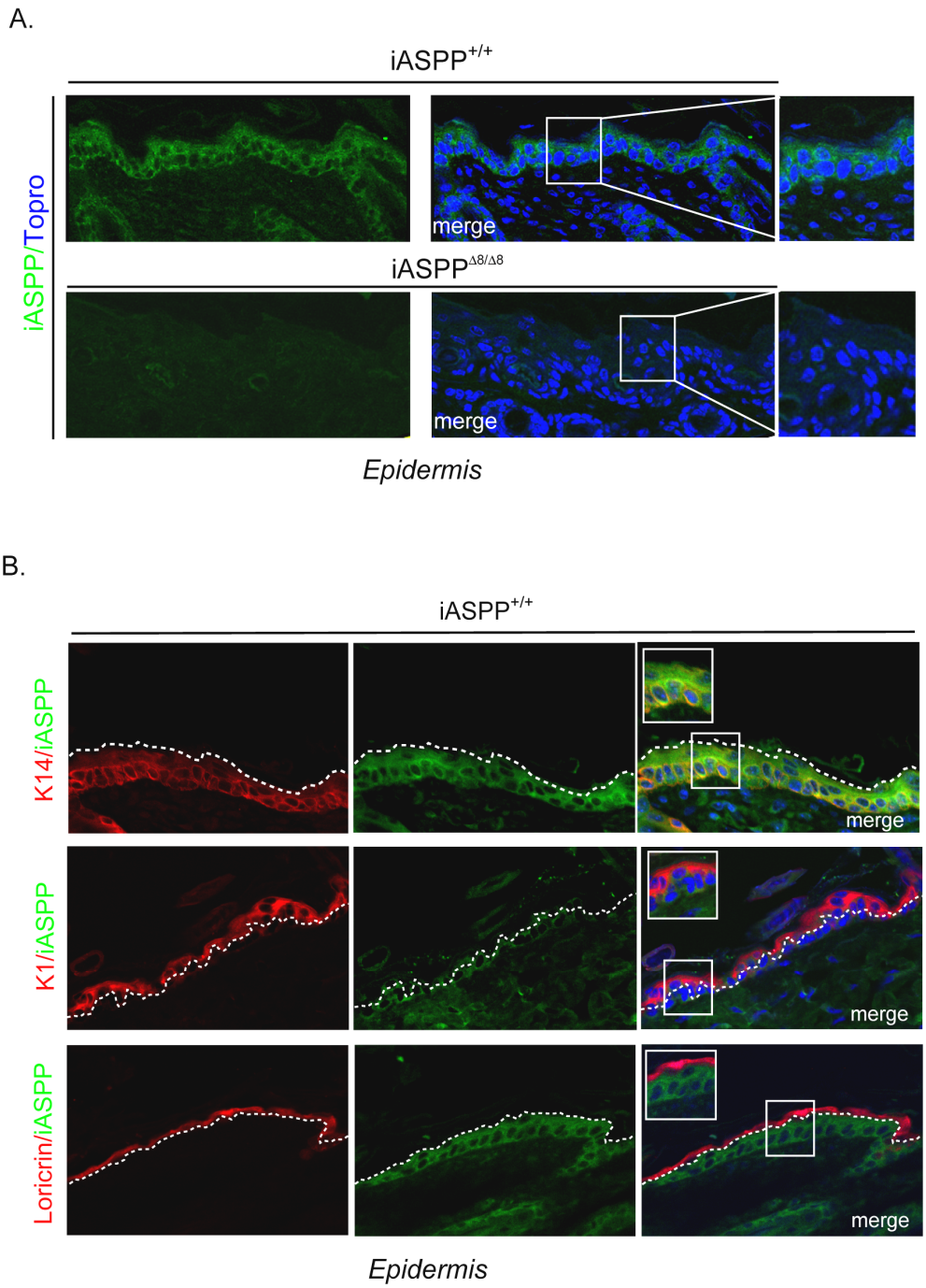


Figure 5.4. iASPP protein is expressed in the epidermal basal layer. (A) Specificity of anti-iASPP antibody LX049.3. Immunofluorescence of skin sections from iASPP$^{+/+}$ mice shows iASPP's location *(top panel)*. iASPP expression was not detected in iASPP$^{\Delta 8/\Delta 8}$ sections *(bottom panel)*. Squares represent higher magnification of the epidermal region. (B) Immunolocation analysis of iASPP in epidermal sections from wild type (iASPP$^{+/+}$) mice in association with different epidermal markers. iASPP is strongly expressed in the basal layer of mouse epidermis in association with K14 *(upper panel)*. Double staining of iASPP and spinous (K1) or granular (Loricrin) differentiation markers suggests different locations of the two proteins *(middle and lower panel)*. The white dotted line represents the separation between iASPP and the epidermal markers K14, K1 and loricrin. Squares represent higher magnification of the epidermal region.

5.2.4 iASPP is a negative regulator of keratinocyte differentiation.

iASPP cellular localisation with K14 demonstrated that iASPP's expression is confined to the basal layer of the epidermis *in vivo*. The basal layer of the epidermis is an active proliferative epidermal layer where stem cells and keratinocytes with higher growth capacities locate (Candi, Cipollone et al. 2008). Therefore, iASPP could play an important role in maintaining the proliferative potential, or inhibiting the differentiation process, of mouse keratinocytes. Given the evidence that a higher number of cells were noted in the suprabasal layer of the epidermis, it was important for us to examine whether iASPP could play a role in inhibiting cellular differentiation.

In order to investigate this hypothesis an experimental model using primary epidermal keratinocytes was established to mimic our *in vivo* system. Regulation of epidermal cell growth and terminal differentiation has been broadly investigated in primary cultures of mouse keratinocytes (KCs), through the modulation of extracellular Ca^{2+} levels as a method for inducing cellular differentiation (Hennings, Michael et al. 1980). Cultivation of primary KCs in low Ca^{2+} conditions (<0.05 mM; low Ca^{2+} conditions) promotes the expansion of a proliferative population of undifferentiated, epidermal basal-like cells. Raising extracellular Ca^{2+} levels (>1 mM; high Ca^{2+} conditions) in non-confluent cultures triggers differentiation in a manner that closely resembles the *in vivo* event, including cell cycle withdrawal, cytoskeletal changes, stratification and cornification (Hennings, Michael et al. 1980). Growth arrest and morphological changes in these cultures are accompanied by the induction of differentiation-related genes, such as K1 and K10, loricrin, transglutaminases and filaggrin (Yuspa, Kilkenny et al. 1989). We, therefore, examined whether iASPP's expression is regulated during primary keratinocyte differentiation *in vitro.*

Primary keratinocytes were purified from iASPP-depleted and wild type new born mice, and the differentiation process induced by increasing calcium concentration in the culturing media. Cells were then harvested at two specific time points as undifferentiated and differentiated (five days into the differentiation process) *(figure 5.5A)*. Morphological and molecular differences distinguished the undifferentiated and differentiated keratinocytes (Hennings, Michael et al. 1980). As shown in

figure 5.5A, undifferentiated keratinocytes are single cellular entities that have a characteristic triangular shape with no cell-to-cell contacts, while differentiated keratinocytes assume a more enlarged, square shape and form strong cell-to-cell connections with neighbouring cells without leaving any intercellular spaces between them *(figure 5.5A)*. Of note, no differences in appearance or morphology was noticed between $iASPP^{\Delta 8/\Delta 8}$ and $iASPP^{+/+}$ primary keratinocytes in undifferentiated or differentiated states *(figure 5.5A)*.

To investigate whether iASPP could play a role in controlling keratinocyte differentiation, mouse keratinocytes were purified from iASPP wild type and deficient newborn mice, and maintained in low Ca^{2+} medium to mimic undifferentiated conditions. Differentiation was induced by adding high Ca^{2+} medium for five days. Keratinocyte differentiation was confirmed by the disappearance of p63 expression and translocation of E-cadherin to cell-to-cell junctions (Owens, Brunton et al. 2000; Koster, Kim et al. 2004) *(figure 5.5B)*. Interestingly, in this experiment we observed a significant reduction of iASPP expression in differentiated keratinocytes. This result suggests that iASPP may play a role in inhibiting keratinocyte differentiation *in vitro*. To further explore this hypothesis, we generated mouse primary keratinocytes from $iASPP^{+/+}$ and $iASPP^{\Delta 8/\Delta 8}$ mice. Protein lysates were purified from undifferentiated or five day differentiated keratinocyte cultures, and iASPP expression was investigated by western blot analysis using LX049.3 antibody. Figure 5.5B clearly demonstrates that iASPP expression was reduced upon Ca^{2+} differentiation *(figure 5.5B)*. In addition, we also investigated the expression level of ASPP1 and ASPP2 proteins upon keratinocyte differentiation. Quantification analysis revealed that the two proteins have reduced expression in keratinocyte lysates when compare to iASPP but, more importantly ASPP2 was only detected in protein extracts obtained from differentiated keratinocytes *(figure 5.5C)*, while ASPP1 (similar to iASPP) was only observed in undifferentiated keratinocytes. This suggests a possible antagonist relationship between iASPP and ASPP2 in modulating epidermal homeostasis. In order to obtain additional supporting evidence of iASPP being an inhibitor of epidermal differentiation, we used a different *in vitro* system to achieve iASPP down-

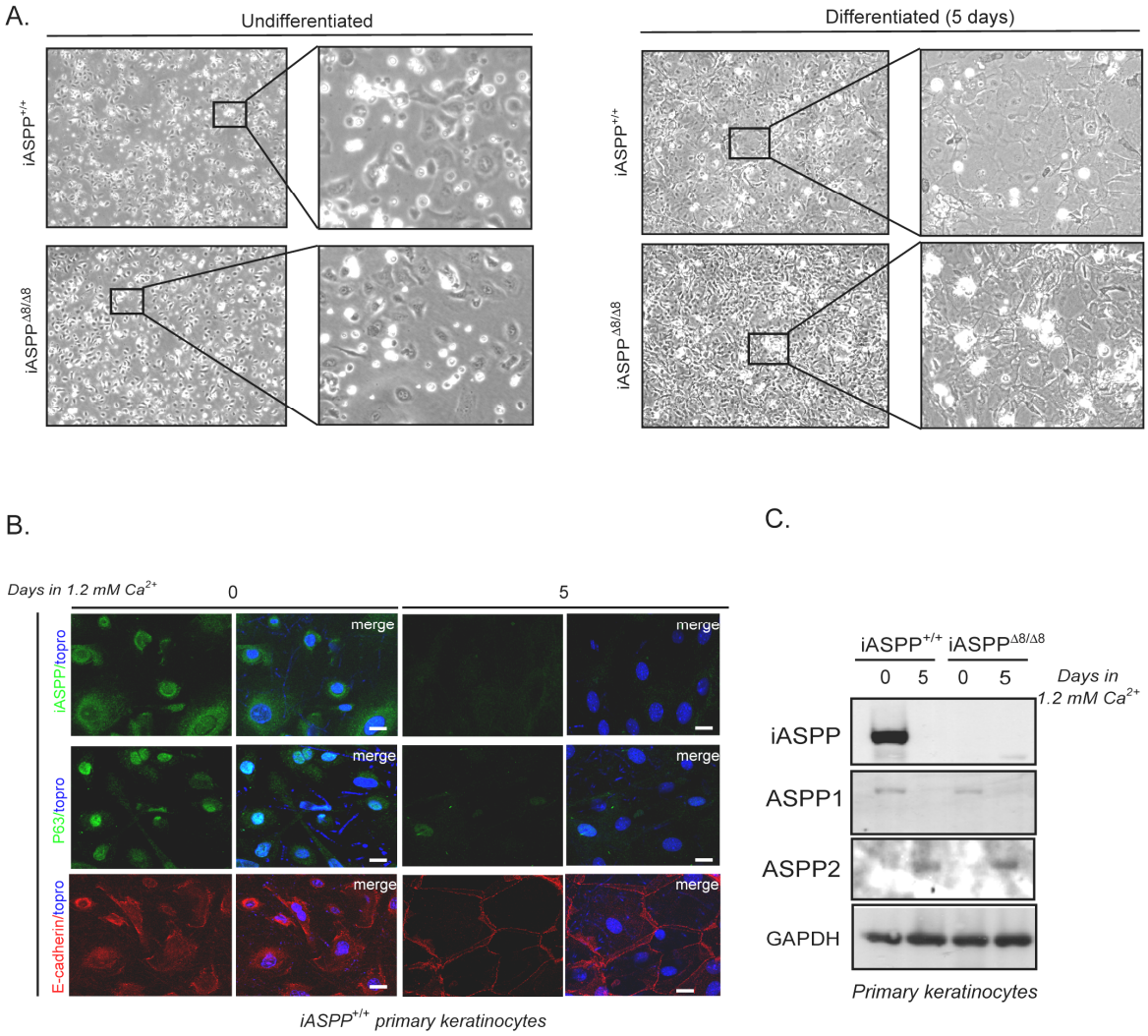


Figure 5.5. iASPP expression is lost upon Ca^{2+} differentiation in mouse primary keratinocytes (KCs). (A) Primary mouse KCs were purified from newborn $iASPP^{+/+}$ and $iASPP^{\Delta 8/\Delta 8}$ mice and cultured in low Ca^{2+} (undifferentiated) or high Ca^{2+} (differentiated) medium for the indicated time. Picture shows the different cellular morphology between undifferentiated and differentiated keratinocytes. (B) Immunofluorescence analyses using iASPP, p63 and E-cadherin monoclonal specific antibodies of undifferentiated and differentiated KCs. TO-PRO was used as nuclear marker. Scale bar 20µm. (B) Immunoblot analysis of iASPP, ASPP1 and ASPP2 protein expression was performed in primary mouse KCs cultured in 1.2mM Ca^{2+} for the indicated time. GAPDH was used as a loading control.

regulation, in which Cre recombinase expression was controlled by the presence of 4-hydroxytamoxifen (4-OHT). Briefly iASPP$^{flox/flox}$ mice were crossed with Rosa 26 Cre^{+}ER mice (Indra, Warot et al. 1999) to generate iASPP$^{flox/flox}$;Cre^{+}ER mice in which Cre expression was controlled by the presence of 4-OHT. MEFs were then generated and the absence of iASPP expression was verified by western blot analysis upon addition of 4-OHT *(figure 5.6A)*. The results in figure 5.6A show clearly that iASPP expression is severely reduced 3 days after the addition of 4-OHT at a concentration of 1 μM, and completely deleted 4 days after induction of the Cre enzyme *(figure 5.6A).* To test whether iASPP can influence the early epidermal stratification process, we generated mouse KCs from newborn iASPP$^{flox/flox}$;Cre^{+}ER^{T} mice. The expression of iASPP was deleted by adding 4-OHT to low Ca^{2+} media for four days, and the absence of iASPP subsequently was confirmed by immunoblot analysis *(figure 5.6B*). The ability of iASPP to affect keratinocyte differentiation was tested by incubating KC cultures in high Ca^{2+}-containing media for 24 or 48 hours, as indicated in figure 5.6B. The expression levels of differentiation markers such as K1 and loricrin were compared between iASPP-expressing and -deficient mouse KC cultures by immunoblot analysis. Interestingly, iASPP deficiency resulted in a small but detectable increase in the expression levels of K1 and loricrin *(figure 5.6A*). This increase in keratinocyte differentiation markers occurred as early as 24 hours after the Ca^{2+} switch.

Collectively, these results suggest that iASPP may negatively regulate keratinocyte differentiation.

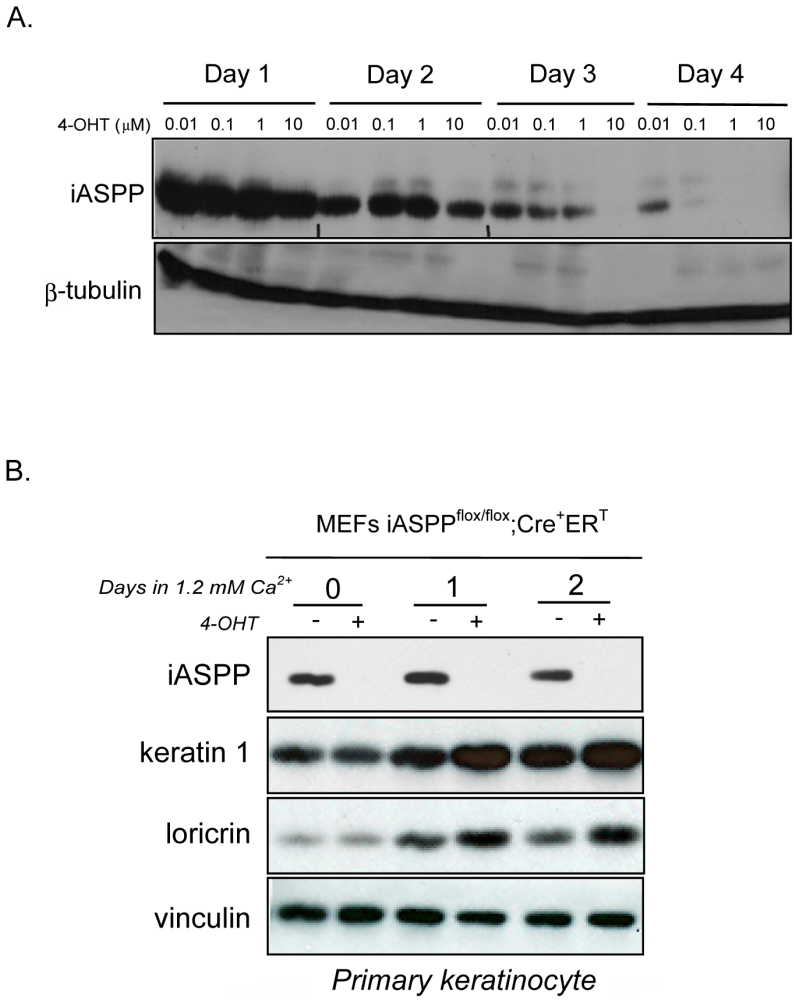


Figure 5.6. Loss of iASPP expression increases the expression of early differentiation markers in primary mouse keratinocytes upon differentiation. (A) Immunoblot analysis of protein lysates from iASPP$^{flox/flox}$;Cre^{+} ER^{T} MEFs under different 4-OHT concentrations. A noticeable decrease in iASPP protein expression was achieved after 3 days with 1μM 4-OHT. Complete deletion of iASPP protein was achieved after 4 days with 1μM 4-OHT. β-tubulin was used as a loading control. (B) iASPP$^{flox/flox}$;Cre^{+}ER^{T} KCs were purified from newborn mice and cells were treated with 4-OHT for four days prior to exposure of 1.2 mM Ca^{2+} media for the indicated time. Immunoblot demonstrates lack of iASPP in presence of 4-OHT *(lanes 2, 4 and 6, top panel)*. Immunoblot analysis of differentiation markers for spinous (K1) and granular (Loricrin) layers was performed. Vinculin expression was used as a loading control.

5.2.5 iASPP deficiency does not affect epithelial cell-to-cell junctions.

We previously showed that iASPP is expressed at the polar-end of cardiomyocytes *(figure 4.14)*, and observed that iASPP deficiency leads to the dissolution of the cell-to-cell junction. Hence, we proposed a possible role for iASPP in maintaining the integrity of the ID structures in the myocardium. In order to investigate whether the expression of cell-to-cell junction markers is affected by the loss of iASPP in mouse epidermis, immunofluorescence was performed using antibodies against E-cadherin, α-catenin and β-catenin in epidermal samples from wild type and iASPP$^{\Delta 8/\Delta 8}$ *(figure 5.6 A-C)* mice. Surprisingly, no significance differences in the location or intensity of the staining were noted between wild type and iASPP-deficient mice. Cell junctional components were visible in both samples with a characteristic location along the plasma membrane of keratinocytes, which gradually became flatter towards the SC *(figure 5.6 A-C)*. Diversity in the thickness of the epidermis was notable in iASPP-depleted samples when compared to wild-type counterparts, confirming the previous morphological analysis in which iASPP loss led to an increase in the thickness of the epidermis.

Together, these data indicate that epidermal junctions are not affected by the loss of iASPP protein. However, we did not investigate the strength of the intercellular junctions under mechanical stress conditions (i.e. heart beat).

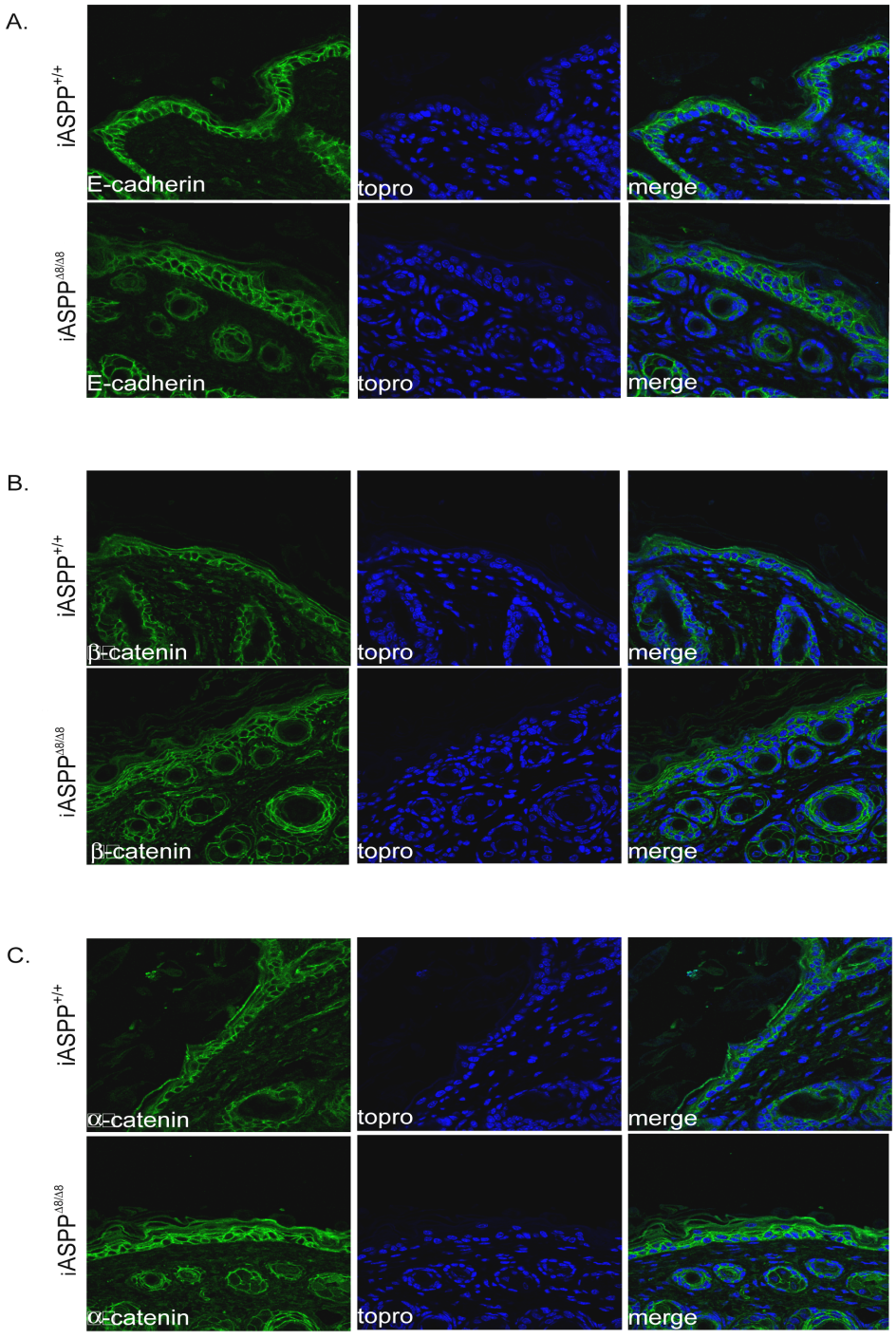


Figure 5.9. Loss of iASPP does not affect cell-to-cell junctions in mouse epidermis. (A-C) Paraffin-wax epidermal sections obtained from iASPP$^{+/+}$ and iASPP$^{\Delta 8/\Delta 8}$ mice were immunostained using specific antibodies against E-cadherin, β-catenin and α-catenin. Topro was used as nuclear marker.

5.2.6 iASPP binds p63 and antagonises the transcriptional activity of TAp63.

To date, the ASPP proteins have not been shown to possess any intrinsic enzymatic activity, and their effects are mediated through protein/protein interactions and the modulation of transcription factors (Sullivan and Lu 2007). *In vitro* studies have shown that iASPP was able to bind p63 with a relatively weak affinity in comparison to p53 (Robinson, Lu et al. 2008). However, *in vivo*, it is known that p63 but not p53 is the key transcription factor that controls epithelial stratification (Mills, Zheng et al. 1999; Yang, Schweitzer et al. 1999). Knowing that iASPP is predominantly expressed in the basal layers of stratified epithelium in mouse skin, we investigated whether its expression pattern also exists in humans. Immunohistochemistry of human epidermal samples showed that iASPP is mainly expressed as a nuclear protein in the basal and suprabasal layers of epidermal stratified epithelia *(figure 5.10A)*. Using adjacent sections from human epidermis, we observed that iASPP's expression pattern overlaps with p63 and that they are both highly expressed in the basal and suprabasal layers, suggesting a functional link between p63 and iASPP (Victoria Salter and Anna Pagotto personal communication, *figure 5.10A*).

By generating specific p63 isoforms, it was recently demonstrated that TAp63 can act as a tumour suppressor and is a key regulator of epithelial stratification (Su, Paris et al. 2009). Thus, TAp63 and iASPP could have opposing effects in controlling epithelial stratification. Since the DNA binding domain of p63 and the C-terminus of iASPP interact *in vitro* (Robinson, Lu et al. 2008), we hypothesised that iASPP may antagonise p63's function in controlling epithelial stratification. Hence, we investigated whether iASPP was able to bind endogenous p63 in primary keratinocytes, *in vitro*. An immortalised human keratinocyte cell line, HaCaT cells, was used to test this hypothesis. Interestingly, when endogenous iASPP was immunoprecipitated with a polyclonal antibody raised against the N-terminal part of the protein (pbN_1), p63 was found to co-immunoprecipitate (Ying Hu personal communication, *figure 5.10B*).

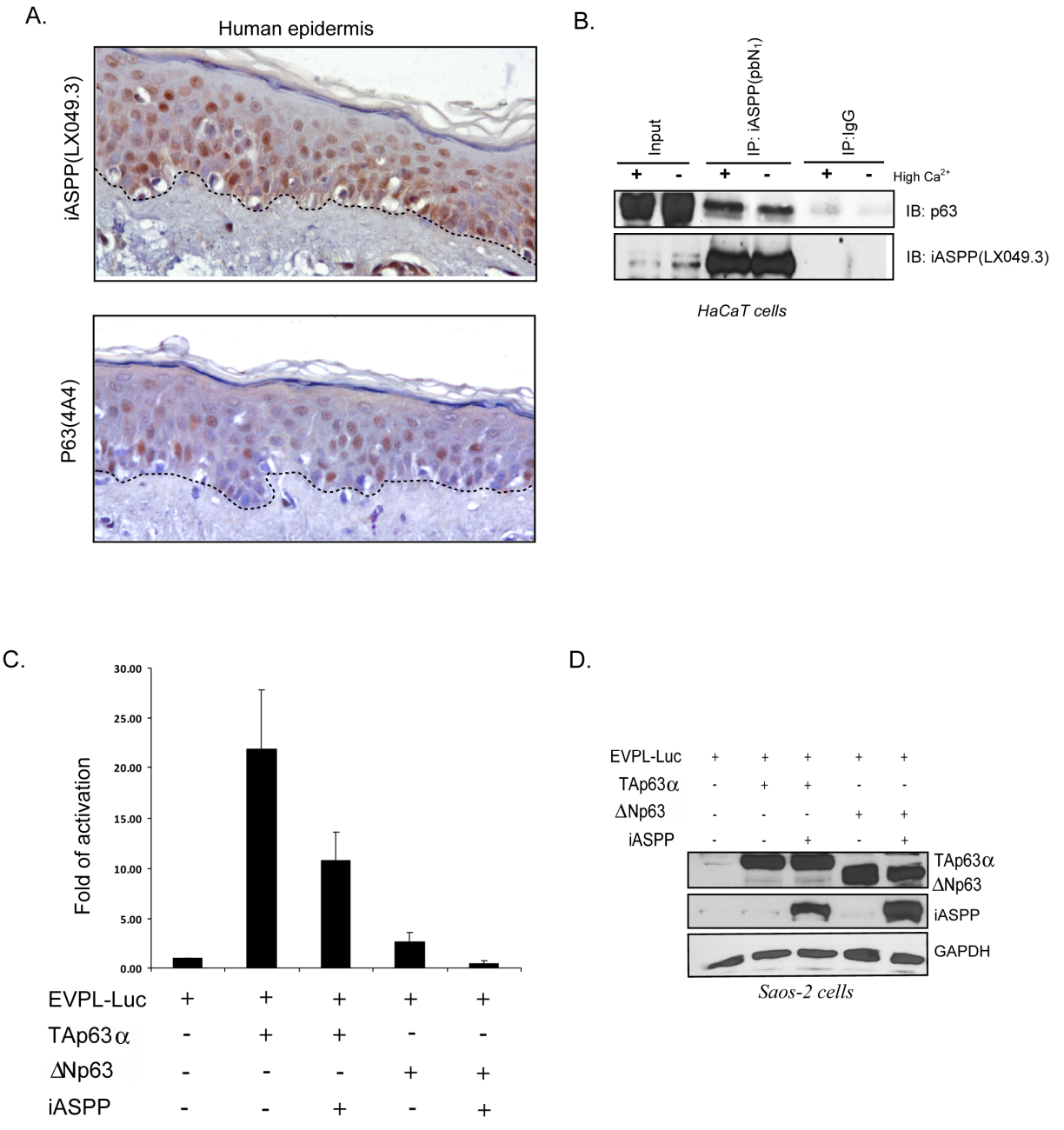


Figure 5.10. iASPP binds p63 and negatively regulates the transcription function of TAp63α. (A) Immunohistochemical staining for iASPP and p63's locations. Normal human epidermal sequential sections reveal an almost identical expression pattern of the two proteins. Dotted line represents the dermo-epidermal boundary. (B) Endogenous iASPP was immunoprecipitated with anti-iASPP rabbit polyclonal antibody pAbiASPPN1 (pbN_1). Anti-IgG rabbit polyclonal antibody was used as a negative control. iASPP (LX049.3) and p63 (4A4) were detected by SDS-Page/Immunoblotting and indicated exposure of HaCaT cells at high Ca^{2+} for 24 h. (C) The bar graph shows the effect of iASPP on the transactivation activity of TAp63α on the envoplakin promoter (EVLP-Luc). Values are the mean ± SD of three independent experiments (n=3). (D) The expression levels of various transfected proteins were detected using LX049.3 and p63 (4A4) antibodies. GAPDH was used as a loading control marker.

This suggests that the ability of iASPP to bind to p63 may be of importance in the regulation of p63's target genes.

Next, we investigated the ability of iASPP to influence the transcriptional activity of TAp63. One of the best established transcriptional targets of TAp63 that contributes to terminal differentiation in mouse epidermal stratification, is envoplakin, a member of the plakin family and part of the early constituents of the cornified envelops (Osada, Park et al. 2005). The envoplakin promoter linked to the luciferase reporter gene (EVPL-Luc) was used as a read out for the transcriptional activity of TAp63α. To investigate the ability of iASPP to influence the transcriptional activity of TAp63, Saos-2 cells were transfected with a TAp63α expression plasmid, in association or not with exogenous iASPP expression. As expected, TAp63α was able to enhance the transcription of EVPL-Luc by more than 20-fold when compared with cells transfected with EVLP-Luc alone (Caroline Baer personal communication, *figure 5.10C*). Interestingly, co-expression of iASPP and TAp63α halved the transcriptional activity of the latter by 50% when compared with cells transfected with TAp63α alone (*figure 5.10C*). This decrease in transcriptional activity was not due to a reduction in TAp63α expression, as similar amounts of TAp63α were detected by immunoblot in cells transfected or not with an iASPP expression plasmid. Under the same conditions, ΔNp63α had minimal or no effect on the transcriptional activity of EVPL-Luc *(figure 5.10D)*.

These data suggest that one of the mechanisms by which iASPP could affect epithelial stratification and cell cycle withdrawal is through its ability to bind p63 and inhibit the transcriptional activity of TAp63.

5.2.7 Genetic interaction between the iASPP and p63 proteins in mouse epidermis: generation of $iASPP^{\Delta 8/\Delta 8}$;$p63^{+/.}$

We previously demonstrated that both p63 and iASPP are expressed within the basal layer of the epidermis, both in mouse and human specimens. Moreover, we showed that iASPP and p63 interact and that iASPP inhibits the transcriptional activity of TAp63α on the promoter of envoplakin, suggesting that one of the mechanisms by which iASPP could affect epithelial stratification is through its ability to bind p63 and inhibit the transcriptional activity of TAp63. Hence, whether the iASPP-null epidermal phenotype could be dependent on p63 expression was investigated. In order to test this hypothesis, the $p63^{+/-}$ allele was introduced into an iASPP-null background. Mice double heterozygous for p63 and iASPP were inter-crossed in order to generate the double mutant progeny $p63^{+/-}$;$iASPP^{\Delta 8/\Delta 8}$. Among the 96 pups generated by double heterozygous crosses, the expected combination of p63-iASPP genotypes were obtained, expect for the p63-null allele that, according to the literature, is not viable (Mills, Zheng et al. 1999; Yang, Schweitzer et al. 1999). In agreement with our previous analyses of the segregation of iASPP-null alleles, we noted a slight decrease in the number of mice in the iASPP-null cohort *(Chapter IV, table 4.3)*. However, the total number of genotypes originating from double heterozygous couples needed to be increase to be statistically relevant.

In order to understand the impact of p63 on iASPP's epidermal phenotype, $p63^{+/-}$;$iASPP^{\Delta 8/\Delta 8}$ mice were first analysed by gross examination. Looking at the fur on the back of the double mutant mice, the absence of one p63 allele did not rescue the "spikey" hair phenotype typical of $iASPP^{\Delta 8/\Delta 8}$ mice. In fact, the fur of $p63^{+/-}$;$iASPP^{\Delta 8/\Delta 8}$ mice looked less shiny and with the characteristic "wavy" hair *(figure 5.11)*. However, the absence of one p63 allele in the iASPP wild type background ($p63^{+/-}$; $iASPP^{+/+}$) resulted in abnormal hair coats as well. In addition, the $p63^{+/-}$ progeny in the pure Balb/c genetic background showed a hair phenotype which resembled that of $iASPP^{\Delta 8/\Delta 8}$ mice *(figure5.11A)*. Of note, $p63^{+/-}$;$iASPP^{\Delta 8/\Delta 8}$ newborn mice had significantly reduced weights when compared with wild type littermates. The weight loss in $p63^{+/-}$;$iASPP^{\Delta 8/\Delta 8}$ mice was not due to the

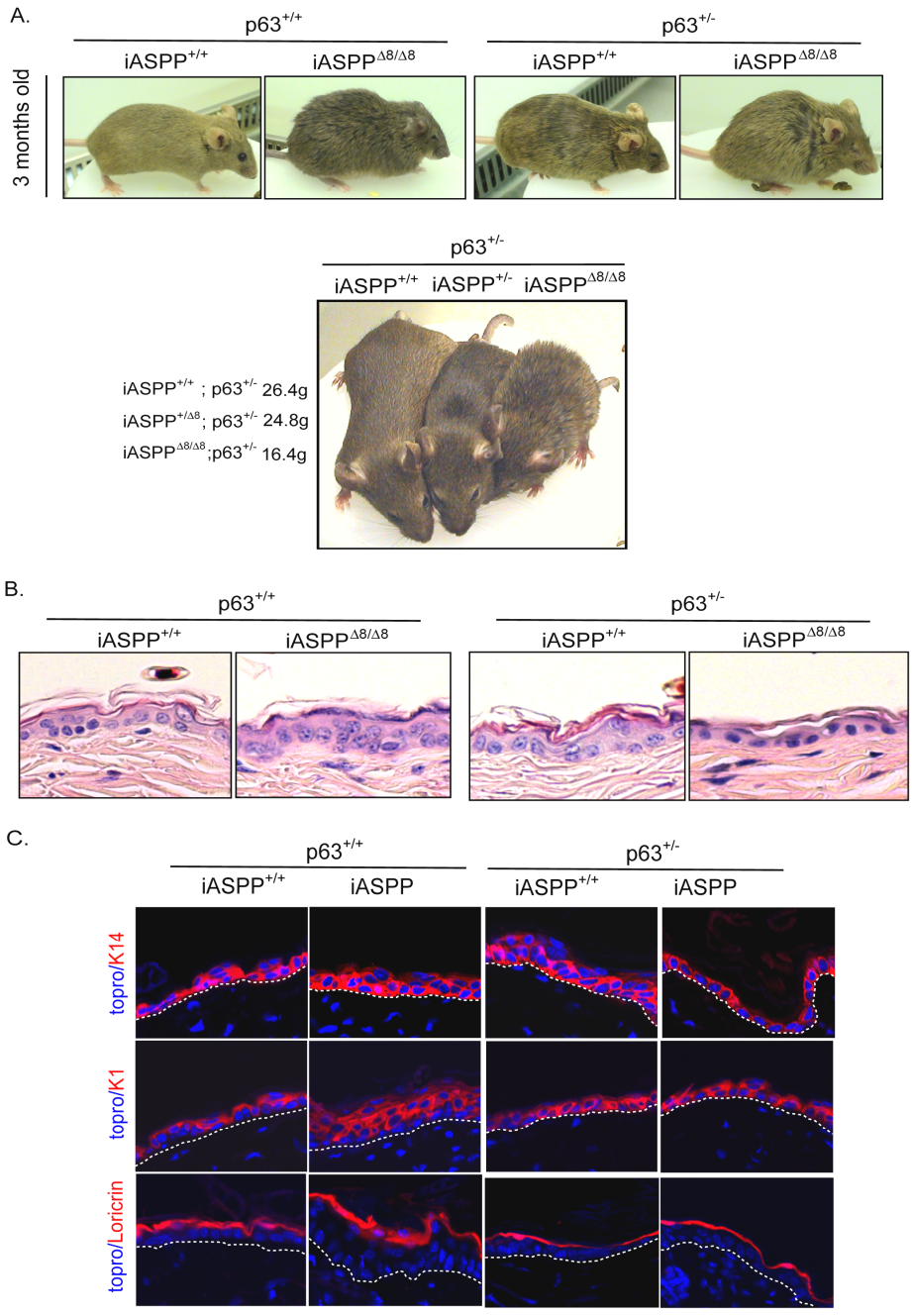


Figure 5.11. Inactivation of one p63 allele ($p63^{+/-}$) partially rescues the epidermal phenotype of $iASPP^{\Delta8/\Delta8}$ mice. (A) Gross analyses of the coat of $p63^{+/+}$;$iASPP^{+/+}$, $p63^{+/+}$;$iASPP^{\Delta8/\Delta8}$, $p63^{+/-}$;$iASPP^{+/+}$ and $p63^{+/-}$;$iASPP^{\Delta8/\Delta8}$ mice. Expression of only one p63 allele did not affect the "wavy" hair coat of $iASPP^{\Delta8/\Delta8}$ mice. (B) Paraffin wax sections of epidermis obtain from $p63^{+/+}$;$iASPP^{+/+}$, $p63^{+/+}$;$iASPP^{\Delta8/\Delta8}$, $p63^{+/-}$;$iASPP^{+/+}$ and $p63^{+/-}$;$iASPP^{\Delta8/\Delta8}$ mice were H&E stained. The increased epithelial stratification process seen in $iASPP^{\Delta8/\Delta8}$ ($p63^{+/+}$;$iASPP^{\Delta8/\Delta8}$) mice was partially rescued by the loss of one p63 allele ($p63^{+/-}$;$iASPP^{\Delta8/\Delta8}$). (C) Immunostaining of paraffin wax epidermal sections obtained from $p63^{+/+}$;$iASPP^{+/+}$, $p63^{+/+}$;$iASPP^{\Delta8/\Delta8}$, $p63^{+/-}$;$iASPP^{+/+}$ and $p63^{+/-}$;$iASPP^{\Delta8/\Delta8}$ mice using different antibodies against epidermal markers (K14, K1 and loricrin). Pictures show partial rescue of K1 and loricrin in $p63^{+/-}$;$iASPP^{\Delta8/\Delta8}$ mice, when compared to $p63^{+/+}$;$iASPP^{\Delta8/\Delta8}$ mice.

reduction in p63 expression alone as $p63^{+/-}$;$iASPP^{+/+}$ mice showed a slight, but not significant, decrease in body weight *(figure 5.11B)*. Although when the animals reached adultness, this difference was lost. To understand whether the deletion of one allele of the *TP63* gene could rescue the thicker $iASPP^{\Delta 8/\Delta 8}$ epidermis phenotype, skin samples were dissected from $p63^{+/+}$;$iASPP^{+/+}$ (wild type), $p63^{+/-}$;$iASPP^{\Delta 8/\Delta 8}$ mice, together with $p63^{+/-}$;$iASPP^{+/+}$ and $p63^{+/+}$;$iASPP^{\Delta 8/\Delta 8}$ mice. Adult mice from the four different genotypes were sacrificed and back skin samples prepared for histological examination. H&E staining was carried out to investigate the overall integrity of the epidermal structure. Consistent with our previous results, light microscopy analysis revealed that $iASPP^{\Delta 8/\Delta 8}$ epidermis was thicker when compared to wild type controls, in association with an increased number of cells in the basal layer of the epidermis *(figure 5.11 B)*. Interestingly, in the absence of only one p63 allele, the thickness of the epidermis in $iASPP^{\Delta 8/\Delta 8}$ samples was sensibly reduced *(figure 5.10)*, suggesting that a reduced amount of p63 expression could restore the proliferative capacity or differentiation program of $iASPP^{\Delta 8/\Delta 8}$ mice. However, reduced amounts of basal layer cells were also in evidence in $p63^{+/-}$;$iASPP^{\Delta 8/\Delta 8}$ mice *(figure 5.11 B).* To further confirm that a reduced amount of p63 could rescue the impaired proliferation or early differentiation phenotype in $iASPP^{\Delta 8/\Delta 8}$ epidermal samples, immunofluorescence was performed to understand whether the differentiation program was restored in $p63^{+/-}$;$iASPP^{\Delta 8/\Delta 8}$ mice. Different epidermal markers were used to visualise basal (K14), spinous (K1) and granular (loricrin) layers. Coherent with our previous report that iASPP loss can affect the distribution of various epidermal differentiation markers *in vivo*, K1 and loricrin staining were found to be displaced in $p63^{+/+}$;$iASPP^{\Delta 8/\Delta 8}$ specimens *(figure 5.11 C)*. Also, a more consistent expansion of the basal layer was noted. Interestingly, all proliferative and early differentiation markers seemed to be rescue in $p63^{+/-}$;$iASPP^{\Delta 8/\Delta 8}$ mice, suggesting that the iASPP epidermal phenotype is dependent on p63 expression *(figure 5.11 C).* Collectively, these preliminary data suggest that iASPP and p63 could interact genetically in influencing the proliferation or early differentiation potential of the basal layer of the epidermis *in vivo*.

5.3 Summary and discussion.

The work described in this Chapter was conducted to investigate the phenotype that affects the hair follicle organisation and epidermal structure in iASPP$^{\Delta 8/\Delta 8}$ mice. Preliminary data showed that iASPP-null progeny were affected by hair follicle abnormalities, indicating the possible involvement of iASPP in maintaining their renewal capacity *in vivo*. Regrettably, only basic information could be concluded from our study, such as that iASPP$^{\Delta 8/\Delta 8}$ mice show an increased number of hair follicles with a disorganised pattern of growth. However, there were a few interesting points for further consideration. Firstly, a hair condition named "wavy" or "wolly hair" has been linked with two particular types of cardiocutaneous syndrome known as Naxos and Carvajal disease, both in humans and in animals (Protonotarios, Tsatsopoulou et al. 1986; Carvajal-Huerta 1998). "Woolly hair" animals are characterised by curlier and thinner hair shafts, with a particularly soft texture (Bolling and Jonkman 2009). Unfortunately, mouse fur can not be curly due to the shortness of the hair shafts, however, Herron and colleagues have already described thinner hair in Wa3 KO mice (Herron, Rao et al. 2005). This suggests a potential correlation between iASPP-deficiency *in vivo* and the two human cardiocutaneous syndromes of Naxos and Carvajal disease. Secondly, as iASPP is expressed in the bulb of the hair follicles where the matrix cells are located, it can be speculated that iASPP is involved in hair regeneration. Matrix cells are trans-amplified cells that are metabolically active only in the growing phase of the hair follicle (Schmidt-Ullrich and Paus 2005). Wnt signalling pathways play a crucial role in the differentiation of matrix cells along different hair shaft lineages (Merrill, Gat et al. 2001). The transcription of different keratins as cell lineage markers has been identified as downstream targets of Wnt signalling (Gat, DasGupta et al. 1998). Moreover, it has been shown that constitutively active β-catenin in mice could lead to an overgrowth of hair follicles and hair tumours composed of only one specific cell lineage (Gat, DasGupta et al. 1998). Collectively, these findings indicate that Wnt signalling is an important player in the hair follicles cycle. As briefly mentioned in Chapter IV, plakoglobin (also called γ-catenin) is known to interact and compete with β-catenin at multiple cellular levels, with a

negative influence on the canonical Wnt/β-catenin signalling pathway (Klymkowsky, Williams et al. 1999; Zhurinsky, Shtutman et al. 2000; Maeda, Usami et al. 2004). In the myocardium, plakoglobin and Wnt signalling have been described as being involved in the pathogenesis of ARVC (Garcia-Gras, Lombardi et al. 2006). As a group, the data presented here suggests an interesting link between the two tissues and the two different phenotypes affecting iASPP-null progeny. Since iASPP deficiency could have an effect on plakoglobin and therefore Wnt signalling in the myocardium, it is possible that it has similar effects on the hair cycle and follicle growth. Although more evidence is needed, the absence of iASPP from the membrane could destabilise cell-to-cell junctions and the signalling pathways in which they are involved. Nevertheless, iASPP-null mice could be use as a valuable tool with which to explore the relationship between hair phenotypes and cardiac abnormalities in more detail, as we know from the literature that "woolly" hair provides a valuable warning signal for the development of fatal cardiomyopathy in humans (Protonotarios, Tsatsopoulou et al. 2001).

Although the phenotype affecting the fur of iASPP-null mice has not been described significantly, more details were obtained on the role of iASPP in the epidermal stratification process. The epidermal phenotype of iASPP$^{\Delta 8/\Delta 8}$ is characterised by an increase in the thickness of the epidermis, associated with an increase in the number of differentiated keratinocytes. Interestingly, the difference in number of primary cells in the basal layer of the epidermis, between wild type and transgenic iASPP mice, was not statistically significant. However, the number of cells within the suprabasal differentiation layers was significantly higher in iASPP$^{\Delta 8/\Delta 8}$ mice, suggesting that iASPP-null keratinocytes were more prone to detach from the basal membrane and undergo the terminal differentiation process. In support of this hypothesis, spinous and granular layers were the most affected in iASPP$^{\Delta 8/\Delta 8}$ epidermal specimens, associated with displacement of the K1 and loricrin expression markers. This is in agreement with the idea that iASPP is an inhibitor of keratinocyte differentiation. Further studies within our lab support this line of evidence. In

particular, in primary murine keratinocytes purified from iASPP$^{\Delta 8/\Delta 8}$ mice, Ca^{2+} differentiation stimuli induced quicker kinetics of K1 and loricrin expression when compared to wild type controls, indicating that iASPP loss induces quicker kinetics of keratinocyte differentiation. Collectively, these results indicate that a cutaneous syndrome, involving both hair follicles and the epidermis, exists in iASPP-null progeny.

According to medical dictionaries, keratosis is a condition common to the majority of palmoplantar keratoderma diseases, which are usually autosomal dominant conditions characterised by a well-demarcated, symmetric thickening of palms and soles in humans, and are often associated with a "dirty" snakeskin-like appearance due to an underlying epidermolysis. Palmoplantar keratodermas are a heterogeneous group of disorders which include non-epidermolysis, focal and punctate keratosis (James, William; Berger, Timothy; Elston, Dirk (2005). *Andrews' Diseases of the Skin: Clinical Dermatology*. 10th ed. Saunders). Interestingly, epidermal sections obtained from iASPP$^{\Delta 8/\Delta 8}$ mice seem to resemble these human conditions with the exception of the epidermolysis. Furthermore, palmoplantar keratoderma has been associated with mutations in K1 expression in non-syndromic disease (Whittock, Smith et al. 2002), and it is intriguing that the main epidermal marker altered in iASPP-null epidermis is K1.

However, the most exciting observation is that iASPP-null mice exhibit cardiocutaneous and hair follicle alterations that closely parallel both Naxos and Carvajal disease (Protonotarios, Tsatsopoulou et al. 1986; Carvajal-Huerta 1998). Therefore, it is possible that iASPP is a potential candidate for the aetiology of cardiocutaneous syndromes. Since mutations in the plakoglobin and desmoplakin genes have been demonstrated to cause Naxos and Carvajal syndrome, it is possible that iASPP has a functional role in maintaining the integrity of desmosomes. However, the mechanism behind the development of palmoplantar keratoderma is still completely obscure. One potential mechanism have been indicating in poor adhesion between keratinocytes. Bolling and colleagues recently proposed that reduced cellular integrity at the site of cell-to-cell junctions in the

epidermis could lead to the activation of compensatory signaling pathways in various epidermal layers, and hyperkeratosis is the end result to protect the skin from further loss of tissue integrity (Bolling and Jonkman 2009). As an alternative explanation, they also proposed that affected proteins responsible for the genesis of the syndrome could influence a particular signaling pathway, and thereby influence the change in the keratinocyte differentiation program. Finally, they also propose that the reduced number of desmosomes could cause proliferation and differentiation discrepancies in the stratification program (Bolling and Jonkman 2009). Controversially, our preliminary data indicates that the integrity of the skin, in particular cell-to-cell junctions, is not affected by the loss of iASPP expression under physiological conditions. However, the epidermis of iASPP transgenic mice has never been examined for fragility or under stress conditions.

It is well-established that the epidermis develops following the activity of the transcription factor p63, as demonstrated by gene KO technologies *in vivo* (Yang, Kaghad et al. 1998; Mills, Zheng et al. 1999). Furthermore, mutations in the *TP63* gene are involved in the pathogenesis of human syndromes that are phenotypically characterised by ectodermal dysplasia, often associated with an increase in epidermal thickness (Celli, Duijf et al. 1999; McGrath, Duijf et al. 2001). The best-known function of the ASPP family of proteins is their ability to regulate the apoptotic function of p53 and its family members, and the p63 DNA binding domain has been demonstrated to interact with the C-terminus of iASPP (Sullivan and Lu 2007; Robinson, Lu et al. 2008). Hence, it is possible that iASPP could modulate the transcription of target genes important for epidermal homeostasis through its binding with p63. In agreement with this hypothesis, both iASPP and p63 are predominantly expressed in the basal layer of stratified epithelia. Its expression pattern supports the notion that iASPP may control epithelial stratification via p63. However, how p63 controls epithelial stratification remains complex (Candi, Cipollone et al. 2008). Investigation of target genes induced by either ΔNp63 or TAp63α has revealed that TAp63α predominately controls the expression of genes that contribute to epidermal differentiation, such as K1, K10, iKKα or envoplakin, whereas ΔNp63 transcriptional targets are predominantly basal epidermal markers such

as K14 (Osada, Park et al. 2005; Candi, Rufini et al. 2006; Candi, Terrinoni et al. 2006). Recently, it was reported that TAp63 also plays a key role in the maintenance of adult stem cells in murine skin. In our study, it has been demonstrated that iASPP could affect the transcriptional activity of TAp63α on the promoter of an envoplakin luciferase plasmid. Therefore, cellular factors like iASPP that can bind both TAp63 and ΔNp63 are likely to influence epithelial stratification by affecting the balancing act of TAp63 and ΔNp63. Further studies are needed to elucidate whether iASPP predominantly functions through either TAp63 or ΔNp63, or both, to regulate epithelial stratification. However, these results suggest a possible interaction between iASPP and the master epidermal regulator p63, providing a possible new mechanism for the development of keratosis. Although more evidence is needed, it can be speculated that iASPP may have a role in modulating p63's transcriptional selectivity of specific target genes important for the switch between proliferation and early differentiation processes. Further evidence supporting this hypothesis has come from the generation of a colony of mice in which the p63-null allele was been introduced into the iASPP$^{\Delta 8/\Delta 8}$ background. Since p63-null mice are not viable (Mills, Zheng et al. 1999; Yang, Schweitzer et al. 1999), only p63$^{+/-}$;iASPP$^{\Delta 8/\Delta 8}$ mice could be analysed. Interestingly, diminished expression of p63 was able to alleviate the epidermal phenotype seen in iASPP-null mice, suggesting increased expression of the protein or its increased activity on selected target genes when iASPP is absent. Nevertheless, this newly identified property of iASPP as a regulator of epithelial stratification and an inhibitor of p63 agrees with the fact that both iASPP and p63 are evolutionary conserved, and that iASPP is an inhibitor of p63 in *C. elegans* (Yang, Kaghad et al. 2002; Belyi and Levine 2009)**.**

Chapter 6
Conclusions and future work

Although many points of discussion have already been considered in individual results chapters, a few key issues raised by the findings presented in this study will be discussed in this section, with a focus on directions for future work.

6.1 iASPP$^{flox/flox}$ mice: a new conditional mouse model to investigate the biological importance of iASPP *in vivo*.

DNA amplification analysis of iASPP$^{flox/+}$ mice obtained from Ingenius Targeting Laboratory demonstrate the successful insertion of two loxP sites at the ends of *PPP13R1L* exon 8. Deletion of exon 8 in primary cells originating from iASPP$^{flox/flox}$ embryos resulted in a complete removal of iASPP expression upon activation of the Cre enzyme. The same results were obtained by analyzing protein extracts originating from mouse tissues in which the recombinase enzyme was genetically activated. In this panel of experiments, it was also noted that iASPP was differentially express in various mouse organs. Mouse tissues in which iASPP was expressed the most were also the organs in which clear gross phenotypes was noted in iASPP-null progeny, indicating that iASPP may play an important role in the biology of these tissues. With the inducible KO system validated, iASPP expression could be targeted in a tissue specific manner, diminishing the possibility of "non-specific" effects of iASPP loss in the biology of the "target" organs. In addition, this inducible system allowed the generation of primary cell lines from different *in vivo* tissues, and specific silencing of iASPP expression to study its functions by "loss and gain of function" experiments. Consistent with the findings obtained in this study, we will now generate a transgenic mouse line by

crossing our iASPP$^{flox/flox}$ with α-smooth muscle-Cre^{+} mice (αMyHC-Cre^{+}), in which the expression of Cre recombinase is under the control of a cardiac specific promoter (Agah, Frenkel *et al*. 1997). These mice will be useful to confirm that the cardiomyopathy seen in iASPP$^{\Delta 8/\Delta 8}$ mice is indeed cause by the absence of iASPP. Moreover, we plan to generate a novel transgenic mouse line in which Cre recombinase will be controlled by the keratin 14 promoter, in order to drive the excision of *PPP13R1L* exon 8 in the basal layer of the epidermis only.

In view of the above, experimental procedures have already begun for the creation of iASPP$^{flox/flox}$;Cre^{+}ER^{T}, in which Cre expression is under the control of 4-hydrotamoxifen (4-OHT) (Chapter V, section 5.5). By painting the skin of these mice with solutions containing 4-OHT, we could delete iASPP expression only in the area where the 4-OHT was applied (data not shown). Preliminary data has demonstrated that a high efficiency of iASPP silencing can be achieved by this method. Moreover, an increase in differentiation associated with thickening of the basal and suprabasal epidermal layers, and a "flaky" skin phenotype were evident in treated mice (data not shown).

In conclusion, it is believed that this study has generated the first model that allows the assessment of iASPP's function in a tissue specific/cell specific manner.

6.2 iASPP and ARVC: are iASPP$^{\Delta 8/\Delta 8}$ mice a new *in vivo* model with which to study ARVC?

Cardiovascular disease is considered to be the major cause of morbidity and mortality in the western world (Ahmad, Seidman *et al*. 2005). Over the past few years, great achievements have been made in the management of various cardiomyopathies, which have mainly come from the use of experimental animal models (Ou, Li *et al*. 2010). In Chapter IV, we showed that iASPP deletion leads to a severe cardiac myopathy associated with shorter life span, sudden death and diminished heart performance of the transgenic animals. These results are in line with the cardiac failure end points that are typical of various cardiomyopathies (Franz, Muller *et al*. 2001; Ahmad, Seidman *et*

al. 2005). Moreover, clear signs of arrhythmias were evident in iASPP$^{\Delta 8/\Delta 8}$ ECG analyses, indicating an arrhythmogenic pattern of the myopathy and an arrhythmic mode of death of the mutant mice(Chapter IV, section 4.2.4). Extensive characterization of the iASPP-null hearts revealed striking similarities with the histopathological features of human ARVC disease. Firstly, hearts depleted of iASPP expression showed grave dilatation of both ventricles associated with extensive focal fibrosis deposits and myocardial disarray. Interestingly, our embryonic imaging analysis, associated with histological investigation of the embryonic heart at different stages, suggested that the observed myopathy started at the site of the right ventricle, with cardiomyocyte loss and thinning of the ventricular wall (Chapter IV, section 4.3.3-4). Secondly, fibrotic deposits were infiltrated with adipocyte droplets, indicating a fatty component of fibrotic tissue present only in iASPP-null specimens (Chapter IV, section 4.2.2). The presence of fibro-fatty deposits and myocyte degenerative changes in iASPP KO mice fulfills the requirement for the histological diagnosis of ARVC (Marcus, McKenna et al. 2010). Finally, Asimaki and colleagues have proposed a new diagnostic tool for the diagnosis of ARVC in humans which consists of the dislocation of plakoglobin staining patterns in ARVC myocardial sections (Asimaki, Tandri et al. 2009). As shown in this study, iASPP-null hearts have severely reduced expression of plakoglobin at the sites of cell-to-cell junctions. Moreover, in young adult mice a clear disproportion between right and left ventricular staining for IDs components was evident, indicating a predominant right ventricular phenotype in iASPP-depleted mice (Chapter IV, section 4.2.5). Collectively, these data strongly indicate that iASPP-deficient mice are affected by ARVC.

In view of the above, it will be of particular importance to investigate whether iASPP expression is reduced in human ARVC samples. This can be achieved by immunohistochemistry experiments using iASPP-specific antibodies on normal and ARVC samples. Since Asimaki et al. have demonstrated that components of ID junctions are affected differently in different cardiomyopathies (Asimaki, Tandri et al. 2009), it would be of great interest to explore whether a loss of iASPP expression can be specifically associated to ARVC patients. Moreover, iASPP$^{\Delta 8/\Delta 8}$ could serve as an

animal model in which the molecular pathways and underlying mechanisms involved in the pathogenesis of the myopathy could be investigated. In addition, this model could also be used to develop and test treatments designed to be specifically effective for dilated cardiomyopathies.

As this study has demonstrated that in the heart, iASPP deficiency leads to the destabilization of ID junctions and abnormal apoptotic activity, iASPP expression appears to be necessary for the preservation of both contractile and electrical function of the heart. The dilated myopathy phenotype of our model agrees with that seen in patients with ARVC, thus our results suggest that genetic screening for iASPP mutations in patients with a family history of lethal arrhythmias or cardiac dysfunction may be prudent.

6.3 iASPP and ARVC: iASPP as a new component of the intercalated disc junctions in the myocardium.

Several studies have identified iASPP to be a potent suppressor of p53-mediated apoptosis (Bergamaschi, Samuels et al. 2003; Liu, Wang et al. 2009). Consistent with this, mice lacking iASPP expression gradually lost myocytes via apoptosis, and the initiation of a remodeling process of the right ventricular chambers was observed (Chapter IV, section 4.4 and 4.3). This is in agreement with previous reports of abnormally enhanced apoptosis in the heart (Jones, Roe et al. 1995; Montes de Oca Luna, Wagner et al. 1995; Grier, Xiong et al. 2006; Xiong, Van Pelt et al. 2007). However, the contemporary deletion of iASPP and p53 decreased the number and extension of the fibro-fatty deposits in iASPP$^{\Delta 8/\Delta 8}$ mice, but did not result in a complete rescue of the cardiac phenotype, suggesting an active role for apoptosis in the pathogenesis of ARVC. This unexpected result suggests a differently driven mechanism for the establishment of ARVC. A growing body of evidence indicates that the replacement of the myocardial tissue with fibro-fatty deposits seems to be a degenerative process caused by death of cardiomyocytes via apoptosis (McKenna, Thiene et al. 1994; Franz, Muller et al. 2001; Ahmad, Seidman et al. 2005). This is consistent with our observation that focal fibrotic deposits are dependent on the presence of p53 (Chapter IV, section

4.4.2). Since proliferation and apoptosis are important processes in heart development (Fisher, Langille et al. 2000), the evidence outlined in Chapter IV indicates that iASPP is important for the regulation of apoptosis, but it demonstrates that it not essential for the correct development of the embryonic heart, in contrast to mdm2 (Grier, Xiong et al. 2006). On the other hand, it is possible that iASPP could control p53's activity during maladaptive remodeling processes or under stress conditions. This hypothesis is supported by the observation that mice deficient for mdm4 have shorter life spans due to underlying dilated cardiomyopathies. Hence, mdm4 is important but not essential for heart development, but its presence is vital for protecting differentiated cardiomyocytes from apoptosis upon stress conditions applied to the heart (Xiong, Van Pelt et al. 2007). It would, therefore, be of great interest to understand whether iASPP collaborates with mdm4 to protect myocytes from p53-mediated apoptosis triggers under stress conditions. This could be achieved by isolating cardiac primary myocytes and investigating their responses upon different *in vitro* stress conditions in the presence of absence of iASPP.

Although the molecular pathogenesis of ARVC remains to be elucidated, its genetic basis is only partially understood. Several genetic loci have been mapped, and four genes encoding the desmosomal proteins desmoplakin, plakoglobin, plakophillin-2 and desmoglein-2 have been linked with the cause of the disease (Sen-Chowdhry, Syrris et al. 2005; Pilichou, Nava et al. 2006). In particular, an elegant report from Ali J. Marian's group in 2006 revealed an interesting connection between a genetic KO mouse model, which had reduced desmoplakin expression, and the rise of ARVC (Garcia-Gras, Lombardi *et al*. 2006). They demonstrated that a loss of desmoplakin from the IDs could cause plakoglobin (γ-catenin) to relocate into the nucleus, where it could suppress canonical Wnt/β-catenin signaling. Such suppression of Wnt signaling provokes fibrogenesis, adipogenesis and can induce apoptosis (Ross, Hemati et al. 2000; Chen, Guttridge et al. 2001). Using a specific monoclonal antibody for the detection of iASPP protein, which does not co-react with tissue samples obtained from iASPP-deficient mice, it has been demonstrated in this study that

full-length iASPP is clearly expressed at the polar ends of cardiomyocytes (Chapter IV, section 4.2). Desmosomes, and adherens and gap junctions are all located at the polar ends of cardiomyocytes and maintain the integrity of the heart tissue (Chapter I, section 1.3). Based on this model, we can speculate that loss of iASPP could destabilize adherens or desmosomal junctions and free γ–catenin into the cytoplasm. This pool of γ–catenin could then translocate into the nucleus, where it could influence canonical Wnt signaling. It will, therefore, be of interest to investigate whether the molecular mechanism proposed by Gracia-Gras et al. can be verified in our iASPP$^{\Delta 8/\Delta 8}$ mouse model. Moreover, as the leading causes of ARVC have been linked with abnormalities in the structure or in the maintenance of the intercalated discs (Franz, Muller et al. 2001; Ahmad, Seidman et al. 2005), it is of fundamental importance to study whether iASPP is involved in maintaining ID structure, and at what level. While it has not yet been definitively demonstrated iASPP is a new component of ID structure, the right ventricular phenotype observed in embryos and young adult animal suggests that iASPP plays a fundamental role in maintaining the integrity of cell-cell junctions. In order to fully understand the role of iASPP within the ID structures, it will be of particular importance to identify which junctional structures iASPP directly interacts with, and which domains are required for these interactions. iASPP contains several domains involved in protein-protein interactions, such as the ankyrin repeat and SH-3 domains. However, it can not be excluded that another part of the protein may play a role in its interaction with IDs.

6.4 iASPP and Naxos-Carvajal syndrome.

Mutations in some ID junctional proteins are responsible for human syndromes characterized by cardiocutaneous symptoms such as cardiomyopathy, woolly hair and palmo-keratoderma. Specifically, Naxos and Carvajal diseases are rare autosomal recessive pathologies that are cause by the mutation of plakoglobin and desmoplakin, respectively (McKoy, Protonotarios et al. 2000; Norgett, Hatsell et al. 2000). In particular, Naxos disease affects the right ventricular chamber of the heart, in association with a high incidence of arrhythmias and sudden cardiac death (Protonotarios,

Tsatsopoulou *et al*. 1986). The disease has been linked to the somatic mutation of two nucleotides within the plakoglobin gene, which causes a frame shift resulting in the truncation of the C-terminal domain (McKoy, Protonotarios et al. 2000). Naxos disease also results in thickening of the epidermis and a hair phenotype, as seen in iASPP mutant mice. In the course of the disease, affected hearts show right ventricular dilatation with fibro-fatty replacement of myocardial tissue typical of ARVC (McKenna, Thiene et al. 1994; Basso, Tsatsopoulou et al. 2001). With further disease progression, left ventricular involvement become significant and heart failure develops. Thus, Naxos disease and the iASPP$^{\Delta 8/\Delta 8}$ mouse model developed in this study bear striking similarities. Cardiocutaneous syndrome have also been described in Indian and Arab family (Rao, Reddy et al. 1996; Djabali, Martinez-Mir et al. 2002). Mutations in several candidates gene such as plakoglobin, desmoplakin, plakophilins-2 and desmocollins/desmogleins were search for and not found. Thus, mutations in additional genes may be the genetic cause of the disease therefore, iASPP might be involved in the etiology of these cardiocutaneous syndromes. Hence, it would be of particular interest screen for iASPP genetic mutations in idiopathic Naxos or Carvajal patients.

Moreover, desmoplakin have been indicated as the mutant protein in Carvajal syndrome (Carvajal-Huerta 1998; Norgett, Hatsell et al. 2000). These junctional proteins link the cytoskeletal filaments to each other and to membrane-associated adhesion complex (section 1.3.2). Desmoplakin contains three functional domain: an N-terminal domain which binds to desmosomal cadherins via interaction of plakoglobin and plakophillin; a long rod shape central domain; and a C-terminal domain, which bind desmin-based intermediated filament (Kowalczyk, Bornslaeger et al. 1999). In Carvajal syndrome, a deletion in exon 24 produces a premature stop codon and thereby truncates the C-terminal domain (Norgett, Hatsell et al. 2000). Immunofluorescence analysis, revealed marked reductions in desmoplakin, plakoglobin and desmin staining at intracellular junctions in iASPP$^{\Delta 8/\Delta 8}$ heart sections (figure 4.21). Deletion of iASPP from the IDs site may therefore interfere with molecular interactions among desmoplakin, plakoglobin and desmin. Although the sarcomeric distribution of the desmin in iASPP$^{\Delta 8/\Delta 8}$ mice there was a marked loss of its signal at the ID

structures, strongly suggesting that loss of iASPP may weaken the binding between the intermediate filament and the cardiac desmosomes. Therefore, it is plausible to speculate that iASPP is important to maintain force transmission between the cytoskeleton and the cellular-junction. In view of the above, we are already investigating a possible physical link between iASPP, desmoplakin and desmin. Of great interest would be investigate whether the Carvajal mutation of 7901delG (Norgett, Hatsell et al. 2000) would disrupt the possible association between iASPP, desmoplakin and desmin.

6.5 iASPP and cardiotoxicity of anticancer drugs.

As mentioned in Chapter I, cytotoxic agents and more recently developed targeted anticancer therapies have been shown to induce acute or chronic side-effects, which specifically target the cardiovascular system (Chapter I, section 1.3.1). In particular, new classes of molecules specifically designed to inhibit surface receptors involved in growth signalling pathways (i.e. monoclonal antibodies against ErbB2 receptors), or small molecules that inhibit tyrosine kinase signalling cascades, selectively disrupt pathways that are centrally involved in cell survival, growth and inflammatory activation (see Chapter IV, section 1.3.4). These new anticancer drugs have been shown to induce cardiovascular side-effects associated with substantial risks to the patient health (Albini, Pennesi et al. 2010; Raschi, Vasina et al. 2010). Specifically, the use of antibodies against ErbB2 has been shown to interfere with various intracellular signaling pathways, including PI3-kinase/akt and MAP kinase (Kerkela, Grazette et al. 2006; Valabrega, Montemurro et al. 2007). Genetic ablation of the ErbB2 receptor tyrosine kinase in a restricted ventricular manner suggests an important role for this molecule in the prevention of dilated cardiomyopathy (Crone, Zhao et al. 2002). Moreover, imatinib mesylate (Gleevec), a small molecule inhibitor of the fusion protein Bcr-Abl which is the causal agent in chronic myelogenous leukemia (Wong and Witte 2004), has been directly related to left ventricular dysfunction and heart failure (Chapter I, section 1.3.1). Cardiac myocytes infected with an imatinib-resistant mutant form of c-able are largely protected from

imatinib side-effects, suggesting that c-abl has an as yet unrecognized survival role in cardiomyocytes (Kerkela, Grazette et al. 2006). Based on these observations, it is possible that one of the targets of imatinib mesylate (i.e. c-able, PDGF or c-kit) may have a survival function in cardiomyocytes. Interestingly, studies conducted in our laboratory indicate iASPP to be a specific substrate of c-abl and SRC kinase (Ying Hu personal communication). Preliminary data suggests that iASPP phosphorylation relocates the protein to the cell-cell membrane in *in vitro* studies using primary keratinocytes (Ying Hu personal communication). In light of the above, it would be extremely interesting to determine whether the clinical use of tyrosine kinase inhibitors as antineoplastic compounds could affect the phosphorylation status of iASPP, thus affecting its membrane location and impairing cell-to-cell junctions.

6.6 iASPP as a new modulator of TAp63 transcriptional activity.

Using mouse primary keratinocytes from iASPP$^{+/+}$ and iASPP$^{\Delta 8/\Delta 8}$ mice, this study has identified an important role for iASPP in inhibiting epidermal differentiation. This was further supported by the *in vivo* finding that iASPP-null epidermis is thicker compared to wild type controls, and that both iASPP and p63 are predominantly expressed in the basal layer of stratified epithelium (Chapter V, section 5.3-5.4). iASPP's expression pattern supports the notion that iASPP may control epithelial stratification via p63. However, how p63 controls epithelial stratification remains unclear (Candi, Cipollone *et al.* 2008), mainly because multiple isoforms of p63 are expressed during the epidermal stratification process. To date, two main groups have been identified: transactivation domain-containing TAp63 versus N-terminal transactivation domain-deleted ΔNp63 (Candi, Cipollone et al. 2008). In theory, ΔNp63 could act as a dominant negative regulator of TAp63 in the basal layer of the epidermis (Yang, Kaghad et al. 1998). However, it is also known that ΔNp63 isoforms can activate the transcription of target genes through a second transactivation domain found in their C-termini (Dohn, Zhang *et al.* 2001; King, Ponnamperuma et al. 2003). Investigation of target genes induced by either ΔNp63 or TAp63α has revealed that TAp63α predominately controls the

expression of genes related to epidermal terminal differentiation, whereas ΔNp63 transcriptional targets are predominantly proliferative epidermal markers (Osada, Park et al. 2005; Candi, Rufini et al. 2006; Candi, Terrinoni et al. 2006).

ΔNp63 is a master transcription factor and is essential for the maintenance of the self-renewal and proliferative potential of the epidermis (Nylander, Vojtesek et al. 2002). How TAp63 and ΔNp63 function, either individually or together, remains unclear. In some *in vitro* experimental assays, TAp63 and ΔNp63 can regulate the same transcriptional target genes, such as IKKα, directly (for TAp63) or indirectly (for ΔNp63) (Candi, Terrinoni et al. 2006). However, for other transcriptional targets such as K14, ΔNp63 and not TAp63 induces their expression (Candi, Rufini et al. 2006). Cellular factors like iASPP, which can bind both TAp63 and ΔNp63, are therefore likely to influence epithelial stratification by affecting the activity of TA- and ΔNp63. Further studies are needed to elucidate whether iASPP predominantly functions through either TAp63, ΔNp63 or both, to regulate epithelial stratification.

Finally, in a previous report on Wa3 mice, it was proposed that iASPP may maintain epithelial homeostasis by binding and inhibiting the activity of p65RelA (Herron, Rao et al. 2005). In Chapter VI, we showed that iASPP can also affect epithelial stratification by binding p63 and inhibiting TAp63's ability to transactivate epithelial terminal differentiation genes. Since IKKα is a direct transcriptional target of TAp63 (Candi, Terrinoni et al. 2006), and IKKα is an upstream activator of p65RelA, it is possible that iASPP could inhibit p65RelA indirectly. This is consistent with the finding that both Wa3 and iASPP$^{\Delta 8/\Delta 8}$ mice share some overlapping defects in the epidermis. Finally, as iASPP is able to bind p63 and p65RelA, future genetic studies are needed to determine whether iASPP predominantly maintains epidermal homeostasis through its ability to bind and regulate p63, p65RelA or both. Nevertheless, the evidence reported here suggests that iASPP is able to inhibit epidermal differentiation by influencing TAp63's transcriptional activity. This finding is further supported by the partial genetic rescue of the epidermal phenotype, by the introduction of an inactive form of the p63 allele into iASPP$^{\Delta 8/\Delta 8}$ mice.

Bibliography

Abdelwahid, E., L. J. Pelliniemi, et al. (1999). "Apoptosis in the pattern formation of the ventricular wall during mouse heart organogenesis." Anat Rec **256**(2): 208-217.

Adams, J. W., Y. Sakata, et al. (1998). "Enhanced Galphaq signaling: a common pathway mediates cardiac hypertrophy and apoptotic heart failure." Proc Natl Acad Sci U S A **95**(17): 10140-10145.

Agah, R., P. A. Frenkel, et al. (1997). "Gene recombination in postmitotic cells. Targeted expression of Cre recombinase provokes cardiac-restricted, site-specific rearrangement in adult ventricular muscle in vivo." J Clin Invest **100**(1): 169-179.

Agirre, X., J. Roman-Gomez, et al. (2006). "ASPP1, a common activator of TP53, is inactivated by aberrant methylation of its promoter in acute lymphoblastic leukemia." Oncogene **25**(13): 1862-1870.

Ahmad, F., J. G. Seidman, et al. (2005). "The genetic basis for cardiac remodeling." Annu Rev Genomics Hum Genet **6**: 185-216.

Ahn, J., I. J. Byeon, et al. (2009). "Insight into the structural basis of pro- and antiapoptotic p53 modulation by ASPP proteins." J Biol Chem **284**(20): 13812-13822.

Ai, Z., A. Fischer, et al. (2000). "Wnt-1 regulation of connexin43 in cardiac myocytes." J Clin Invest **105**(2): 161-171.

Albini, A., G. Pennesi, et al. (2010). "Cardiotoxicity of anticancer drugs: the need for cardio-oncology and cardio-oncological prevention." J Natl Cancer Inst **102**(1): 14-25.

Alessi, D. R. and P. Cohen (1998). "Mechanism of activation and function of protein kinase B." Curr Opin Genet Dev **8**(1): 55-62.

Amagai, M., V. Klaus-Kovtun, et al. (1991). "Autoantibodies against a novel epithelial cadherin in pemphigus vulgaris, a disease of cell adhesion." Cell **67**(5): 869-877.

Amagai, M., N. Matsuyoshi, et al. (2000). "Toxin in bullous impetigo and staphylococcal scalded-skin syndrome targets desmoglein 1." Nat Med **6**(11): 1275-1277.

An, W., J. Kim, et al. (2004). "Ordered cooperative functions of PRMT1, p300, and CARM1 in transcriptional activation by p53." Cell **117**(6): 735-748.

Anderson, R. H., N. A. Brown, et al. (2006). "Development and structures of the venous pole of the heart." Dev Dyn **235**(1): 2-9.

Antoniades, L., A. Tsatsopoulou, et al. (2006). "Arrhythmogenic right ventricular cardiomyopathy caused by deletions in plakophilin-2 and plakoglobin (Naxos disease) in families from Greece and Cyprus: genotype-phenotype relations, diagnostic features and prognosis." Eur Heart J **27**(18): 2208-2216.

Arber, S., J. J. Hunter, et al. (1997). "MLP-deficient mice exhibit a disruption of cardiac cytoarchitectural organization, dilated cardiomyopathy, and heart failure." Cell **88**(3): 393-403.

Arbustini, E., M. Diegoli, et al. (1998). "Mitochondrial DNA mutations and mitochondrial abnormalities in dilated cardiomyopathy." Am J Pathol **153**(5): 1501-1510.

Armstrong, D. K., K. E. McKenna, et al. (1999). "Haploinsufficiency of desmoplakin causes a striate subtype of palmoplantar keratoderma." Hum Mol Genet **8**(1): 143-148.

Armstrong, J. F., M. H. Kaufman, et al. (1995). "High-frequency developmental abnormalities in p53-deficient mice." Curr Biol **5**(8): 931-936.

Asimaki, A., H. Tandri, et al. (2009). "A new diagnostic test for arrhythmogenic right ventricular cardiomyopathy." N Engl J Med **360**(11): 1075-1084.

Azaouagh, A., S. Churzidse, et al. (2011). "Arrhythmogenic right ventricular cardiomyopathy/dysplasia: a review and update." Clin Res Cardiol **100**(5): 383-394.

Baker, S. J., E. R. Fearon, et al. (1989). "Chromosome 17 deletions and p53 gene mutations in colorectal carcinomas." Science **244**(4901): 217-221.

Barboza, J. A., T. Iwakuma, et al. (2008). "Mdm2 and Mdm4 loss regulates distinct p53 activities." Mol Cancer Res **6**(6): 947-954.

Barrandon, Y. and H. Green (1987). "Three clonal types of keratinocyte with different capacities for multiplication." Proc Natl Acad Sci U S A **84**(8): 2302-2306.

Basso, C., A. Tsatsopoulou, et al. (2001). ""Petrified" right ventricle in long-standing naxos arrhythmogenic right ventricular cardiomyopathy." Circulation **104**(23): E132-133.

Beltrami, A. P., K. Urbanek, et al. (2001). "Evidence that human cardiac myocytes divide after myocardial infarction." N Engl J Med **344**(23): 1750-1757.

Belyi, V. A. and A. J. Levine (2009). "One billion years of p53/p63/p73 evolution." Proc Natl Acad Sci U S A **106**(42): 17609-17610.

Ben-Ze'ev, A. and B. Geiger (1998). "Differential molecular interactions of beta-catenin and plakoglobin in adhesion, signaling and cancer." Curr Opin Cell Biol **10**(5): 629-639.

Bergamaschi, D., Y. Samuels, et al. (2004). "ASPP1 and ASPP2: common activators of p53 family members." Mol Cell Biol **24**(3): 1341-1350.

Bergamaschi, D., Y. Samuels, et al. (2003). "iASPP oncoprotein is a key inhibitor of p53 conserved from worm to human." Nat Genet **33**(2): 162-167.

Bergamaschi, D., Y. Samuels, et al. (2006). "iASPP preferentially binds p53 proline-rich region and modulates apoptotic function of codon 72-polymorphic p53." Nat Genet **38**(10): 1133-1141.

Bers, D. M. (2002). "Cardiac excitation-contraction coupling." Nature **415**(6868): 198-205.

Blankesteijn, W. M., Y. P. Essers-Janssen, et al. (1996). "Increased expression of a homologue of drosophila tissue polarity gene "frizzled" in left ventricular hypertrophy in the rat, as identified by subtractive hybridization." J Mol Cell Cardiol **28**(5): 1187-1191.

Blanpain, C., W. E. Lowry, et al. (2006). "Canonical notch signaling functions as a commitment switch in the epidermal lineage." Genes Dev **20**(21): 3022-3035.

Bolling, M. C. and M. F. Jonkman (2009). "Skin and heart: une liaison dangereuse." Exp Dermatol **18**(8): 658-668.

Bornslaeger, E. A., C. M. Corcoran, et al. (1996). "Breaking the connection: displacement of the desmosomal plaque protein desmoplakin from cell-cell interfaces disrupts anchorage of intermediate filament bundles and alters intercellular junction assembly." J Cell Biol **134**(4): 985-1001.

Botchkarev, V. A., N. V. Botchkareva, et al. (1999). "Noggin is a mesenchymally derived stimulator of hair-follicle induction." Nat Cell Biol **1**(3): 158-164.

Brade, T., J. Manner, et al. (2006). "The role of Wnt signalling in cardiac development and tissue remodelling in the mature heart." Cardiovasc Res **72**(2): 198-209.

Brette, F. and C. Orchard (2007). "Resurgence of cardiac t-tubule research." Physiology (Bethesda) **22**: 167-173.

Brooke, M. A., D. Nitoiu, et al. (2011). "Cell-cell connectivity: desmosomes and disease." J Pathol.

Brune, R. M., J. B. Bard, et al. (1999). "A three-dimensional model of the mouse at embryonic day 9." Dev Biol **216**(2): 457-468.

Bukhari, I. and N. Juma'a (2004). "Naxos disease in Saudi Arabia." J Eur Acad Dermatol Venereol **18**(5): 614-616.

Burke, A. P., A. Farb, et al. (1998). "Arrhythmogenic right ventricular cardiomyopathy and fatty replacement of the right ventricular myocardium: are they different diseases?" Circulation **97**(16): 1571-1580.

Cabral, R. M., L. Liu, et al. (2010). "Homozygous mutations in the 5' region of the JUP gene result in cutaneous disease but normal heart development in children." J Invest Dermatol **130**(6): 1543-1550.

Caelles, C., A. Helmberg, et al. (1994). "p53-dependent apoptosis in the absence of transcriptional activation of p53-target genes." Nature **370**(6486): 220-223.

Camelliti, P., J. O. Gallagher, et al. (2006). "Micropatterned cell cultures on elastic membranes as an in vitro model of myocardium." Nat Protoc **1**(3): 1379-1391.

Candi, E., R. Cipollone, et al. (2008). "p63 in epithelial development." Cell Mol Life Sci **65**(20): 3126-3133.

Candi, E., A. Rufini, et al. (2006). "Differential roles of p63 isoforms in epidermal development: selective genetic complementation in p63 null mice." Cell Death Differ **13**(6): 1037-1047.

Candi, E., A. Terrinoni, et al. (2006). "p63 is upstream of IKK alpha in epidermal development." J Cell Sci **119**(Pt 22): 4617-4622.

Cao, Y., T. Hamada, et al. (2004). "Hepatitis C virus core protein interacts with p53-binding protein, 53BP2/Bbp/ASPP2, and inhibits p53-mediated apoptosis." Biochem Biophys Res Commun **315**(4): 788-795.

Capecchi, M. R. (1989). "Altering the genome by homologous recombination." Science **244**(4910): 1288-1292.

Carroll, D. K., J. S. Carroll, et al. (2006). "p63 regulates an adhesion programme and cell survival in epithelial cells." Nat Cell Biol **8**(6): 551-561.

Carvajal-Huerta, L. (1998). "Epidermolytic palmoplantar keratoderma with woolly hair and dilated cardiomyopathy." J Am Acad Dermatol **39**(3): 418-421.

Cecconi, F., G. Alvarez-Bolado, et al. (1998). "Apaf1 (CED-4 homolog) regulates programmed cell death in mammalian development." Cell **94**(6): 727-737.

Celli, J., P. Duijf, et al. (1999). "Heterozygous germline mutations in the p53 homolog p63 are the cause of EEC syndrome." Cell **99**(2): 143-153.

Chan, I., J. I. Harper, et al. (2004). "ADULT ectodermal dysplasia syndrome resulting from the missense mutation R298Q in the p63 gene." Clin Exp Dermatol **29**(6): 669-672.

Chen, D., E. Padiernos, et al. (2005). "Apoptosis-stimulating protein of p53-2 (ASPP2/53BP2L) is an E2F target gene." Cell Death Differ **12**(4): 358-368.

Chen, J. and K. R. Chien (1999). "Complexity in simplicity: monogenic disorders and complex cardiomyopathies." J Clin Invest **103**(11): 1483-1485.

Chen, S., D. C. Guttridge, et al. (2001). "Wnt-1 signaling inhibits apoptosis by activating beta-catenin/T cell factor-mediated transcription." J Cell Biol **152**(1): 87-96.

Chen, Y., W. Liu, et al. (2003). "APP-BP1 mediates APP-induced apoptosis and DNA synthesis and is increased in Alzheimer's disease brain." J Cell Biol **163**(1): 27-33.

Chen, Y., W. Liu, et al. (2003). "ASPP2 inhibits APP-BP1-mediated NEDD8 conjugation to cullin-1 and decreases APP-BP1-induced cell proliferation and neuronal apoptosis." J Neurochem **85**(3): 801-809.

Cheng, W., B. Li, et al. (1995). "Stretch-induced programmed myocyte cell death." J Clin Invest **96**(5): 2247-2259.

Chidgey, M., C. Brakebusch, et al. (2001). "Mice lacking desmocollin 1 show epidermal fragility accompanied by barrier defects and abnormal differentiation." J Cell Biol **155**(5): 821-832.

Classon, M. and E. Harlow (2002). "The retinoblastoma tumour suppressor in development and cancer." Nat Rev Cancer **2**(12): 910-917.

Conlon, I. and M. Raff (1999). "Size control in animal development." Cell **96**(2): 235-244.

Contente, A., A. Dittmer, et al. (2002). "A polymorphic microsatellite that mediates induction of PIG3 by p53." Nat Genet **30**(3): 315-320.

Corrado, D., C. Basso, et al. (1997). "Sudden death in young people with apparently isolated mitral valve prolapse." G Ital Cardiol **27**(11): 1097-1105.

Corrado, D., C. Basso, et al. (1997). "Spectrum of clinicopathologic manifestations of arrhythmogenic right ventricular cardiomyopathy/dysplasia: a multicenter study." J Am Coll Cardiol **30**(6): 1512-1520.

Cotsarelis, G., T. T. Sun, et al. (1990). "Label-retaining cells reside in the bulge area of pilosebaceous unit: implications for follicular stem cells, hair cycle, and skin carcinogenesis." Cell **61**(7): 1329-1337.

Cowin, P., H. P. Kapprell, et al. (1986). "Plakoglobin: a protein common to different kinds of intercellular adhering junctions." Cell **46**(7): 1063-1073.

Cox, G. F. and L. M. Kunkel (1997). "Dystrophies and heart disease." Curr Opin Cardiol **12**(3): 329-343.

Crone, S. A., Y. Y. Zhao, et al. (2002). "ErbB2 is essential in the prevention of dilated cardiomyopathy." Nat Med **8**(5): 459-465.

Dalal, D., K. Nasir, et al. (2005). "Arrhythmogenic right ventricular dysplasia: a United States experience." Circulation **112**(25): 3823-3832.

DasGupta, R. and E. Fuchs (1999). "Multiple roles for activated LEF/TCF transcription complexes during hair follicle development and differentiation." Development **126**(20): 4557-4568.

DeChiara, T. M., A. Efstratiadis, et al. (1990). "A growth-deficiency phenotype in heterozygous mice carrying an insulin-like growth factor II gene disrupted by targeting." Nature **345**(6270): 78-80.

Degterev, A., M. Boyce, et al. (2003). "A decade of caspases." Oncogene **22**(53): 8543-8567.

Delaughter, M. C., G. E. Taffet, et al. (1999). "Local insulin-like growth factor I expression induces physiologic, then pathologic, cardiac hypertrophy in transgenic mice." FASEB J **13**(14): 1923-1929.

Delmar, M. and W. J. McKenna (2010). "The cardiac desmosome and arrhythmogenic cardiomyopathies: from gene to disease." Circ Res **107**(6): 700-714.

Descargues, P., A. K. Sil, et al. (2008). "IKKalpha, a critical regulator of epidermal differentiation and a suppressor of skin cancer." Embo J **27**(20): 2639-2647.

Djabali, K., A. Martinez-Mir, et al. (2002). "Evidence for extensive locus heterogeneity in Naxos disease." J Invest Dermatol **118**(3): 557-560.

Dohn, M., S. Zhang, et al. (2001). "p63alpha and DeltaNp63alpha can induce cell cycle arrest and apoptosis and differentially regulate p53 target genes." Oncogene **20**(25): 3193-3205.

Dolci, A., R. Dominici, et al. (2008). "Biochemical markers for prediction of chemotherapy-induced cardiotoxicity: systematic review of the literature and recommendations for use." Am J Clin Pathol **130**(5): 688-695.

Dominguez, G., J. M. Garcia, et al. (2006). "DeltaTAp73 upregulation correlates with poor prognosis in human tumors: putative in vivo network involving p73 isoforms, p53, and E2F-1." J Clin Oncol **24**(5): 805-815.

Donehower, L. A., M. Harvey, et al. (1992). "Mice deficient for p53 are developmentally normal but susceptible to spontaneous tumours." Nature **356**(6366): 215-221.

el-Deiry, W. S., S. E. Kern, et al. (1992). "Definition of a consensus binding site for p53." Nat Genet **1**(1): 45-49.

Elliott, P. (2000). "Cardiomyopathy. Diagnosis and management of dilated cardiomyopathy." Heart **84**(1): 106-112.

Espanel, X. and M. Sudol (2001). "Yes-associated protein and p53-binding protein-2 interact through their WW and SH3 domains." J Biol Chem **276**(17): 14514-14523.

Fatkin, D., B. K. McConnell, et al. (2000). "An abnormal Ca(2+) response in mutant sarcomere protein-mediated familial hypertrophic cardiomyopathy." J Clin Invest **106**(11): 1351-1359.

Ferreira-Cornwell, M. C., Y. Luo, et al. (2002). "Remodeling the intercalated disc leads to cardiomyopathy in mice misexpressing cadherins in the heart." J Cell Sci **115**(Pt 8): 1623-1634.

Finch, R. A., D. B. Donoviel, et al. (2002). "mdmx is a negative regulator of p53 activity in vivo." Cancer Res **62**(11): 3221-3225.

Finlay, C. A., P. W. Hinds, et al. (1989). "The p53 proto-oncogene can act as a suppressor of transformation." Cell **57**(7): 1083-1093.

Fisher, S. A., B. L. Langille, et al. (2000). "Apoptosis during cardiovascular development." Circ Res **87**(10): 856-864.

Flores, E. R., S. Sengupta, et al. (2005). "Tumor predisposition in mice mutant for p63 and p73: evidence for broader tumor suppressor functions for the p53 family." Cancer Cell **7**(4): 363-373.

Flores, E. R., K. Y. Tsai, et al. (2002). "p63 and p73 are required for p53-dependent apoptosis in response to DNA damage." Nature **416**(6880): 560-564.

Fogal, V., J. K. Hsieh, et al. (2005). "Cell cycle-dependent nuclear retention of p53 by E2F1 requires phosphorylation of p53 at Ser315." Embo J **24**(15): 2768-2782.

Fomenkov, A., Y. P. Huang, et al. (2003). "P63 alpha mutations lead to aberrant splicing of keratinocyte growth factor receptor in the Hay-Wells syndrome." J Biol Chem **278**(26): 23906-23914.

Force, T., D. S. Krause, et al. (2007). "Molecular mechanisms of cardiotoxicity of tyrosine kinase inhibition." Nat Rev Cancer **7**(5): 332-344.

Franke, W. W., C. M. Borrmann, et al. (2006). "The area composita of adhering junctions connecting heart muscle cells of vertebrates. I. Molecular definition in intercalated

disks of cardiomyocytes by immunoelectron microscopy of desmosomal proteins." Eur J Cell Biol **85**(2): 69-82.

Franz, W. M., M. Muller, et al. (2000). "Association of nonsense mutation of dystrophin gene with disruption of sarcoglycan complex in X-linked dilated cardiomyopathy." Lancet **355**(9217): 1781-1785.

Franz, W. M., O. J. Muller, et al. (2001). "Cardiomyopathies: from genetics to the prospect of treatment." Lancet **358**(9293): 1627-1637.

Fuchs, E. (2007). "Scratching the surface of skin development." Nature **445**(7130): 834-842.

Fuchs, E. and H. Green (1980). "Changes in keratin gene expression during terminal differentiation of the keratinocyte." Cell **19**(4): 1033-1042.

Gao, C. and N. Tsuchida (1999). "Activation of caspases in p53-induced transactivation-independent apoptosis." Jpn J Cancer Res **90**(2): 180-187.

Garcia-Gras, E., R. Lombardi, et al. (2006). "Suppression of canonical Wnt/beta-catenin signaling by nuclear plakoglobin recapitulates phenotype of arrhythmogenic right ventricular cardiomyopathy." J Clin Invest **116**(7): 2012-2021.

Gat, U., R. DasGupta, et al. (1998). "De Novo hair follicle morphogenesis and hair tumors in mice expressing a truncated beta-catenin in skin." Cell **95**(5): 605-614.

Gerull, B., A. Heuser, et al. (2004). "Mutations in the desmosomal protein plakophilin-2 are common in arrhythmogenic right ventricular cardiomyopathy." Nat Genet **36**(11): 1162-1164.

Godley, L. A., J. B. Kopp, et al. (1996). "Wild-type p53 transgenic mice exhibit altered differentiation of the ureteric bud and possess small kidneys." Genes Dev **10**(7): 836-850.

Gorina, S. and N. P. Pavletich (1996). "Structure of the p53 tumor suppressor bound to the ankyrin and SH3 domains of 53BP2." Science **274**(5289): 1001-1005.

Grier, J. D., S. Xiong, et al. (2006). "Tissue-specific differences of p53 inhibition by Mdm2 and Mdm4." Mol Cell Biol **26**(1): 192-198.

Grossmann, K. S., C. Grund, et al. (2004). "Requirement of plakophilin 2 for heart morphogenesis and cardiac junction formation." J Cell Biol **167**(1): 149-160.

Grunig, E., J. A. Tasman, et al. (1998). "Frequency and phenotypes of familial dilated cardiomyopathy." J Am Coll Cardiol **31**(1): 186-194.

Gumbiner, B. M. (2000). "Regulation of cadherin adhesive activity." J Cell Biol **148**(3): 399-404.

Guo, X., W. M. Keyes, et al. (2009). "TAp63 induces senescence and suppresses tumorigenesis in vivo." Nat Cell Biol **11**(12): 1451-1457.

Hakimelahi, S., H. R. Parker, et al. (2000). "Plakoglobin regulates the expression of the anti-apoptotic protein BCL-2." J Biol Chem **275**(15): 10905-10911.

Haq, S., A. Michael, et al. (2003). "Stabilization of beta-catenin by a Wnt-independent mechanism regulates cardiomyocyte growth." Proc Natl Acad Sci U S A **100**(8): 4610-4615.

Hardman, M. J., K. Liu, et al. (2005). "Desmosomal cadherin misexpression alters beta-catenin stability and epidermal differentiation." Mol Cell Biol **25**(3): 969-978.

Hartsock, A. and W. J. Nelson (2008). "Adherens and tight junctions: structure, function and connections to the actin cytoskeleton." Biochim Biophys Acta **1778**(3): 660-669.

Hatzfeld, M., C. Haffner, et al. (2000). "The function of plakophilin 1 in desmosome assembly and actin filament organization." J Cell Biol **149**(1): 209-222.

Heidt, A. B. and B. L. Black (2005). "Transgenic mice that express Cre recombinase under control of a skeletal muscle-specific promoter from mef2c." Genesis **42**(1): 28-32.

Helps, N. R., H. M. Barker, et al. (1995). "Protein phosphatase 1 interacts with p53BP2, a protein which binds to the tumour suppressor p53." FEBS Lett **377**(3): 295-300.

Hennings, H., K. Holbrook, et al. (1980). "Growth and differentiation of mouse epidermal cells in culture: effects of extracellular calcium." Curr Probl Dermatol **10**: 3-25.

Hennings, H., D. Michael, et al. (1980). "Calcium regulation of growth and differentiation of mouse epidermal cells in culture." Cell **19**(1): 245-254.

Herron, B. J., C. Rao, et al. (2005). "A mutation in NFkB interacting protein 1 results in cardiomyopathy and abnormal skin development in wa3 mice." Hum Mol Genet **14**(5): 667-677.

Hershko, T., M. Chaussepied, et al. (2005). "Novel link between E2F and p53: proapoptotic cofactors of p53 are transcriptionally upregulated by E2F." Cell Death Differ **12**(4): 377-383.

Hirashima, M., K. Sano, et al. (2008). "Lymphatic vessel assembly is impaired in Aspp1-deficient mouse embryos." Dev Biol **316**(1): 149-159.

Hooper, M., K. Hardy, et al. (1987). "HPRT-deficient (Lesch-Nyhan) mouse embryos derived from germline colonization by cultured cells." Nature **326**(6110): 292-295.

Hughes, S. E. and W. J. McKenna (2005). "New insights into the pathology of inherited cardiomyopathy." Heart **91**(2): 257-264.

Ieda, M., T. Tsuchihashi, et al. (2009). "Cardiac fibroblasts regulate myocardial proliferation through beta1 integrin signaling." Dev Cell **16**(2): 233-244.

Indra, A. K., X. Warot, et al. (1999). "Temporally-controlled site-specific mutagenesis in the basal layer of the epidermis: comparison of the recombinase activity of the tamoxifen-inducible Cre-ER(T) and Cre-ER(T2) recombinases." Nucleic Acids Res **27**(22): 4324-4327.

Irwin, M., M. C. Marin, et al. (2000). "Role for the p53 homologue p73 in E2F-1-induced apoptosis." Nature **407**(6804): 645-648.

Irwin, M. S. and W. G. Kaelin, Jr. (2001). "Role of the newer p53 family proteins in malignancy." Apoptosis **6**(1-2): 17-29.

Ito, N., Y. Kagaya, et al. (1997). "Endothelin and angiotensin II stimulation of Na+-H+ exchange is impaired in cardiac hypertrophy." J Clin Invest **99**(1): 125-135.

Iwabuchi, K., P. L. Bartel, et al. (1994). "Two cellular proteins that bind to wild-type but not mutant p53." Proc Natl Acad Sci U S A **91**(13): 6098-6102.

Jacobson, M. D., M. Weil, et al. (1997). "Programmed cell death in animal development." Cell **88**(3): 347-354.

Jin, Z. and W. S. El-Deiry (2005). "Overview of cell death signaling pathways." Cancer Biol Ther **4**(2): 139-163.

Joerger, A. C., H. C. Ang, et al. (2005). "Structures of p53 cancer mutants and mechanism of rescue by second-site suppressor mutations." J Biol Chem **280**(16): 16030-16037.

Jones, S. N., A. E. Roe, et al. (1995). "Rescue of embryonic lethality in Mdm2-deficient mice by absence of p53." Nature **378**(6553): 206-208.

Jonkman, M. F., A. M. Pasmooij, et al. (2005). "Loss of desmoplakin tail causes lethal acantholytic epidermolysis bullosa." Am J Hum Genet **77**(4): 653-660.

Joo, W. S., P. D. Jeffrey, et al. (2002). "Structure of the 53BP1 BRCT region bound to p53 and its comparison to the Brca1 BRCT structure." Genes Dev **16**(5): 583-593.

Kaghad, M., H. Bonnet, et al. (1997). "Monoallelically expressed gene related to p53 at 1p36, a region frequently deleted in neuroblastoma and other human cancers." Cell **90**(4): 809-819.

Kajstura, J., W. Cheng, et al. (1996). "Apoptotic and necrotic myocyte cell deaths are independent contributing variables of infarct size in rats." Lab Invest **74**(1): 86-107.

Kajstura, J., W. Cheng, et al. (1996). "Necrotic and apoptotic myocyte cell death in the aging heart of Fischer 344 rats." Am J Physiol **271**(3 Pt 2): H1215-1228.

Kaplan, S. R., J. J. Gard, et al. (2004). "Structural and molecular pathology of the heart in Carvajal syndrome." Cardiovasc Pathol **13**(1): 26-32.

Kaplan, S. R., J. J. Gard, et al. (2004). "Remodeling of myocyte gap junctions in arrhythmogenic right ventricular cardiomyopathy due to a deletion in plakoglobin (Naxos disease)." Heart Rhythm **1**(1): 3-11.

Kaufman, M. H. and V. Navaratnam (1981). "Early differentiation of the heart in mouse embryos." J Anat **133**(Pt 2): 235-246.

Keeler, C. E. (1935). "Headdot: An Incompletely Recessive White Spotting Character of the House Mouse." Proc Natl Acad Sci U S A **21**(6): 379-383.

Kerkela, R., L. Grazette, et al. (2006). "Cardiotoxicity of the cancer therapeutic agent imatinib mesylate." Nat Med **12**(8): 908-916.

Kerr, J. F., A. H. Wyllie, et al. (1972). "Apoptosis: a basic biological phenomenon with wide-ranging implications in tissue kinetics." Br J Cancer **26**(4): 239-257.

Keyes, W. M., H. Vogel, et al. (2006). "p63 heterozygous mutant mice are not prone to spontaneous or chemically induced tumors." Proc Natl Acad Sci U S A **103**(22): 8435-8440.

Kilic, T., K. Babaoglu, et al. (2007). "Biventricular involvement in a Turkish boy with palmoplantar hyperkeratosis and curly hair, an unusual presentation of Naxos-Carvajal syndrome." Int J Cardiol **115**(3): e122-125.

King, K. E., R. M. Ponnamperuma, et al. (2003). "deltaNp63alpha functions as both a positive and a negative transcriptional regulator and blocks in vitro differentiation of murine keratinocytes." Oncogene **22**(23): 3635-3644.

Klues, H. G., A. Schiffers, et al. (1995). "Phenotypic spectrum and patterns of left ventricular hypertrophy in hypertrophic cardiomyopathy: morphologic observations and significance as assessed by two-dimensional echocardiography in 600 patients." J Am Coll Cardiol **26**(7): 1699-1708.

Klymkowsky, M. W., B. O. Williams, et al. (1999). "Membrane-anchored plakoglobins have multiple mechanisms of action in Wnt signaling." Mol Biol Cell **10**(10): 3151-3169.

Koster, M. I. (2010). "p63 in skin development and ectodermal dysplasias." J Invest Dermatol **130**(10): 2352-2358.

Koster, M. I., S. Kim, et al. (2004). "p63 is the molecular switch for initiation of an epithelial stratification program." Genes Dev **18**(2): 126-131.

Kostetskii, I., J. Li, et al. (2005). "Induced deletion of the N-cadherin gene in the heart leads to dissolution of the intercalated disc structure." Circ Res **96**(3): 346-354.

Kostin, S., S. Hein, et al. (1999). "Spatiotemporal development and distribution of intercellular junctions in adult rat cardiomyocytes in culture." Circ Res **85**(2): 154-167.

Kowalczyk, A. P., E. A. Bornslaeger, et al. (1999). "Desmosomes: intercellular adhesive junctions specialized for attachment of intermediate filaments." Int Rev Cytol **185**: 237-302.

Kubota, T., C. F. McTiernan, et al. (1997). "Cardiac-specific overexpression of tumor necrosis factor-alpha causes lethal myocarditis in transgenic mice." J Card Fail **3**(2): 117-124.

Kuhl, M., L. C. Sheldahl, et al. (2000). "The Wnt/Ca2+ pathway: a new vertebrate Wnt signaling pathway takes shape." Trends Genet **16**(7): 279-283.

Kuida, K., T. S. Zheng, et al. (1996). "Decreased apoptosis in the brain and premature lethality in CPP32-deficient mice." Nature **384**(6607): 368-372.

Kupatt, C., R. Wichels, et al. (2002). "Retroinfusion of NFkappaB decoy oligonucleotide extends cardioprotection achieved by CD18 inhibition in a preclinical study of myocardial ischemia and retroinfusion in pigs." Gene Ther **9**(8): 518-526.

Kurrelmeyer, K., D. Kalra, et al. (1998). "Cardiac remodeling as a consequence and cause of progressive heart failure." Clin Cardiol **21**(12 Suppl 1): I14-19.

Lai Cheong, J. E., V. Wessagowit, et al. (2005). "Molecular abnormalities of the desmosomal protein desmoplakin in human disease." Clin Exp Dermatol **30**(3): 261-266.

Laurikkala, J., M. L. Mikkola, et al. (2006). "p63 regulates multiple signalling pathways required for ectodermal organogenesis and differentiation." Development **133**(8): 1553-1563.

Lechler, T. and E. Fuchs (2005). "Asymmetric cell divisions promote stratification and differentiation of mammalian skin." Nature **437**(7056): 275-280.

Legue, E. and J. F. Nicolas (2005). "Hair follicle renewal: organization of stem cells in the matrix and the role of stereotyped lineages and behaviors." Development **132**(18): 4143-4154.

Leung, C. L., K. J. Green, et al. (2002). "Plakins: a family of versatile cytolinker proteins." Trends Cell Biol **12**(1): 37-45.

Li, J. and G. L. Radice (2010). "A new perspective on intercalated disc organization: implications for heart disease." Dermatol Res Pract **2010**: 207835.

Li, P., D. Nijhawan, et al. (1997). "Cytochrome c and dATP-dependent formation of Apaf-1/caspase-9 complex initiates an apoptotic protease cascade." Cell **91**(4): 479-489.

Lin, K. K., D. Chudova, et al. (2004). "Identification of hair cycle-associated genes from time-course gene expression profile data by using replicate variance." Proc Natl Acad Sci U S A **101**(45): 15955-15960.

Liu, H., M. Wang, et al. (2009). "siRNA-mediated down-regulation of iASPP promotes apoptosis induced by etoposide and daunorubicin in leukemia cells expressing wild-type p53." Leuk Res **33**(9): 1243-1248.

Liu, Z. J., X. Lu, et al. (2005). "Downregulated mRNA expression of ASPP and the hypermethylation of the 5'-untranslated region in cancer cell lines retaining wild-type p53." FEBS Lett **579**(7): 1587-1590.

Longo, K. A., J. A. Kennell, et al. (2002). "Wnt signaling protects 3T3-L1 preadipocytes from apoptosis through induction of insulin-like growth factors." J Biol Chem **277**(41): 38239-38244.

Lopez, C. D., Y. Ao, et al. (2000). "Proapoptotic p53-interacting protein 53BP2 is induced by UV irradiation but suppressed by p53." Mol Cell Biol **20**(21): 8018-8025.

Louis, J. M., V. W. McFarland, et al. (1988). "The phosphoprotein p53 is down-regulated post-transcriptionally during embryogenesis in vertebrates." Biochim Biophys Acta **950**(3): 395-402.

Lowe, S. W., E. Cepero, et al. (2004). "Intrinsic tumour suppression." Nature **432**(7015): 307-315.

Maeda, O., N. Usami, et al. (2004). "Plakoglobin (gamma-catenin) has TCF/LEF family-dependent transcriptional activity in beta-catenin-deficient cell line." Oncogene **23**(4): 964-972.

Malekar, P., M. Hagenmueller, et al. (2010). "Wnt signaling is critical for maladaptive cardiac hypertrophy and accelerates myocardial remodeling." Hypertension **55**(4): 939-945.

Marcus, F. I., W. J. McKenna, et al. (2010). "Diagnosis of arrhythmogenic right ventricular cardiomyopathy/dysplasia: proposed modification of the task force criteria." Circulation **121**(13): 1533-1541.

Marine, J. C. and A. G. Jochemsen (2004). "Mdmx and Mdm2: brothers in arms?" Cell Cycle **3**(7): 900-904.

Maron, B. J. (1997). "Hypertrophic cardiomyopathy." Lancet **350**(9071): 127-133.

Maron, B. J. and E. K. Louie (1986). "Apical hypertrophic cardiomyopathy: a view from the U. S. A." J Cardiogr **16**(3): 513-517.

Maron, B. J., P. F. Nichols, 3rd, et al. (1984). "Patterns of inheritance in hypertrophic cardiomyopathy: assessment by M-mode and two-dimensional echocardiography." Am J Cardiol **53**(8): 1087-1094.

Maron, B. J., I. Olivotto, et al. (2000). "Epidemiology of hypertrophic cardiomyopathy-related death: revisited in a large non-referral-based patient population." Circulation **102**(8): 858-864.

Masuelli, L., R. Bei, et al. (2003). "Beta-catenin accumulates in intercalated disks of hypertrophic cardiomyopathic hearts." Cardiovasc Res **60**(2): 376-387.

McGrath, J. A., P. H. Duijf, et al. (2001). "Hay-Wells syndrome is caused by heterozygous missense mutations in the SAM domain of p63." Hum Mol Genet **10**(3): 221-229.

McGrath, J. A., J. R. McMillan, et al. (1997). "Mutations in the plakophilin 1 gene result in ectodermal dysplasia/skin fragility syndrome." Nat Genet **17**(2): 240-244.

McKenna, W. J., G. Thiene, et al. (1994). "Diagnosis of arrhythmogenic right ventricular dysplasia/cardiomyopathy. Task Force of the Working Group Myocardial and Pericardial Disease of the European Society of Cardiology and of the Scientific Council on Cardiomyopathies of the International Society and Federation of Cardiology." Br Heart J **71**(3): 215-218.

McKoy, G., N. Protonotarios, et al. (2000). "Identification of a deletion in plakoglobin in arrhythmogenic right ventricular cardiomyopathy with palmoplantar keratoderma and woolly hair (Naxos disease)." Lancet **355**(9221): 2119-2124.

Meldrum, D. R. (1998). "Tumor necrosis factor in the heart." Am J Physiol **274**(3 Pt 2): R577-595.

Melino, G., X. Lu, et al. (2003). "Functional regulation of p73 and p63: development and cancer." Trends Biochem Sci **28**(12): 663-670.

Melkonyan, H. S., W. C. Chang, et al. (1997). "SARPs: a family of secreted apoptosis-related proteins." Proc Natl Acad Sci U S A **94**(25): 13636-13641.

Merrill, B. J., U. Gat, et al. (2001). "Tcf3 and Lef1 regulate lineage differentiation of multipotent stem cells in skin." Genes Dev **15**(13): 1688-1705.

Micheau, O. and J. Tschopp (2003). "Induction of TNF receptor I-mediated apoptosis via two sequential signaling complexes." Cell **114**(2): 181-190.

Migliorini, D., E. Lazzerini Denchi, et al. (2002). "Mdm4 (Mdmx) regulates p53-induced growth arrest and neuronal cell death during early embryonic mouse development." Mol Cell Biol **22**(15): 5527-5538.

Mikkola, M. L. (2009). "Molecular aspects of hypohidrotic ectodermal dysplasia." Am J Med Genet A **149A**(9): 2031-2036.

Mills, A. A., B. Zheng, et al. (1999). "p63 is a p53 homologue required for limb and epidermal morphogenesis." Nature **398**(6729): 708-713.

Milner, D. J., G. Weitzer, et al. (1996). "Disruption of muscle architecture and myocardial degeneration in mice lacking desmin." J Cell Biol **134**(5): 1255-1270.

Minami, M., S. Matsumoto, et al. (2010). "Cardiovascular side-effects of modern cancer therapy." Circ J **74**(9): 1779-1786.

Miwa, T., T. Koyama, et al. (2000). "Muscle specific expression of Cre recombinase under two actin promoters in transgenic mice." Genesis **26**(2): 136-138.

Mogensen, J., T. Kubo, et al. (2003). "Idiopathic restrictive cardiomyopathy is part of the clinical expression of cardiac troponin I mutations." J Clin Invest **111**(2): 209-216.

Molkentin, J. D., J. R. Lu, et al. (1998). "A calcineurin-dependent transcriptional pathway for cardiac hypertrophy." Cell **93**(2): 215-228.

Montes de Oca Luna, R., D. S. Wagner, et al. (1995). "Rescue of early embryonic lethality in mdm2-deficient mice by deletion of p53." Nature **378**(6553): 203-206.

Moon, R. T., B. Bowerman, et al. (2002). "The promise and perils of Wnt signaling through beta-catenin." Science **296**(5573): 1644-1646.

Mori, S., G. Ito, et al. (2004). "p53 apoptotic pathway molecules are frequently and simultaneously altered in nonsmall cell lung carcinoma." Cancer **100**(8): 1673-1682.

Morimoto, T., M. Fujita, et al. (2008). "Myocardial regulation of p300 and p53 by doxorubicin involves ubiquitin pathways." Circ J **72**(9): 1506-1511.

Muller, M., S. Wilder, et al. (1998). "p53 activates the CD95 (APO-1/Fas) gene in response to DNA damage by anticancer drugs." J Exp Med **188**(11): 2033-2045.

Munclinger, M. J., J. J. Patel, et al. (2000). "Follow-up of patients with arrhythmogenic right ventricular cardiomyopathy dysplasia." S Afr Med J **90**(1): 61-68.

Murray-Zmijewski, F., D. P. Lane, et al. (2006). "p53/p63/p73 isoforms: an orchestra of isoforms to harmonise cell differentiation and response to stress." Cell Death Differ **13**(6): 962-972.

Murray-Zmijewski, F., E. A. Slee, et al. (2008). "A complex barcode underlies the heterogeneous response of p53 to stress." Nat Rev Mol Cell Biol **9**(9): 702-712.

Nagase, T., K. Ishikawa, et al. (1998). "Prediction of the coding sequences of unidentified human genes. IX. The complete sequences of 100 new cDNA clones from brain which can code for large proteins in vitro." DNA Res **5**(1): 31-39.

Nagase, T., K. Ishikawa, et al. (1998). "Prediction of the coding sequences of unidentified human genes. XI. The complete sequences of 100 new cDNA clones from brain which code for large proteins in vitro." DNA Res **5**(5): 277-286.

Nakagawa, H., K. Koyama, et al. (2000). "APCL, a central nervous system-specific homologue of adenomatous polyposis coli tumor suppressor, binds to p53-binding protein 2 and translocates it to the perinucleus." Cancer Res **60**(1): 101-105.

Nakamura, T., J. G. Pichel, et al. (1995). "An apoptotic defect in lens differentiation caused by human p53 is rescued by a mutant allele." Proc Natl Acad Sci U S A **92**(13): 6142-6146.

Naumovski, L. and M. L. Cleary (1996). "The p53-binding protein 53BP2 also interacts with Bc12 and impedes cell cycle progression at G2/M." Mol Cell Biol **16**(7): 3884-3892.

Nava, A., B. Bauce, et al. (2000). "Clinical profile and long-term follow-up of 37 families with arrhythmogenic right ventricular cardiomyopathy." J Am Coll Cardiol **36**(7): 2226-2233.

Nicol, C. J., M. L. Harrison, et al. (1995). "A teratologic suppressor role for p53 in benzo[a]pyrene-treated transgenic p53-deficient mice." Nat Genet **10**(2): 181-187.

Nikolova, V., C. Leimena, et al. (2004). "Defects in nuclear structure and function promote dilated cardiomyopathy in lamin A/C-deficient mice." J Clin Invest **113**(3): 357-369.

Norgett, E. E., S. J. Hatsell, et al. (2000). "Recessive mutation in desmoplakin disrupts desmoplakin-intermediate filament interactions and causes dilated cardiomyopathy, woolly hair and keratoderma." Hum Mol Genet **9**(18): 2761-2766.

Norimura, T., S. Nomoto, et al. (1996). "p53-dependent apoptosis suppresses radiation-induced teratogenesis." Nat Med **2**(5): 577-580.

Nylander, K., B. Vojtesek, et al. (2002). "Differential expression of p63 isoforms in normal tissues and neoplastic cells." J Pathol **198**(4): 417-427.

Oda, E., R. Ohki, et al. (2000). "Noxa, a BH3-only member of the Bcl-2 family and candidate mediator of p53-induced apoptosis." Science **288**(5468): 1053-1058.

Ohnemus, U., M. Uenalan, et al. (2006). "The hair follicle as an estrogen target and source." Endocr Rev **27**(6): 677-706.

Ollmann, M., L. M. Young, et al. (2000). "Drosophila p53 is a structural and functional homolog of the tumor suppressor p53." Cell **101**(1): 91-101.

Opie, L. H., P. J. Commerford, et al. (2006). "Controversies in ventricular remodelling." Lancet **367**(9507): 356-367.

Osada, M., M. Ohba, et al. (1998). "Cloning and functional analysis of human p51, which structurally and functionally resembles p53." Nat Med **4**(7): 839-843.

Osada, M., H. L. Park, et al. (2005). "Differential recognition of response elements determines target gene specificity for p53 and p63." Mol Cell Biol **25**(14): 6077-6089.

Oshima, H., A. Rochat, et al. (2001). "Morphogenesis and renewal of hair follicles from adult multipotent stem cells." Cell **104**(2): 233-245.

Ou, L., W. Li, et al. (2010). "Animal models of cardiac disease and stem cell therapy." Open Cardiovasc Med J **4**: 231-239.

Owens, D. W., V. G. Brunton, et al. (2000). "E-cadherin at the cell periphery is a determinant of keratinocyte differentiation in vitro." Biochem Biophys Res Commun **269**(2): 369-376.

Oxford, E. M., H. Musa, et al. (2007). "Connexin43 remodeling caused by inhibition of plakophilin-2 expression in cardiac cells." Circ Res **101**(7): 703-711.

Parant, J., A. Chavez-Reyes, et al. (2001). "Rescue of embryonic lethality in Mdm4-null mice by loss of Trp53 suggests a nonoverlapping pathway with MDM2 to regulate p53." Nat Genet **29**(1): 92-95.

Park, B. J., S. J. Lee, et al. (2000). "Frequent alteration of p63 expression in human primary bladder carcinomas." Cancer Res **60**(13): 3370-3374.

Paus, R. and G. Cotsarelis (1999). "The biology of hair follicles." N Engl J Med **341**(7): 491-497.

Paus, R. and K. Foitzik (2004). "In search of the "hair cycle clock": a guided tour." Differentiation **72**(9-10): 489-511.

Payne, A. S., Y. Hanakawa, et al. (2004). "Desmosomes and disease: pemphigus and bullous impetigo." Curr Opin Cell Biol **16**(5): 536-543.

Perez, C. A., J. Ott, et al. (2007). "p63 consensus DNA-binding site: identification, analysis and application into a p63MH algorithm." Oncogene **26**(52): 7363-7370.

Perriard, J. C., A. Hirschy, et al. (2003). "Dilated cardiomyopathy: a disease of the intercalated disc?" Trends Cardiovasc Med **13**(1): 30-38.

Pilichou, K., A. Nava, et al. (2006). "Mutations in desmoglein-2 gene are associated with arrhythmogenic right ventricular cardiomyopathy." Circulation **113**(9): 1171-1179.

Plikus, M. V., J. A. Mayer, et al. (2008). "Cyclic dermal BMP signalling regulates stem cell activation during hair regeneration." Nature **451**(7176): 340-344.

Poelmann, R. E. and A. C. Gittenberger-de Groot (2005). "Apoptosis as an instrument in cardiovascular development." Birth Defects Res C Embryo Today **75**(4): 305-313.

Popat, S. and I. E. Smith (2008). "Therapy Insight: anthracyclines and trastuzumab--the optimal management of cardiotoxic side effects." Nat Clin Pract Oncol **5**(6): 324-335.

Pozniak, C. D., S. Radinovic, et al. (2000). "An anti-apoptotic role for the p53 family member, p73, during developmental neuron death." Science **289**(5477): 304-306.

Prindull, G. (1995). "Apoptosis in the embryo and tumorigenesis." Eur J Cancer **31A**(1): 116-123.

Protonotarios, N. and A. Tsatsopoulou (2004). "Naxos disease and Carvajal syndrome: cardiocutaneous disorders that highlight the pathogenesis and broaden the spectrum of arrhythmogenic right ventricular cardiomyopathy." Cardiovasc Pathol **13**(4): 185-194.

Protonotarios, N., A. Tsatsopoulou, et al. (2001). "Genotype-phenotype assessment in autosomal recessive arrhythmogenic right ventricular cardiomyopathy (Naxos disease) caused by a deletion in plakoglobin." J Am Coll Cardiol **38**(5): 1477-1484.

Protonotarios, N., A. Tsatsopoulou, et al. (2001). "Naxos disease: keratoderma, scalp modifications, and cardiomyopathy." J Am Acad Dermatol **44**(2): 309-311.

Protonotarios, N., A. Tsatsopoulou, et al. (1986). "Cardiac abnormalities in familial palmoplantar keratosis." Br Heart J **56**(4): 321-326.

Purcell, N. H., G. Tang, et al. (2001). "Activation of NF-kappa B is required for hypertrophic growth of primary rat neonatal ventricular cardiomyocytes." Proc Natl Acad Sci U S A **98**(12): 6668-6673.

Rajewsky, K., H. Gu, et al. (1996). "Conditional gene targeting." J Clin Invest **98**(3): 600-603.

Rampazzo, A., A. Nava, et al. (2002). "Mutation in human desmoplakin domain binding to plakoglobin causes a dominant form of arrhythmogenic right ventricular cardiomyopathy." Am J Hum Genet **71**(5): 1200-1206.

Rao, B. H., I. S. Reddy, et al. (1996). "Familial occurrence of a rare combination of dilated cardiomyopathy with palmoplantar keratoderma and curly hair." Indian Heart J **48**(2): 161-162.

Raschi, E., V. Vasina, et al. (2010). "Anticancer drugs and cardiotoxicity: Insights and perspectives in the era of targeted therapy." Pharmacol Ther **125**(2): 196-218.

Richard, P., P. Charron, et al. (2003). "Hypertrophic cardiomyopathy: distribution of disease genes, spectrum of mutations, and implications for a molecular diagnosis strategy." Circulation **107**(17): 2227-2232.

Richardson, P., W. McKenna, et al. (1996). "Report of the 1995 World Health Organization/International Society and Federation of Cardiology Task Force on the Definition and Classification of cardiomyopathies." Circulation **93**(5): 841-842.

Rickman, L., D. Simrak, et al. (1999). "N-terminal deletion in a desmosomal cadherin causes the autosomal dominant skin disease striate palmoplantar keratoderma." Hum Mol Genet **8**(6): 971-976.

Riley, T., E. Sontag, et al. (2008). "Transcriptional control of human p53-regulated genes." Nat Rev Mol Cell Biol **9**(5): 402-412.

Robinson, R. A., X. Lu, et al. (2008). "Biochemical and structural studies of ASPP proteins reveal differential binding to p53, p63, and p73." Structure **16**(2): 259-268.

Robles, A. I., N. A. Bemmels, et al. (2001). "APAF-1 is a transcriptional target of p53 in DNA damage-induced apoptosis." Cancer Res **61**(18): 6660-6664.

Rogel, A., M. Popliker, et al. (1985). "p53 cellular tumor antigen: analysis of mRNA levels in normal adult tissues, embryos, and tumors." Mol Cell Biol **5**(10): 2851-2855.

Ross, S. E., N. Hemati, et al. (2000). "Inhibition of adipogenesis by Wnt signaling." Science **289**(5481): 950-953.

Runge, M. S., G. A. Stouffer, et al. (2000). "Morphological patterns of death by myocytes in arrhythmogenic right ventricular dysplasia." Am J Med Sci **320**(5): 310-319.

Sah, V. P., L. D. Attardi, et al. (1995). "A subset of p53-deficient embryos exhibit exencephaly." Nat Genet **10**(2): 175-180.

Samuels-Lev, Y., D. J. O'Connor, et al. (2001). "ASPP proteins specifically stimulate the apoptotic function of p53." Mol Cell **8**(4): 781-794.

Santorelli, F. M., S. C. Mak, et al. (1996). "Maternally inherited cardiomyopathy and hearing loss associated with a novel mutation in the mitochondrial tRNA(Lys) gene (G8363A)." Am J Hum Genet **58**(5): 933-939.

Sasaki, Y., S. Ishida, et al. (2002). "The p53 family member genes are involved in the Notch signal pathway." J Biol Chem **277**(1): 719-724.

Sasaki, Y., Y. Naishiro, et al. (2005). "Identification of pigment epithelium-derived factor as a direct target of the p53 family member genes." Oncogene **24**(32): 5131-5136.

Sauer, B. and N. Henderson (1988). "Site-specific DNA recombination in mammalian cells by the Cre recombinase of bacteriophage P1." Proc Natl Acad Sci U S A **85**(14): 5166-5170.

Sawa, Y., R. Morishita, et al. (1997). "A novel strategy for myocardial protection using in vivo transfection of cis element 'decoy' against NFkappaB binding site: evidence for a role of NFkappaB in ischemia-reperfusion injury." Circulation **96**(9 Suppl): II-280-284; discussion II-285.

Schmid, P., A. Lorenz, et al. (1991). "Expression of p53 during mouse embryogenesis." Development **113**(3): 857-865.

Schmidinger, M., C. C. Zielinski, et al. (2008). "Cardiac toxicity of sunitinib and sorafenib in patients with metastatic renal cell carcinoma." J Clin Oncol **26**(32): 5204-5212.

Schmidt-Ullrich, R. and R. Paus (2005). "Molecular principles of hair follicle induction and morphogenesis." Bioessays **27**(3): 247-261.

Schneider, M. R., R. Schmidt-Ullrich, et al. (2009). "The hair follicle as a dynamic miniorgan." Curr Biol **19**(3): R132-142.

Schneider, V. A. and M. Mercola (2001). "Wnt antagonism initiates cardiogenesis in Xenopus laevis." Genes Dev **15**(3): 304-315.

Schumacher, B., K. Hofmann, et al. (2001). "The C. elegans homolog of the p53 tumor suppressor is required for DNA damage-induced apoptosis." Curr Biol **11**(21): 1722-1727.

Schwenk, F., U. Baron, et al. (1995). "A cre-transgenic mouse strain for the ubiquitous deletion of loxP-flanked gene segments including deletion in germ cells." Nucleic Acids Res **23**(24): 5080-5081.

Seidman, A., C. Hudis, et al. (2002). "Cardiac dysfunction in the trastuzumab clinical trials experience." J Clin Oncol **20**(5): 1215-1221.

Sen-Chowdhry, S., R. D. Morgan, et al. (2010). "Arrhythmogenic cardiomyopathy: etiology, diagnosis, and treatment." Annu Rev Med **61**: 233-253.

Sen-Chowdhry, S., P. Syrris, et al. (2005). "Genetics of right ventricular cardiomyopathy." J Cardiovasc Electrophysiol **16**(8): 927-935.

Seto, E., A. Usheva, et al. (1992). "Wild-type p53 binds to the TATA-binding protein and represses transcription." Proc Natl Acad Sci U S A **89**(24): 12028-12032.

Sgroi, D. C., S. Teng, et al. (1999). "In vivo gene expression profile analysis of human breast cancer progression." Cancer Res **59**(22): 5656-5661.

Shan, K., A. M. Lincoff, et al. (1996). "Anthracycline-induced cardiotoxicity." Ann Intern Med **125**(1): 47-58.

Sil, A. K., S. Maeda, et al. (2004). "IkappaB kinase-alpha acts in the epidermis to control skeletal and craniofacial morphogenesis." Nature **428**(6983): 660-664.

Simon, M. I., M. P. Strathmann, et al. (1991). "Diversity of G proteins in signal transduction." Science **252**(5007): 802-808.

Sivasubramanian, N., M. L. Coker, et al. (2001). "Left ventricular remodeling in transgenic mice with cardiac restricted overexpression of tumor necrosis factor." Circulation **104**(7): 826-831.

Slee, E. A., S. Gillotin, et al. (2004). "The N-terminus of a novel isoform of human iASPP is required for its cytoplasmic localization." Oncogene **23**(56): 9007-9016.

Slee, E. A., D. J. O'Connor, et al. (2004). "To die or not to die: how does p53 decide?" Oncogene **23**(16): 2809-2818.

Smalley, M. J. and T. C. Dale (1999). "Wnt signalling in mammalian development and cancer." Cancer Metastasis Rev **18**(2): 215-230.

Smith, E. A. and E. Fuchs (1998). "Defining the interactions between intermediate filaments and desmosomes." J Cell Biol **141**(5): 1229-1241.

Sottocornola, R., C. Royer, et al. (2010). "ASPP2 binds Par-3 and controls the polarity and proliferation of neural progenitors during CNS development." Dev Cell **19**(1): 126-137.

St-Jacques, B., H. R. Dassule, et al. (1998). "Sonic hedgehog signaling is essential for hair development." Curr Biol **8**(19): 1058-1068.

Stenn, K. S. and R. Paus (2001). "Controls of hair follicle cycling." Physiol Rev **81**(1): 449-494.

Stiewe, T., S. Zimmermann, et al. (2002). "Transactivation-deficient DeltaTA-p73 acts as an oncogene." Cancer Res **62**(13): 3598-3602.

Su, X., M. Paris, et al. (2009). "TAp63 prevents premature aging by promoting adult stem cell maintenance." Cell Stem Cell **5**(1): 64-75.

Sullivan, A. and X. Lu (2007). "ASPP: a new family of oncogenes and tumour suppressor genes." Br J Cancer **96**(2): 196-200.

Takahashi, N., S. Kobayashi, et al. (2004). "Expression of 53BP2 and ASPP2 proteins from TP53BP2 gene by alternative splicing." Biochem Biophys Res Commun **315**(2): 434-438.

Tan, M., J. Bian, et al. (2001). "p53CP is p51/p63, the third member of the p53 gene family: partial purification and characterization." Carcinogenesis **22**(2): 295-300.

Taylor, G., M. S. Lehrer, et al. (2000). "Involvement of follicular stem cells in forming not only the follicle but also the epidermis." Cell **102**(4): 451-461.

Testoni, B., S. Borrelli, et al. (2006). "Identification of new p63 targets in human keratinocytes." Cell Cycle **5**(23): 2805-2811.

Thiene, G., A. Nava, et al. (1988). "Right ventricular cardiomyopathy and sudden death in young people." N Engl J Med **318**(3): 129-133.

Thornberry, N. A. and Y. Lazebnik (1998). "Caspases: enemies within." Science **281**(5381): 1312-1316.

Thornton, J. K., C. Dalgleish, et al. (2006). "The tumour-suppressor protein ASPP1 is nuclear in human germ cells and can modulate ratios of CD44 exon V5 spliced isoforms in vivo." Oncogene **25**(22): 3104-3112.

Toker, A. and L. C. Cantley (1997). "Signalling through the lipid products of phosphoinositide-3-OH kinase." Nature **387**(6634): 673-676.

Tomic-Canic, M., M. Komine, et al. (1998). "Epidermal signal transduction and transcription factor activation in activated keratinocytes." J Dermatol Sci **17**(3): 167-181.

Tong, X. and P. A. Coulombe (2006). "Keratin 17 modulates hair follicle cycling in a TNFalpha-dependent fashion." Genes Dev **20**(10): 1353-1364.

Tosti, A., C. Misciali, et al. (1994). "Woolly hair, palmoplantar keratoderma, and cardiac abnormalities: report of a family." Arch Dermatol **130**(4): 522-524.

Trigiante, G. and X. Lu (2006). "ASPP [corrected] and cancer." Nat Rev Cancer **6**(3): 217-226.

Tsubata, S., K. R. Bowles, et al. (2000). "Mutations in the human delta-sarcoglycan gene in familial and sporadic dilated cardiomyopathy." J Clin Invest **106**(5): 655-662.

Tyner, S. D., S. Venkatachalam, et al. (2002). "p53 mutant mice that display early ageing-associated phenotypes." Nature **415**(6867): 45-53.

Valabrega, G., F. Montemurro, et al. (2007). "Trastuzumab: mechanism of action, resistance and future perspectives in HER2-overexpressing breast cancer." Ann Oncol **18**(6): 977-984.

van Empel, V. P. and L. J. De Windt (2004). "Myocyte hypertrophy and apoptosis: a balancing act." Cardiovasc Res **63**(3): 487-499.

Vives, V., J. Su, et al. (2006). "ASPP2 is a haploinsufficient tumor suppressor that cooperates with p53 to suppress tumor growth." Genes Dev **20**(10): 1262-1267.

Vogelstein, B., D. Lane, et al. (2000). "Surfing the p53 network." Nature **408**(6810): 307-310.

Vousden, K. H. and X. Lu (2002). "Live or let die: the cell's response to p53." Nat Rev Cancer **2**(8): 594-604.

Wager, M., J. Guilhot, et al. (2006). "Prognostic value of increase in transcript levels of Tp73 DeltaEx2-3 isoforms in low-grade glioma patients." Br J Cancer **95**(8): 1062-1069.

Walker, N. P., R. V. Talanian, et al. (1994). "Crystal structure of the cysteine protease interleukin-1 beta-converting enzyme: a (p20/p10)2 homodimer." Cell **78**(2): 343-352.

Weber, A., U. Bellmann, et al. (2002). "Expression of p53 and its homologues in primary and recurrent squamous cell carcinomas of the head and neck." Int J Cancer **99**(1): 22-28.

Wei, C. L., Q. Wu, et al. (2006). "A global map of p53 transcription-factor binding sites in the human genome." Cell **124**(1): 207-219.

Weissleder, R. and U. Mahmood (2001). "Molecular imaging." Radiology **219**(2): 316-333.

Weninger, W. J., K. Lopes Floro, et al. (2005). "Cited2 is required both for heart morphogenesis and establishment of the left-right axis in mouse development." Development **132**(6): 1337-1348.

Weninger, W. J., S. Meng, et al. (1998). "A new episcopic method for rapid 3-D reconstruction: applications in anatomy and embryology." Anat Embryol (Berl) **197**(5): 341-348.

Weninger, W. J. and T. Mohun (2002). "Phenotyping transgenic embryos: a rapid 3-D screening method based on episcopic fluorescence image capturing." Nat Genet **30**(1): 59-65.

Westfall, M. D., D. J. Mays, et al. (2003). "The Delta Np63 alpha phosphoprotein binds the p21 and 14-3-3 sigma promoters in vivo and has transcriptional repressor activity that is reduced by Hay-Wells syndrome-derived mutations." Mol Cell Biol **23**(7): 2264-2276.

Whittock, N. V., F. J. Smith, et al. (2002). "Frameshift mutation in the V2 domain of human keratin 1 results in striate palmoplantar keratoderma." J Invest Dermatol **118**(5): 838-844.

Whittock, N. V., H. Wan, et al. (2002). "Compound heterozygosity for non-sense and mis-sense mutations in desmoplakin underlies skin fragility/woolly hair syndrome." J Invest Dermatol **118**(2): 232-238.

Wong, S. and O. N. Witte (2004). "The BCR-ABL story: bench to bedside and back." Annu Rev Immunol **22**: 247-306.

Wu, G. S., T. F. Burns, et al. (1997). "KILLER/DR5 is a DNA damage-inducible p53-regulated death receptor gene." Nat Genet **17**(2): 141-143.

Wu, W., W. L. Lee, et al. (2000). "Expression of constitutively active phosphatidylinositol 3-kinase inhibits activation of caspase 3 and apoptosis of cardiac muscle cells." J Biol Chem **275**(51): 40113-40119.

Wyllie, A. H. (1997). "Apoptosis: an overview." Br Med Bull **53**(3): 451-465.

Xiong, S., C. S. Van Pelt, et al. (2007). "Loss of Mdm4 results in p53-dependent dilated cardiomyopathy." Circulation **115**(23): 2925-2930.

Yamaguchi, H., K. Inokuchi, et al. (2001). "Mutation of the p51/p63 gene is associated with blastic crisis in chronic myelogenous leukemia." Leukemia **15**(11): 1729-1734.

Yang, A., M. Kaghad, et al. (2002). "On the shoulders of giants: p63, p73 and the rise of p53." Trends Genet **18**(2): 90-95.

Yang, A., M. Kaghad, et al. (1998). "p63, a p53 homolog at 3q27-29, encodes multiple products with transactivating, death-inducing, and dominant-negative activities." Mol Cell **2**(3): 305-316.

Yang, A. and F. McKeon (2000). "P63 and P73: P53 mimics, menaces and more." Nat Rev Mol Cell Biol **1**(3): 199-207.

Yang, A., R. Schweitzer, et al. (1999). "p63 is essential for regenerative proliferation in limb, craniofacial and epithelial development." Nature **398**(6729): 714-718.

Yang, A., N. Walker, et al. (2000). "p73-deficient mice have neurological, pheromonal and inflammatory defects but lack spontaneous tumours." Nature **404**(6773): 99-103.

Yang, J. P., M. Hori, et al. (1999). "Identification of a novel inhibitor of nuclear factor-kappaB, RelA-associated inhibitor." J Biol Chem **274**(22): 15662-15670.

Yang, J. P., M. Hori, et al. (1999). "NF-kappaB subunit p65 binds to 53BP2 and inhibits cell death induced by 53BP2." Oncogene **18**(37): 5177-5186.

Yee, K. S. and K. H. Vousden (2005). "Complicating the complexity of p53." Carcinogenesis **26**(8): 1317-1322.

Yoshida, K., T. Taga, et al. (1996). "Targeted disruption of gp130, a common signal transducer for the interleukin 6 family of cytokines, leads to myocardial and hematological disorders." Proc Natl Acad Sci U S A **93**(1): 407-411.

Yu, J. and L. Zhang (2003). "No PUMA, no death: implications for p53-dependent apoptosis." Cancer Cell **4**(4): 248-249.

Yu, J., L. Zhang, et al. (2001). "PUMA induces the rapid apoptosis of colorectal cancer cells." Mol Cell **7**(3): 673-682.

Yuspa, S. H., A. E. Kilkenny, et al. (1989). "Expression of murine epidermal differentiation markers is tightly regulated by restricted extracellular calcium concentrations in vitro." J Cell Biol **109**(3): 1207-1217.

Zhang, J., A. Kumar, et al. (2001). "Clinical and molecular studies of a large family with desmin-associated restrictive cardiomyopathy." Clin Genet **59**(4): 248-256.

Zhang, X., S. Diao, et al. (2007). "Identification of a novel isoform of iASPP and its interaction with p53." J Mol Biol **368**(4): 1162-1171.

Zhang, X., M. Wang, et al. (2005). "The expression of iASPP in acute leukemias." Leuk Res **29**(2): 179-183.

Zhao, J., G. Wu, et al. (2010). "Epigenetic silence of ankyrin-repeat-containing, SH3-domain-containing, and proline-rich-region- containing protein 1 (ASPP1) and ASPP2 genes promotes tumor growth in hepatitis B virus-positive hepatocellular carcinoma." Hepatology **51**(1): 142-153.

Zhu, J., W. Zhou, et al. (1998). "Identification of a novel p53 functional domain that is necessary for mediating apoptosis." J Biol Chem **273**(21): 13030-13036.

Zhu, Z., J. Ramos, et al. (2005). "Control of ASPP2/(53BP2L) protein levels by proteasomal degradation modulates p53 apoptotic function." J Biol Chem **280**(41): 34473-34480.

Zhurinsky, J., M. Shtutman, et al. (2000). "Differential mechanisms of LEF/TCF family-dependent transcriptional activation by beta-catenin and plakoglobin." Mol Cell Biol **20**(12): 4238-4252.

Zong, W. X., T. Lindsten, et al. (2001). "BH3-only proteins that bind pro-survival Bcl-2 family members fail to induce apoptosis in the absence of Bax and Bak." Genes Dev **15**(12): 1481-1486.

Zou, Y. R., W. Muller, et al. (1994). "Cre-loxP-mediated gene replacement: a mouse strain producing humanized antibodies." Curr Biol **4**(12): 1099-1103.